Defining the Metabolic Effect of Peroxisome Proliferator-Activated Receptor δ Activation

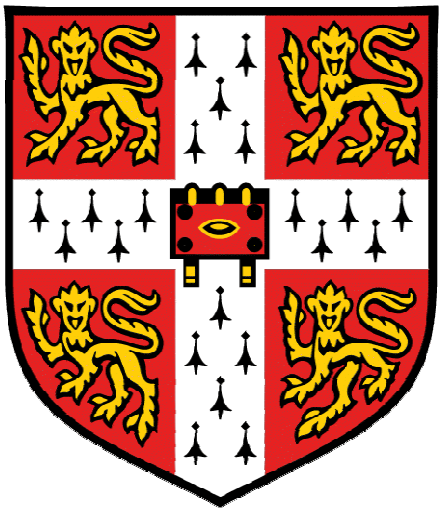

A dissertation submitted for the degree of Doctor of Philosophy

at the University of Cambridge

Lee Daniel Roberts

King's College

"My main thesis will be that in the study of the intermediate processes of metabolism we have to deal not with complex substances which elude ordinary chemical methods, but with the simple substances undergoing comprehensible reactions... I intend also to emphasise the fact that it is not alone with the separation and identification of products from the animal that our present studies deal; but with their reactions in the body; with the dynamic side of biochemical phenomena."

-Sir Frederick Gowland Hopkins
Biochemist and Nobel Laureate
The Dynamic Side of Biochemistry (1914) *Report on the 83rd Meeting of the British Association for the Advancement of Science*, **653**.

"Never express yourself more clearly than you are able to think."

-Niels Henrik David Bohr
Danish Physicist and Nobel Laureate

Declaration

This thesis is a summary of research conducted within the Department of Biochemistry, University of Cambridge, between October 2006 and February 2010. This dissertation is the result of my own work and includes nothing which is the outcome of work done in collaboration, except where specifically indicated in the text. None of the research described, in its entirety or in part, has been submitted for any other qualification at any other University.

Abstract

Peroxisome proliferator-activated receptors (PPARs) are nuclear receptors that function as ligand activated transcription factors. There are three identified isotypes: PPARα, PPARγ and PPARδ, together controlling the expression of genes involved in inflammation, cell differentiation, proliferation, lipid and carbohydrate metabolism and energy homeostasis. The PPARs are potential targets for the treatment of dyslipidaemia, type II diabetes mellitus and the metabolic syndrome. This thesis uses a multi-platform metabolomics approach, ^{13}C-isotope substrate flux analysis, respirometry and transcriptomics to determine the role PPARδ and PPARγ play in metabolic control both in adipose tissue and systemically. To achieve this, the metabolic phenotype of the 3T3-L1 adipocyte cell line was defined to generate a metabolically phenotyped *in vitro* model of adipose tissue. The importance of fatty acid α-oxidation in the differentiation of adipocytes was emphasised The effects of PPARδ and PPARγ activation in white adipose tissue from the *ob/ob* mouse model of insulin resistance, and in the phenotyped 3T3-L1 adipocyte model, were investigated. PPARδ activation was distinguished by oxidative catabolism of fatty acids and citric acid cycle intermediates. Conversely, PPARγ activation was identified by the sequestration of lipids into adipose tissue. Moreover, to address the systemic influence of PPAR activation, with a focus on the Cori cycle and the interactions of the liver and skeletal muscle, the metabolic changes that occur in these tissues following PPARδ and PPARγ activation in the *ob/ob* mouse were examined. PPARδ activation was characterised by the mobilisation and release of triacylglycerols (TAGs) into circulation as an energy source for peripheral tissues whereas PPARγ activation was defined by a reduction and sequestration of circulating TAGs. This thesis has better characterised the role of the PPARs as master regulators of metabolism and emphasised their potential as therapeutic targets for metabolic diseases of global importance.

Publications

Roberts, L.D., Hassall, D.G., Winegar, D.A., Haselden, J.N., Nicholls, A.W., Griffin J.L. (2009) Increased hepatic oxidative metabolism distinguishes the action of Peroxisome Proliferator-Activated Receptor delta from Peroxisome Proliferator-Activated Receptor gamma in the Ob/Ob mouse. *Genome Med*. **1**, 115.

Roberts, L.D., Virtue, S., Vidal-Puig, A., Nicholls, A.W., Griffin, J.L. (2009) Metabolic phenotyping of a model of adipocyte differentiation. *Physiol. Genomics*. **39**, 109-19.

Roberts, L.D., McCombie, G., Titman, C.M., Griffin, J.L. (2008) A matter of fat: an introduction to lipidomic profiling methods. *J. Chromatogr. B Analyt. Technol. Biomed. Life Sci.* **871**, 174-81

Acknowledgements

I would like to take this opportunity to express my gratitude to the many people who have helped me over the years, without you this thesis could never have been. Specifically I would like to take the time to thank both those that have contributed to my work over the last three years, culminating in this thesis, and to those who have offered me their friendship and support, it is due to you that I have so enjoyed my time in Cambridge.

Foremost I would like to thank my supervisor Dr Jules Griffin. Thank you for the opportunity of researching in your lab and visiting international meetings and conferences. I have learnt a great deal, not only in terms of the science but also on how to conduct research; this is a grounding I will call upon for my entire academic career. I would also like to thank my industrial supervisor Dr Andrew Nicholls at GlaxoSmithKline who has provided a great deal of support and advice throughout the last three years. In addition I would thank all those at GlaxoSmithKline who have been of help.

Thanks also go to those who have offered their technical expertise and advice, to Sam Virtue for all his support with cell culture, and Andrew Murray and David Menassa for their guidance and help with respirometry.

Thanks should also go to the past and present members of the JLG lab for keeping life in the lab entertaining and being around for a trip to the pub when it wasn't. It has been a pleasure. A special thanks go to Bal it was a delight to introduce you to "flatliners", Cheng for stats advice (congratulations on starting the family), Chris for all the help and advice but especially for all the cake, Claire my shins will never be the same again, Denis thanks for recommending the cold cure, to Gregor we will write the LIIT book eventually ("Brooklyn, Bronx, Queens and Staten"), Helen thanks for all the dancing and lab bay

decorations (sorry about the pants thing), Martin thanks for putting up with sitting next to me, the conversations (I'll miss those!) and the nights out (What and you're still single?!), Mel thanks for my "stripette", Oli my festival tent partner, Reza for 2D NMR advice, Sarah for her inspirational teaching tips on how to keep undergraduates awake during supervisions and lastly Steve for Halloween dressing up, introducing me to Cambridge United and the joys of Ely (my sofa will miss you).

Next I would like to address my friends from King's College and especially the graduate community, an almost constant source of fun and great memories, thank you for all the formals, mingles, May Week events, parties and "grad trips". To Kev and Louis thanks for the ups (California, Mexico and Las Vegas), the downs (The Mill), the nickname and the "witty" banter. Steve you must have been scraping the barrel to have ended up with me as best man but thanks (congratulations on the Dylan Thomas challenge!), Adrienne for being "house mum" and the most entertaining cleaning session ever. To Anne, thank you for your understanding, patience and support during the more stressful periods (moods and hysterics) whilst writing this thesis. Our chats are amazing and the motivational postcards kept me going.

To the SPH boys Marcus, JJ, Joe, Mark and Mel thank you for your friendship for all these years and the ability you have to keep my feet on the ground, but head in the clouds (yes we are getting old but still not growing up).

Lastly I would like to thank my family, with special reference to Mark and Ames, siblings without parallel who know how to keep their big brother in check ("What's going on in Bristol?"). To my grandmother Vera, who passed away during the preparation of this thesis, you are sorely missed and never forgotten. Finally for their unquestioning and unwavering love, support and encouragement throughout my life I dedicate this thesis to my family and especially to my parents Carole and Bill Roberts.

Table of Contents

Abbreviations

API	Atmospheric pressure ionisation
ATMA	Automatic tuning and matching
BEH	Bridged ethyl hybrid
CID	Collision induced dissociation
^{13}C-NMR	^{13}C-Nuclear magnetic resonance
DI-MS	Direct infusion-mass spectrometry
DMEM	Dulbecco's modified eagles media
DMSO	Dimethylsulphoxide
EGIR	European group for the study of insulin resistance
EI	Electron impact
EPA	Environmental protection agency
ESI	Electrospray ionisation
FAMEs	Fatty acid methyl esters
FBS	Foetal bovine serum
FFA	Free fatty acid
GC-FID	Gas chromatography-flame ionisation detection
GC-MS	Gas chromatography-mass spectrometry
h	Planck's constant
HCA	Hierarchical cluster analysis
HDL	High density lipoprotein
HPLC	High performance liquid chromatography
^{1}H-NMR	^{1}H-Nuclear magnetic resonance
HSQC	Heteronuclear single-quantum coherence
I	Nuclear spin
IDF	International Diabetes Federation
IGT	Impaired glucose tolerance

Abbreviations

LC-MS	Liquid chromatography-mass spectrometry
LDL	Low density lipoprotein
MALDI	Matrix assisted laser desorption/ionisation
MS/MS	Tandem-MS
MSTFA	*N*-methyl-*N*-(trimethylsilyl)-trifluoroacetamide
m/z	Mass to charge ratio
NCEP	National cholesterol education program
Ncor1	Transcription of nuclear receptor corepressor
NIH	National institute of health
NIST	National institute of standards and technology
OGTT	Oral glucose tolerance test
OSC	Orthogonal signal correction
PBS	Phosphate buffered saline
PC	Principal component
PCA	Principal components analysis
PLS	Partial least squares
PLS-DA	Partial least squares discriminate analysis
PPAR	Peroxisome proliferator-activated receptor
PPREs	Peroxisome proliferator response elements
PRESS	Predicted residual sum of squares
QToF	Quadrupole-time-of-flight
RPC	Reversed phase chromatography
RXR	9-cis-retinoic acid receptor
σ	Shielding constant
TAG	Triacylglycerol
THF	Tetrahydrofuran
TIIDM	Type II diabetes mellitus
TOF	Time-of-flight
TSP	Sodium-3-(trimethylsilyl)-2,2,3,3-tetradeuteriopropionate
TZD	Thiazolidinediones
VIP	Variable influence on projection

VLDL	Very low density lipoproteins
WHO	World health organisation

Chapter 1

Introduction

1.1 Metabolomics

1.1.1. The Omics Revolution and Metabolomics

The central biochemical and molecular biological dogma declares that information flows directionally from the genomic DNA through mRNA transcripts, which are then translated to protein. The protein products, amongst them enzymes, then influence the concentrations of their substrates and products which are integrated in tightly controlled metabolic pathways. It is the flux of these small molecular weight metabolites within a cell, tissue or organism that generates the phenotype. Whilst much of this holds true it is now understood that the movement of information is far from unidirectional. Cellular communication is now known to occur via a complex system of interactions between DNA, RNA, protein and metabolite with feed forward and negative feed back loops in play (**Figure 1.1**); the new methodologies of the omics revolution of the 1980s and 1990s, in particular genomics, provided invaluable tools for the study of these interactions on a global level and offered an alternative means of investigation to that of the more reductionist molecular biology approaches.

Genomics, that is the determination of the entire genetic DNA sequence of organisms accounting for the often indefinite line between genetic and non-genetic regions of DNA, fine-scale genetic mapping, and intragenomic interactions between loci and alleles within

the genome of an organism, gave rise to the related field of functional genomics. The fundamental goal of functional genomics is the exploration of gene function on a global scale by elucidating the functions of genes, their products and how they interact to translate into the complex organisation of cells, tissues and organisms. The importance of such a stratagem becomes clear when it is considered that approximately 40% of all open reading frames have no known function[1]; functional genomics is an ideal device for mining these potential genes. A common approach in functional genomics involves gene modification which disturbs the system and generates an altered phenotype; the adapted phenotype can then be characterised and compared to that of the wild type. Functional analysis at the gene expression level is known as transcriptomics and examines the expression level of mRNAs in a population of cells or tissue using high-throughput techniques often based on microarray technology. Investigations at the level of protein translation, defined as proteomics aims to identify and localise proteins and determine protein pathways within an organelle, cell, or organism[2, 3]. More recently study of metabolic network interactions have been designated as metabolomics. When integrated, the variety of approaches in functional genomics can contribute to research in systems biology, which examines the interactions between the components of the central dogma, and how these interactions give rise to the function and behaviour of the biological systems to which they belong.

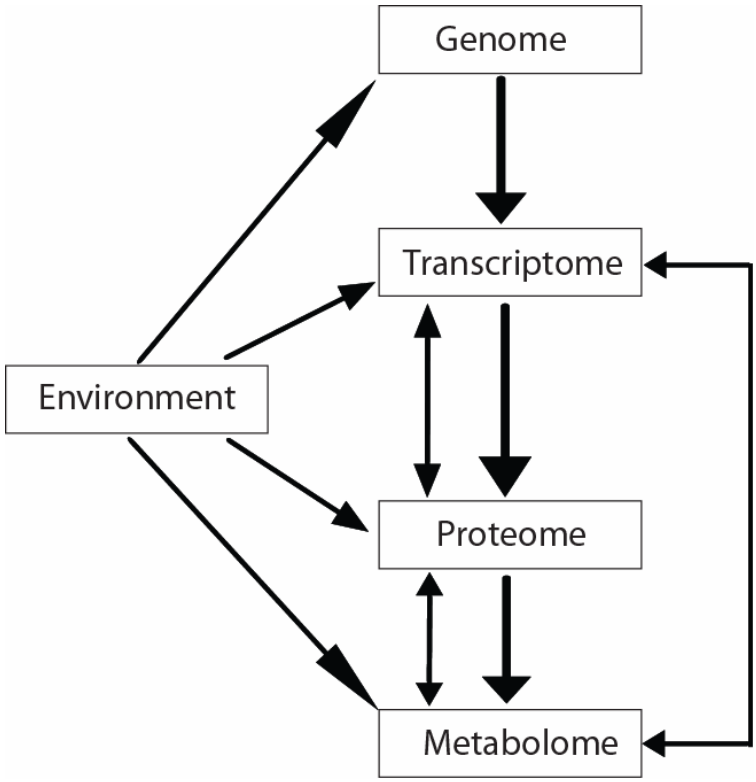

Figure 1.1: The central molecular biological dogma states information flows directionally from genomic DNA through mRNA transcripts, to protein. However, each tier of organization is now known to depend on the other. In addition, the environment has a vital impact on expression and concentrations of mRNA transcripts, proteins, metabolites and even affects the genome.

1.1.2 Metabolomics

Metabolomics was defined in the late 1990s as a term which describes techniques aimed at measuring the metabolites present within a cell, tissue or organism during a genetic alteration or physiological stimulus[4, 5]. Measurement of time-related metabolic changes in animal models in response to genetic manipulation can be used to define the varying phenotypes[6]. Through this methodology metabolomics has proved complementary to the other omic techniques; identifying so called silent phenotypes, genes that when perturbed have no influence on apparent physical characteristics or behaviour[7].

The metabolome is the terminal downstream product of the genome and consists of the total complement of all the low molecular weight molecules (metabolites) in a cell, tissue or organism required for growth, maintenance or normal function in a specific physiological state[8, 9]. However when the potential size of the metabolome is considered, it is often heavily disputed, with an estimated range from ~ 600 metabolites in *S. Cerevisiae*[10] to ~200,000 metabolites in the plant kingdom[11]. Alongside the variety of chemical classes and physical properties (small polar volatiles through to large hydrophobic lipids) that constitute metabolites and the dynamic range of metabolite concentrations across large orders of magnitude (from picomolar to millimolar) it becomes clear why it is necessary to employ an extensive array of analytical techniques within metabolomics research.

Analytical approaches used within metabolomics to identify the changes in the concentrations and fluxes of endogenous metabolites include, but are not limited to, ^{1}H-Nuclear Magnetic Resonance (^{1}H-NMR) Spectroscopy, ^{13}C-Nuclear Magnetic Resonance (^{13}C-NMR) Spectroscopy, Gas Chromatography-Mass Spectrometry (GC-MS), Gas Chromatography-Flame Ionisation Detection (GC-FID), Direct Infusion-Mass Spectrometry (DI-MS) and Liquid Chromatography-Mass Spectrometry (LC-MS).

Given the extensive amount of raw data that is generated using these spectroscopic and spectrometric techniques, robust chemometric techniques and bioinformatic tools are a necessity. Pattern recognition allows the description of inherent patterns of changing metabolites. Through multivariate techniques such as the unsupervised principal components analysis (PCA) and supervised techniques such as projection to latent structures through partial least squares discriminate analysis (PLS-DA) metabolites that vary between treatment groups can be identified[12].

Due to the wide array of metabolites and the dynamic nature of their concentrations within the cell, a complete analysis of the metabolome has thus far eluded description even when a range of analytical approaches have been employed. Despite this

disadvantage metabolomics has been used successfully within the field of functional genomics to understand gene function in a range of model organisms.

1.1.3 Lipidomics

Although the lipidome is a sub fraction of the metabolome, the complexity of lipid classes and their distinct chemical properties has necessitated focused approaches to the study of these constituents of the metabolome. Lipidomics has been defined as "the full characterisation of lipid molecular species and of their biological roles with respect to expression of proteins involved in lipid metabolism and function, including gene regulation"[13]. A distinction is drawn between lipidomics and lipid profiling by some but the differences are subtle and the terms are extensively used interchangeably[14, 15]. The interest in lipidomics has also been driven by the widening knowledge of the role of lipid species in the cell. In the past the majority of lipids were considered to be either membrane components or an energy store. However, these molecules are now known to have diverse roles in transcriptional and translational control, cellular signalling, cell-cell interactions, and as indicators of changes to the environs of a cell or organism over time. To study the various functions of lipids a multidisciplinary approach has been employed within lipidomics. These have encompassed: profiling of the lipid species using a range of chromatographic and spectrometric techniques (many of which are well established metabolomic methods) and multivariate statistical data analysis[16], use of traditional biochemical techniques to study lipid-lipid or lipid-protein interactions such as immobilised lipid assays[17] and lipid-protein complex antibody assays[18], and localisation of lipids using imaging methods, for instance fluorescently tagged lipids or optical probes for their detection[19]. Lipidomics has also proved a powerful means of defining the part lipids play in pathological states, both for diseases where lipids are known to play a prominent role such as diabetes[20] and where their roles are less well characterised such as Alzheimer's disease[21]. The development of the lipidomic field has composed an additional tier to data from proteomics and genomics and metabolomics of small molecules, furthering our knowledge of the function of lipids within the cell[22].

1.1.4 Application of Metabolomics and Lipidomics

In the interest of relevance to this thesis the applications discussed will primarily relate to the instances in which metabolomics has been utilised in the investigation of cardiovascular disease, the metabolic syndrome, pharmacological studies and phenotyping chemotaxonomy. However, it is worthy of note that metabolomics has been employed in the investigation of a diverse range of other fields including neuroscience[23, 24], cancer biology[25, 26], microbiology[27] and cellular lipid signalling[28].

To a significant extent metabolomics has been an application driven discipline and much of the momentum within the field can be attributed to the study of diseases. An early progression from single metabolite analysis was the attempted exploitation of metabolomics to find biomarkers of disease; the hope being that in finding valid biomarkers, metabolomics could be used as a viable diagnostic tool. A prominent example of this premise has employed ^{1}H-NMR spectroscopy analysis to blood serum, followed by pattern recognition analysis to examine the changes in lipoprotein metabolism associated with coronary artery disease and diabetes[29]. The pattern recognition models generated from this study predicted that pre-diabetic serum is characteristic of a pro-atherogenic state in which there is a decrease in small high density lipoprotein (HDL) particles and an increase in very low density lipoproteins (VLDL). The authors continue to suggest that lipoprotein profiling may assist in diagnosing patients at an increased risk of developing diabetes. In the study of clinical cardiology, a targeted mass spectrometry metabolomics investigation was utilised in the study of patients subjected to exercise stress testing with myocardial perfusion imaging[30]. The study aimed to investigate whether metabolomics could be used to discriminate the occurrence of ischaemia in coronary artery disease; a goal that could aid the diagnosis, selection of therapy and understanding of disease mechanism. The study employed a control group of 18 patients with no evidence of ischaemia and a case group of 18 patients with inducible ischaemia. Plasma was analysed by LC-MS using a triple quadrupole mass spectrometer operating under selected reaction monitoring conditions. Metabolites involved in skeletal muscle AMP catabolism, lactic acid, as well as

hypoxanthine and inosine, increased in both the inducible ischaemic and non-ischaemic groups. However there was a significant difference in a number of the metabolic changes between control and case groups. The TCA cycle was profoundly effected and 6 of the 23 most significantly changed metabolites were intermediates in this pathway. Six metabolites displayed significant discordant changes in case and control groups, using these metabolites, case subjects could be distinguished from control subjects with a high degree of accuracy ($p < 0.0001$; c-statistic = 0.83). Metabolomics has also been employed in the correlation of metabolite changes within blood plasma to measure blood pressure[31].

The applications of metabolomics in the study of disease are not limited to its diagnostic and biomarker identification properties; the metabolomic method has been employed in the study of a diverse range of diseases to elucidate mechanisms of pathology. Salek *et al* employed an NMR-based metabolomic analysis to examine urinary metabolic changes in the Zucker rat (*fa/fa*) and *db/db* mouse, models of type II diabetes mellitus (TIIDM), as well as in human diabetes patients[32]. Disease dependent metabolic changes were identified in the subjects, demonstrating similarity in metabolic perturbation between the three species examined. Of significance were metabolic disturbances related to systemic stress, the TCA cycle, nucleotide metabolism and methylamine metabolism. Lipidomic analysis has also enabled new insights into biological disease processes[33]. The potential application of LC-MS lipidomic analysis in both preclinical and clinical research has not gone unnoticed due to the importance of lipids in cardiovascular, TIIDM and related inflammatory disorders[34]. For example, LC-MS analysis of liver tissue from the *ob/ob* mouse, a classic model of obese insulin resistance and hepatic steatosis, using reversed-phase LC-MS revealed an increase of tri- and di-acylglycerols, diacylphosphoglycerols and certain ceramides and a decrease in the concentration of sphingomyelins[35]. Pietilainen *et al* used reversed phase LC-MS lipidomics to study the serum lipid profiles from monozygotic twins, determining that acquired obesity, independent of genetic influences, was linked with an increase in the concentration of lysophosphatidylcholines[36]. These results were correlated and considered alongside clinical measurements revealing the propriety of LC-MS lipidomic analyses in human

studies. Lipidomic investigation by normal phase LC-MS has also been exploited in the determination of lipid changes associated with the conversion of normal HDL to pro-inflammatory HDL (acute-phase HDL) associated with cardiovascular disease. Phosphatidylcholine and sphingomyelin ratios were increased and diacyl and alkenylacyl glycerophosphatidylethanolamine and phosphatidylinositol were decreased, which may be indicative of proinflammatory and proatherogenic roles[37]. In addition a LC-MS based lipidomics approach has been applied in a clinical study of TIIDM patients[38]. The study identified over 100 phospholipids in the blood plasma and demonstrated changes in the plasma phospholipid profile that distinguished patients from control subjects. An increased concentration of two phosphoethanolamine species (phosphoethanolamine C16:0/C22:6 and C18:0/C20:4) and a decrease in the concentration of two lyso-phosphocholine species (lyso-phosphocholine C16:0 and C18:0) discriminated diabetic patients from controls.

Metabolomics has also been successfully applied as a phenotyping device for laboratory model *in vitro* and *in vivo* biological mediums and chemotaxonomy, which is profiling for strain differences; this concept was initially proved in a ^{1}H-NMR spectroscopy study of the metabolic changes induced in two yeast mutants of 6-phosphofructo-2-kinase which was capable of distinguishing between the silent phenotypes of the yeast[39]. The phenotyping approach was then expanded upon by a study that demonstrated it could be applied to the media in which the yeast was grown, giving rise to the technique of metabolic footprinting[40]. Plant biochemistry has also exploited the rigorous phenotyping capabilities of metabolomics; in a seminal paper Fiehn *et al* were able to use GC-MS to quantify 326 distinct metabolites from *Arabidopsis* using these to separate four genotypes[41]. GC-MS metabolomic analysis has also been exploited to identify changes in lipid metabolism upon hormone induced differentiation of 3T3-L1 cells into mature adipocytes[42]. A metabolic profiling approach has been utilised to phenotype mouse models of cardiac diseases[43]. Analysis of cardiac tissue from mouse models of Duchenne muscular dystrophy, cardiac arrhythmia and cardiac hypertrophy using NMR spectroscopy in conjunction with multivariate statistics was capable of classifying mouse models of cardiac disease. Strain background was identified as a substantial contributor

to the metabolic phenotype of the mouse models. Independently of strain differences each mouse model could be separated from its control strain. Numerous further examples of the application of metabolomics in this manner exist across a diverse range of species and include discrimination between different species of *Ephedra*[44], use of DI-MS to determine different species of fungal strains[45] and selection of pathogenic and non-pathogenic species of *Bacillus cereus* isolated from meningitis patients[46].

The potential for developing metabolomics within the pharmaceutical industry has also been realised, especially in preclinical compound toxicology screening; these screens generate thoroughly definable end-points that are usually monitored over a relatively short period of time, providing robust candidates for metabolomic analysis which can associate metabolites with the distinct end-points. Toxicological studies conducted in this manner have implicated phenyl-acetyl glycine as a candidate biomarker for drug induced phospholipidosis[47], 2-aminoadipate as a mechanism associated biomarker for hydrazine induced neurotoxicity[48] and urinary D-β-hydroxybutyrate or trimethylamine and dimethylamine as region specific markers of nephrotoxicity in the proximal tubules and renal papilla respectively[49, 50]. One of the most significant studies in the area of drug toxicity was the COMET project which aimed to construct databases of drug toxicity using approximately 100,000 ^{1}H-NMR spectra of biofluids from animals treated with model toxins[51]. The COMET project has since been expanded to include COMET II which aims to elucidate the biological mechanisms behind drug toxicity with a combination of omics techniques.

1.1.5 Integrated Omics

The integration of genomics, transcriptomics, proteomics and metabolomics is a key goal of systems biology. The potential benefit for integrating the omics has been realised in the fields of disease research, where for some conditions conventional approaches have been inconclusive, and population, nutrition and toxicogenomic studies, where integration allows connections between environmental factors (for example diet), exposure to toxic compounds and environmentally induced diseases to be drawn. The

potential to use an integrated methodology to identify genes whose functions are as yet unknown remains a tempting research approach. However, reaching definitive conclusions from integrated omics approaches can be challenging; the generation of multiple metabolites from a single gene set can result from translational control of mRNA, transcriptional and translational processes that produce isoenzymes, or poor enzyme specificity and lead to confounding results.

In the area of disease research a combined transcriptomic and metabolomic approach has been used to investigate fatty liver disease induced by orotic acid in Kyoto rats, identifying uridine metabolism, choline turnover and the stearoyl-CoA desaturase as key to disease progression[52]. Integration of transcriptomics, proteomics and metabolomics has been employed to investigate the ApoE*3-Leiden transgenic mouse[53]. The mouse model over expresses the human ApoE protein that is involved in the transport of fats in blood plasma, preventing the clearance of lipid from the blood, resulting in the development of atherosclerotic plaques by 25 weeks of age. LC-MS analysis identified perturbation of lipid metabolism characterised by a decrease in plasma lysophosphocholine and increase in Triacylglycerols (TAGs) occurring pre-symptomatically at 9 weeks in the ApoE mouse. Transcriptomics, proteomics and metabolomic analyses were then applied to the liver tissue from the ApoE mouse; a total of 21,000 components were measured using the three approaches and facilitated the development of correlation networks to highlight perturbed metabolic pathways. The identification of new mechanisms in cardiovascular disease is being realised by exploitation of the complementarities of the omic techniques. Metabolomics and proteomics in combination have been employed to characterise atrial tissue that predispose patients to the development of atrial fibrillation[54]. In addition there is the hope that future genome-wide association studies will identify genomic sequence variants precipitating the further integration of the omics. At the forefront several loci have already been identified, which are associated with early-onset myocardial infarction[55, 56, 57].

An example of the integration of omics techniques in a toxicological study is provided by research conducted by Coen *et al* which examined acetaminophen induced hepatotoxicity in the mouse using transcriptomics and metabolomics[58]. The results from both the transcriptomics and metabolomics indicated increases in glycolytic flux, highlighting the complementarities of the omics for the use in the evaluation of drug safety.

1.2 Analytical Techniques

To verify changes in low molecular weight metabolites from complex biological samples, analytical methods which are sensitive to a range of sample components, well resolved, robust, relatively cheap on a per sample basis, suitable for application and offer high throughput capabilities are required. Recent and rapid developments in the areas of NMR spectroscopy, mass spectrometry and chromatography have lead to significant advances within the fields of metabolomics and lipidomics. As a result an extensive range of profiling technologies is now available and their applications have proven to be diverse.

Metabolomic analysis is most commonly performed using ^{1}H-NMR spectroscopy and mass spectrometry, often coupled to a prior chromatographic technique, most commonly liquid or gas chromatography. However other analytical techniques such as Fourier transform infrared spectroscopy[59], capillary electrophoresis[60] and high-performance liquid chromatography ultra violet detection[61] have been applied. Through a combined analytical approach utilising a range of technologies a more inclusive picture of the metabolome can be acquired by overcoming the limitations of individual techniques, although, due to the extensive variety and complex nature of metabolite species a fully comprehensive metabolomic map remains an unattained goal. It seems likely that to achieve this formidable objective will require a collective approach allying traditional biochemistry, metabolomic profiling and the swiftly evolving area of bioinformatics. The principles behind and effectiveness of the techniques used within this thesis will now be explored.

1.2.1 Mass Spectrometry in Metabolomics and Lipidomics

The field of metabolomics and lipidomics in particular has been strongly influenced by developments in mass spectrometry. Mass spectrometric analysis comprises three distinct events: analyte ionisation, mass dependent ion separation and ion detection. Ionic separation can be achieved by a variety of mass analysers including time-of-flight (TOF),

quadrupoles, magnetic and / or electric sectors, ion trap and Fourier transform ion cyncotron resonance[62]. The analysers vary in their dynamic range, resolution, suitability for tandem-MS (MS/MS) experiments and mass accuracy. The identification and separation of analytes by mass to charge ratio (*m/z*) can be improved with higher resolution and mass accuracy instruments. However, there is a correlation between the resolution of an instrument and its relative cost! To a degree, lower resolution and mass accuracy can be compensated for by MS/MS capability, and this has meant an extensive range of instruments are utilised in metabolomic studies.

The most common methods of analyte ionisation in metabolomic and lipidomic mass spectrometry are electrospray ionisation (ESI), electron impact (EI) ionisation and to a lesser extent matrix assisted laser desorption/ionisation (MALDI); the last of these has not been exploited in this thesis and will not be discussed further.

EI ionisation is used almost exclusively in combination with GC as it requires the analyte to be volatile. In EI high energy electrons bombard the volatile analyte causing analytes to fragment and generate a reproducible pattern of signals, which can be matched to spectral databases for the purpose of identification. GC-MS within the context of metabolomics and lipidomics will be discussed in greater detail later.

The late 1980s saw the development of the, so called, soft ionisation technique ESI[63], which allowed the mass spectrometric detection of non volatile and high mass analytes, such as peptides, proteins or intact lipids. The principal advantages of the soft ionisation techniques are that they do not require chemical derivatisation, although derivatisation can be used to enhance or enable ionisation[64], and they minimise analyte fragmentation, which can assist in the analytical interpretation of complex mixtures.

Briefly, ESI elutes the analyte by spraying it through a highly charged needle tip. The charged analyte spray droplets are heated, evaporating the solvent and resulting in ionisation and entry of analyte ions into the mass separation unit[65]. ESI is by far the most commonly applied ionisation technique in lipidomics, partially due to the ease of

coupling the eluent of an analytical LC experiment to the mass spectrometer. The use of ESI, in metabolomics, to analyse polar aqueous soluble metabolites has lagged behind that of lipid analysis, although it has been employed extensively in drug pharmacokinetic analysis[66]. However the analysis of polar metabolites by LC-MS in metabolomics is now experiencing a rapid period of growth[67,68]. DI-MS, LC-MS and ESI are explored more extensively in **sections 1.2.2** and **1.2.3** of this thesis.

1.2.2 Electrospray Ionisation and Direct Infusion-Mass Spectrometry in Lipidomics

The development of the ESI and closely related nano-spray technique in the 1980s resulted from pioneering work, conducted in the laboratory of John Fenn, producing a novel atmospheric pressure interface for the coupling of a liquid chromatograph and a mass spectrometer[69]. The ESI source functions as an electrochemical cell, generating gas-phase ions. Analytes are typically dissolved in a polar or volatile solvent and pumped into a fine capillary with a diameter ranging from 75-150 μm with a flow rate ranging from 1 μl min^{-1} to 1 ml min^{-1} [70]. A voltage, generally in the region of 1-4 kV depending on the elution solvent (typically 2-3 kV for methanol/acetonitrile and 4 kV for water), is applied to the capillary tip and results in a charge migration of species in solution to the capillary/solution interface producing an electric double layer; a novel adaptation meaning in ESI the pre-organisation of charges occurs in solution[71].

A Taylor cone is produced when the electrostatic forces on the preformed ions in the electric double layer of the capillary counterbalance the surface tension. The Taylor cone is destabilised by the increase in voltage resulting in the sample emerging from the capillary being dispersed as a fine spray of charged droplets; this process is enhanced by the co-axial nebulising gas, frequently nitrogen, which flows around the capillary. Solvent evaporation then reduces the size of the charged droplet causing an increase in the concentration of charge on the droplet surface up to the Rayleigh limit[72]; at this point "Coulombic explosion" occurs as the Coulombic repulsion surmounts the surface tension of the droplet and the droplet explodes forming smaller droplets of lesser charge. Solvent

evaporation and Coulombic explosion continues eventually forming individually charged solvent free analyte ions, creating the spray of charged species (**Figure 1.2**).

There are two competing theories as to how gaseous ions are formed in ESI during droplet desolvation[73]. The charge residual model states that successive droplet fissions occur until individual ions are formed in the gas phase. The second model, known as the ion evaporation model, proposes that ions are expelled from droplets to the gas phase prior to total droplet fissions.

The spray of the charged analyte species can be introduced into a sampling cone, then into an intermediate sampling vacuum before entering the mass analyser of the mass spectrometer, which is maintained under high vacuum, where they are analysed for *m/z*. The charges are distributed along charge sites on the analyte, under certain conditions, resulting in the formation of multiply charged ions.

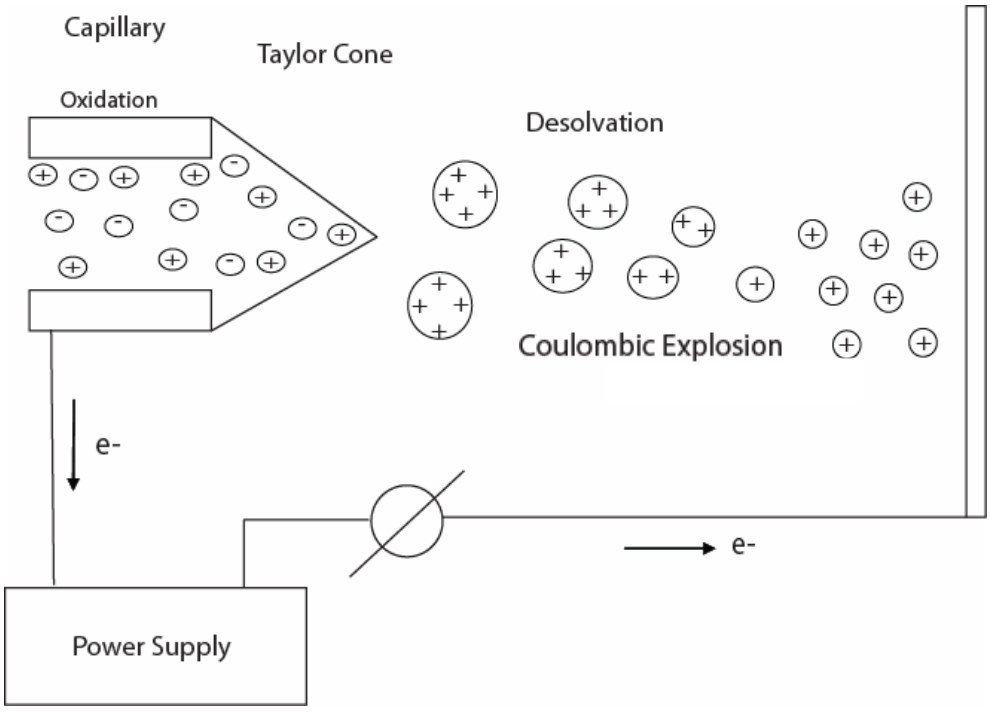

Figure 1.2: Gas phase ion formation by ESI.

ESI has been used effectively in DI-MS, in which the analyte mixture is directly infused into the mass spectrometer. Direct infusion ESI has also been dubbed "shotgun" in reference to the more frequently known shotgun proteomics[74].

The attention of the reader is also drawn to the capabilities of the different ionisation modes to measure varying lipid species. In negative mode there is a preference for anionic lipid species to ionise. After addition of lithium hydroxide, ammonium acetate or formic acid, negative ion mode can detect the weak anionic lipids and positive mode detects the neutral and polar lipids.

Direct infusion lipidomics has facilitated identification and relative quantification of over 450 phospholipids from mammalian cells[75]. By means of a triple quadrupole mass spectrometer, Milne *et al*, were able to measure four major lipid classes in positive mode and 7 in negative ion mode in directly infused lipid extract from approximately $3x10^6$ WEHI-231 cells[75].

Mass spectrometry provides significant analyte separation, is highly sensitive[76] and extremely versatile. As a consequence it is utilised in a range of experiments. The mass spectrum of a mixture may be used in metabolic “fingerprinting” experiments. Fingerprinting is so called as it necessitates a rapid biochemical ‘fingerprint’ of a sample without the time consuming process of metabolite identification[11]. Koulman *et al* exploited whole spectra from raw plant metabolite extractions as fingerprints before carrying out further experiments to identify the signals with MS/MS in a high throughput manner[77]. MS/MS isolates individual *m/z* species for fragmentation. In a process known as collision induced dissociation (CID), the molecular ions are accelerated by an electrical potential increasing their kinetic energy. The ions then collide with neutral gas molecules such as helium or nitrogen within a collision cell in the mass spectrometer. As the molecules collide the kinetic energy is converted into internal energy, resulting in the breakage of chemical bonds and the fragmentation of the molecular ion. The fragments are then separated by *m/z* in a second mass analyser. The *m/z* values of the fragments aid the identification of the isolated ions. For instance, phospholipid headgroups often give

characteristic fragment signals either in the form of a neutral loss or a characteristic signal at a specific *m/z* value[74]. The speed, relative robustness and potential for automation of this technique have been extensively exploited.

As mentioned previously there is an array of mass analysers engaged in metabolomic and lipidomic analysis. The DI-MS investigation conducted in this study utilised a quadrupole linear ion trap mass spectrometer. The Thermo Finnigan linear ion trap mass spectrometer employed in investigations conducted in this study consists of an ion beam generated at an ESI source, directed through a heated capillary and focused through two successive rod arrays. Entry into the ion trap is gated by a lens which pulses from positive to negative voltages to repel and attract the ions into the aperture leading to the ion trap. The allowed entry time of ions into the ion trap maximises signal whilst reducing the unwanted space-charge effects which would result from an excessive quantity of ions entering the trap. Three hyperbolic quadrupole rod arrays constitute the ion trap itself; ions are restrained radially by a two-dimensional radio frequency trapping field in the centre section of the ion trap. Axial confinement is by direct current potentials applied to the front and rear end electrodes. The ion trap is filled with helium to a pressure of ~1 mtorr, as collisions with helium reduce the kinetic energy of the ions, in a process known as kinetic cooling, and contract the trajectories of molecular ions to the centre of the trap. The ion trap functions as a mass spectrometer when the field within the device is altered, by dipole excitation generated with auxiliary alternating current voltages on the X-rods, destabilising the trajectories of concurrently trapped ions of successive *m/z* ratio; consequentially the ions leave the trapping field in order of their *m/z* ratio[78]. On leaving the ion trap the ions strike a detector, typically a conversion diode and electron multiplier (**Figure 1.3**).

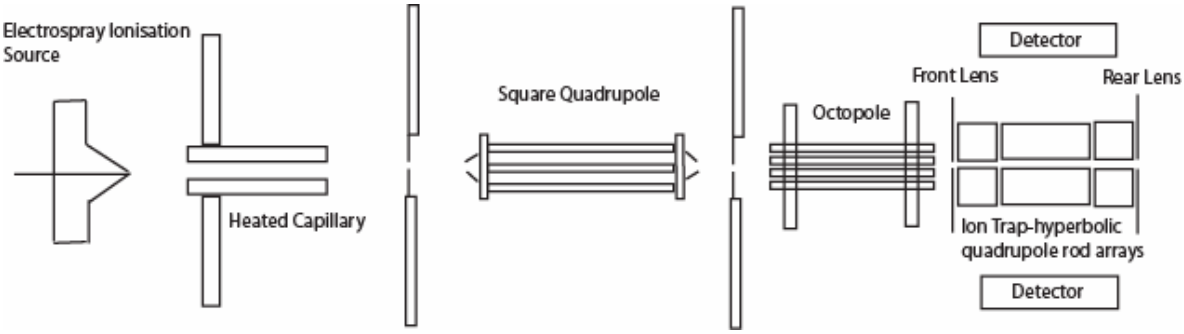

Figure 1.3: Schematic diagram of the Thermo Finnigan Linear Ion Trap Mass Spectrometer. Ions pass through the instrument from left to right.

The MS/MS function of the quadrupole linear ion trap operates in a pulsed mode and so mass selected ions can be accumulated over time. Fragment ions arising from 90% of isolated ions can be confined using the ion trap and as a consequence several mass-selective operations can be performed; ion traps are capable of performing MS/MS to the *n*th degree[79].

ESI can suffer from a number of disadvantages. The most prominent being strong ion suppression effects when analysing complex molecular mixtures[80]. Ion suppression is generated by analytes competing for charge during the ionisation process, with an individual analytes' ionisation efficiencies based on their chemical characteristics[81]. Therefore, the observed ion count for a particular ion can change, depending on what other analytes or contaminants are being co-ionised. The problem is compounded in that ion suppression can occur even when the interfering compound is not seen in the mass spectrum. Thus, measurement must assume the mixtures are roughly the same between the groups of samples analysed. The drawback may be circumvented, to a degree, by separating the analytes via one or more chromatographic techniques prior to mass spectrometric analysis[82].

1.2.3 Liquid Chromatography-Mass Spectrometry

It was previously mentioned that a number of metabolomic and lipidomic studies have utilised DI-MS, introducing a sample directly into an ESI source[83, 84, 85, 86]. However the

ion suppression phenomenon caused by certain metabolites including prominent phospholipids, especially when using positive ionisation, can affect both low and high concentration analytes[87]. Detrimental ionisation properties can be minimised with an initial, either offline or online, high performance liquid chromatography (HPLC) separation. The use of HPLC for lipid analysis is a well established approach; normal phase chromatography in the separation of lipid classes, particularly phospholipids, is well documented, though HPLC was originally, and often still is, coupled to either evaporative light scattering detection[88, 89] or ultra-violet detection[90]. These detectors are susceptible to serious constraints in lack of selectivity and the choice of mobile phase[91]. As a consequence, metabolomic and lipidomic applications of HPLC often interface the liquid chromatograph to an ESI-MS detector[92].

LC-MS is suitable for the analysis of thermally labile, polar or high molecular mass compounds but is disposed to certain constraints with respect to these; the temperatures used in ESI may be limiting when analysing particularly labile compounds and due to the intrinsic nature of ESI there must be a degree of innate polarity in analyte molecules. To aid the subsequent ionisation of analytes ammonium acetate can be added to the mobile phase to produce ammonium adducts. In addition the volatile organic acid, formic acid can be included in the mobile phase to improve ionisation of analytes from the eluent in mass spectrometric investigation.

The sample is injected onto a LC column which consists of a narrow tube packed with chemically modified silica. Separation of analytes occurs due to their interaction with the stationary phase (the column packing) and the mobile phase (the solvent passing through the column). There is an extensive range of column chemistries available including partition, normal phase, ion exchange, size exclusion, displacement and reversed phase chromatography and their ability to separate chemical classes of analyte varies. LC-MS conducted in the course of this thesis has extensively employed reversed phase chromatography (RPC).

RPC column chemistry exploits a non-polar stationary phase and a moderately polar, aqueous mobile phase. The stationary phase utilised in the LC-MS investigations detailed in this thesis is a silica based surface which was subsequently treated with $C_8H_{17}Me_2SiCl$. RPC relies on the principles of electrostatic and hydrophobic forces. The column chemistry functions in such a way that the binding of analytes to the stationary phase relies on the contact surface area around the non-polar segment of the analyte molecule with the chemistry of the stationary phase within the aqueous eluent and is described by the solvophobic theory. Retention of molecules by the stationary phase can be decreased by reducing the polarity of the mobile phase solvent and so lessening the water surface tension. Elution of analytes from the column is brought about by reducing the polarity and surface tension of the mobile phase over a gradient. Therefore, in reversed phase analysis the retention time for larger non polar molecules is longer when compared to polar molecules[93, 36]. The use of columns with sub-2 μm particle size along with elevated column temperature or temperature gradients is favoured for higher resolutions and faster separations[94]. It is worthy of note that the elevated column temperature is necessary; as flow rates increase with smaller column packing particles, resolution is improved but the pressure is increased due to the reduced particle size; by increasing the temperature the effective pressure is reduced.

Following chromatographic separation the analytes are then introduced into a mass spectrometer via an ionisation interface, the most common of which is Atmospheric Pressure Ionisation (API), which includes ESI and Atmospheric Pressure Chemical Ionisation. The LC-MS analysis conducted in this study was performed using ESI and a quadrupole-time-of-flight (QToF) mass spectrometer. The ESI interface introduces the ions generated to a radio frequency quadrupole lens which functions as an ion guide and collisional dampening cell. The ions are then accelerated into the second mass analyser quadrupole, which for single mass spectrometry functions to transmit the ions through the machine. A quadrupole is formed of four parallel metal rods. One set of opposing rods have the applied potential $(U+V\cos(\varpi t))$. The other pair of rods have the potential $-(U+V\cos(\varpi t))$. U is a direct current voltage and $V\cos(\varpi t)$ an alternating current voltage. Voltages applied to the rods are used to control the course of ions as they move along the

ion flight path at the centre of the four rods. By altering the voltages ions of a particular *m/z* are allowed through the quadrupole filter (**Figure 1.4**).

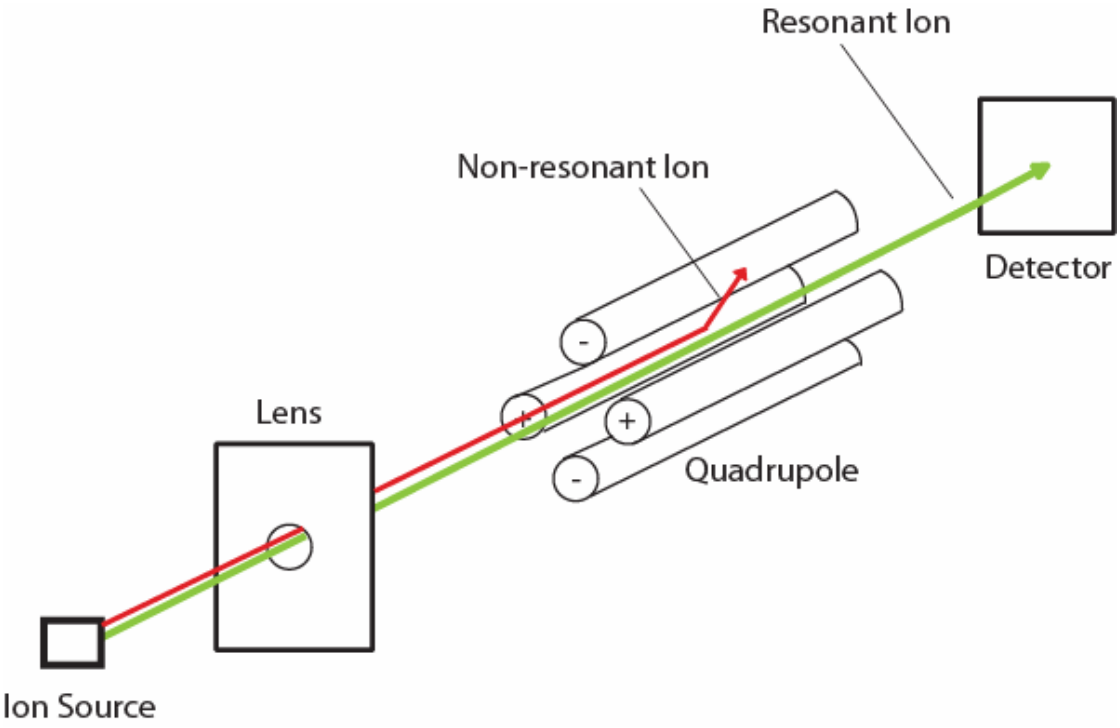

Figure 1.4: Schematic Diagram of a Quadrupole Mass Analyser. Ionisation occurs at the source. Ions are then accelerated and focussed by a lens into the quadrupole. Opposing rods have the same applied potential. Voltages applied to the rods are used to control the course of ions as they move along the ion flight path at the centre of the four rods. The green arrow represents the flight path of a resonant ion. The red arrow is the flight path of a non-resonant ion.

However, in MS/MS mode, the quadrupole functions as a mass filter transmitting the ion of interest. The ions are accelerated into a hexapole collision cell, operated in radio-frequency only mode when performing single mass spectrometry. When performing MS/MS the ion of interest is accelerated before it enters the collision hexapole, where the ion is subjected to CID. In both single mass spectrometry and MS/MS mode the ions are reaccelerated as they leave the collision cell and focused using ion optics into the ion modulator of the TOF analyser. A pulsed electric field pushes ions into the accelerating column from here the ions enter the field free space. A reflectron is then employed to correct the kinetic energy distribution of the ions. A constant electrostatic field reflects

the ion beam towards the detector. The greater the kinetic energy of an ion the deeper it penetrates the reflectrons electrostatic field and therefore the longer its flight path to the detector; in this way the energy distribution of ions with the same *m/z* is corrected resulting in the simultaneous arrival of ions of identical *m/z* at the detector, referred to as time-of-flight focus. Ions are detected with two microchannel plates and mass spectra are recorded with a time-to-digital converter[95]. (**Figure 1.5**).

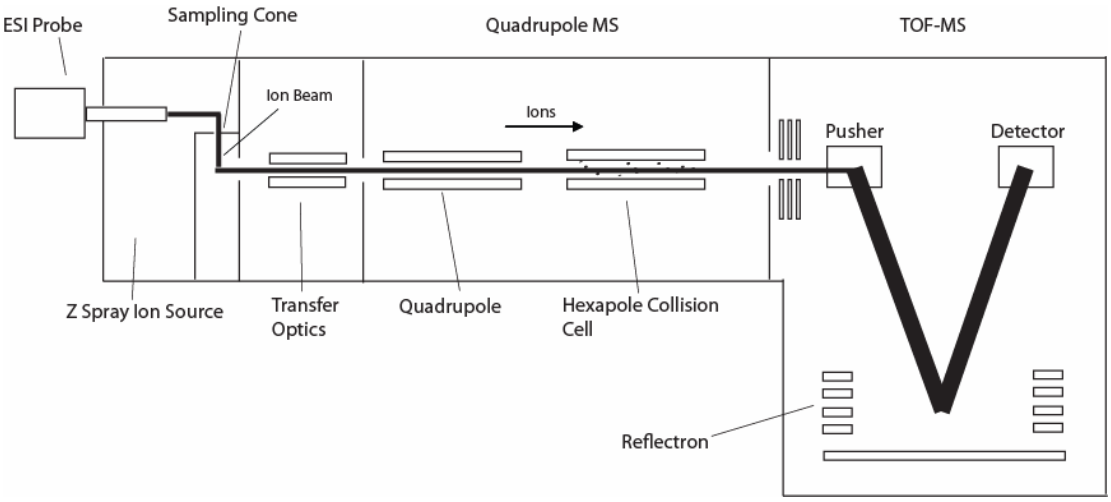

Figure 1.5: Schematic Diagram of the Micromass QToF Ultima Mass Spectrometer operating in V-mode. When the mass spectrometer is operated in W-mode higher resolution is achieved but as a consequence there is a decrease in sensitivity due to ion loss.

LC-MS has many advantages as a technique for metabolomic analysis; it is a relatively high throughput method that combines a good dynamic range with the potential for metabolite identification from the spectral data. LC-MS can also be very sensitive with good mass accuracy and resolution[96].

Libraries to assist in sample identification for LC-MS lipidomic and metabolomic data are limited, partly because ESI-MS is affected by the instrument type, ion source, ion source potentials, mobile phases and other factors affecting fragmentation patterns[97]. However, a number of resources are available. These provide pertinent reference material and structural information of MS/MS fragmentation. Examples of these include

LIPID MAPS (www.lipidmaps.org[98]), The Lipid Library (http://www.lipidlibrary.co.uk/), Cyber Lipid Center (http://www.cyberlipid.org/), LIPIDAT (http://www.lipidat.ul.ie/,[99]) and LipidBank (http://lipidbank.jp/).

1.2.4 Gas Chromatography-Mass Spectrometry

Gas-chromatography was first proposed in a 1941 paper by Martin and Synge in which it was suggested that the mobile phase in a liquid-liquid chromatography system could be replaced with a vapour[100]. Following advances in technology, it became possible to couple the chromatographic technique to mass spectrometry. During the 1950s Gohlke and McLafferty united a gas chromatograph to a TOF mass spectrometer founding the technique of GC-MS[101]. GC-MS has since become a key research technique in a vast array of fields and is a core tool in lipid biochemistry, lipidomics and metabolomics.

Since GC-MS requires the analytes to be volatile and thermally stable, derivatisation is used to reduce unwanted absorption effects, increase the volatility of polar compounds, remove polar functional groups or generate derivatives as an aid to identification. The derivatisation of aqueous soluble metabolites has been conducted using a variety of methods; however a two step protocol using methoxylamine hydrochloride followed by *N*-methyl-*N*-(trimethylsilyl)-trifluoroacetamide (MSTFA) is most commonly used in metabolomic analysis[102]. The initial methoxymation converts the keto group of monosaccharides to an oxime; limiting the monosaccharide to the *syn* and *anti* isomer reduces the tautomeric forms of monosaccharides from 5 to 2 and therefore reduces the complexity of a chromatogram and also improves subsequent derivatisation. The subsequent silylation reaction using MSTFA diminishes the intrinsic dipole-dipole interactions of the analyte molecules by substituting the active hydrogens in hydroxyl (OH), amine (NH) and thiol (SH) groups with a silyl; thereby increasing the volatility of the metabolites. (**Figure 1.6**).

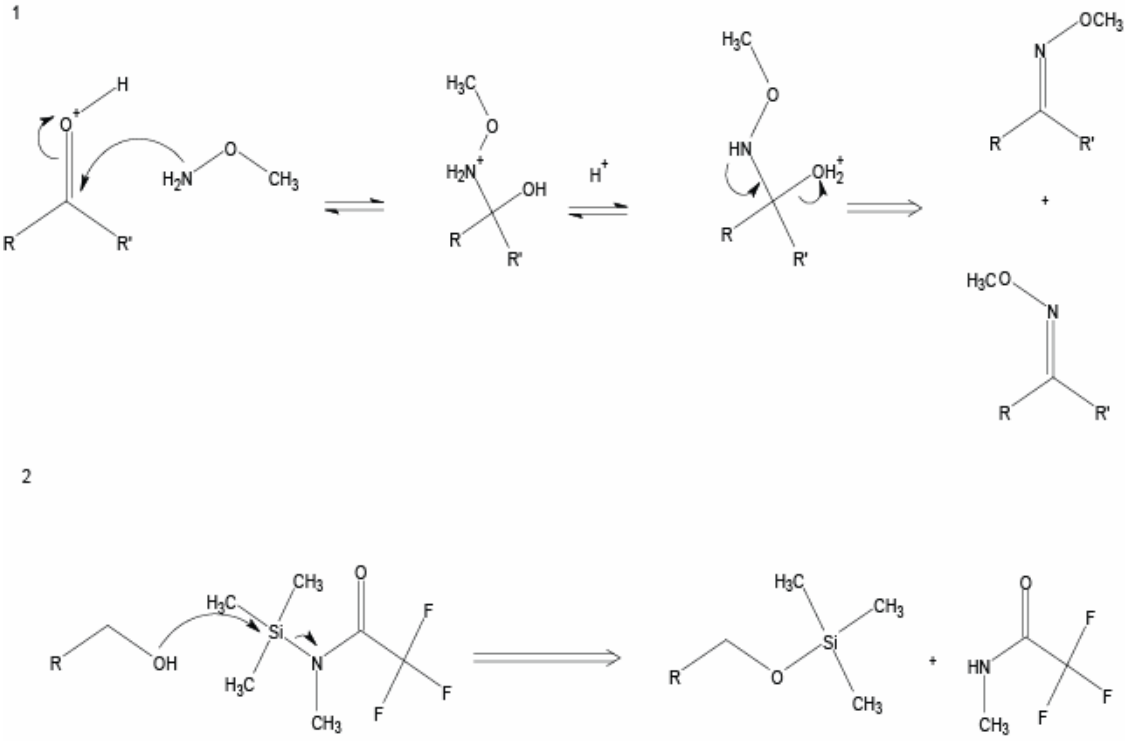

Figure 1.6: The reaction mechanisms for the derivatisation of aqueous phase metabolites. **1.** Methoxymation of keto groups from monosaccharides. **2.** Silylation of hydroxyls.

The most frequent derivatisation of fatty acids is hydrolysis of complex lipids, to release esterified fatty acids, followed by the methylation of the fatty acids to form fatty acid methyl esters (FAMEs). A range of methods have been described in the literature to perform methylation of fatty acids[103, 104]; research conducted in this thesis exploited acidic esterification using boron trifluoride and methanol. Methylation increases the volatility of the fatty acids whilst masking their polar functional carboxyl group (**Figure 1.7**).

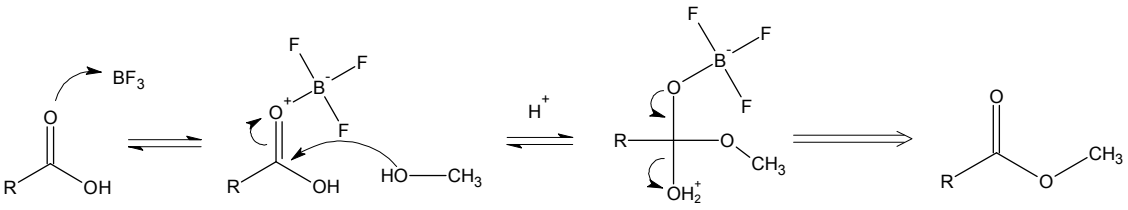

Figure 1.7: The reaction mechanism for the methyl esterification of fatty acids.

The analyte mixture is injected, vaporised and introduced onto the GC column by a carrier gas. The carrier gas, which functions as the mobile phase, pushes the sample through the heated column. As different compounds dissolve to varying degrees in the stationary phase, a polymer layer bound to an inert solid (commonly a silicone liquid), they move through the column at differing rates which are dependent on the partition of the compounds between the stationary phase and the mobile carrier gas. As separation is partially reliant on volatility, a programmed temperature gradient is applied. The separation of compounds within the sample is dependent on carrier gas flow rate, column dimensions, stationary phase type, analyte chemistry and the temperature of the column.

A key aspect of metabolomics and lipidomics is the ability to identify the metabolites once they have been detected. The stationary phase of the GC column selected for analysis has a significant impact on the identification process. For example non polar silicone phases separate fatty acid methyl esters based almost exclusively on molecular weight, whereas using high molecular weight hydrocarbons allow for separation of saturated and unsaturated components of the same chain length. The use of polar polyester columns also permits the separation of esters of the same chain length to the extent that, using highly polar cyanoalkylpolysiloxane phases gives excellent discrimination of cis and trans isomers of monounsaturated fatty acids, albeit requiring relatively long chromatography times. Given suitable chromatographic separation provisional identifications can be made using a comparison of the analyte retention times with those of commercially available standard mixtures. However, these identifications must only be viewed as tentative and highlight the benefit of a combined chromatographic-spectrometric technique.

In GC-MS analysis, the end of the GC column is interfaced with the mass spectrometer by passing the column through a heated transfer line to the ion source where the eluting compounds are ionised. EI ionisation is most commonly used in GC-MS experimentation to ionise the analyte molecules (**Figure 1.8**). The analyte is subjected to an energetic beam of electrons generated by a filament, which causes the analyte to lose an electron and a radical cation to be produced. Ionised analytes can fragment as a relaxation

pathway removing the excess internal energy gained through ionisation and producing further smaller ions. Fragmentation provides structural information in the form of a "finger print" which can then be used for identification[62]. As a consequence of the amount of energy absorbed by the analytes and the low stability of the radical gas phase ions, fragmentation of analytes is extremely reproducible. The ionisation energy typically used is 70 eV allowing standardisation of fragmentation libraries. There are a number of commercially available databases, for example the National Institute of Standards and Technology (NIST)/ Environmental Protection Agency (EPA)/ National Institutes of Health (NIH) mass spectral library**,** designed to aid the identification of metabolites from GC-MS analysis and are therefore well suited to metabolomic investigation.

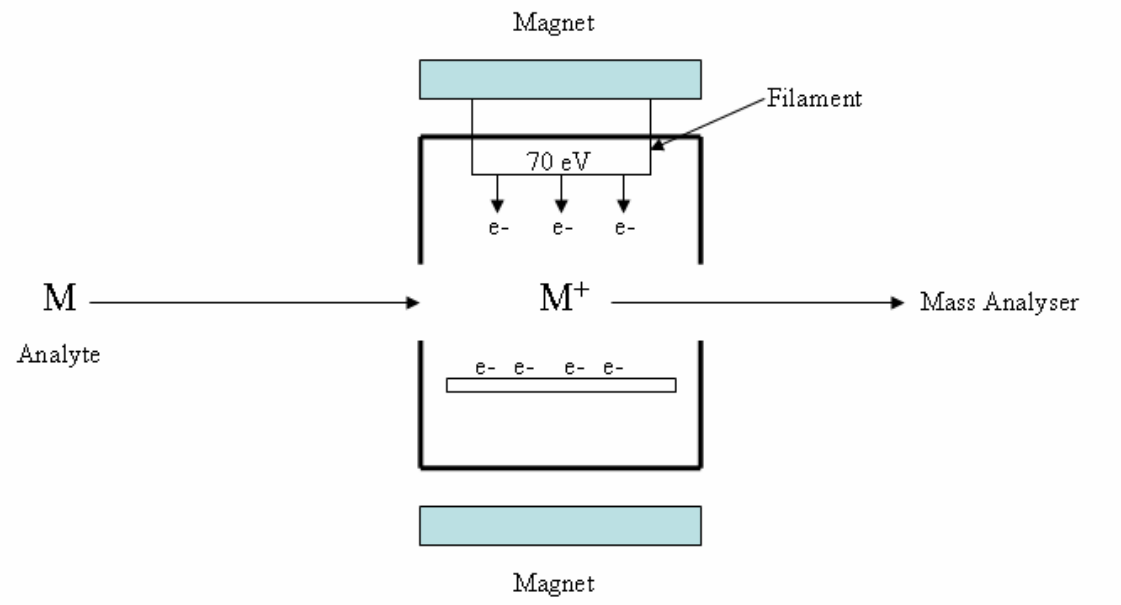

Figure 1.8: Schematic of Electron Impact Ionisation.

The ions generated by EI are then repelled out of the ionisation chamber with a small positive charge. The ions enter a mass analyser which functions to separate the ions based on their *m/z*. Quadrupole mass analysers are the most commonly used and have been discussed previously. Mass spectra are generated by examining the ions progressing through the quadrupole whilst the applied voltages are adjusted. Once filtered, the ions

enter the detector where the electrical impulses are amplified and sent to a computer where the signal is converted into a visual display.

GC-MS is a robust system that is highly sensitive and provides good resolution. Nevertheless, the technique is limited by its *m/z* range, preventing the analysis of larger metabolite species. The technique also requires that compounds be thermally stable with high enough vapour pressure to volatilise during injection. Chemical derivatisation for GC-MS has been used to overcome this problem but in itself can introduce variability to the samples and can mask metabolite structural information. Chemical derivatisation also increases sample preparation and when combined with an extensive chromatographic run (as is often required in metabolomics to separate the variety of chemical classes of metabolites) reduces the throughput of GC-MS as an analytical technique. The multiple procedures required prior to GC-MS analysis also increase the risk of contamination and recovery losses. However by using GC-MS in combination with other analytical techniques not only are these restrictions surmounted but the coverage of the metabolome can be significantly increased.

1.2.5 ^{1}H-Nuclear Magnetic Resonance Spectroscopy

Analysis of biofluids and tissue extracts using ^{1}H-NMR spectroscopy is a well established technique that has diversified within the field of metabolomics[105, 106]. The popularity of the technique arises partly from its application in the determination of the structures of small organic molecules allowing the identification of metabolites from biological samples, but also from its low cost per sample basis and, due to its spectroscopic, quantitative, robust and reproducible nature. The technique is also non-destructive allowing multiple analyses of samples. The use of high-resolution NMR spectroscopy with field strengths greater than 9.4 Tesla are utilised to overcome some of the disadvantages of NMR due to low sensitivity and small chemical shift range for ^{1}H-NMR spectra. The analysis of mouse tissue metabolite extracts using ^{1}H-NMR typically detects 20-40 metabolites; when applied to urine the number of metabolites observed reaches 100-200[107]. Despite the relatively low coverage of the metabolome ^{1}H-NMR

analysis can be highly discriminatory; this arises because metabolic pathways are connected by a small number of metabolite nodes, which are observed using ^{1}H-NMR analysis, whose concentrations are significant indicators of changes in the steady states of metabolic pathways[43]. Much of the criticism directed at metabolomic studies using NMR spectroscopy has not been concentrated on the analysis itself but on biological discrepancy. However, within rodent studies variables such as diet, sex, choice of vehicle and strain can be controlled and therefore limit sources of variations.

Nuclear magnetic resonance spectroscopy is reliant on magnetic nuclei having an intrinsic angular momentum called spin. Nuclei with non-zero spin are detectable by NMR; these include ^{1}H, ^{13}C and ^{31}P. The magnitude of spin angular momentum is defined by the equation: $[I(I+1)]^{1/2}\ \hbar$, where I is the spin quantum number of a nucleus. The nuclear spin quantum number of ^{1}H is ½. The spin angular momentum $\boldsymbol{I}$ is a vector that in a spin-I nucleus has $2I+1$ projections onto an axis, this allows the quantisation of a particular axis component of $\boldsymbol{I}$, known as $I_{x,y\ or\ z}$ depending on the axis. Therefore $I_{x,y\ or\ z} = m\ \hbar$ where the term m is the magnetic quantum number which has $2I+1$ values at integral steps from $+I$ to $-I$. These parameters mean that for the ^{1}H nucleus, which has $I=½$, the angular momentum has two allowed directions, $I_{x,y\ or\ z} = \pm ½\ \hbar$ (**Figure 1.9)**.

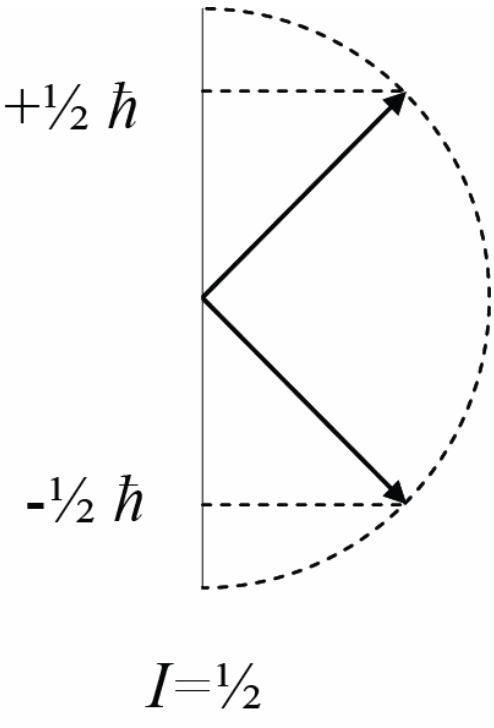

Figure 1.9: Space quantisation of spin-½ nuclei.

2*I*+1 orientations of a spin-*I* nucleus have the same energy until a magnetic field is applied. The energy of the nucleus is altered by an amount proportional to the strength of the magnetic field **B**, the gyromagnetic ratio and the axis component of the angular momentum. Therefore the 2*I*+1 states for spin-*I* nuclei are spaced with an energy gap $\hbar\gamma B$. Since for NMR $\Delta m=\pm 1$ transitions occur between adjacent energy levels and therefore $\Delta E=h\nu=\hbar\gamma B$ (**Figure 1.10**). If electromagnetic radiation is applied at frequency ν the nuclei will move from the lower energy state to that of the higher energy state; this frequency is the Larmor frequency.

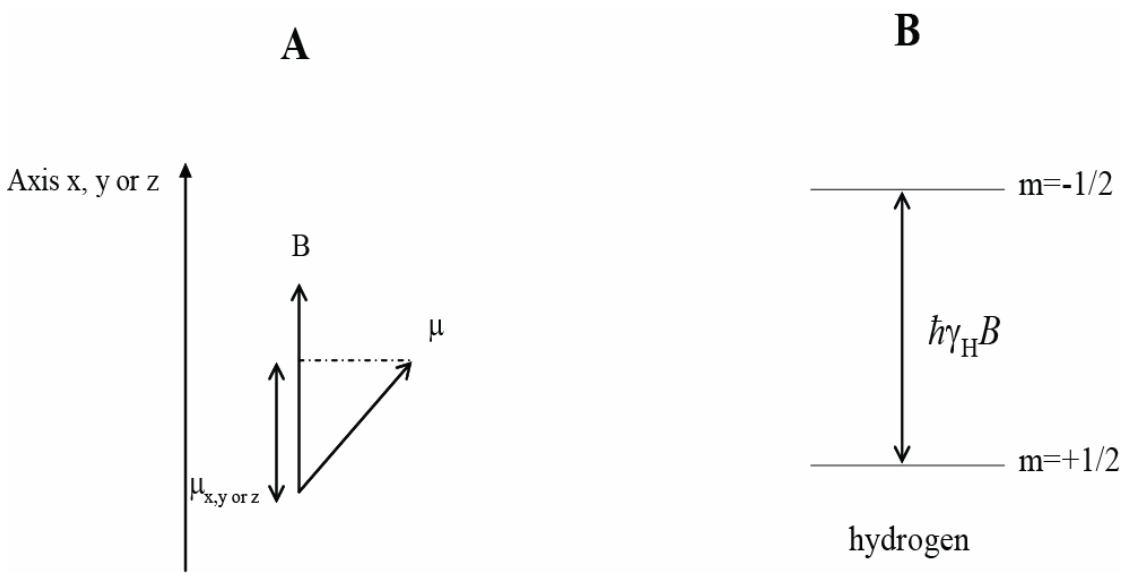

Figure 1.10: **A.** The interaction between the magnetic field *B*, the nuclear magnetic moment μ and the projection of μ onto *B*, $\mu_{x,\ y\ or\ z}$. **B.** Energy level for ^{1}H nuclei in a magnetic field.

In a magnetic field, magnetic nuclei are separated between the $2I+1$ energy levels according to the Boltzmann distribution with the ratio of the two levels given by $n_{upper}/n_{lower}=e^{-\Delta E/kT}$ (where k is the Boltzmann's constant) which is comparable to the thermal energy of the system at room temperature. However, NMR signals are weak, with the intensity of the transition depending on the difference in the populations of the energy levels which are very small. The population differences are often ≤0.001%, explaining the relative insensitivity of ^{1}H-NMR. By using stronger field strengths ΔE can be maximised and the sensitivity of NMR spectroscopy increased. Regardless, the population difference between energy states is large enough to produce a net magnetic moment which aligns with the magnetic field.

When a radiofrequency pulse is applied along the x-axis of the magnetisation its rotation can be moved away from its equilibrium position rotating about the z-axis so it is aligned by 90º into the x,y plane. Short radiofrequency pulses, referred to as hard pulses, are large enough to excite a range of frequencies simultaneously, and therefore populations of all spin energy levels will be equalised. Populations of higher spin levels will then resonantly emit energy as they slowly decay to their equilibrium positions. The emission

of energy can be detected using a coil of wire that surrounds the sample and is mounted in the xy-plane; when the magnetisation precession intersects the wire it is detected as a current is induced. This is known as the free induction decay (FID) which is Fourier transformed from the time to the frequency domain producing a spectrum (**Figure 1.11**). The chemical shift and coupling identified within the spectrum are used to assign resonances.

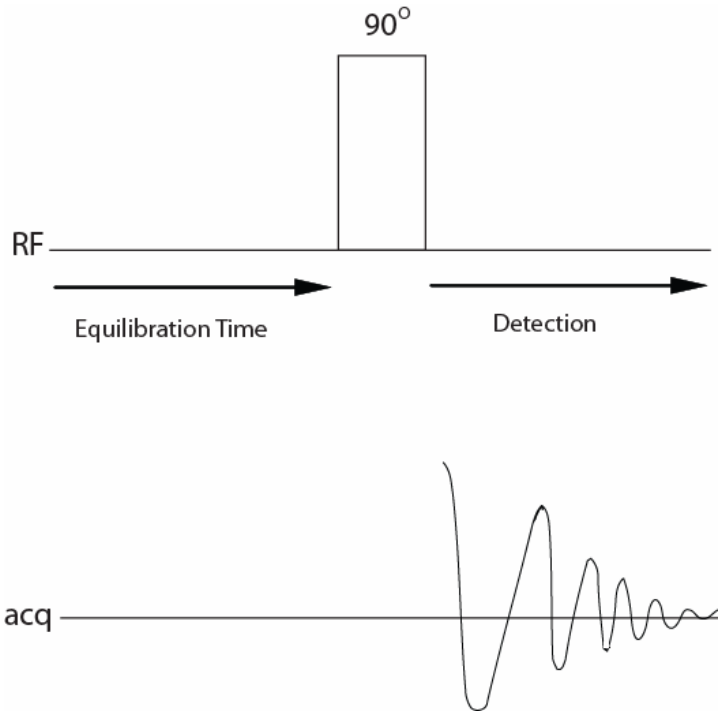

Figure 1.11: A simple pulse sequence for a pulse-aquire experiment. Post equilibration a 90º radiofrequency pulse is applied, rotating the magnetisation into the y-axis. The precession of the magnetisation generates the free induction decay signal.

The resonance frequency of nuclei is dependent upon the position of the nucleus in a molecule. This effect is known as the chemical shift and occurs because the external magnetic field causes electrons to circulate in their orbitals. This motion generates a small magnetic field *B'*, in the opposite direction to B_0 that shields the nucleus from the external field. The magnetic field experienced by the nucleus (B_N) is determined by the equation $B_N = B_0 (1-\sigma)$, σ being the shielding constant. For nuclei in molecules the motion of the electrons may induce fields that either augment or oppose the external field,

and so influence their resonant frequencies. The frequency is presented as a shift in parts per million (ppm) from a reference nucleus. Besides the chemical shift additional data from NMR spectra can be obtained from magnetic interactions between nuclei which generate extra peaks in the spectra providing information on the arrangement of the nuclei in an analyte, known as spin-spin coupling. Spin-spin coupling arises when non-symmetrically equivalent adjacent nuclei interact, splitting the corresponding NMR signal. The number of lines generated by a signal coupling is given by the equation $(2nI+1)$, where n is the equivalent nuclei and I is spin of these nuclei. The term J defines the difference between the components and is a measure of electronic overlap measured in Hz. J aids in the identification of compounds analysed by NMR since it provides information about the bonds linking nuclei.

1.2.6 Two-dimensional Heteronuclear Single-Quantum Coherence ^{13}C-Nuclear Magnetic Resonance Spectroscopy

Conventional one-dimensional NMR generates a spectrum which plots intensity against frequency; however two-dimensional NMR plots intensity against two frequency axes, meaning each peak in a two-dimensional spectrum has intensity and two frequency co-ordinates, aiding greatly the separation of different resonances. Two-dimensional NMR experiments start with a preparation period in which the equilibrium magnetisation is transformed into a coherence which evolves during the evolution period, t_1. The preparation period involves a 90º pulse generating a single-quantum coherence (transverse magnetisation). The evolution, t_1, is systematically incremented in a series of experiments. During the mixing period the coherence present at the end of t_1 is manipulated into an observable signal which is then recorded in the detection period, known as t_2. In the mixing period the magnetisation is transferred from one spin nuclei to another. In a two dimensional NMR experiment the FID is detected at regular time intervals in t_1 and t_2 generating a series of data points representing the time-domain function. Initially t_1 is set to 0, the pulse sequence is run and the FID detected and recorded as a function of t_2 (**Figure 1.12**). The process is then repeated for Δ_1 and then

$2\Delta_1$ and so on. Free inductions are generated for both t_1 and t_2 which are then Fourier transformed for both dimensions.

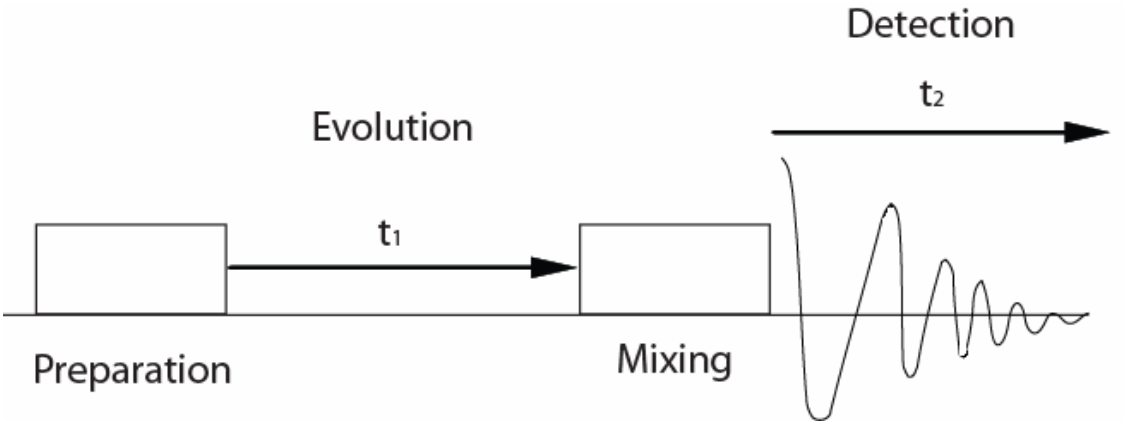

Figure 1.12: General scheme for two-dimensional NMR. The preparation and mixing periods can be a single radiofrequency pulse. Coherence generated during the preparation phase evolves for time t_1, the signal is detected during t_2.

In a Heteronuclear Single-Quantum Coherence (HSQC) experiment one frequency co-ordinate gives the ^{13}C chemical shift, whilst the second frequency co-ordinate is that of the attached proton, the observed nuclei in this case is the proton. Cross peaks in a heteronuclear correlation spectrum arise as a result of transfer through one bond heteronuclear coupling, identifying shifts of directly attached nuclei and aiding assignment (**Figure 1.13**). The HSQC pulse sequence functions by first transferring magnetisation from the proton to the ^{13}C nuclei making the approach more sensitive than NMR pulse sequences that detect ^{13}C resonances directly. The ^{13}C spin magnetisation evolves for t_1, acquiring a frequency label according to the offset of ^{13}C. Magnetisation is then transferred back to ^{1}H and observed. The spectra produced have peaks centred at the offset of the ^{13}C spin and at the offset of the ^{1}H spin.

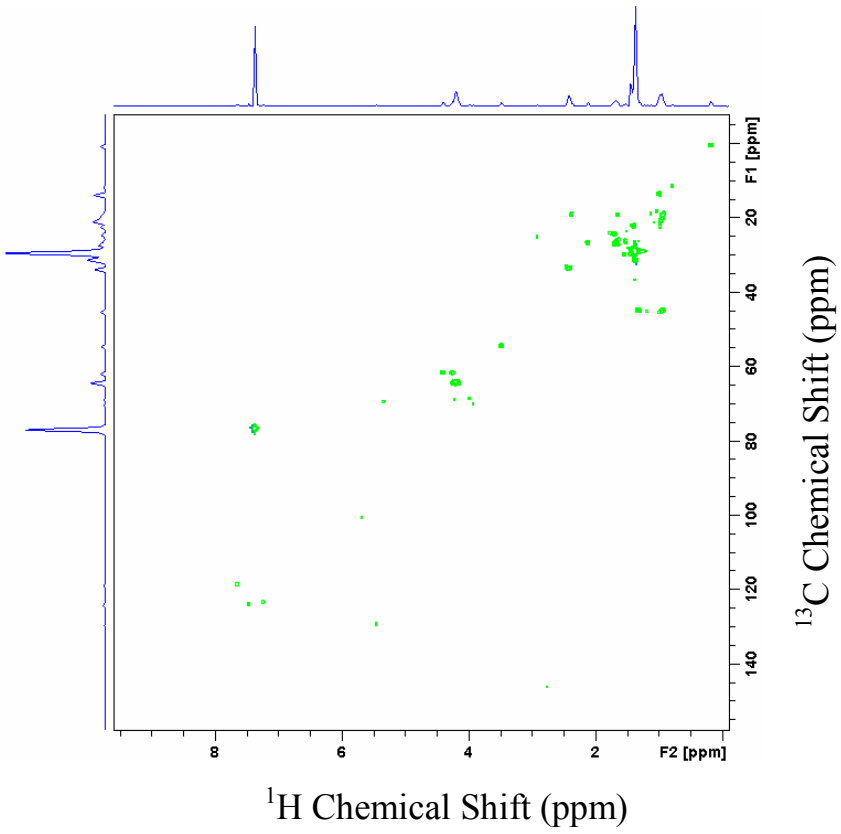

Figure 1.13: An example ^{1}H-^{13}C HSQC spectrum recorded at 500 MHz.

^{13}C NMR spectroscopy has been used extensively to measure concentrations of ^{13}C labelled metabolites and for mapping flux through metabolic pathways in biological systems both *in vitro* and *in vivo*. Pioneering research using ^{13}C NMR to track metabolic pathways using labelled substrates such as glucose tagged with the stable ^{13}C isotope was first conducted in the 1970s[108]; these experiments were initially performed in microorganisms and perfused organs and determined rates of metabolic pathways by measuring the label appearance in pathway products as a function of time[109]. The 1980s saw an expansion of the technique when it was first applied in animal models[110] and with in vivo NMR spectroscopy in humans[111]. ^{13}C labelled metabolite tracing studies provide a bridge between the distinct scientific approaches of reductionist molecular biochemistry and global systems biology, contributing to the elucidation of the mechanisms of metabolic regulation.

1.3 Multivariate Statistical Techniques

1.3.1 Multivariate Statistics in Metabolomics

As metabolomic analysis evolves the number of metabolites measured and the coverage of the metabolome will continue to increase. The result is the generation of extensive amounts of raw data, containing the concentrations of a large array of metabolites, which must be contained in intricate data tables. In order to mine these vast resources for statistically relevant variation in metabolism requires potent statistical techniques proficient in data reduction and simplification.

Multivariate statistics, and especially pattern recognition processes, examine the relationships between multiple variables simultaneously permitting visualisation of the prominent trends within complex data sets. In analysing large data sets, where the number of variables often exceeds the number of samples, especially when the variables are co-linear as is the case in metabolomic analysis, multivariate statistics becomes a superior tool to more traditional univariate analysis. Multivariate analysis has a number of advantages over univariate techniques in that it concurrently analyses all variables, taking into account their co-linear nature, it can manage with omitted data and is robust to noise[112]; overcoming the risk of generating ambiguous results from monitoring and assessing each variable independently as is the case in univariate statistics.

Multivariate statistical methods are commonly classed as either unsupervised or supervised. Methods such as PCA and hierarchical cluster analysis (HCA) are classified as unsupervised techniques as they do not assume a priori knowledge of classification in the data set and so examine intrinsic variation of the data set. Supervised methods include partial least squares (PLS), orthogonal signal correction (OSC) and PLS-DA; these statistical analyses exploit information on classification to distinguish the intrinsic variation from variation generated by class membership, optimising discrimination between classes[113]. Within a metabolomics setting, where the variance of interest may not essentially be the greatest variance in the dataset, the supervised techniques can be valuable in distinguishing particular biological queries; particular illustrative examples

include differentiating drug treatment doses or severity of disease. The principles behind multivariate statistical techniques used within this thesis are explored in further detail in **Chapter 2 Materials and Methods** (section 2.11 *Data Handling for Metabolomics*).

1.4 The Metabolic Syndrome

1.4.1 Regulation of Metabolism, Insulin Resistance and the Metabolic Syndrome

Insulin is the primary hormone regulator of intermediary metabolism in mammals, controlling the utilisation of fuels for storage or oxidation. Insulin exerts its influence over carbohydrate and lipid metabolism, as well as on protein and mineral metabolism. As a consequence, perturbations in the systemic insulin signalling network will have severe detrimental effects, not only on specific target organs but also on the whole organism.

The release of insulin, from the β-cells in the islets of Langerhans found in the pancreas, as a result of elevated levels of blood glucose facilitates uptake, utilisation and storage of glucose in a range of tissues. Activation of the insulin receptor in muscle and adipose tissue leads to an increase in the recruitment of the GLUT 4 transporter on the surface of cells in these tissues and therefore increases the rate of entry of glucose into the cells[114]. Insulin also has a profound effect on liver metabolism; the hormone stimulates the uptake of glucose into hepatocytes and its conversion to glycogen, once glycogen stores are full, insulin also promotes the de novo synthesis of fatty acids from glucose in the liver. The exposure of adipose tissue to insulin inhibits the intracellular lipase and therefore prevents the hydrolysis and release of fatty acids from TAGs, concomitantly the synthesis of glycerol from glucose is enhanced. These processes lead to further accumulation of TAGs in the adipocytes.

There is a distinctive variation in the concentration of insulin required to arbitrate the metabolic responses in tissues between individuals in a population[115]. In the case of insulin insensitivity, referred to as insulin resistance, peripheral metabolic tissues fail to respond effectively to increases in the concentration of insulin in circulation[116]. This can lead to hyperglycaemia. In some individuals the ability to produce enough insulin to negate insulin resistance is impaired and this gives rise to TIIDM. Increased insulin resistance, when combined with hyperinsulinaemia and obesity, increases an individual's

risk of associated disorders such as dyslipidaemia and microalbuminuria which in turn increase the prevalence of atherosclerosis and hypertension leading to cardiovascular morbidity and mortality[117]. The increased risk of cardiovascular disease as a direct result of perturbed insulin pathway function in non-type I diabetics was first defined as metabolic syndrome in 1988[118]. A number of biomarkers have been identified that decidedly correlate with the degree of insulin resistance; these include low density lipoprotein (LDL) particle size[119] and fibrinogen[120].

1.4.2 Aetiology of the Metabolic Syndrome

The aetiology of the metabolic syndrome is complex and poorly understood with roots likely to lie in both environmental and polygenic factors. The theory that hyperinsulinaemia caused by a loss of insulin sensitivity is a primary contributing factor to the development of metabolic syndrome has become widely established[121]. The syndrome associates insulin resistance, visceral obesity, dyslipidaemia and hypertension, which are known to be interrelated. However there is continued controversy as to whether the condition is a homogeneous disorder or disease and whether it can be truly recognised as a syndrome[122]. The pathophysiology is further complicated by the recognition that individuals with a lone component of the metabolic syndrome are not at as high a risk of cardiovascular disease or TIIDM demonstrating the individual components are more than additive.

The principal contributing factors of the metabolic syndrome have been grouped together in four main categories: insulin resistance, visceral obesity, atherogenic dyslipidaemia and endothelial dysfunction. The first two factors seem to be central and metabolic predisposition to insulin resistance and obesity appear to be necessary for the metabolic syndrome phenotype. Dyslipidaemia often arises from the insulin resistance and obesity and is further broken down to include high serum TAG concentrations and decreased HDL particle concentrations. Endothelial dysfunction is thought to come from adipokines and free fatty acids (FFAs) released by adipose tissue in the obese phenotype. Endothelial dysfunction manifests symptomatically as hypertension. Together the

dyslipidaemia and hypertension contribute to the emergence of cardiovascular disease. Candidate genetic factors that may combine to the pathology of the metabolic syndrome have been identified in a number of large cohort patient studies[123].

1.4.3 Diagnosis and Current Definitions of Metabolic Syndrome

As previously mentioned the etiology of the metabolic syndrome is complex and this has meant that the diagnosis and definitions of the disorder have controversially varied. The most commonly used definitions for diagnosis come from the World Health Organisation (WHO), first developed in 1998, the European Group for the Study of Insulin Resistance (EGIR), who proposed an amendment to the WHO definition in 1999, the National Cholesterol Education Program (NCEP), who devised their definition in 2001 and which has since been amended by the National Heart Lung and Blood Institute in 2005, and the International Diabetes Foundation (IDF) whose definition was first published in 2005. These definitions are summarised in **Table 1.1**.

Given the multiple definitions arising from the variation of emphasis, for example the WHO definition classifies individuals at risk of developing TIIDM whereas the IDF definition focuses on adiposity, the Food and Drug Administration, the European Association for the Study of Diabetes and the American Diabetes Association have questioned diagnosing patients as suffering from metabolic syndrome and instead called for the identification and treatment of individual risk factors[124].

	NCEP (2005)	WHO (1998)	EGIR (1999)	IDF (2005)
Essential	N/a	Insulin Resistance (IGT or TIIDM)	Hyperinsulinaemia (plasma insulin >75th percentile)	Central obesity (waist >94cm male, >80 cm female)
Criteria	Three of the five criteria defined below	Insulin resistance or TIIDM and two of the five criteria below	Hyperinsulinaemia and two of the four criteria below	Obesity and two of the four criteria below
Obesity Definition	Waist >101 cm male and >89 cm female	Waist/hip ratio >0.9 Male and >0.85 Female or BMI >30 kg/m^2	Waist >94 cm Male and >80 cm Female	Central Obesity required
Hyperglycaemia	Fasting glucose >5.6 mmol/l	Insulin resistance required	Insulin resistance required	Fasting glucose >5.6 mmol/l
Dyslipidaemia	TAG >1.7 mmol/l and HDL-Cholesterol <1 mmol/l male and <1.3 mmol/l Female	TAG >1.7 mmol/l or HDL-Cholesterol <0.9 mmol/l Male and <1 mmol/l Female	TAG >2 mmol/l or HDL-Cholesterol <1 mmol/l	TAG > 1.7 mmol/l and HDL-Cholesterol <1 mmol/l Male and <1.3 mmol/l Female
Hypertension	>130 mmHg systolic of >85 mmHg diastolic	>140/90 mmHg	>140/90 mmHg	>130 mmHg systolic of >85 mmHg diastolic
Additional		Microalbuminuria		

Table 1.1: Definitions of the metabolic syndrome. Impaired Glucose Tolerance (IGT). Microalbuminuria, >20 mg/min urinary albumin excretion or albumin-to-creatinine ratio of >30 mg/g. Adapted from Huang, P.L., 2009 [125].

1.5 Peroxisome Proliferator-Activated Receptors

In 1990 a novel murine orphan receptor was cloned and characterised that was activated by a range of peroxisome proliferators[126]; this was the first peroxisome proliferator-activated receptor (PPAR) isoform to be characterised and was named PPARα. Peroxisomes are cellular organelles involved in the β-oxidation of long-chain fatty acids and catabolism of cholesterol in the formation of bile acids. The PPARs are a subgroup of the nuclear receptor superfamily and ligand-activated transcription factors that control the expression of genes involved in a range of vital biological processes[127]. Since the discovery of PPARα further PPAR isoforms have been identified and named PPARγ and PPARδ, each demonstrating its own specific tissue distribution and ligand preference[128]. As opposed to PPARα neither PPARδ nor PPARγ are activated by peroxisome proliferators or increase the number or size of peroxisomes in rodent tissues[129]. PPARδ is also known as PPARβ, a complexity resulting from the initial isolation of PPARβ in *Xenopus* oocytes[130]. The mammalian PPARβ appeared to have little homology with that identified in amphibians and so was named PPARδ. The mammalian genome was later revealed to only contain three PPAR isoforms; PPARδ was recognised as the mammalian ortholog of PPARβ[131].

The PPARs share a great deal of structural homology with other members of the nuclear receptor superfamily. The DNA binding domain of the receptors is comprised of an approximately 70 amino acid binding domain containing two highly conserved zinc fingers. The receptors also include a more variable ligand binding domain of approximately 250 amino acids which besides its ligand binding capacities includes dimerisation and transcriptional activation domains as well as the extensively studied transcriptional activation function 2 domain at the extreme C-terminal section of the receptor.

Ongoing research into the physiological role of PPARs has revealed that they have a primary role as master regulators of metabolism and as nutritional sensors. The three

PPAR isoforms are activated by a range of unsaturated fatty acids and essential fatty acid metabolic pathway products and their derivatives, the eicosanoid and prostaglandin classes. As PPARs have been implicated in the metabolic control of pathways involving a number of their ligands it has been suggested that the ability of PPARs to act as nutritional sensors comes from their ability to function through these positive and negative feed back loops[132]. However it has also been postulated that activation of the PPARs is less specific; a theory emanating from the discovery that the binding affinity fatty acids have for the PPARs is relatively low when compared to other hormone-receptor couplings[133] and from the elucidation of the structure of the binding domain of the receptor class which is large in comparison to other members of the nuclear receptor superfamily, and so binds promiscuously to a diverse range of heterogenic compounds[134].

1.5.1 PPAR Ligand Activated Transcription Factors

The PPARs form obligate heterodimers with the 9-cis-retinoic acid receptor (RXR) and bind to two half sites of the direct repeat of the hexameric DNA consensus sequence, AGGTCA separated by one nucleotide[135] (**Figure 1.14**). The consensus binding sequences are known as Peroxisome Proliferator Response Elements (PPREs) and have been identified in numerous genes involved in organogenesis, inflammation, cell differentiation and proliferation and carbohydrate and lipid metabolism. In the absence of ligand binding, the PPAR-RXR complex recruits co-repressors, associated histone deacetylases and chromatin-modifying enzymes that silence transcription by active repression[136,137]. Upon ligand binding a conformational change occurs in the PPAR-RXR complex releasing transcriptional repressors in exchange for co-activators; these complexes function to recruit the basal transcriptional machinery enhancing the expression of target genes. There is mounting evidence that the different functional properties of the three PPAR subtypes arises from subtle differences in binding site preference, tissue distribution and their ability to bind different co-repressors and co-activators[138].

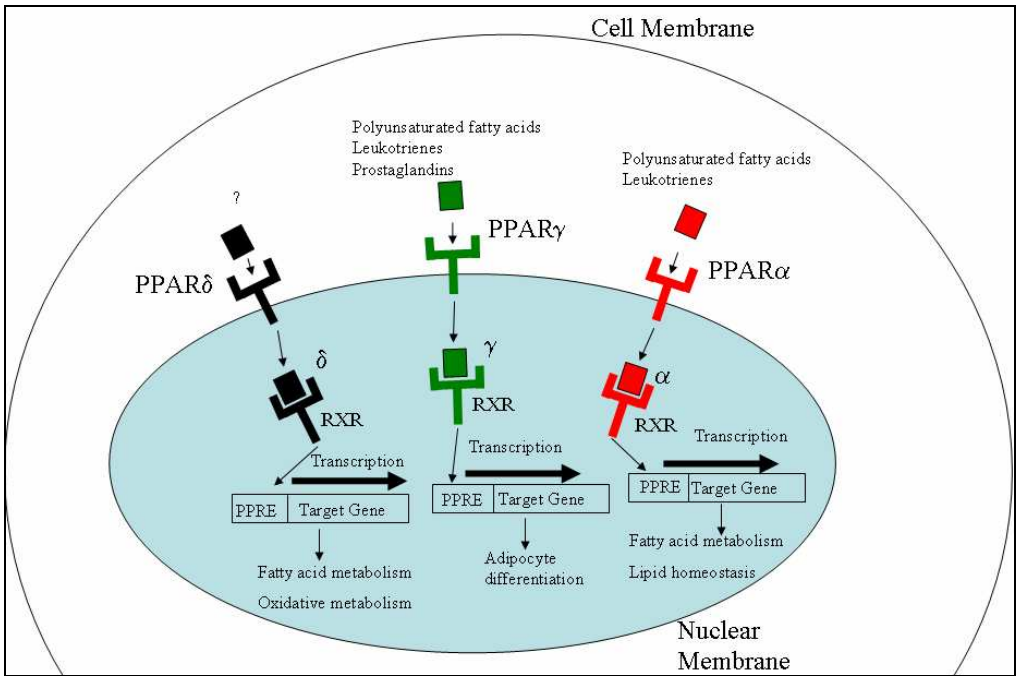

Figure 1.14: The peroxisome proliferator-activated receptor mechanism for the activation of gene transcription.

1.5.2 Peroxisome Proliferator-Activated Receptor α

PPARα is primarily expressed in highly catabolic tissues such as the heart, liver, macrophages, intestines, kidneys and skeletal muscle[139]. The receptor is bound by a range of saturated and unsaturated fatty acids including palmitoleate and oleate[138], as well as polyunsaturated fatty acids and leukotriene B4[140]. PPARα plays a crucial role in the regulation of FFA transport, uptake and catabolism[141].

The response to hypoglycaemic conditions is partially co-ordinated by PPARα. The nuclear receptor increases the expression of a panel of genes including the fatty acid transporter, fatty acid transport protein, acyl-CoA oxidase, and keto-acyl-CoA thiolase. The result is an increase in uptake of fatty acids into the liver accompanied by upregulation of peroxisomal β-oxidation of these fatty acids, shortening their chain length and facilitating entry into the mitochondria. The mitochondrial β-oxidation pathways also come under PPARα transcriptional control with increased expression of carnitine

palmitoyltransferase I[142] and medium-chain-acyl-CoA dehydrogenase[143]. As a consequence circulating TAG concentrations are reduced and lipidaemic profiles normalised by PPARα activation.

Due to the low levels of expression of PPARα in white adipose tissue the receptor is thought to play a limited role in adipogenesis. Activation of PPARα in 3T3-L1 preadipocytes fails to stimulate their differentiation[144]; however when the receptor is co-expressed with the transcriptional co-activator PPARγ-coactivator 1 in this cell line the expression of enzymes participating in the β-oxidation pathway is increased[145]. Rat primary adipocytes were also found to respond in a similar way to PPARα activation by fibrates in a process involving the upregulation of fatty acid uptake and β-oxidation[146]. *In vivo* mice lacking the PPARα gene appear to have normal white adipose tissue; however they are susceptible to spontaneous late onset obesity and adipocyte hypertrophy[147].

It is worthy of note that PPARα is also the target for the fibrate pharmacological compound class used in the treatment of hypercholesterolaemia and hyperlipidaemia. Members of this class include fenofibrate and bezafibrate. Activation of PPARα by fibrates results in a decrease in very low-density lipoprotein-cholesterol, chylomicrons and circulating TAGs through a mechanism involving increased expression of lipoprotein lipase and apolipoprotein A-V[148]. HDL-Cholesterol concentrations also increase following fibrate treatment, a result of increased transcription and subsequent translation of apoA-I and apoA-II[149] and ABC binding cassette transporter A1 induction, which stimulates macrophage cholesterol efflux[150]; since macrophages containing high concentrations of lipids are primary facilitators of inflammation and atherosclerotic plaque formation in the vasculature these processes contribute to a reduction in the risk of cardiovascular disease[151].

1.5.3 Peroxisome Proliferator-Activated Receptor γ

PPARγ was initially identified using homology cloning in *Xenopus*[130] and then mice[152], before it was isolated by identification and cloning of the ARF6 factor controlling the function of the adipose-specific enhancer of the *aP2* gene[153]. ARF6 was discovered to be PPARγ associated with its heterodimeric partner RXR[153]. The PPARγ gene is transcribed to give three mRNAs, termed $PPAR_{\gamma 1}$, $PPAR_{\gamma 2}$ and $PPAR_{\gamma 3}$, which are generated by alternative splicing and differential promoter utilisation. Only the $PPAR_{\gamma 1}$ and $PPAR_{\gamma 2}$ isoforms are expressed as proteins in mice and humans. The $PPAR_{\gamma 2}$ protein is larger than $PPAR_{\gamma 1}$, comprising of an additional 30 amino acids located at the N-terminus. The function of the extended N-terminus in $PPAR_{\gamma 2}$ is as yet unknown but several studies have suggested that it may play a role in adipogenesis[154, 155]. The tissue expression of the two isoforms also differs; $PPAR_{\gamma 2}$ is primarily expressed in the white and brown adipose tissue whereas $PPAR_{\gamma 1}$ is more ubiquitously expressed with higher concentrations of the mRNA found in kidneys, pancreas, heart, intestines and adipose tissue[139, 156].

PPARγ has been established as the master regulator of adipogenesis; no other transcriptional regulator has yet been shown to promote adipogenesis in the absence of the nuclear receptor. However, *in vivo* study of PPARγ null mice has proven difficult due to embryonic lethality arising from placental insufficiency[157]. The generation of chimeric mice containing PPARγ null cells demonstrated that these cells do not contribute to adipocyte formation[158]. Later research has shown that inactivation of PPARγ specifically in embryonic cells rather than trophoblasts lead to the production of mice with PPARγ deficiency that demonstrated lipodystrophy, insulin resistance and hypotension. In addition PPARγ selective ablation in adipose tissue verified the nuclear receptor's importance for post-differentiation adipocyte survival[159]. *In vitro* studies have also emphasised the importance of PPARγ for adipogenic processes; PPARγ knock out fibroblasts and embryonic stem cells have been shown to be differentiation incompetent[158] whilst pre-adipocytes carrying a dominant negative PPARγ mutation failed to undergo adipogenesis[160].

Besides PPARγ's critical role in adipogenesis, the nuclear receptor is also a principle regulator of fatty acid metabolism in white adipose tissue. The receptor promotes FFA uptake and consequent storage as TAGs. Activation of PPARγ increases expression of an array of genes required for a range of lipid metabolic pathways in adipocytes; the genes regulated by PPARγ include fatty acid transport protein 1, crucial for FFA uptake, lipoprotein lipase, necessary for the release of FFA from TAGs, fatty acid binding protein 4, required for intra-cellular FFA transport, as well as acyl-CoA synthase and phosphoenolpyruvate carboxykinase 1, essential for FFA activation and esterification, via glyceroneogenesis, respectively[161]. The active nuclear receptor also promotes storage of TAGs in unilocular lipid vesicles within adipocytes[162].

PPARγ activation is of clinical importance in the treatment of TIIDM and the metabolic syndrome; the thiazolidinedione (TZD) class of antidiabetic drugs are PPARγ agonists. Two members of the TZD pharmacological compound class, rosiglitazone and pioglitazone are currently utilised in the clinic. TZDs were of interest initially due to their ability to lower blood glucose levels in rodents and later in humans[163]; subsequently it was discovered that the TZDs were direct pharmacological agonists for PPARγ[164]. The mechanism by which activation of PPARγ by TZDs brings about insulin sensitisation and normalisation of hyperglycaemia has been the focus of a great deal of research over the last decade. Evidence thus far supports the conviction that adipose tissue is the primary target and mediator for the systemic effects of TZD treatment, a theory described by the "lipid steal" hypothesis[165,166]. The hypothesis states that PPARγ activation in white adipose tissue enhances dietary fatty acid storage. TIIDM is characterised by increased plasma FFA concentrations and inappropriate deposition of lipids in peripheral and metabolic tissues such as liver and skeletal muscle, which is associated with insulin resistance and impaired glucose utilisation[167]. Therefore PPARγ activation in the adipose tissue is thought to facilitate sequestration of the FFAs into the white adipose tissue, as a safe storage depot, and away from the peripheral tissues where their deposition is deleterious. However, the theory is less than comprehensive since the insulin sensitising effects of TZDs are not shared by alternative drug classes that also lower circulating

plasma FFA concentrations, suggesting additional mechanisms are involved in the antidiabetic processes initiated by PPARγ activation.

1.5.4 Peroxisome Proliferator-Activated Receptor δ

In comparison to PPARα and PPARγ, the third member of the family, PPARδ has come under a lesser degree of scrutiny. However, the research that has been conducted thus far indicates PPARδ may be a potential clinical target for the treatment of obesity, the metabolic syndrome and TIIDM. PPARδ is expressed almost ubiquitously, though some tissues express higher concentrations of the mRNA including the brain, adipose tissue, skin, liver and skeletal muscle[139]. In addition PPARδ protein expression has recently been shown to be high in liver, colon, small intestine and keratinocytes[168]. PPARδ is activated by several 14 to 18 carbon containing polyunsaturated fatty acids, including eicosanoids such as prostaglandin A_1, iloprost and carbaprostacyclin, in the micromolar range[132]. Nevertheless, the physiological ligands of PPARδ remain undefined.

In vivo studies using PPARδ null rodents have proven difficult since deficiency of the receptor results in embryonic lethality of over 90% due to placental defects. However, the surviving animals have been found to expend less energy than the wild type and consequently are more susceptible to weight gain[169]. The development of a number of high affinity synthetic PPARδ ligands has identified the receptor as a potential therapeutic target for the metabolic syndrome; PPARδ ligands retard weight gain in models of high-fat diet induced obesity. Insulin resistant obese rhesus monkeys treated with the selective PPARδ agonist GW501516 demonstrated significant increases in HDL-cholesterol with concomitant decreases in TAGs and LDL-cholesterol[170]. PPARδ is expressed at 10 and 50 times the concentrations of PPARα and PPARγ, respectively, in skeletal muscle and administration of PPARδ agonists to rodents results in an increase in expression of genes involved in fatty acid oxidation, mitochondrial respiration, oxidative metabolism and slow twitch contractile apparatus[171]. These changes would be expected to bring about a decrease in muscle fatigability and positively impact fatty acid homeostasis.

The role of PPARδ in adipose tissue appears to be that of a regulator of tissue metabolism and energy homeostasis. *In vitro* investigation has shown that expression of PPARδ is induced early in the differentiation of the 3T3-L1 murine clonal white preadipocyte cell line[172] and during early brown adipogenesis[173]. PPARδ is also implicated in the stimulation of adipogenesis via the induction of PPARγ expression and mitotic clonal expansion[174, 175]. *In vivo* targeted activation of PPARδ in white adipose tissue results in increased expression of genes involved in FFA oxidation and the electron transport chain uncoupling protein 1; these transcriptional changes coincided with a reduction in adiposity through reduced intracellular TAG accumulation and improved lipid profiles[169].

However, the ubiquitous expression of PPARδ may result in diverse and unwanted side effects upon activation of this receptor. PPARδ has been the subject of contrasting studies relating to its role in carcinogenesis. The nuclear receptor has been implicated in the acceleration of intestinal adenoma growth and increased growth in breast and prostate cancer cell lines, but contradictory to these studies PPARδ has also been shown to attenuate colon cancer[176, 177, 178]. The role of PPARδ in development and carcinogenesis is complex and has been extensively reviewed elsewhere[179]. Given the ubiquity of expression of PPARδ and its apparent diverse effects, an unambiguous comprehension of the global effects of activation of the nuclear receptor is necessary before it can be considered as a therapeutic target.

1.5.5 The Application of Metabolomics to the Study of the PPARs

Metabolomics has been employed to study mouse models of PPAR function. ^{13}C isotope labelling strategies identified hypoglycaemia and impaired liver fatty acid β-oxidation in fasting PPARα null mice, demonstrating that the receptor regulates hepatic gluconeogenesis in both fed and fasted mice[180, 181]. Atherton and colleagues used a combined ^{1}H-NMR spectroscopy and GC-MS metabolomics strategy to analyse the effect of the ageing process on metabolism in the liver, heart, skeletal muscle and adipose tissue of PPARα null mice and wild-type mice between 3 and 13 months of age[182]. The

PPARα null mouse was characterised by hepatic steatosis and reduced glucose and glycogen liver and muscle concentrations. The hepatic concentrations of glucose and glycogen also decreased in an age dependent manner in both mouse genotypes. The study highlighted the role the receptor plays in the ageing process and provides a model for the investigation of the interaction between age and genotype.

The functions of the PPARs have also been investigated using synthetic agonist compound treatment studies of model organisms. PPARγ activation by rosiglitazone in the heart, adipose tissue, liver and plasma of the NZO x NON mouse, a model of TIIDM, has also been investigated using a lipidomics platform[183]. The mass spectrometry based study employed thin layer chromatography to separate lipids into their chemical classes followed by GC-MS to investigate constituent fatty acids that were esterified to each complex lipid class. There was a detected decrease in several lipid classes in the serum, alterations in cardiolipin, and an accumulation of polyunsaturated fatty acids in adipose tissue. The metabolomic changes were also correlated with transcriptional changes analysed by reverse transcriptase polymerase chain reaction. The metabolic effect on exposure of rats to two PPARα agonists, a PPARγ agonist and a PPARδ agonist has been studied using a ^{1}H-NMR spectroscopy based metabolomics investigation of urine[184]. Two biomarkers from the tryptophan-NAD+ pathway, N-methyl-4nicotinamide and N-methyl-4-pyridone-3-carboxamide, were found to correlate with peroxisome proliferation measured by electron microscopy of liver tissue.

1.5.6 Selective Pharmacological PPAR Agonists

The research conducted within this thesis employs two high affinity, specific and extensively characterised PPAR agonists. GW347845 is a specific PPARγ agonist with an EC_{50} value of 1.2 nM for murine PPARγ. GW610742 is a PPARδ agonist with an EC_{50} value of 28 nM for murine PPARδ compared to 8900 nM and >10,000 nM for PPARα and PPARγ respectively[185].

1.6 Project Aims

Given the crucial role of both PPARδ and PPARγ in white adipose tissue, it is the aim of this thesis to use a metabolomics approach to investigate and define the metabolic effects of PPARδ and PPARγ activation in both *in vivo* adipose tissue and in an *in vitro* model of adipose tissue.

To achieve the outlined aim the metabolic phenotype of the adipose tissue specific cell line, differentiating 3T3-L1 preadipocytes, as they mature into adipocyte cells will be defined and compared to differentiating murine primary cells using metabolomics to generate a metabolically phenotyped *in vitro* model of adipose tissue.

The effects of PPARδ and PPARγ activation in white adipose tissue from a mouse model of insulin resistance, and in the adipose tissue specific cell line within a cell culture system, will then be investigated in order to generate an *in vivo* and an *in vitro* model of adipose tissue specific PPAR activation. In addition the thesis aims to deconvolute the metabolic mechanisms by which PPARδ and PPARγ alter the metabolism of the adipose tissue specific cell line using stable isotope labelling, transcriptomics and additional complementary methodologies.

Further to these aims it is intended to use a metabolomics approach to investigate and define the global physiological and pharmacological effects of PPARδ and PPARγ activation through the characterisation of a range of tissues from a pharmacological compound treatment study performed in a mouse model of insulin resistance.

AIM	
To metabolically phenotype the 3T3-L1 adipocyte model of differentiation and compare the model to differentiating murine primary preadipocytes using metabolomic techniques.	**Chapter 3**
To investigate the metabolic effects of pharmacological PPARδ activation in white adipose tissue from the *ob/ob* mouse model of insulin resistance, and in the 3T3-L1 adipose tissue specific cell line within a cell culture system, to generate an *in vivo* and an *in vitro* model of adipose tissue specific PPARδ activation.	**Chapter 4**
To deconvolute the metabolic mechanisms by which PPARδ activation alters the metabolism of the 3T3-L1 adipose tissue specific cell line using stable isotope labelling, transcriptomics and respirometry.	**Chapter 4**
To investigate the metabolic effects of pharmacological PPARγ activation in white adipose tissue from the *ob/ob* mouse model of insulin resistance, and in the 3T3-L1 adipose tissue specific cell line within a cell culture system, to generate an *in vivo* and an *in vitro* model of adipose tissue specific PPARγ activation.	**Chapter 5**
To deconvolute the metabolic mechanisms by which PPARγ activation alters the metabolism of the 3T3-L1 adipose tissue specific cell line using stable isotope labelling and transcriptomics.	**Chapter 5**
To use a metabolomics approach to investigate and define the global physiological and pharmacological effects of PPARδ and PPARγ activation through the metabolic characterisation of blood serum, skeletal muscle and liver tissue from a pharmacological compound treatment study performed in the *ob/ob* mouse model of insulin resistance.	**Chapter 6**

Chapter 2

Materials and Methods

2.1 3T3-L1 and Primary Murine Adipocyte Cell Culture Techniques

2.1.1. 3T3-L1 Cell Culture and Adipocyte Differentiation

3T3-L1 preadipocytes were grown in T75 flasks and maintained in Dulbecco's modified Eagles media (DMEM) (high glucose 4.5 g/l; Sigma-Aldrich) supplemented with 10% (v/v) new born calf serum (Sigma-Aldrich), 50 units/ml penicillin, and 50 µg/ml streptomycin (Sigma-Aldrich) in a humidified 5% CO_2 incubator at 37ºC. At 2 days post-confluence cells were induced to differentiate with DMEM supplemented with 10% v/v FBS, 1 µM dexamethasone (Sigma-Aldrich), 0.5 mM isobutylmethylxanthine (Sigma-Aldrich), 100 nM insulin (Sigma-Aldrich), 50 units/ml penicillin, and 50 µg/ml streptomycin. The cells were maintained in this media for 72 h as this was found to improve the reproducibility of differentiation between flasks. After 72 h the media was replaced with DMEM supplemented with 10% FBS, 100 nM insulin, 50 units/ml penicillin, and 50 µg/ml streptomycin. The media was subsequently changed for DMEM supplemented with 10% FBS, 50 units/ml penicillin, and 50 µg/ml streptomycin every 48 h.

2.1.2. Primary Adipocyte Cell Isolation and Differentiation

The gonadal fat pad was isolated from four week old mice post mortem. Four mice were required per primary adipocyte culture. The adipose tissue was finely ground and then

digested in a solution of Hanks Balanced Salt Solution (7 ml) containing collagenase type II (10 mg; Sigma-Aldrich) and Bovine Serum Albumin (BSA 7.5% w/v 3 ml) in an incubator for 35 min at 37 ºC. Following digestion, the solution was filtered through a 250 μm mesh (BD Biosciences**,** San Jose, CA.). The solution was left to settle on ice for 20 min. The upper white adipose tissue layer, containing mature adipocytes, was removed. The next stratum, which contains the preadipocytes, was then filtered through a 100 μm mesh. The filtered digest media was diluted 1:1 with 10% FBS media. The cells were centrifuged at 700 *g* for 10 min. The cell pellet was re-suspended in plating media constituting DMEM supplemented with 10% v/v NCS (newborn calf serum), 50 units/ml penicillin, 50 μg/ml streptomycin, 2.4 nM insulin and 250 μM sodium ascorbate (Sigma-Aldrich). The cells were then centrifuged at 700 g for 10 min and once again resuspended in plating media. Cells were plated on four well plates. The media was changed every 24 h for the first three days and subsequently every 48 h up to day 7.

2.1.3. Activation of PPARδ in 3T3-L1 Adipocytes

At day 11 post differentiation induction the media on the cells was replaced with DMEM supplemented with 10% FBS, 100 nM insulin, 50 units/ml penicillin, and 50 μg/ml streptomycin containing either dimethylsulphoxide DMSO (Sigma-Aldrich) (control, n=6) or GW610742 PPARδ selective agonist (GlaxoSmithKline plc.) (n=6 at 100 nM and 1 μM) for 2 days prior to cell collection and metabolite extraction described in sections **2.1.6** and **2.3**.

2.1.4. Activation of PPARγ in 3T3-L1 Adipocytes

At day 11 post differentiation induction the media on the cells was replaced with DMEM supplemented with 10% FBS, 100 nM insulin, 50 units/ml penicillin, and 50 μg/ml streptomycin containing either DMSO (control, n=7) or GW GW347845 PPARγ selective agonist (GlaxoSmithKline plc.) (n=7 at 10 nM and 100 nM) for 2 days prior to cell collection and metabolite extraction described in sections **2.1.6** and **2.3**.

2.1.5. Oil Red O Staining and Intracytoplasmic Lipid Accumulation

Cell cultures were washed with phosphate buffered saline (PBS; Severn Biotech Ltd) and fixed overnight with 10% formalin in PBS at 4 °C. The cultures were then incubated for 1 h with 0.3% Oil Red O (Sigma-Aldrich) in 60% isopropanol at room temperature and washed with PBS. Digital images of the cells were taken using a Nikon D100 camera. The stain was extracted from the cells with 60% isopropyl alcohol for 1 h (10 mL/flask) and 1 ml measured at 510 nm in a spectrophotometer.

2.1.6. Adipocyte Cell Collection

Cells were collected by removing the media and washing each T75 flask with 10 ml of PBS. Cells were then washed with 1.5 ml trypsin-EDTA solution (5 BAEE units trypsin/ml, 1.8 µg EDTA/ml; Sigma-Aldrich) for 2 min at 37ºC to remove the cells from the surface of the flask. 8.5 ml DMEM supplemented with 10% (v/v) new born calf serum, 50 units/ml penicillin, and 50 µg/ml streptomycin was added to each flask. The DMEM containing the cells was transferred to a falcon tube and centrifuged at 200 *g* for 2 min to pellet the cells. The remaining media was removed and the cells washed with physiological saline (0.9% NaCl) solution.

2.2 Animal and Tissue Handling

2.2.1. Animal Handling

All animal studies were performed by GlaxoSmithKline (Research Triangle Park, N.C., U.S.A) within the relevant local legislation. Two month old male *ob/ob* mice (Jackson Labs, Bar Harbor, ME), were fed standard laboratory chow *ad libitum* and housed 4 per cage on alpha-dri bedding under controlled temperature, lighting and humidity (20-22 ºC, 12-h light/dark cycle, Humidity 48-50%). Prior to selection for the study, all mice were examined ensuring they were physically normal and exhibited normal activity. During the studies, body weight and food consumption (cage average) were recorded.

The *ob/ob* mice were assigned to six groups of eight and dosed orally daily at 8 am with 0.5% Hydroxypropylmethylcellulose/0.1% Tween80 vehicle control, a PPARδ agonist, GW610742 (30 mg/kg) and a PPARγ agonist GW347845 (5 mg/kg). Injection volume was adjusted daily according to body weight at 10 ml/kg.

2.2.2. Clinical Chemistry

All clinical chemistry measurements were performed using an Olympus AU 400e analyser at GlaxoSmithKline (Research Triangle Park, N.C., U.S.A)[186]. Plasma was analysed for the following parameters: alkaline phosphatase, alanine transaminase, total bilirubin, thymidine phosphorylase, albumin, blood urea nitrogen, creatine, glucose, cholesterol, high density lipoprotein-cholesterol, triacylglycerides, non-esterified fatty acids, creatine kinase, lactate dehydrogenase, sodium, potassium and β-hydroxybutyrate. Insulin measurements were performed by ELISA (Millipore Mouse Insulin ELISA kit).

2.2.3. Oral Glucose Tolerance Test (OGTT)

The OGTT was performed at GlaxoSmithKline (Research Triangle Park, N.C., U.S.A). Animals were fasted overnight prior to the OGTT (day 12). Glucose concentrations were measured using the FreeStyle Blood Glucose Monitoring System (TheraSense, U.K.). Animals were dosed orally with 1 g/kg glucose. Baseline fasted glucose values were collected at the 0 min time point. Glucose concentrations were collected at 15, 30, 60 and 90 min intervals. All samples were collected via tail snips.

2.2.4. Tissue Handling

Serum was collected via cardiac stick under isofluorane anaesthesia at completion of the study (day 15). Skeletal muscle (gastrocnemius) white adipose and liver tissue were rapidly dissected (<60 s post mortem), snap frozen in liquid nitrogen and stored at -80 ºC until extraction.

2.3 3T3-L1 Cell, Primary Adipocyte and Tissue Metabolite Extraction

Metabolites were extracted from serum, liver, skeletal muscle, white adipose tissue, 3T3-L1 cells and primary adipocyte cells using a modified Bligh and Dyer method[187]. Frozen tissue was pulverised with liquid nitrogen. Methanol-chloroform (2:1 600 µl) was added to the tissues (100 mg for NMR and 50 mg for GC-MS analysis), serum (50 µl), 5 mg cell pellets (3T3-L1 cells) or 1 mg cell pellets (primary cells) and the samples were sonicated for 15 min. Chloroform-water (1:1) was then added (200 µl of each). Samples were centrifuged (16,100 *g*, 20 min) and the organic and aqueous phases were separated and stored at -80°C until analysis. Of these fractions, 100 µl of the organic phase was used for LC-MS, and the remaining organic phase was used for GC-MS. Prior to analysis the organic fractions were dried in a fume hood. For the aqueous phase, 100 µl of the aqueous phase was taken for GC-MS analysis, and the remaining aqueous phase sample was used for ^{1}H-NMR spectroscopy. Prior to further analysis the aqueous fractions were dried in an evacuated centrifuge overnight (Eppendorf, Hamburg, Germany).

2.4. ^{13}C Substrate Labelling Studies

2.4.1 ^{13}C-glucose Substrate Labelling Study in PPARδ Activated Cells

At 2 days post differentiation media was removed from the T75 flasks and replaced with DMEM (10% (v/v) FBS, 50 units/ml penicillin, and 50 µg/ml streptomycin) and either 4.5 g/l ^{12}C unlabelled glucose with DMSO (control, n=6) or with 1µM GW610742 PPARδ selective agonist (n=7) or 4.5 g/l 1-^{13}C-glucose with (DMSO control, n=7) or with 1 µM GW610742 PPARδ selective agonist (n=7). After 2 days cells were collected and metabolites extracted as previously described in sections **2.1.6** and **2.3**.

2.4.2. ^{13}C-glucose Substrate Labelling Study in PPARγ Activated Cells

At 2 days post differentiation media was removed from the T75 flasks and replaced with DMEM (10% (v/v) FBS, 50 units/ml penicillin, and 50 µg/ml streptomycin) and either 4.5 g/l ^{12}C unlabelled glucose with DMSO (control, n=6) or with 1 µM GW347845

PPARγ selective agonist (n=7) or 4.5 g/l 1-^{13}C-glucose (Cambridge Isotope Laboratories, Andover, MA) with DMSO (control, n=7) or with 1 μM GW347845 PPARγ selective agonist (n=7). After 2 days cells were collected and metabolites extracted as previously described in sections **2.1.6** and **2.3**.

2.4.3. Preparation of ^{13}C and ^{12}C-palmitate Solution

75 ml of PBS was heated to 37 ºC. BSA (20g) was added to the PBS. Separately deionised water (15 ml), 95% ethanol solution (10 ml) and Na_2CO_3 (0.106 g) (Sigma-Aldrich) were mixed under nitrogen. Either unlabelled palmitate (0.2115 g) or U-^{13}C labelled palmitate (0.2247 g) (Cambridge Isotope Laboratories, Andover, MA) was added, and then heated to ~78 ºC to evaporate the ethanol. The fatty acid solution was added to the albumin solution and well mixed. The palmitate/albumin mixture was dialysed (Spectra/Por dialysis tubing; Molecular weight cut off 6000-8000) in deionised water at 4 ºC overnight.

2.4.4. ^{13}C-palmitate Substrate Labelling Study in PPARδ Activated Cells

At 2 days post-differentiation media was removed from the T75 flasks and replaced with DMEM (serum free, 50 units/ml penicillin, and 50 μg/ml streptomycin) and either 70 μM unlabelled palmitate (n=6) with DMSO (control, n=6) or with 1 μM GW610742 PPARδ selective agonist (n=7) or 70 μM U-^{13}C labelled palmitate (n=7) with DMSO (control, n=6) or with 1 μM GW610742 PPARδ selective agonist (n=7). After 2 days cells were collected and metabolites extracted as previously described in sections **2.1.6** and **2.3**.

2.4.5. ^{13}C-palmitate Substrate Labelling Study in PPARγ Activated Cells

At 2 days post-differentiation media was removed from the T75 flasks and replaced with DMEM (serum free, 50 units/ml penicillin, and 50 μg/ml streptomycin) and either 70 μM ^{12}C-U-palmitate (n=6) with DMSO (control, n=6) or with 1 μM GW347845 PPARγ selective agonist (n=7) or 70 μM U-^{13}C labelled palmitate (n=7) with DMSO (control,

n=6) or with 1 μM GW347845 PPARγ selective agonist (n=7). After 2 days cells were collected and metabolites extracted as previously described in sections **2.1.6** and **2.3**.

2.5. Respirometric Analysis of PPARδ Agonist Treated 3T3-L1 Cells

Cells were grown, treated with GW610742 PPARδ agonist and collected as has already been described in sections **2.1.1**, **2.1.3** and **2.1.7** with the exception that they were collected into respiration medium (100 mM KCl, 50 mM MOPS, 1.0 mM KH_2PO_4, 1.0 mg/ml defatted BSA, pH 7.4). Respiratory rates of *in situ* permeabilised control and PPARδ agonist treated 3T3-L1 cells were measured using a Clark-type oxygen electrode (Strathkelvin Instruments Ltd, Glasgow, UK) with methods developed by Kuznetsov *et al*[188]. Respiration rates were recorded and quantified using 782 Oxygen System v3.0 software (Strathkelvin Instruments). Oxygen concentrations were measured continuously in 0.5 ml respiration medium containing 250,000 cells in a respiration chamber maintained at 37 °C. The cells were initially permeabilised with the addition of digitonin (25 μg/ml), before malate (5 mM) plus palmitoyl-carnitine (0.04 mM) were added as respiratory substrates to measure the fatty acid oxidation rates. Respiration was stimulated by the addition of a saturating concentration of ADP (2 mM) plus $MgCl_2$ (0.6 mM) and subsequently measured. Antimycin (5 μM) was then added to inhibit complex III of the electron transport chain, and respiration ceased. Complex IV respiration was stimulated by addition of the artificial substrates TMPD (N,N,N',N'-tetramethyl-p-phenylenediamine dihydrochloride, 0.5 mM) and ascorbate (2 mM). Finally respiration was terminated by addition of the complex IV inhibitor, sodium azide (3 mM).

2.6. Metabolomic Analysis by Nuclear Magnetic Resonance

2.6.1. Spectrometer

All samples were analysed using a Bruker AVANCE II+ spectrometer operating at 500.13 MHz for the ^1H frequency (Bruker BioSpin GmbH, Rheinstetten, Germany) using a 5mm Broadband TXI Inverse Automatic Tuning and Matching (ATMA) probe.

2.6.2. Sample Preparation

Dried extracts were dissolved in 600 μl of D_2O and buffered in 0.24 M sodium phosphate (pH 7.4) containing 1 mM sodium-3-(trimethylsilyl)-2,2,3,3-tetradeuteriopropionate (TSP; Cambridge Isotope Laboratories, Andover, MA) and 0.02 M sodium azide.

2.6.3. 1-dimensional ^{1}H-Nuclear Magnetic Resonance Spectroscopy Experimental Method

A presaturation pulse sequence for water suppression based on a one-dimensional nuclear Overhauser effect spectroscopy pulse sequence was used to saturate the residual water proton signal (relaxation delay = 2 s, t_1 = 4 μs, mixing time = 50 ms, presaturation applied during the relaxation time and mixing time). 128 and 256 transients were collected for tissue extracts and 3T3-L1 cell extracts, respectively, into 64k data points over a spectral width of 8000 Hz at 300K.

2.6.4. Processing 1-dimensional ^{1}H-Nuclear Magnetic Resonance Data

NMR spectra were processed in ACD 1D NMR Manager (version 8; Advanced Chemistry Development Inc, Toronto, Canada), multiplied by an exponential weighting function of 1 Hz, Fourier transformed, phased, baseline corrected and referenced to TSP at 0.0 ppm. The NMR spectra were integrated using 0.04-ppm integral regions between 0.2 and 9.56 ppm (excluding water resonance between 4.20 and 5.08 ppm). Spectra were normalised to total integrated area to account for differences in concentration between samples and assigned by comparison with previous literature and, in the case of 3T3-L1 cells, Chenomx NMR suite 5.0 libraries.

2.6.5. 2-dimensional Heteronuclear Single-Quantum Coherence ^{13}C-Nuclear Magnetic Resonance Experimental Method

Dried 3T3-L1 adipocyte cell organic phase extracts from ^{13}C-labelling studies were dissolved in 600 μl of deuterated Chloroform. Samples were analyzed using a DRX

Avance II+ spectrometer interfaced to a 5-mm TXI ATMA probe. Analysis was performed using 2D H-1/X correlation via double inept transfer with sensitivity improvement. Phase sensitive using Echo/Antiecho-TPPI and gradient selection with decoupling during acquisition. Trim pulses in inept transfer using shaped pulses for all 180 degree pulses on f2-channel with gradients in back-inept. Spectral widths of 10.00 ppm and 160 ppm were used in the F2 (1H) and F1 (13C) dimensions respectively with an offset of 75.00 ppm. Spectra were acquired using 96 scans with a relaxation delay of 1.0 s. Datasets were zero-filled and multiplied by sine bell squared functions prior to fourier transformation.

2.6.6. Processing 2-dimensional Heteronuclear Single-Quantum Coherence ^{13}C-Nuclear Magnetic Resonance Data

2D-NMR spectra were processed in Bruker TOPSPIN (version 2.0, Bruker BioSpin GmbH, Rheinstetten, Germany). Peaks were selected using the automated peak picking algorithm with the sensitivity set to lowest contour level. The peaks were then integrated and normalised to total integrated area and assigned by comparison with previous literature.

2.7. Analysis by Gas Chromatography-Mass Spectrometry

2.7.1. Derivatisation of Aqueous Phase Metabolites

Dried aqueous phase samples were derivatised by adding 30 µl of methoxyamine hydrochloride solution (20 mg/ml in pyridine, Sigma-Aldrich Ltd), vortex mixed for 1 min then incubated at 25 ºC for 17 h. Samples were silylated with 30 µL of *N*-methyl-*N*-trimethylsilyltrifluoroacetamide (MSTFA; Macherey-Nagel, Germany) for 1 h at 25 ºC[189]. The tissue samples were diluted by addition of 200 µL of analytical grade hexane prior to GC-MS analysis.

2.7.2. Derivatisation of Organic Phase Metabolites

Acid-catalysed esterification was used to derivatise the organic phase samples. Chloroform-methanol (1:1, 0.25 ml) and BF_3-methanol (10%; 0.125 ml) (Sigma-Aldrich) was added to the organic phase and incubated at 90 ºC for 90 min. Water (0.15 ml; mQ) and hexane (0.3 ml) were added and the samples vortex mixed for 1 min and left to form a bilayer. The aqueous phase was discarded and the organic layer evaporated to dryness prior to reconstitution in analytical grade hexane (200 µl) before GC-MS analysis.

2.7.3. Gas Chromatography-Mass Spectrometry Methods

All GC-MS analyses were made using a Trace GC Ultra coupled to a Trace DSQ II single-quadrupole mass spectrometer (Thermo Scientific, Cheshire, UK).

2.7.3.1 Gas Chromatography-Mass Spectrometry methods for aqueous phase samples

Derivatised aqueous samples were injected splitless onto a ZB-5ms column (30 m x 0.25 mm, 0.25 µm 5%-Phenyl-Arylene - 95% Dimethylpolysiloxane stationary phase, with an integral 5 m Guardian guard column; Phenomenex). The injector temperature was 230 ºC and the helium carrier gas was used at a flow rate of 1.2 mL/min. The initial column temperature of 70 ºC was increased by 10 ºC/min to 130 ºC and then increased at a rate of 5 ºC/min to 230 ºC followed by an increase of 20 ºC/min to 310 ºC and held for 5 min (transfer line temperature = 250 ºC; ion source = 250 ºC; electron ionisation = 70 eV). The detector was turned on after 240 s and full-scan spectra were collected using 3 scans/s over a range of 50-650 *m*/*z*.

2.7.3.2 Gas Chromatography-Mass Spectrometry methods for organic phase samples

The derivatised organic samples were injected with a split ratio of 60 for white adipose tissue and 8 for 3T3-L1 cells, liver, skeletal muscle and serum onto a 30 m × 0.25 mm 70% cyanopropyl polysilphenylene-siloxane 0.25 µm TR-FAME stationary phase column (Thermo Electron). The injector temperature was set to 230 ºC and the helium carrier gas was at a flow rate of 1.2 mL/min. The column temperature was 60 ºC for 2 min, increased by 15 ºC/min to 150 ºC and then increased at a rate of 4 ºC/min to 230 ºC

(transfer line = 240 ºC; ion source = 250 ºC, EI = 70 eV). The detector was set as above for the ZB-5ms column.

2.7.4. Gas Chromatography-Mass Spectrometry Analysis, Processing and Data Handling for 3T3-L1 Adipocyte ^{13}C-labelled Substrate Studies.

Analysis of organic and aqueous phases was carried out as previously described in sections **2.7.1**, **2.7.2** and **2.7.3**. Enrichment of metabolites was identified by calculating isotope ratios of the M and M+1 ions for the parent ion of the fragmentation pattern in the case of ^{13}C-Glucose metabolism analysis and TCA cycle intermediates originating from ^{13}C-Palmitate oxidation. For fatty acid synthesis and desaturation products from ^{13}C-labelled palmitate an ion ratio of M+16/M was used and for fatty acids originating from oxidation of ^{13}C-labelled palmitate an ion ratio of M+n/M, where n = the carbon chain length of the fatty acid was used. Statistical analysis was performed using a univariate Student's *t*-test.

2.7.5. Processing Gas Chromatography-Mass Spectrometry Data

GC-MS chromatograms were processed using Xcaliber (version 2.0; Thermo Electron). Each individual peak was integrated and then normalised so that the total sum of peaks in a chromatogram was set to 10000. Overlapping peaks were separated using traces of single ions. Peak assignment was based on mass fragmentation patterns matched to the NIST/ EPA/NIH mass spectral library and to previously reported literature. Identification of metabolites from organic phase GC-MS analysis was supported by comparison with a FAME standard mix (Supelco 37 Component FAME Mix; Sigma Aldrich).

2.8. Analysis by Ultra Performance Liquid Chromatography-Mass Spectrometry

2.8.1. Chromatography and Mass Spectrometry Parameters

Chromatography was performed using an ACQUITY UPLC® system (Waters Corporation, Centennial Park, Elstree, Hertfordshire) equipped with an Acquity UPLC 1.7 μm Bridged Ethyl Hybrid (BEH) C8 column (2.1×100 mm Waters) which was kept at 65 ºC and coupled to a Micromass QTof-Ultima™ with a Z-spray™ electrospray source. The electrospray source was operated in positive ion mode with the source temperature set at 100 ºC and a cone gas flow of 50 L/h. The desolvation gas temperature was 300 ºC and the nebuliser gas flow rate was set at 600 L/h. The capillary voltage was 3 kV and the cone voltage was 50 V. Reserpine was used as the lock reference and was introduced into the LockSpray interface at a concentration of 50 μM in 1:1 methanol-water 0.1% formic acid (Fluka). Centroid mode was used for data collection. The lock reference sampling frequency was 10 s and the lock mass data was averaged over 10 scans. The binary solvent system used was solvent A: HPLC grade water (chromosolv plus Sigma-Aldrich), 1% 1 M ammonium acetate (NH_4Ac; Fluka), 0.1% formic acid and solvent B: HPLC grade acetonitrile (chromosolv Sigma-Aldrich)/isopropanol (Fisher Scientific) 5:2, 1% 1 M NH_4Ac, 0.1% formic acid[190]. The temperature of the sample organiser was set at 4 °C. Mass spectrometric data was collected in full scan mode from 100-1350 m/z for tissue and 100-1500 m/z for 3T3-L1 cells from 0-14 min with a scan duration of 0.5 s and an interscan delay of 0.1 s.

2.8.2. Sample Preparation and Chromatographic Gradient

2.8.2.1 Adipose tissue preparation and chromatographic gradient

The organic phase of adipose tissue extracts was reconstituted in methanol-chloroform (2:1, 500 μl). This was further diluted 10-fold prior to injection onto the C8 column (5 μl). The column mobile phase was held at 85% solvent B for 0.5 min followed by an increase from 85%-100% solvent B over 0.5-8 min. The mobile phase was then held at 100% B for 4 min. Between 12 and 12.25 min the mobile phase was returned to 85% B

held for 1.75 min to re-equilibrate the column. The total UPLC cycle was 14 min and the eluent flow rate was 600 µl/min.

2.8.2.2 Liver tissue preparation and chromatographic gradient

The organic phase of liver was reconstituted in methanol-chloroform (2:1, 500 µl). This was further diluted 7.5-fold prior to injection onto the C8 column (5 µl). The column mobile phase was held at 70% solvent B for 0.5 min followed by an increase from 70%-100% solvent B over 0.5-6.5 min. The mobile phase was then held at 100% B for 3.5 min. Between 10 and 10.25 min the mobile phase was returned to 70% B held for 3.75 min to re-equilibrate the column. The total UPLC cycle was 14 min. The eluent flow rate was 600 µl/min.

2.8.2.3 Serum preparation and chromatographic gradient

The organic phase of serum was reconstituted in methanol-chloroform (2:1, 500 µl). This was further diluted 4 fold prior to injection onto the C8 column (10 µl). The column mobile phase was held at 70% solvent B for 0.5 min followed by an increase from 70%-100% solvent B over 0.5-6.5 min. The mobile phase was then held at 100% B for 3.5 min. Between 10 and 10.25 min the mobile phase was returned to 70% B held for 3.75 min to re-equilibrate the column. The total UPLC cycle was 14 min. The eluent flow rate was 600 µl/min.

2.8.2.4 3T3-L1 adipocyte preparation and chromatographic gradient

3T3-L1 Cell Organic phase metabolites were reconstituted in methanol-chloroform (2:1, 1 ml). Aliquots of diluted organic phase sample (5 µl) were injected onto the C8 column. The column mobile phase was held at 50% solvent B for 0.5 min followed by an increase from 50%-100% solvent B over 0.5-6.5 min. The mobile phase was then held at 100% B for 3.5 min. Between 10 and 10.25 min the mobile phase was returned to 50% B held for 3.75 min to re-equilibrate the column. The total UPLC cycle was 14 min and the eluent flow rate was 600 µl/min.

2.8.3 Tandem Mass Spectrometry Method

Tandem mass spectrometry was used for the identification of selected lipids. MS/MS runs were performed using ESI+ mode and collision energies of 16, 18, 20, 25, 28 V and a mass range of 80-1500 m/z. Other conditions were as described in section **2.8.1**.

2.8.4. Processing Liquid Chromatography-Mass Spectrometry Data

Data was processed using Micromass Markerlynx Applications Manager (Waters Corporation). Each peak was detected, deconvoluted, noise-reduced and integrated. The ion-intensities for each peak are detected and normalised. Individual peaks were normalised to the total integrated area of the sample. Lipids were identified using the tandem mass spectrometry data.

2.9. Analysis by Direct Infusion-Mass Spectrometry

Direct infusion mass spectrometric analysis was performed using a Thermo Finnigan LTQ linear ion trap mass spectrometer equipped with a Finnigan Surveyor pump and Finnigan Micro AS Autosampler (Thermo Scientific, Waltham, MA).

2.9.1. Sample Preparation

2.9.1.1 3T3-L1 adipocytes

The 3T3-L1 organic phase samples for DI-MS were reconstituted in 500 µl methanol:tetrahydrofuran (THF) (2:1 v/v). 100 µl of each sample was added to a 96 well plate.

2.9.1.2 Liver tissue

The liver organic phase samples for DI-MS were reconstituted in 500 µl methanol:THF (2:1 v/v). 50 µl of each sample was aliquoted into a 96 well plate where the samples were diluted by the addition of a further 150 µl methanol:THF (2:1 v/v).

2.9.1.2 White adipose tissue

The white adipose tissue organic phase samples for DI-MS were reconstituted in 1 ml methanol:THF (2:1 v/v). 60 µl of each sample was aliquoted into a 96 well plate where the samples were diluted by the addition of a further 600 µl methanol:THF (2:1 v/v).

2.9.2. Direct Infusion and Mass Spectrometry Parameters

The infusion solvent (methanol-THF, 2:1 v/v) was initially pumped at 50 µl/min. The sample (10 µl) was introduced via infusion and the flow rate maintained at 50 µl/min for 1.2 min. Flow rate was then increased to 300 µl/min for 0.8 min and returned to 50 µl/min prior to the next injection. Infused sample was introduced to, and ionised in, a standard electrospray source with sheath gas flow of 12 units, auxiliary gas flow of 1 unit and sweep gas flow of 1 unit, capillary temperature of 290 °C, and spray voltage of 5 kV. The capillary and tube lens voltages for positive mode analysis were set to 40 and 80 V, respectively. In negative mode the capillary voltage was -50 V; the tube lens voltage was set to -200 V. The scan range was set at 100-1100 m/z in profile mode. To ensure analytical reproducibility samples were analyzed either in triplicate or duplicate using both positive and negative ionisation modes, a pooled sample and a blank sample were also analysed every 6 injections.

2.9.3. Processing of Direct Infusion Mass Spectrometry Data

DI-MS chromatograms were processed using Xcaliber (version 2.0; Thermo Electron). The mass data was averaged from the chromatogram for the period of sample injection and the “exact masses” were exported; the data points summed between M and M+1, to give variables which corresponded to individual peaks, normalised to total spectral area and integrated.

2.9.4. MS/MS Method

MS/MS data was utilised for lipid identification. MS/MS data was collected by infusing a pooled sample by syringe pump at a flow rate of 15 µl/min. Centroid mode was used with a scan width of 100 *m/z* to 1000 *m/z* and a parent mass step value of 1 *m/z*. The isolation width was 1.5 *m/z* and the collision energy was 35 eV; all other parameters were as outlined in section **2.9.2**.

2.10 Transcriptomic Analysis

2.10.1. RNA Extraction

Cells were grown, treated with PPARδ agonist or PPARγ agonist and collected as has already been described in sections **2.1.1**, **2.1.3**, **2.1.4** and **2.1.6.** An RNeasy RNA extraction and purification kit was used to extract total RNA from 3T3-L1 adipocytes (Qiagen GmbH, Hilden, Germany). Approximately 5mg of cells was used per sample for RNA isolation. Procedures were carried out according to the manufacturer's instructions. Extracted RNA was quantified using a Nanodrop ND-1000 Spectrometer (Nanodrop Technologies Inc., Wilmington, USA) to measure the absorbance at 260 nm. Sample purity was assessed using the A_{260}/A_{280} ratio. Samples with an A_{260}/A_{280} ratio above 1.8 were considered sufficiently pure.

2.10.2. Microarray Analysis

Transcriptomic analysis was conducted by Cambridge Genomic Centre for Microarray Resources (Cambridge Genomic Services, Department of Pathology, University of Cambridge). An automated Illumina Infinium Gene Expression BeadArray (Illumina Inc, San Diego, CA) was used to perform mRNA transcriptional profiling. A mouse WG6 array platform was used with 45281 probes.

2.10.3. Processing Microarray Data

Quality control was carried out using the arrayQualityMetrics R package and no samples failed or were identified as outliers to their replicates. Statistical selection was performed using the detection p-value provided by Illumina. This value represents the confidence that a given transcript is expressed above the background defined by the negative control probe. The R package lumi was used for this analysis [191]. The detection p-value threshold was set to 0.01. Probes were required to be successfully detected (p-value<0.01 in Lumi) in at least one sample to pass the selection. The data is transformed using variance stabilisation and then normalised using quantile normalisation[192]. Gene expression was compared between PPARδ agonist treated, PPARγ agonist treated and control 3T3-L1 cells using the R package limma[193]. The threshold utilised in this analysis was the 5% confidence interval. The selected and normalised data was then analysed using the multivariate statistics in the Simca-P+ package as is described in section **2.11**. The 6% of transcripts most responsible for separation in the multivariate models were then examined (3% most increased and 3% most decreased in PPARδ agonist treated cells as identified in the multivariate models).

The Reactome Skypainter tool (www.reactome.org) was used to determine which biological pathways were statistically significant in the 3% of genes most increased and most decreased in transcription in PPAR agonist treated cells. From a given set of genes known to participate in a pathway, the total genes for mus musculus and the submitted list of genes (the genes increased or decreased in expression in PPAR activated cells) of which N genes participate in the given pathway, the probability of observing at least N genes from a pathway if that pathway is not overrepresented in the submitted list of genes is calculated using the one-tailed version of Fisher's exact test. Therefore a p-value smaller than or equal to the significance level suggests that the pathway is statistically significant in the submitted list of genes.

2.11 Data Handling for Metabolomics

2.11.1. Pretreatment of Metabolomic Data for Multivariate Analysis

Pretreatment is often applied to metabolomic data preceding multivariate analysis. The pretreatment of the data usually takes the form of mean centring and scaling. Mean centring involves the calculation of the mean of each variable, which is then subtracted from the variable values for each observation; centring all variables to a mean value of 0. The manipulation is employed in the majority of chemometrics to centre data in scores plots.

Scaling ensures models are not excessively influenced by variables with large ranges as these typically have larger degrees of variance relative to variables possessing smaller ranges and functions by multiplying the data by a specific scaling weighting. The scaling weighting utilised is dependent upon the nature of the data being analysed.

Pareto scaling is used when there is some knowledge of the relative importance of variables within a dataset, for example when analytical noise has been included in a data set and lower weighting needs to be given to these variables; a scaling weight of $1/(S_k)^{1/2}$, S_k being the standard deviation of the variable k, is used in this instance and therefore scales each variable k to the variable's standard deviation. Within metabolomic studies Pareto scaling increases the importance of low concentration metabolites without greatly magnifying the contribution of noise in the subsequent multivariate model.

Univariant scaling is used in the case of data where little is known about the importance of the variables within the data; the variance of each variable is standardised to 1 by multiplying each variable by the scaling weight $1/S_k$. Thus, the influence of any one variable is limited by the scaling and in metabolomic study prevents a single metabolite dominating a data set.

The multivariate analysis in this thesis was conducted by importing the normalised data generated from the analytical platforms into SIMCA-P+ version 11 (Umetrics, Umeå, Sweden). Data was mean centred and scaled. GC-MS data in this thesis was scaled utilising unit variance, ensuring all peaks contribute to the multivariate models generated, as only identified peaks were incorporated into the data sets. Since the bucketing routine used in the processing of NMR data incorporates baseline noise in the data set, Pareto scaling was used for the analysis of 1-dimensional ^{1}H-NMR data; this assigns a lesser weighting to the noise variables. Pareto scaling was also employed for the analysis of LC-MS and DI-MS data.

2.11.2. Multivariate Statistical Analysis: Principal Component Analysis

PCA is a multivariate projection method and an unsupervised technique where a single covariance matrix contains the values for all the variables measured. PCA reduces the dimensionality of multidimensional data sets while the characteristics of the data that are most responsible for variance are retained; via a transformation a data set of dimension N is reduced to dimension M. In PCA correlated variables are transformed into uncorrelated variables called principal components (PCs). Each observation is plotted in k-dimensional space, each dimension corresponding to an individual variable. Each principal component represents a vector within k-dimensional space. PC 1 would represent the greatest variance in the dataset, PC 2 the second most variance, and so forth. The principal components must intercept the origin and have the minimal square of the distance between each observation and itself. The observations are projected onto the principal components to generate a coordinate; this value is the score, t_1, for PC 1 or t_2 for PC 2. PC 1 and PC 2 are orthogonal and so define a plane in the data (**Figure 2.1**). Clustering of observations can be seen when their scores are plotted.

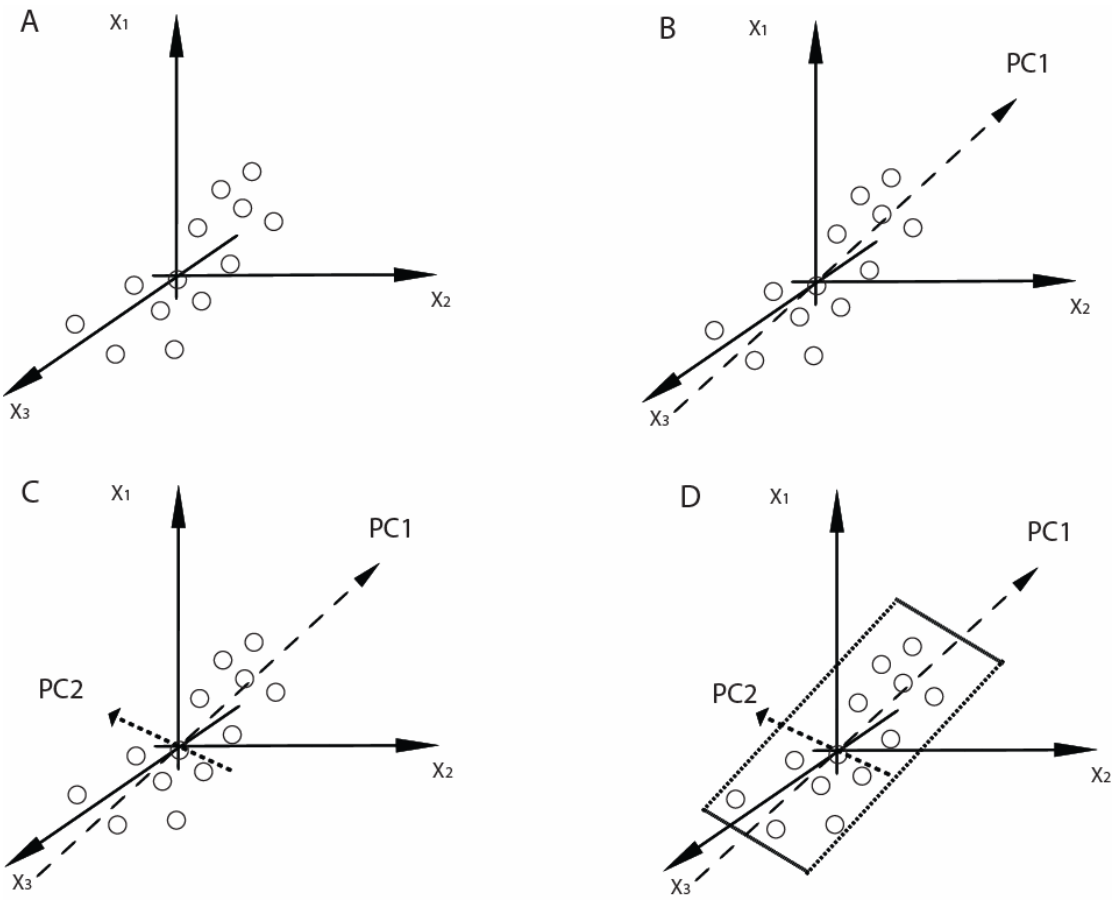

Figure 2.1: **A.** Mean centered observations in the data matrix are plotted in the variable (k-dimensional) space. **B.** The first principal component, PC1, represents the maximum variance direction in the data. Each observation is projected onto the PC to obtain a co-ordinate. The co-ordinate value is the score. **C.** A second principal co-ordinate, PC2 is oriented through the average point and orthogonal to PC1 to represent the second largest variation in the data set. **D.** Two PCs generate a plane in the variable space. By projecting each observation onto the plane the scores can be visualised graphically in a scores plot.

Clustering of data is shown in the scores plots but in order to examine which variables generate the differences in clustered groups a loadings plot is needed. Loadings are Eigenvectors generated from an Eigen transformation of the variables in the original covariance matrix. Loadings describe the orientation of the PCs in the multidimensional space, and thus the contribution of a variable to the separation of clusters depends on its distance from the origin of the loadings plot. Directionality of PC can therefore be

explained by the cosine of the angle between PC 1 and each variable and loadings coefficients can be generated for each PC (**Figure 2.2**). An alternative means of viewing loadings is with coefficient column plots in which the contribution of each variable to a model is represented by the size of the bar and error bars indicate the significance of changes to a set confidence limit.

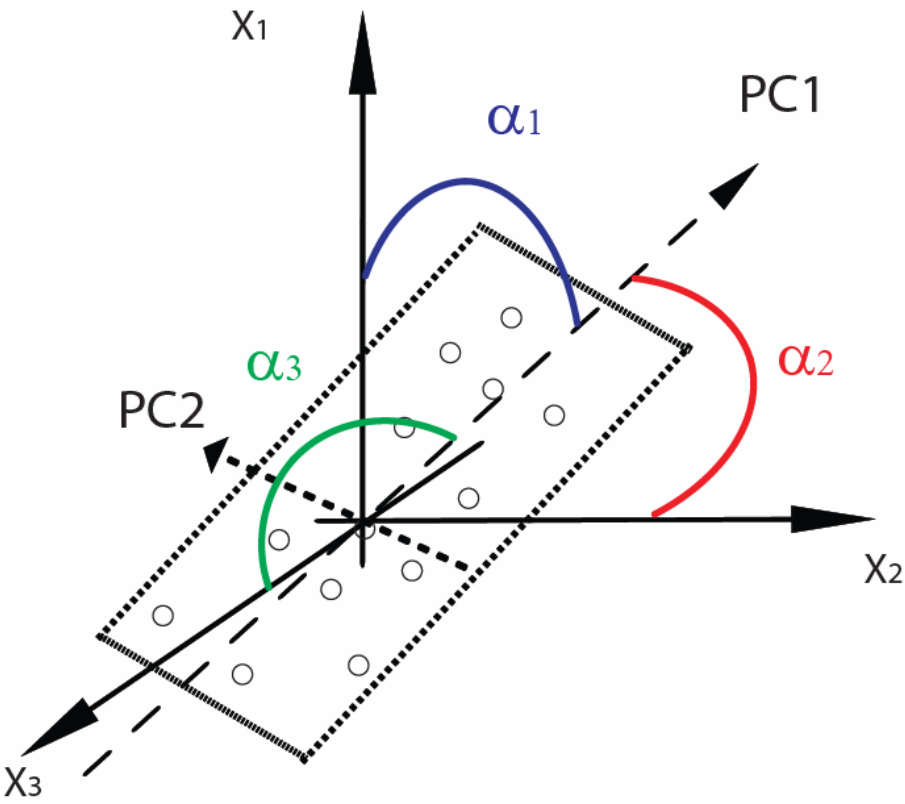

Figure 2.2: PC loadings express the orientation of the model plane in k-dimensional space. The cosine of the angles α_1, α_2, and α_3 gives the direction of PC1 in relation to the original variables. These values demonstrate how the variables X_1, X_2 and X_3 contribute to PC1. An additional set of loading coefficients express the direction of PC2 in relation to the original variables. Therefore, six loading values (cosine of angles) describe the model planes orientation in the k-dimensional space.

2.11.3 Multivariate Statistical Analysis: Projection to Latent Structures by Partial Least Squares

PLS constitutes a regression analysis of PCA, modelling the covariance of a relationship between two sets of variables termed X and Y. Each observation corresponds to a point

in X-space and a point in Y-space. A PLS component represents a line in the X-space which describes maximum variance while concurrently correlating with the Y-vector. The scores in the X-space are attained by projection onto the PLS components; for PLS component 1 the vector t_1 is generated, for PLS component 2 the vector t_2 is generated. The scores are latent variables used to explain the Y variable.

During metabolomics studies it is important to establish which variables, and therefore metabolites, are most significantly contributing to the model; this is achieved by cross-examining both the X-variable weight vectors, known as w^* , which describe how x-variables are linearly combined forming the X score vectors and the Y-variable weight vectors, c.

Traditionally the contribution of a variable to a PLS model is summarised using two methods. The variable influence on projection (VIP) parameter is a weighted sum of squares of PLS weights (w^*), taking account of the residual variation in Y, per dimension. The second method involves plotting the regression coefficients, indicating how the X variables influence Y. A variable with a coefficient that has a confidence limit above 95% is statistically significant in explaining Y.

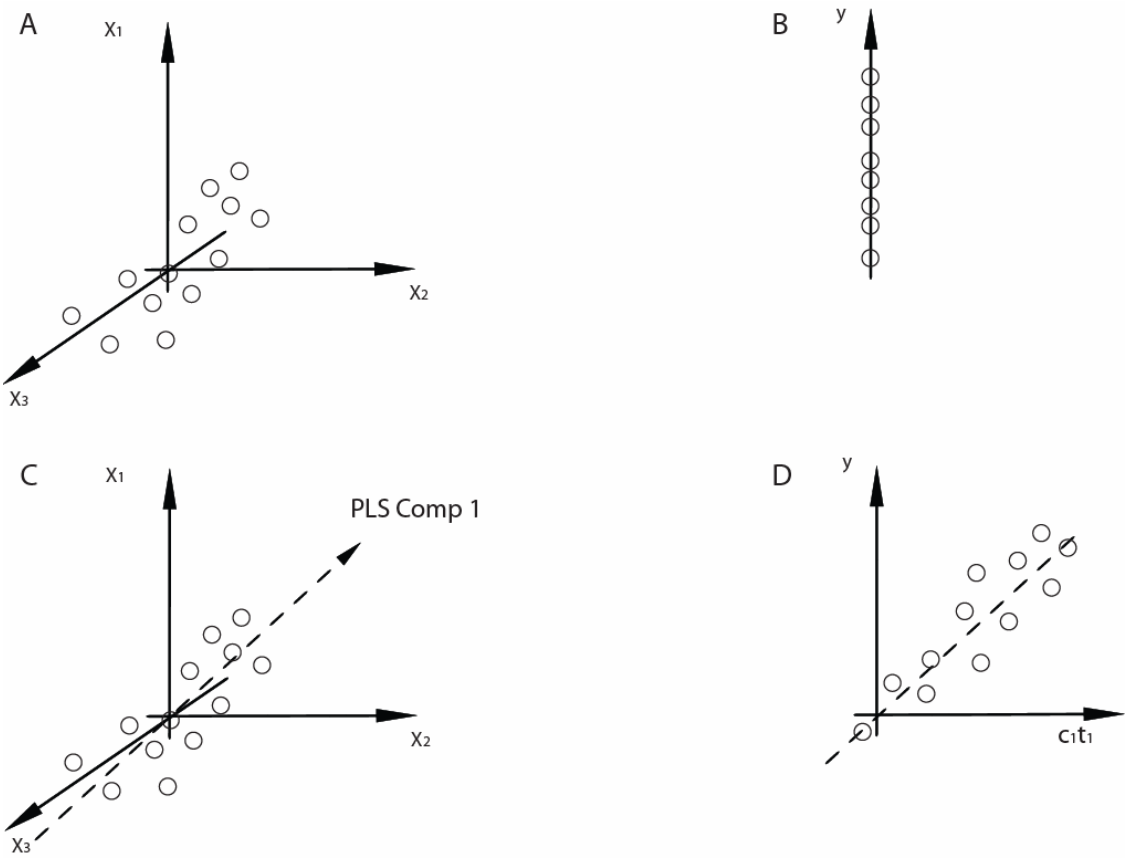

Figure 2.3: PLS analysis. **A.** Observations are plotted in x-dimensional space **B.** The observations are simultaneously plotted in y-dimensional space, which is reduced to a 1-dimensional y-vector. **C.** PLS component 1 is calculated, modelling the distribution of the observations in the x-dimensional space whilst providing correlation with the y-vector. When observations are projected onto the PLS component they receive a t-score; the t-scores taken together give the score vector t_1 **D.** Multiplying t_1 by the weight of the y vector, c_1 gives an estimate of y. The difference in the y values and the estimated y values can be modelled by employing additional PLS components.

2.11.4 Multivariate Statistical Analysis: Partial Least Squares-Discriminant Analysis

PLS-DA is a supervised extension of PCA which uses prior knowledge of class membership and regression trends to augment the separation between groups. Class membership is assigned using an artificial Y matrix with *N* columns, where *N* is the

number of classes. The column corresponding to a particular class contains ones whilst all other columns contain zeros for observations that belong to that specific class. PLS-DA components represent projections in the X-space that optimise separation between the projected observations based on class. Metabolomic investigation establishes which metabolites contribute most significantly to separation in the models by concurrently investigating the corresponding weights for the X-matrix (w^*) and Y matrix (c).

2.11.5 Validation of Multivariate Models

Validation of multivariate models requires examination of the model dimensionality. This is calculated by the degree of variation described by a model, and by the accuracy with which a model can predict the X data.

For both PLS-DA and PCA the variation in the model given by a component is known as R^2. The term R^2 is defined as $R^2=1\text{-}RSS/SXX_{tot.corr.}$ where RSS is the residual sum of squares of the data from the component and $SXX_{tot.corr.}$ is the total variation in the X matrix post mean centring. If the R^2 was 1 that would indicate the total variation in the data matrix had been explained by the model.

Validation of PLS models generates two R^2 values defined as R^2X and R^2Y, describing the variation the model explains in the X matrix and the Y matrix. By increasing the components in a model, the R^2 can be increased though this risks over-fitting the model making it statistically insignificant; this can be avoided by cross validating the model.

The term Q^2, defined as $Q^2=1\text{-}PRESS/SXX_{tot.corr.}$, where PRESS is the sum of the squared differences between the predicted and real values (predictive residual sum of squares) is used as an indicator of the predictive nature of the model. For every successive component built for a model the cross validation is calculated up to the point where generation of new components no longer improves the model's predictive power. Significantly predictive models are considered to have Q^2 values greater than 0.4.

Outliers are readily identified in multivariate analysis; significantly deviant observations will be obvious in scores plots as the plots contain an ellipse which indicates the 95% confidence interval established using a multivariate generalisation of the Student's t-test known a *Hotelling's* T^2. The outliers can also be identified using the distance to model in X space defined as DModX; this equals the residual standard deviation of an observation. When DModX is larger than the D_{crit} (>95%) then the observation is a moderate outlier.

2.11.6 Multivariate Statistical Analysis Methodology

PCA models within this thesis were generated in SIMCA-P+11.0 (Umetrics AB, Umeå, Sweden) to indentify the major trends and outliers in the datasets. The supervised techniques PLS-DA and, where appropriate, PLS were utilised to examine differences between specific groups and probe the metabolic changes producing the separation between groups. Metabolites identified in the VIP/coefficients plots were deemed to have changed globally if they contributed to separation in the models with a confidence limit of 95% or greater as determined by a jack-knifing routine within the SIMCA package. To assess the variation explained by each model the R^2 values were used. In order to assess the robustness of the predictive nature of the models, Q^2 values were used. The SIMCA-P+ validation function was also employed to monitor that PLS-DA and PLS models were not over fitted.

2.11.7 Univariate Statistical Analysis Methodology

Gas Chromatography-Mass Spectrometry ^{13}C labelled substrate, clinical chemistry data and selected microarray transcriptomic data was analysed by univariate techniques. Univariate analysis was performed using an unpaired Student's t-*t*est with a significance level set to $p<0.05$. An F-test was also utilised to compare the variance of two distributions. All univariate analysis was conducted in the GraphPad Prism package (version 4).

Chapter 3

Metabolic Phenotyping of a Model of Adipocyte Differentiation

3.1 Introduction

The 3T3-L1 murine cell line was developed by Green and co-workers and is a derivative of the 3T3 mouse fibroblast cell line[194, 195]. It was found that, if 3T3-L1 cells were allowed to reach a resting condition in a confluent state the cells develop an adipocyte phenotype. This cell-line has become a well established and widely used model for the study of the biochemical processes undergone during mammalian adipogenesis. In the preconfluent state 3T3-L1 cells morphologically and biochemically resemble fibroblasts[196, 197]. However, once the cells reach 100% confluency they can be differentiated into mature adipocytes by initial treatment with insulin, which activates the IGF-1 receptor, dexamethasone, a synthetic glucocorticoid, and 1-methyl-3-isobutylxanthine a cyclic nucleotide phosphodiesterase inhibitor increasing cAMP and cGMP, activating cyclic nucleotide dependent protein kinases[198]. The process is robust and relatively uniform with 70-90% of cells differentiating and mirroring reactions to lipogenic/lytic hormones, morphological changes and metabolic processes observed during mammalian adipocyte development[199]. The cells accumulate TAG, acquire the rounded morphology of adipocytes and lose the ability to revert to a growth state.

A recent resurgence in the use of the 3T3-L1 adipose tissue differentiation model has accompanied expansion of research into the developing global obesity crisis. The adipocyte is not merely a lipid depository, as it was once viewed, but a key metabolic

regulator responsible for the production of cytokines, metabolic substrates and adipokines; wielding influence over metabolism both locally and on a systemic level. Adipocytes function as a secure fatty acid storage depot, capable of accumulating extensive lipid concentrations without toxic side effects to the cell itself or on the level of the whole organism. The adipocyte is now regarded as a key player in the aetiology of insulin resistance and the resultant metabolic syndrome. Once the fatty acid storage capacity of white adipose tissue is exceeded, as occurs in the obese state and certain lipodystrophies, lipid can accumulate in peripheral tissues, including the muscle and liver; a phenomenon highly correlated with lipotoxicity and insulin resistance[200]. Therefore, research has concentrated on the deregulation of metabolism within adipose tissue, which may contribute to the wider effects of TIIDM, the metabolic syndrome and obesity[201, 202, 203].

The differentiation of preadipocyte cells into mature adipocytes requires a complex interaction of metabolic pathways that as yet remain to be fully defined. A diverse range of pathways have been implicated as vital to the differentiation process including polyamine biosynthesis[204], essential fatty acid pathways[205], eicosanoid biosynthesis[206], fatty acid desaturation[207] as well as fatty acid synthesis[208] and the TCA cycle[209]. Many of these pathways may be critical to differentiation at specific points during the process, either being perturbed by a process associated with differentiation or alternatively providing metabolic cues to induce other processes.

3.2 Aims and Objectives

In this study, the metabolic changes associated with adipocyte differentiation of the 3T3-L1 cell line have been studied using combined GC-MS, ^{1}H-NMR spectroscopy, LC-MS, DI-MS and ^{13}C substrate labelling detected by HSQC NMR and GC-MS in conjunction with multivariate statistics. The metabolic changes identified were then compared and contrasted to the metabolic differences between pre- and post-differentiation primary adipocytes observed using GC-MS and LC-MS. The changes in metabolite concentrations at distinct periods during differentiation have been defined including alterations in the TCA cycle, glycolysis, the production of odd chain fatty acids by α-oxidation, fatty acid synthesis, fatty acid desaturation, polyamine biosynthesis and trans-esterification to produce complex lipids. These metabolic alterations reflect the changing role of the 3T3-L1 cells during differentiation, as well as possibly providing metabolic triggers to stimulate the processes which occur during differentiation. Defining the metabolic phenotype of differentiating 3T3-L1 preadipocytes, as they mature into adipocyte cells and comparing this to differentiating murine primary cells using metabolomics has generated a metabolically phenotyped *in vitro* model of adipose tissue.

3.3 Materials and Methods

3.3.1. 3T3-L1 Adipocyte Cell Culture

3T3-L1 preadipocytes were grown and differentiated as described in **Chapter 2 Materials and Methods** (section 2.1.1 *3T3-L1 cell culture and adipocyte differentiation*). The T75 flasks were assigned to groups of 3 flasks each corresponding to 0 h, 2 h, 4 h, 8 h, 16 h, 24 h, 72 h, 120 h and 216 h time points during the differentiation process.

3.3.2. Primary Adipocyte Cell Isolation and Differentiation

Primary preadipocytes were isolated from the gonadal fat pad of mice and differentiated as described in **Chapter 2 Materials and Methods** (section 2.1.2 *Primary adipocyte cell isolation and differentiation*). One mouse was used per 28 cm^2 well. Five wells were collected as undifferentiated preadipocytes. Three wells were fully differentiated up to day 7.

3.3.3. Oil Red O Staining and Intracytoplasmic Lipid Accumulation

Three additional T75 flasks of 3T3-L1 adipocytes were grown per 0 h, 2 h, 4 h, 8 h, 16 h, 24 h, 72 h, 120 h and 216 h time point group (as in section 3.3.1). The cells were stained and the intracytoplasmic lipid accumulation assessed as in **Chapter 2 Materials and Methods** (section 2.1.5 *Oil Red O staining and intracytoplasmic lipid accumulation*).

3.3.4. 3T3-L1 and Primary Adipocyte Cell Collection and Metabolite Extraction

3T3-L1 cells were collected at 0 h, 2 h, 4 h, 8 h, 16 h, 24 h, 72 h, 120 h and 216 h time points following the initiation of differentiation. Primary cells were collected at 0 h and 168 h. 5 mg 3T3-L1 cell pellets and 1 mg primary cell pellets were used for the extraction process. The cells were collected and their metabolites extracted as described in **Chapter**

2 Materials and Methods (sections 2.1.6 and 2.3 *Adipocyte cell collection* and 3T3-L1 cell, primary adipocyte and tissue metabolite extraction).

3.3.5. ^{1}H-NMR Spectroscopy Analysis

All samples were analysed using a Bruker AVANCE II+ spectrometer operating at 500.13 MHz for the ^{1}H frequency using a 5 mm Broadband TXI Inverse ATMA probe. All procedures are as depicted in **Chapter 2 Materials and Methods** (sections 2.6.1. *Spectrometer*, 2.6.2. *Sample preparation*, 2.6.3. *1-dimensional ^{1}H-Nuclear Magnetic Resonance experimental method* and 2.6.4. *Processing 1-dimensional ^{1}H-Nuclear Magnetic Resonance data*).

3.3.6. GC-MS Analysis

The aqueous phase of extracts were derivatised as described in **Chapter 2 Materials and Methods** (section 2.7.1).

The organic phase of extracts were derivatised as described in **Chapter 2 Materials and Methods** (section 2.7.2).

GC-MS analyses were made using a Trace GC Ultra coupled to a Trace DSQ II single-quadrupole mass spectrometer. Parameters for the GC-MS analysis of aqueous phase metabolites and organic phase metabolites were as described in **Chapter 2 Materials and Methods** (sections 2.7.3.1 *Gas Chromatography-Mass Spectrometry methods for aqueous phase samples* and 2.7.3.2 *Gas Chromatography-Mass Spectrometry methods for organic phase samples*). Derivatised aqueous phase samples were injected splitless and organic phase samples were injected with a split ratio of 25.

GC-MS chromatograms were processed using Xcaliber (version 2.0; Thermo Electron) as outlined in **Chapter 2 Materials and Methods** (2.7.5. *Processing Gas Chromatography-Mass Spectrometry data*).

3.3.7. UPLC-MS Analysis

Chromatography was performed using an ACQUITY UPLC® system equipped with an Acquity UPLC 1.7 µm BEH C8 column (2.1×100 mm) coupled to a Micromass QTof-*Ultima* with a Z-spray electrospray source. All chromatography and mass spectrometric parameters were as outlined in **Chapter 2 Materials and Methods (**section 2.8.1. *Chromatography and mass Spectrometry parameters*)

The organic phase of the extracts were reconstituted in methanol-chloroform (2:1, 1 ml). Aliquots of diluted organic phase sample (5 µl) were injected onto the C8 column. The column mobile phase was held at 50% solvent B for 0.5 min followed by an increase from 50%-100% solvent B over 0.5-6.5 min. The mobile phase was then held at 100% B for 3.5 min. Between 10 and 10.25 min the mobile phase was returned to 50% B and held for 3.75 min to re-equilibrate the column. The total UPLC cycle was 14 min. The eluent flow rate was 600 µl/min.

Tandem mass spectrometry procedures were as described in **Chapter 2 Materials and Methods** (2.8.3 *Tandem mass spectrometry method*).

Data was processed using Micromass MarkerLynx Applications Manager as depicted in **Chapter 2 Materials and Methods** (2.8.4. *Processing Liquid Chromatography-Mass Spectrometry data*).

3.3.8. Direct Infusion Mass Spectrometry

Direct infusion mass spectrometric analysis was performed using a Thermo Finnigan LTQ equipped with a Finnigan Surveyor pump and Finnigan Micro AS Autosampler.

The organic phase samples for DI-MS were reconstituted in 500 µl methanol:THF (2:1 v/v). 100 µl of each sample was added to a 96 well plate. Samples were analyzed in duplicate using both positive and negative mode. All other direct infusion and mass

spectrometric parameters were as described in **Chapter 2 Materials and Methods** (section 2.9.2. *Direct infusion and mass spectrometry parameters*).

DI-MS chromatograms were processed using Xcaliber as outlined in **Chapter 2 Materials and Methods** (2.9.3. *Processing of direct infusion mass spectrometry data*).

3.3.9. Multivariate Analysis

Multivariate data analysis was performed using SIMCA-P^+ 11.0 (Umetrics AB, Umeå, Sweden). NMR, DI-MS and UPLC-MS data sets were mean-centered and Pareto-scaled prior to analysis. GC-MS data sets were scaled to UV. Data sets were analyzed using PCA, PLS and PLS-DA. Further details are summarised in **Chapter 2 Materials and Methods** (section 2.11.6 *Multivariate Statistical Analysis Methodology*).

3.3.10. ^{13}C-glucose Substrate Labelling Study

At 2 days post differentiation media was removed from the T75 flasks and replaced with DMEM (10% (v/v) FBS, 50 units/ml penicillin, and 50 µg/ml streptomycin) and either 4.5 g/l ^{12}C unlabelled glucose (n=6) or 4.5 g/l 1-^{13}C-glucose (n=7).

After 2 days cells were collected and metabolites extracted as previously described in **Chapter 2 Materials and Methods** (sections 2.1.6 and 2.3 *Adipocyte cell collection* and *3T3-L1 cell, primary adipocyte and tissue metabolite extraction*). Two-dimensional HSQC ^{13}C-Nuclear Magnetic Resonance spectroscopy was performed on the samples using the methodology in **Chapter 2 Materials and Methods (**2.6.5. *2-dimensional Heteronuclear Single-Quantum Coherence ^{13}C-Nuclear Magnetic Resonance experimental method*).

GC-MS analysis of organic and aqueous phases, processing and analysis was also carried out as previously described in **Chapter 2 Materials and Methods** (section 2.7.4. Gas

Chromatography-Mass Spectrometry analysis, processing and data handling for 3T3-L1 adipocyte ^{13}C labelled substrate studies).

3.3.11. ^{13}C-palmitate Substrate Labelling Study

^{13}C labelled and unlabelled palmitate solutions were prepared as is summarised in **Chapter 2 Materials and Methods** (section 2.4.3. *Preparation of ^{13}C and ^{12}C palmitate solution*).

At 2 days post-differentiation media was removed from the T75 flasks and replaced with DMEM (serum free, 50 units/ml penicillin, and 50 µg/ml streptomycin) and either 70 µM unenriched palmitate (n=6) or 70 µM U-^{13}C labelled palmitate (n=6).

After 2 days cells were collected and metabolites extracted as previously described in **Chapter 2 Materials and Methods** (sections 2.1.6 and 2.3 *Adipocyte cell collection* and *3T3-L1 cell, primary adipocyte and tissue metabolite extraction*).

GC-MS analysis of organic and aqueous phases was also carried out as previously described in **Chapter 2 Materials and Methods** (section 2.7.4. Gas Chromatography-Mass Spectrometry analysis, processing and data handling for 3T3-L1 adipocyte ^{13}C labelled substrate studies).

3.4 Results

3.4.1. 3T3-L1 Adipocytes

High resolution ^{1}H-NMR spectroscopy, GC-MS, LC-MS and DI-MS analysis, combined with multivariate pattern recognition were used to profile metabolism within differentiating 3T3-L1 murine cells. The combination of these analytical tools was used in order to maximise the coverage of the metabolome within the cells. High resolution ^{1}H-NMR spectroscopy detected 25 identifiable metabolites. GC-MS detected 100-150 defined peaks from aqueous phase samples and 60-70 defined peaks from organic phase samples. Matching the mass spectra detected with those held in the NIST/ EPA/ NIH mass spectral library identified 60% of metabolites for aqueous extracts and 65% for lipids. Of the species detected using DI-MS negative mode ionisation that contribute to separation in the multivariate models 40% (~150) were identified both in terms of lipid class and their fatty acyl moieties. Of the species detected using LC-MS that contribute to separation in the multivariate models 60% were identified using MS/MS.

Across all multivariate models used to examine the individual spectra/chromatograms a similar trend in the separation of time points was detected where by the earliest time points showed only subtle variation before diverging steadily up to 24 h. This trend for the first 24 h was along PC 2 which represents the second most amount of correlated variation detected in the dataset. Significant separation then occurs for the latter time points (24-120 h) along PC 1, which represents the most amount of correlated variation detected in the dataset. By 216 h clustering along component 2 has returned to a position similar to the earliest time points; however separation along component 1 remained altered (**Figure 3.1**).

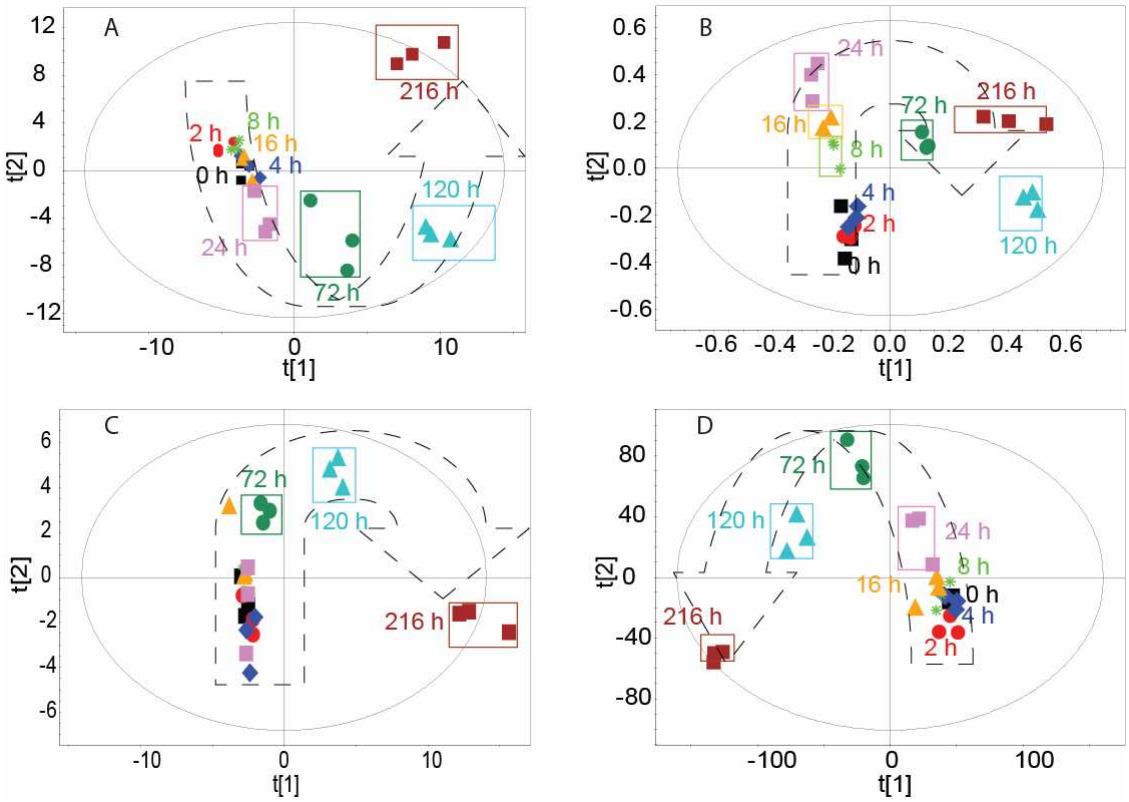

Figure 3.1: **A.** PLS scores plot showing clustering of aqueous phase metabolites analyzed by GC-MS extracted from 3T3-L1 cells at 0 h, 2 h, 4 h, 8 h, 16 h, 24 h, 72 h, 120 h and 216 h time points during the differentiation process. (R^2=0.63, Q^2=0.97). The PLS model was formed by cross correlating the metabolic profile (X variables) against the time of differentiation (Y variable). **B.** PLS scores plot showing clustering of aqueous phase metabolites analyzed by ^{1}H-NMR extracted from 3T3-L1 cells at 0 h, 2 h, 4 h, 8 h, 16 h, 24 h, 72 h, 120 h and 216 h time points during the differentiation process. (R^2=0.99, Q^2=0.97). The PLS model was formed by regressing against time. **C.** PLS scores plot showing clustering of organic phase metabolites analyzed by GC-MS extracted from 3T3-L1 cells at 0 h, 2 h, 4 h, 8 h, 16 h, 24 h, 72 h, 120 h and 216 h time points during the differentiation process. (R^2=0.99, Q^2=0.98). The PLS model was formed by regressing against time. **D.** PCA scores plot showing clustering of metabolites analyzed by LC-MS extracted from 3T3-L1 cells at 0 h, 2 h, 4 h, 8 h, 16 h, 24 h, 72 h, 120 h and 216 h time points during the differentiation process. (R^2=0.73, Q^2=0.61).

3.4.1.1 3T3-L1 preadipocyte differentiation and intracytoplasmic lipid accumulation

Oil red O stained images of the differentiating cells demonstrated that the cells maintained a fibroblastic like morphology for the early time points. By 16 h a number of

cells had altered their morphology to a more rounded phenotype. By 120 h the cells were beginning to resemble adipocytes and accumulate lipid as indicated by the stain. The staining for the final time point showed mature 3T3-L1 cells with a rounded morphology and lipid containing vesicles; 75 percent of the total number of cells differentiated (**Figure 3.2**). Spectrophotometric measurement at 510 nm of the eluted Oil Red O from the stained cells confirmed that the cells had begun to accumulate lipid by 120 h and had significantly differentiated by 216 h (**Figure 3.3**).

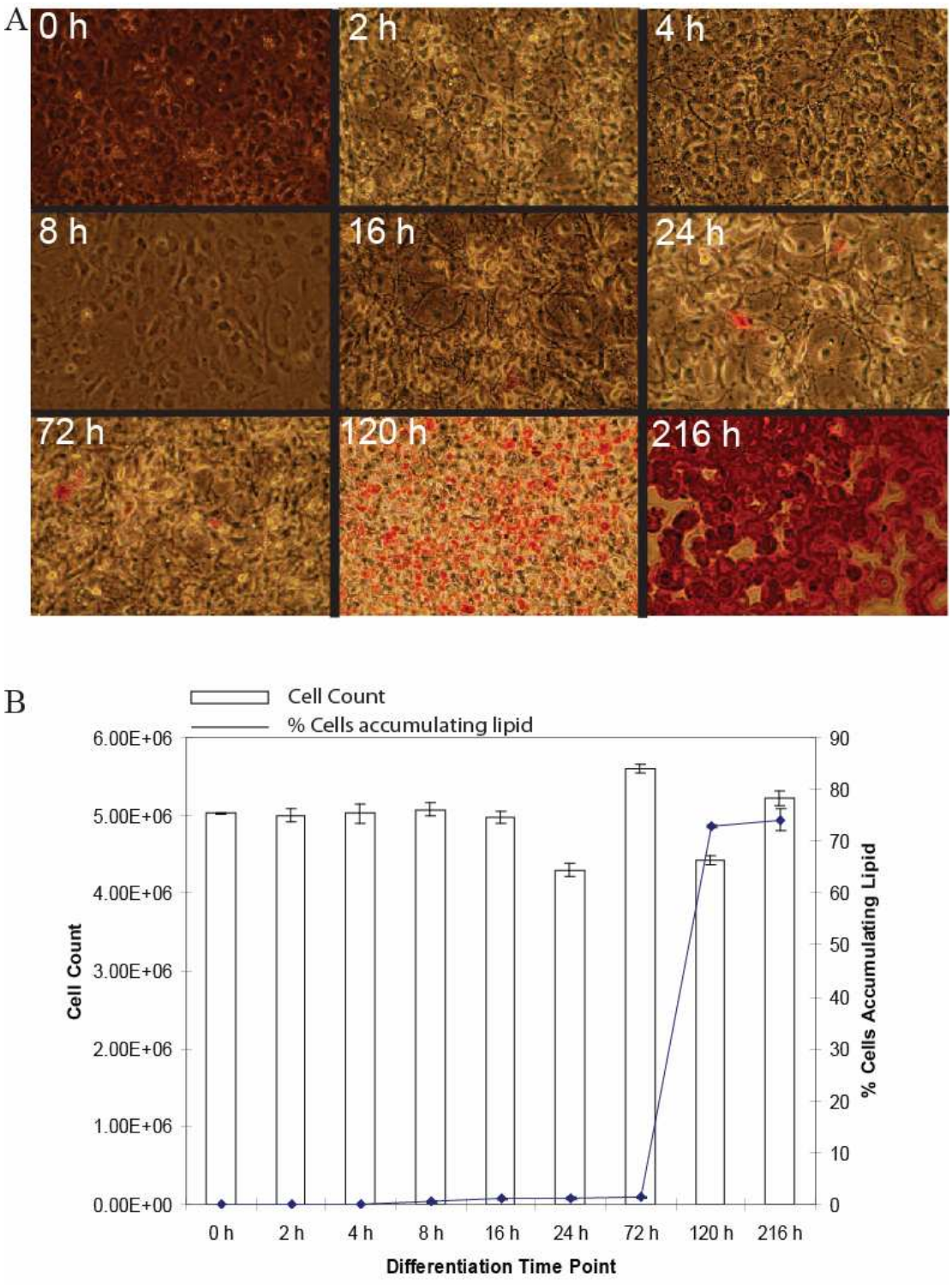

Figure 3.2: **A.** Oil Red O stained images of differentiating 3T3-L1 adipocytes at time points 0-216 h. **B.** Graph showing cell counts and the percentage of differentiating cells at time points 0-216 h.

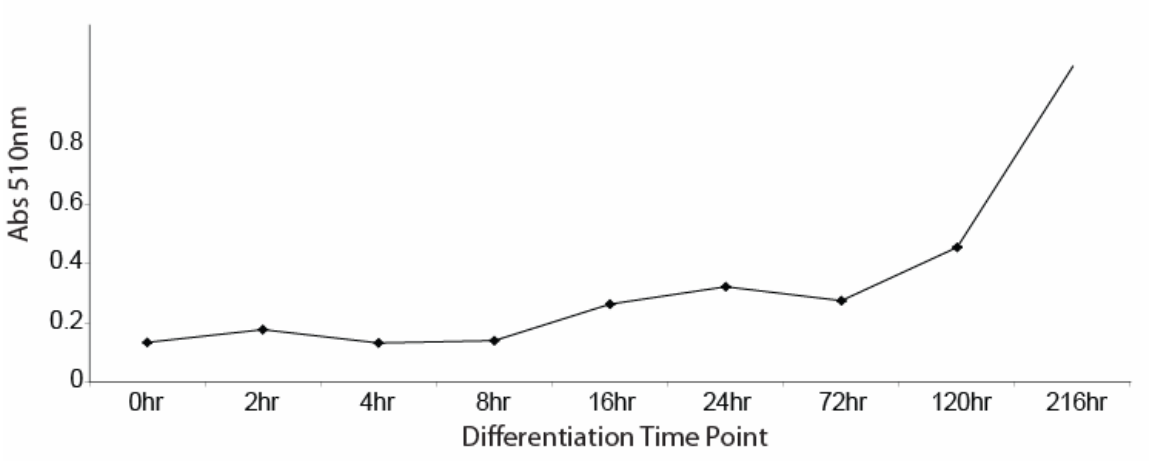

Figure 3.3: Spectrophotometric measurement at 510 nm of Oil Red O eluted from the stained cells at 0-216 h.

3.4.1.2 Total fatty acid metabolism

To establish the fatty acid content of the cell differentiation media prior to addition to the cell cultures the media was extracted and the organic phase fatty acids derivatised and analysed using GCMS (**Figure 3.4**). The media was found to contain relatively high concentrations of palmitate and stearate, however the concentrations of other even chain fatty acids was relatively low. The concentrations of odd chain fatty acids were low with only pentadecanoate and heptadecanoate detectable. Also low in concentration were the Δ9 desaturated fatty acids with only C16:1 and C18:1 detected. The media was also established as a source of the essential fatty acid linoleic acid.

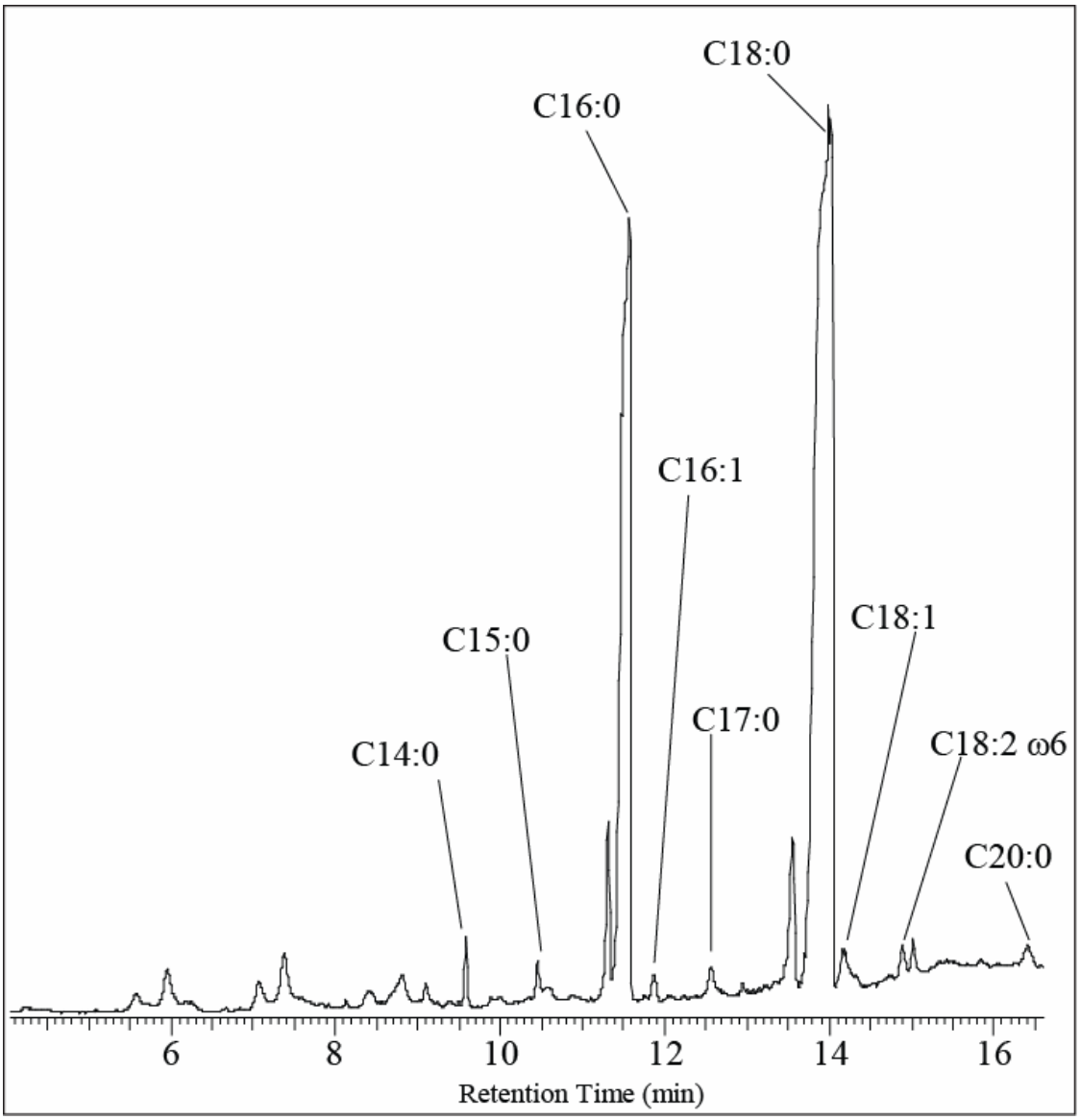

Figure 3.4: A typical GC-MS total ion chromatogram (TIC) from the analysis of methyl esterification-derivatised organic extracts from fresh media. Metabolites are identified from exact retention times and comparison of corresponding mass spectrum with the NIST database and a FAME standard mix.

The total fatty acid concentrations in 3T3-L1 cells were measured using GC-MS analysis of their methyl esterified derivatives from the organic phase of the cell extracts. Between 24-72 h, the even chained fatty acids (C8:0, 10:0, 12:0, 14:0) and the Δ9 desaturase products C14:1, C16:1 and C18:1 increased in concentration as detected by their contribution to PC 2 of the PCA model used to analyze the fatty acid methyl ester dataset.

In addition pantothenate, a key constituent of Co-Enzyme A, was detected at 72 h (**Figure 3.5 A.**) and was accompanied by a decrease in the concentration of acetate which is in part produced from the β-oxidation product acetyl-CoA. Also increased in concentration was carnitine, a key metabolite involved in fatty acid transport across the membrane of several cellular organelles. Accumulation of even chained fatty acids continued 72-120 h (C8:0, C10:0, C14:0) as detected in the loading coefficients for PC 1. In addition this increase was accompanied by an increase in odd chain fatty acids (C9:0, C11:0, C13:0, C15:0, C17:0) (**Figure 3.5 B**). The increase in the concentration of these odd chain fatty acids also pre-empted an increase in the concentration of their desaturation products (C11:1, C15:1, C17:1, C19:1) (**Figure 3.5 C**). Pantothenate and carnitine concentrations continued to increase up to 216 h whilst acetate concentrations decreased by 120 h. At 216 h a decrease in the concentration of all omega-6 fatty acid pathway intermediates and a decrease in the end products of the omega-3 pathway (5,8,11,14,17-20:5 and 4,7,10,13,16,19-22:6) were detected. At this time point there was also a continued increase in the even chain fatty acids (C8:0, 10:0, 12:0 14:0), their monounsaturated products and palmitoleate, accompanied by continued increases in odd chain fatty acids (C9:0, 11:0, 13:0, 15:0 and 17:0) and monounsaturated odd chain fatty acids (C11:1, 15:1, 17:1). The concentration of larger chain fatty acids decreased (20:0, 24:0, 24:1) across the time course. The concentration of palmitate increases between 16-24 h before decreasing, alongside stearate for the remainder of the differentiation process (**Figure 3.5 D and 3.5 E**). Accompanying the changes observed in the concentrations of the essential fatty acid pathway intermediates, the concentration of arachidonic acid esterified to phospholipids increased at 24 h and again at the 216 h time point.

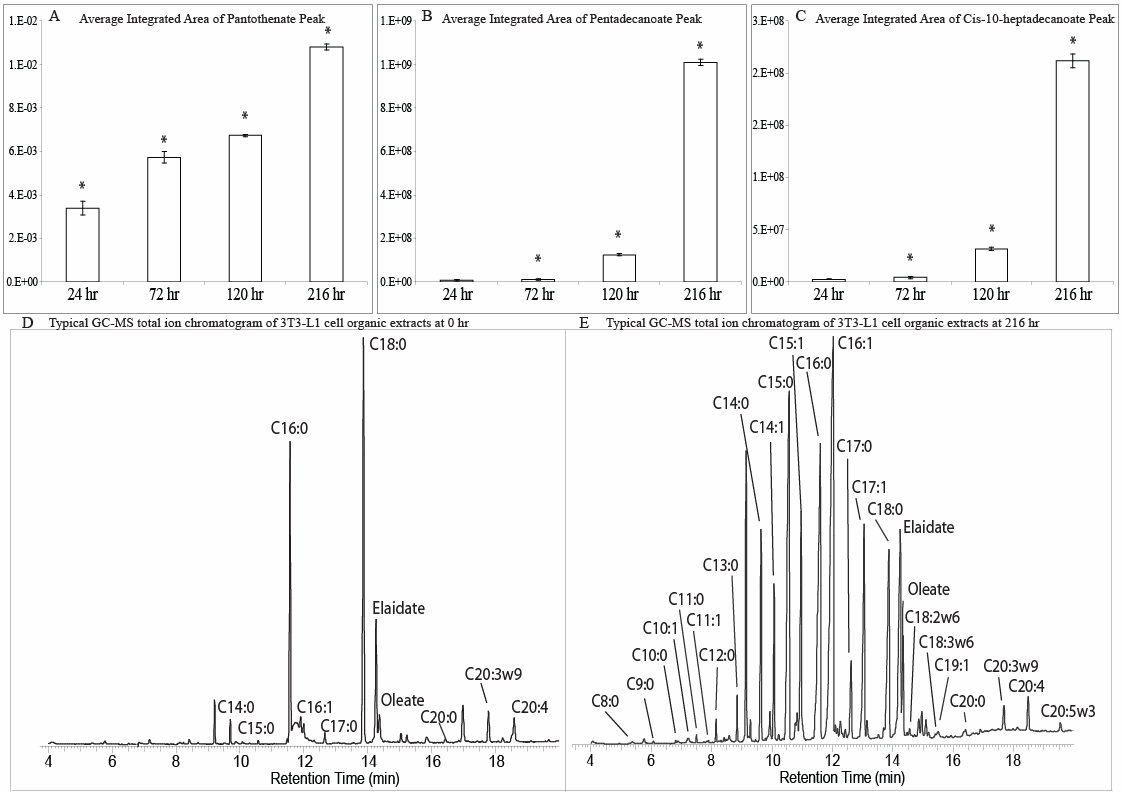

Figure 3.5: **A.** Bar graph showing the average integrated area of the pantothenate peak at 24 h, 72 h, 120 h and 216 h time points as measured by ^{1}H-NMR spectroscopy. Standard error bars are shown. .* $P < 0.05$ calculated between adjacent time points. **B.** Graph showing the average integrated area of the pentadecanoate peak (C15:0) peak at 24 h, 72 h, 120 h and 216 h time points as measured by GC-MS of fatty acid methyl esters. Standard error bars are shown. * $P < 0.05$ calculated between adjacent time points. **C.** Bar graph showing the average integrated area of the cis-10-heptadecanoate peak at 24 h, 72 h, 120 h and 216 h time points. Standard error bars are shown. * $P < 0.05$ calculated between adjacent time points. **D.** A typical GC-MS total ion chromatogram (TIC) from the analysis of methyl esterification-derivatised 3T3-L1 cell organic extracts from the 0 h time point. Metabolites are identified from exact retention times and comparison of corresponding mass spectrum with the NIST database and a FAME standard mix. **E.** A typical GC-MS total ion chromatogram (TIC) from the analysis of methyl esterification-derivatised 3T3-L1 cell organic extracts from the 216 h time point. Metabolites are identified from exact retention times and comparison of corresponding mass spectrum with the NIST database and a FAME standard mix.

3.4.1.3 Carbohydrate metabolism

Concentrations of glycolytic and TCA cycle intermediates were measured using ^{1}H-NMR and GC-MS analysis of their methoximated and silylated derivatives from the aqueous phase of the cell metabolite extraction. During the first 4 h of differentiation a number of TCA cycle intermediates increased in concentration including succinate, fumarate and malate. For the first 2 h of the differentiation process this was also accompanied by an increase in glycolysis as indicated by increases in lactate and pyruvate and a decrease in glucose-6-phosphate. Both changes were accompanied by an increase in the concentration of ATP. Between 8 h and 16 h the concentrations of the latter intermediates (succinate, fumarate and malate) in the TCA cycle decreased as the concentrations of the early intermediates isocitrate and citrate increased indicating the change in steady state for the two halves of the cycle. At the same time the concentrations of glucose and galactose increased and lactate decreased suggestive of a decrease in glycolytic flux consistent with greater coupling between glycolytic flux and the TCA cycle. By 72 h, corresponding to the identified initiation of lipid accumulation, the concentration of the TCA cycle intermediates fumarate, malate, isocitrate and citrate increased; a corresponding increase in ATP concentrations suggests that the flux of the TCA cycle was also increased. The concentration of glucose was also reduced at this time point. The TCA cycle intermediates continued to increase at 120 h, with the concentrations of succinate, fumarate, malate and citrate all increasing across this time period. Accompanying upregulation of glycolytic flux was established with observed decreases in the concentrations of glucose, fructose and galactose and increases in pyruvate and lactate between 24 h and 120 h. At 216 h TCA cycle and glycolytic intermediates were decreased in concentration as the cells reached terminal differentiation – at this time point the concentrations of glucose, galactose and fructose were increased and those of pyruvate, lactate, succinate, fumarate, malate, isocitrate and citrate were decreased compared to 120 h.

3.4.1.4 Amino acid metabolism

Concentrations of amino acids and polyamine biosynthesis intermediates were measured using ^{1}H-NMR spectroscopy and GC-MS analysis. The concentration of glutamine

increased after 4 h and again after 16 h with a concomitant decrease in the concentration of glutamate. Polyamine metabolism was also altered during differentiation with an increase in the concentration of the putrescine precursors aspartate and ornithine detected prior to an increase in the concentration of putrescine detected after 24 h. The levels of the polyamine pathway metabolites, including putrescine, then decreased by 216 h.

3.4.1.5 Complex lipids and free fatty acids

Concentrations of FFAs and glycerophospholipids were measured using DI-MS (**Figure 3.6**). LC-MS was used to measure the concentrations of glycerophospholipids and TAGs.

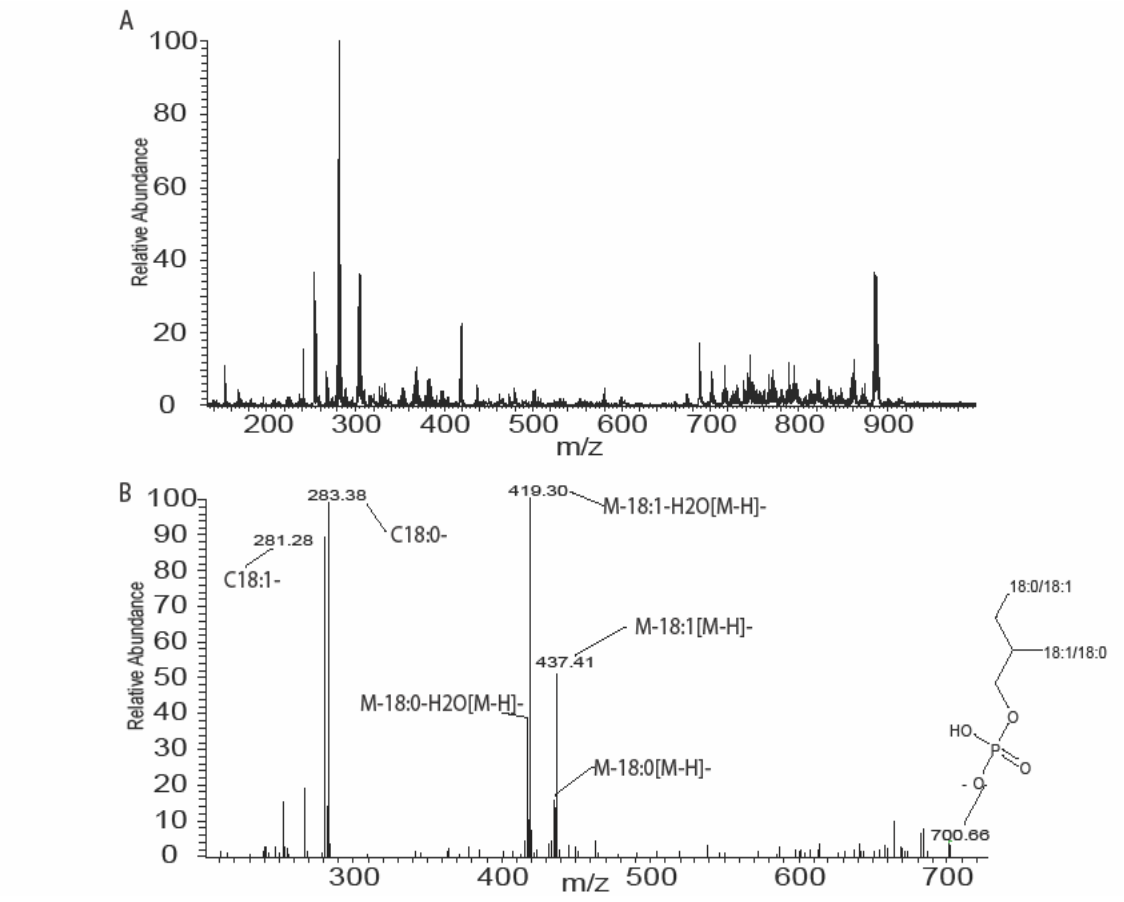

Figure 3.6: Direct infusion of 3T3-L1 cell lipid extraction in negative mode using an LTQ ion trap. **A.** Direct infusion mass spectrum of 3T3-L1 cell lipid extraction fraction. **B.** MS/MS spectrum of an ion at 701 *m/z*. Daughter ions are labelled.

At 24 h an increase in even chain saturated and unsaturated FFAs was detected as was an increase in the intermediates and end products of the omega-3 and omega-6 fatty acid pathways. By 72 h there was an increase in the concentrations of even chain unsaturated fatty acids accompanied by an increase in the concentrations of odd chain saturated and unsaturated fatty acids which continued to the 216 h time point. The concentrations of the longer chain unsaturated even chain fatty acids were decreased by 120 h as were the concentrations of the omega-6 fatty acid pathway intermediates. At the conclusion of the study there was a detected increase in the concentration of α-linolenic acid and concomitant decrease in the essential fatty acid pathway intermediates and end products. A continued decrease in the longer, even chain fatty acids was also detected at 216 h.

The composition of TAGs was also altered with an increase in the incorporation of odd chain saturated and unsaturated fatty acids and a concomitant decrease in the concentration of even chain fatty acids at 72 h. Accumulation of odd chain fatty acids continued at 120 h with a concomitant decrease in even long chain fatty acids. By 216 h the concentration of TAGs esterified with odd chain fatty acids continued to increase while an associated decrease in the concentration of TAGs incorporating C16:0 and C18:0 was detected (**Table 3.1**).

Time Point	72 h	120 h	216 h
Concentration Increased	TAG 15:0/15:0/17:1 NH4 + TAG 15:0/15:1/17:0 NH4 + TAG 15:0/16:0/16:1 NH4 + TAG 14:0/16:0/17:1 NH4 + TAG 14:0/16:1/17:0 NH4 + TAG 16:1/15:0/17:0 NH4 + TAG 16:0/15:0/17:1 NH4 + TAG 15:0/16:0/20:2 NH4 + TAG 19:1/17:1/15:0 NH4 + TAG 18:1/18:1/15:0 NH4 + TAG 49:2 NH4 + TAG 49:1 NH4 + TAG 48:3 NH4 + TAG 48:2 NH4 +	TAG 15:0/15:0/16:1 NH4 + TAG 15:1/15:0/16:0 NH4 + TAG 16:0/16:1/14:0 NH4 + TAG 14:1/16:0/16:0 NH4 + TAG 16:1/15:0/17:0 NH4 + TAG 16:0/15:0/17:1 NH4 + TAG 16:2/17:1/17:1 NH4 + TAG 16:1/16:1/18:2 NH4 + TAG 15:0/16:0/20:2 NH4 + TAG 19:1/17:1/15:0 NH4 + TAG 18:1/18:1/15:0 NH4 + TAG 17:0/16:0/18:1 NH4 + TAG 16:0/16:0/19:1 NH4 + TAG 46:0 NH4 + TAG 47:3 NH4 + TAG 47:2 NH4 + TAG 48:3 NH4 + TAG 48:2 NH4 + TAG 48:0 NH4 + TAG 49:2 NH4 + TAG 49:1 NH4 + TAG 50:3 NH4 + TAG 50:1 NH4 +	TAG 15:0/15:0/16:1 NH4 + TAG 15:1/15:0/16:0 NH4 + TAG 16:0/16:1/14:0 NH4 + TAG 14:1/16:0/16:0 NH4 + TAG 15:0/15:0/17:1 NH4 + TAG 15:0/15:1/17:0 NH4 + TAG 15:0/16:0/16:1 NH4 + TAG 14:0/16:0/17:1 NH4 + TAG 14:0/16:1/17:0 NH4 + TAG 16:1/15:0/17:0 NH4 + TAG 16:0/15:0/17:1 NH4 + TAG 16:2/17:1/17:1 NH4 + TAG 16:1/16:1/18:2 NH4 + TAG 15:0/16:0/20:2 NH4 + TAG 19:1/17:1/15:0 NH4 + TAG 18:1/18:1/15:0 NH4 + TAG 17:0/16:0/18:1 NH4 + TAG 16:0/16:0/19:1 NH4 + TAG 46:0 NH4 + TAG 47:3 NH4 + TAG 48:3 NH4 + TAG 48:2 NH4 + TAG 49:2 NH4 + TAG 49:1 NH4 + TAG 50:3 NH4 + TAG 50:1 NH4 +
Concentration Decreased	16:0/16:0/18:0 NH4 + 18:1/18:2/16:0 NH4 + 18:0/20:0/16:0 NH4 + TAG 48:0 NH4 + TAG 50:3 NH4 + TAG 54:5 NH4 + TAG 54:4 NH4 + TAG 54:3 NH4 + TAG 54:0 NH4 +	TAG 18:1/18:2/16:0 NH4 + TAG 54:5 NH4 + TAG 54:4 NH4 + TAG 54:3 NH4 +	TAG 16:0/16:0/18:0 NH4 + TAG 18:1/18:2/16:0 NH4 + TAG 18:0/16:0/18:0 NH4 + TAG 18:0/20:0/16:0 NH4 + TAG 54:4 NH4 + TAG 54:3 NH4 +

Table 3.1: The changes in TAG concentrations during the differentiation of 3T3-L1 preadipocytes into mature adipocytes at the 72 h, 120 h and 216 h time points. TAGs were detected by LC-MS and identified using MS/MS.

3.4.2. 3T3-L1 Adipocyte ^{13}C-labelled Substrate Study

To investigate the mechanisms generating the changes in the steady state concentrations of metabolites identified in the metabolomic studies ^{13}C stable isotope labelled substrate studies were conducted. Given that the most significant changes were found to occur in the lipid composition of the differentiating cells and especially considering the unusual concentration of odd chain fatty acids we elected to investigate synthesis and metabolic processing of fatty acids directly using stable isotope techniques.

3.4.2.1 ^{13}C-glucose labelling study

^{13}C enrichment of a number of key metabolites was measured using HSQC NMR analysis of the organic phase metabolites and GC-MS analysis of the organic and aqueous phases. When using 1-^{13}C-glucose as a substrate lactate, succinate and glutamate were all found to be enriched when analysed by GC-MS (**Figure 3.7**), as were the lipid resonances in HSQC spectra corresponding to ω 1-3 resonances, allylic carbons, terminal lipid resonances (CH_3 resonances), the methylene envelope and esterified and non-esterified glycerol (**Figure 3.8**). Further investigation, by GC-MS, of the enrichment of individual fatty acid species demonstrated that both C14:0 and C16:0 had clearly incorporated ^{13}C from glucose (**Figure 3.9 A,B**).

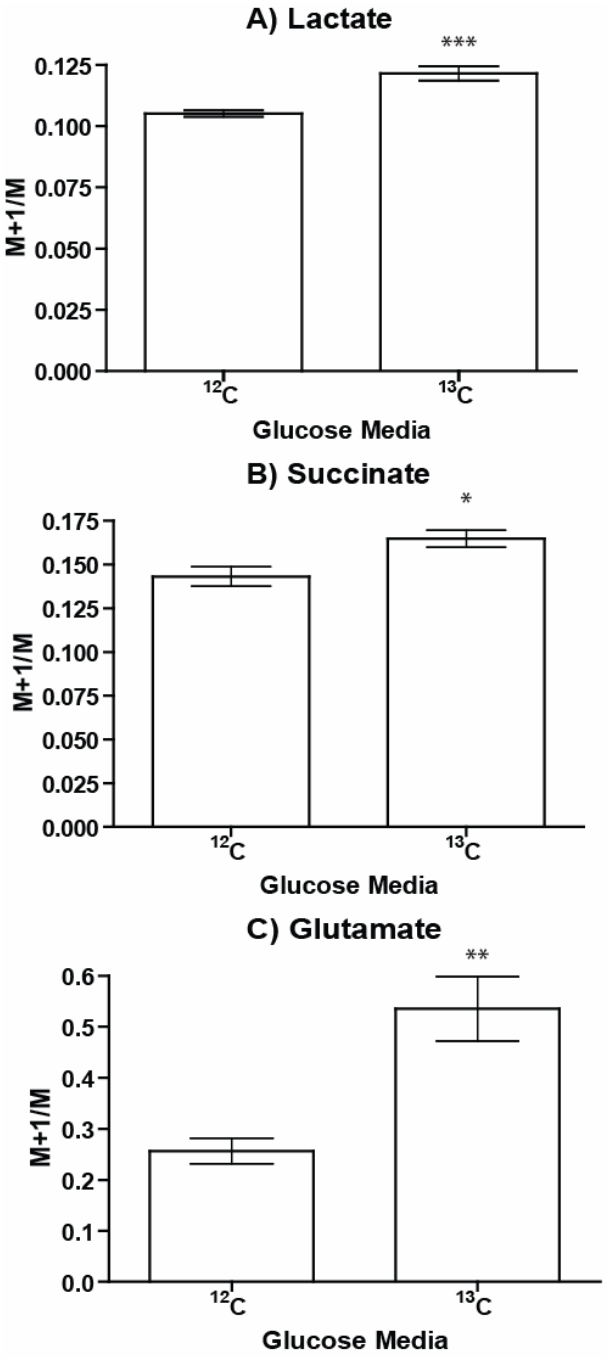

Figure 3.7: **A.** Graph showing GC-MS M+1/M ion ratio for lactate when using 1-^{13}C-glucose and unlabelled glucose. Enrichment of lactate is shown. **B.** Graph showing GC-MS M+1/M ion ratio for succinate when using 1-^{13}C-glucose and unlabelled glucose, showing enrichment of succinate. **C.** Graph showing GC-MS M+1/M ion ratio for glutamate when using 1-^{13}C-glucose and unlabelled glucose, showing enrichment of glutamate. *P < 0.05, **P < 0.01, ***P < 0.005. ^{12}C is unenriched glucose, ^{13}C is 1-^{13}C enriched glucose. Parent ions were used to calculate ion ratio.

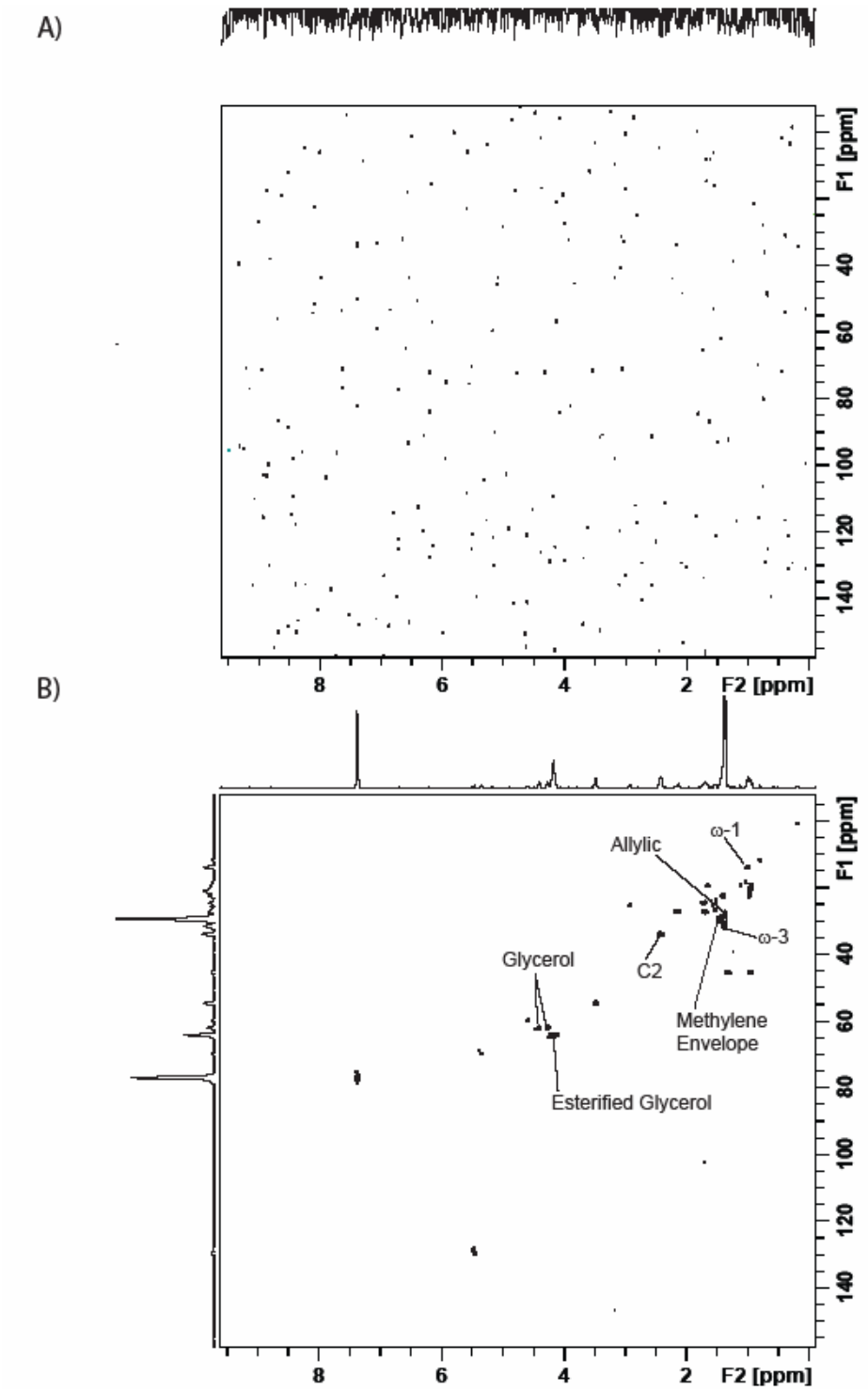

Figure 3.8: HSQC NMR spectra of organic extraction phase of 3T3-L1 cells exposed to unlabelled (**A**) or 1-^{13}C-glucose (**B**). Key: ω 1-3 Carbon signals, allylic carbons, C1-3 signals, the methylene envelope and esterified and non-esterified glycerol ^{13}C cross peaks are labelled.

3.4.2.2 ^{13}C-palmitate labelling study

^{13}C enrichment of a range of metabolites was identified using GC-MS analysis of the organic and aqueous phases (the possibility remains that there were small amounts of 13C labelled fatty acid impurities in the 13C labelled palmitate). Pentadecanoate was found to be enriched confirming the observed increase in odd chain fatty acid abundance detected by analysis of the total pool of FFAs (**Figure 3.9 C**). The palmitate desaturation product palmitoleate was also found to be enriched with ^{13}C in accordance with the observed activity of the Δ9 desaturase from the metabolomic studies (**Figure 3.9 D**).

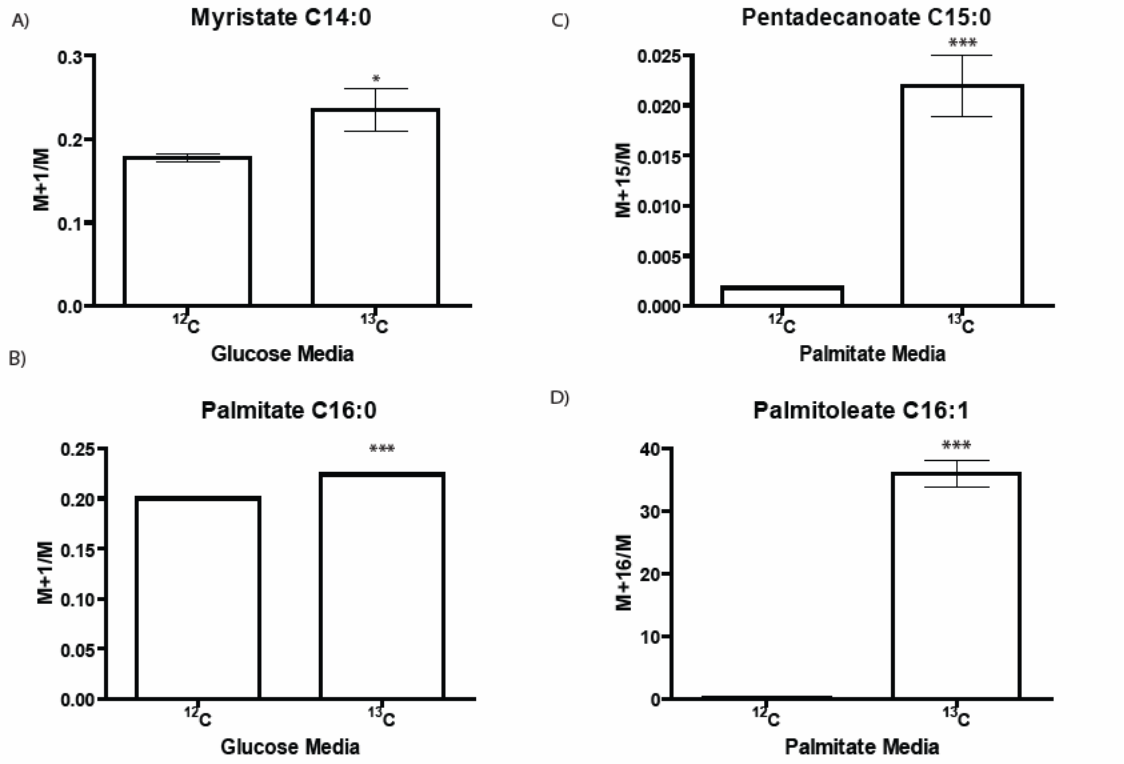

Figure 3.9: **A.** Graph showing GC-MS M+1/M ion ratio for myristate when using 1-^{13}C-glucose and unlabelled glucose. Enrichment of myristate is shown. **B.** Graph showing GC-MS M+1/M ion ratio for palmitate when using 1-^{13}C-glucose and unlabelled glucose, showing enrichment of palmitate. **C.** Graph showing GC-MS M+1/M ion ratio for pentadecanoate when using U-^{13}C-palmitate and unlabelled palmitate, showing enrichment of pentadecanoate. **D.** Graph showing GC-MS M+1/M ion ratio for palmitoleate when using U-^{13}C-palmitate and unlabelled palmitate, showing enrichment of palmitoleate. *P < 0.05, ***P < 0.005.

3.4.3. Primary Adipocytes

To examine the relevance of the 3T3-L1 adipocyte model to mature adipocytes and to investigate how the 3T3-L1 cells recapitulate metabolic changes that occur in adipocytes, the differentiation of primary adipocytes was investigated. As less primary cell material was available for analysis when compared with that available for the 3T3-L1 cells, the decision was taken to focus the investigation on the lipid changes occurring within the primary adipocytes during differentiation. Therefore GC-MS and LC-MS, combined with multivariate pattern recognition were used to compare metabolic differences between primary preadipocytes and differentiated primary adipocytes (**Figure 3.10**).

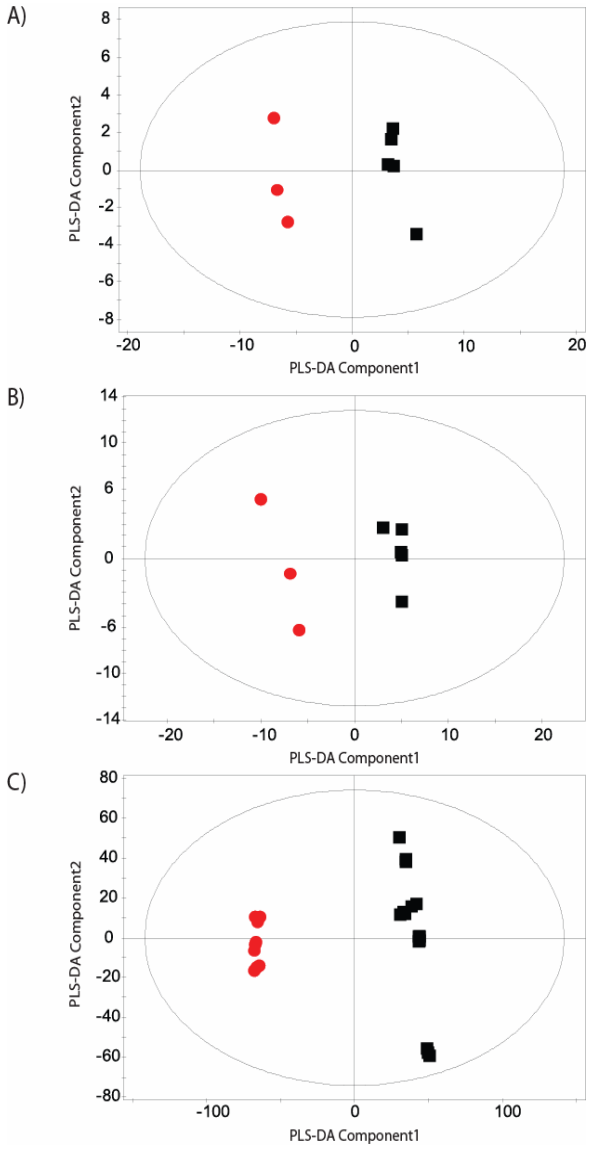

Figure 3.10: **A.** PLS-DA scores plot showing clustering of organic phase metabolites analyzed by GC-MS extracted from ■ primary preadipocytes and ● differentiated primary adipocytes. (R^2=0.76, Q^2=0.97) **B.** PLS-DA scores plot showing clustering of aqueous phase metabolites analyzed by GC-MS extracted from ■ primary preadipocytes and ● differentiated primary adipocytes. (R^2=0.71, Q^2=0.96) **C.** PLS-DA scores plot showing clustering of organic phase metabolites analyzed by LC-MS extracted from ■ primary preadipocytes and ● differentiated primary adipocytes. (R^2=0.443, Q^2=0.99). Two technical replicates were analysed.

3.4.3.1 Total fatty acid metabolism

The total fatty acid concentrations were measured using GC-MS analysis of their methyl esterified derivatives from the organic phase of the cell extracts. An increase in the concentrations of the shorter chain fatty acids (C12:0 and C14:0) and concomitant decrease in the concentrations of the longer chain fatty acids (C16:0, C18:0, C20:0, C 22:0 and C24:0) were observed in the differentiated primary adipocytes when compared to the primary preadipocytes. The odd chain length fatty acids (C13:0 and C15:0) and the Δ9 desaturase products (C14:1, C16:1, C18:1, C19:1, C20:1 and C24:1) were also identified as increased in concentration in the differentiated primary adipocytes.

3.4.3.2 Carbohydrate metabolism

Concentrations of glycolytic and TCA cycle intermediates were measured using GC-MS analysis of their methoximated and silylated derivatives from the aqueous phase of the cell metabolite extraction. The concentrations of glucose-6-phosphate, lactate, fumarate and malate were all found to be increased in the differentiated primary adipocytes compared to the primary preadipocytes. This was a comparable result to the changes identified in the 3T3-L1 cell line.

3.4.3.1 Triacylglycerols

The composition of TAGs was altered during differentiation of the primary adipocytes. There was an increase in the accumulation of odd chain length fatty acids into TAGs. In addition the concentration of desaturated fatty acid constituents of the TAGs was increased (**Table 3.2**).

Primary Adipocyte Differentiation	TAG Species Increased in Concentration
	TAG 14:1/14:1/18:1 NH4+
	TAG 16:1/16:1/14:1 NH4+
	TAG 15:0/16:1/16:1 NH4+
	TAG 16:0/15:0/17:1 NH4+
	TAG 16:0/16:0/16:1 NH4+
	TAG 14:0/17:1/17:0 NH4+
	TAG 14:1/17:0/17:0 NH4+
	TAG 16:1/16:1/18:1 NH4+
	TAG 16:0/16:1/18:2 NH4+
	TAG 14:1/18:1/18:1 NH4+
	TAG 15:1/18:1/18:1 NH4+
	TAG 16:0/17:2/18:1 NH4+
	TAG 18:1/18:1/16:1 NH4+
	TAG 44:2 NH4+
	TAG 46:2 NH4+
	TAG 48:3 NH4+
	TAG 48:2 NH4+
	TAG 49:2 NH4+
	TAG 50:4 NH4+
	TAG 52:2 NH4+
	TAG 54:3 NH4+

Table 3.2: The TAG species increased in concentration during the differentiation of primary preadipocytes into primary adipocytes. TAGs were detected by LC-MS.

3.5 Discussion

During 3T3-L1 adipocyte development the commitment to differentiate occurs between 24-48 h and is followed by the process of lipid accumulation[210]. In the study described in this chapter these processes are reflected in the multivariate models of the various analytical assays. One of the earliest changes in the process of differentiation was associated with upregulation of the TCA cycle, as represented by an increase in the pool sizes of a number of the intermediates, possibly to increase ATP for the differentiation process. By 72 h, corresponding to the identified initiation of lipid accumulation, the intermediates of the TCA cycle again increase in concentration, but at this time point it is dominated by increases in citrate and isocitrate as fatty acid synthesis increases, with citrate being used to supply cytosolic acetyl-CoA, a key intermediate of fatty acid synthesis. Finally at 216 h the metabolite concentrations of the glycolytic pathway and the TCA cycle are such that it would suggest decreased need for these pathways, possibly as the energy demand of the cell decreases following differentiation. Alternatively, it could be viewed that now the dominant pathways involve fatty acid metabolism rather than pathways involving glucose (**Figure 3.11**).

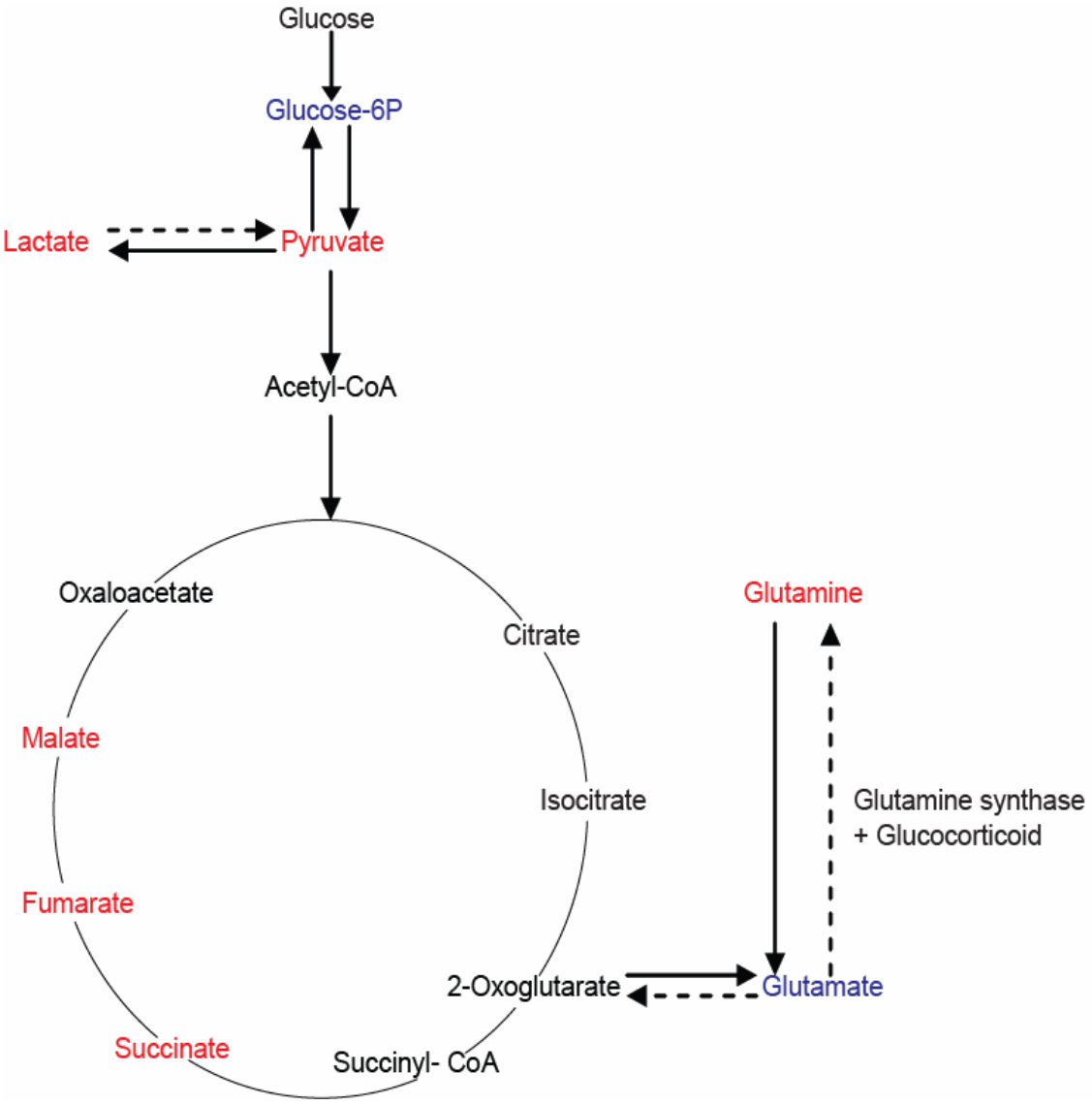

Figure 3.11: Glycolysis and TCA cycle metabolic pathways altered during the initiation phase of 3T3-L1 adipocyte differentiation (0-48 h). Metabolites increased in concentration are marked Red; metabolites decreased in concentration are marked with Blue.

The increase in the concentration of glutamine detected during differentiation has previously been observed and is caused by induction of glutamine synthase as a result of glucocorticoid stimulation during the commitment to differentiate[211]. Furthermore, the detected changes in polyamine biosynthesis are known to be essential for differentiation of 3T3-L1 cells into adipocytes[204]. The observed increase in concentration again corresponds to the induction of lipid accumulation and commitment to differentiate and a

reduction in polyamine biosynthesis intermediates at 216 h also suggest the cells return to a resting state at this time point; an observation which correlates with changes in transcription of ornithine decarboxylase during adipocyte differentiation, with this enzyme producing putrescine from ornithine[212].

From 72 h onwards there is a significant increase in the majority of fatty acids as the process of lipid accumulation occurs following the preadipocytes commitment to differentiate. Accompanying the increase in fatty acids there was also an increase in desaturation and especially of the monounsaturated forms of fatty acids. Stearoyl-CoA desaturase 2 has recently been identified as essential for differentiation. Considering there is a predominance of saturated fatty acids in the growth media and the transcription of the enzyme is upregulated during differentiation[213], it is likely the desaturation observed is carried out by this enzyme[207]. Sequential peroxisomal fatty acid α-oxidation and Δ-9 desaturation of fatty acids has been shown to occur in differentiating 3T3-L1 adipocytes, explaining the detected increase in odd chain fatty acids, their desaturation and accumulation into complex lipids[214]. Analysis of the media eliminated this as the source of the odd chain fatty acids; the highest concentration fatty acids present in the media were palmitate and stearate, and odd chain fatty acids were only detected at low levels. A concomitant increase in the concentration of the CoA constituent pantothenate was detected alongside the lipid changes. CoA is necessary for fatty acid synthesis, transport of fatty acids into peroxisomes and both α and β fatty acid oxidation. Therefore, it appears CoA is increased in response to demand for fatty acid synthesis and α-oxidation. The increase in the concentration of the fatty acid transport molecule carnitine at 72 h, continuing to 216 h, may indicate the requirement for export of odd chain fatty acids from peroxisomes following α-oxidation, since peroxisomes contain short- and medium-chain carnitine acyltransferases functioning to esterify carnitine to fatty acids in order to cross the peroxisomal membrane[215]. The transcription of propionyl CoA carboxylase, an enzyme involved in fatty acid α-oxidation, and the enzyme carnitine acyl transferase have previously been reported as upregulated during 3T3-L1 differentiation[213].

Furthermore the utilisation of glucose to generate fatty acids during 3T3-L1 metabolism has been confirmed through the use of ^{13}C-labelled glucose to monitor the metabolic flux through glycolysis, the TCA cycle and into fatty acid synthesis. Once the fatty acids are synthesised they are subjected to desaturation by the Δ9 desaturase or to α-oxidation, forming odd chain fatty acids as indicated by the metabolomic data and confirmed through the use of U-^{13}C labelled palmitate.

The observed decrease in the end products of the omega-3 essential fatty acid pathway, 5,8,11,14,17-eicosapentaenoic acid and 4,7,10,13,16,19-docosahexaenoic acid, may be necessary for the regulation of differentiation in the 3T3-L1 cell line. Docosahexaenoic acid has been shown to inhibit differentiation and promote lipolysis in the adipocytes[216].

The concentration of arachidonic acid acyl groups in phospholipids appears to increase from 24 h with a decrease in its concentration as a FFA detected by 120 h. Glucocorticoids block release of arachidonic acid from intracellular phospholipid pools[217]. Given arachidonic acid is the initial substrate for the omega-6 essential fatty acid pathway this will lead to the decrease in the intermediates and products of this pathway, as observed in this study. The control of flux through this pathway is vital to differentiation since arachidonic acid as a substrate for cyclooxygenase-2, strongly inhibits adipocyte differentiation via a prostaglandin synthesis pathway[218]. In addition eicosapentaenoic acid represses the expression of peroxisome proliferator-activated receptor-γ, a nuclear receptor vital to adipocyte differentiation[205] (**Figure 3.12**).

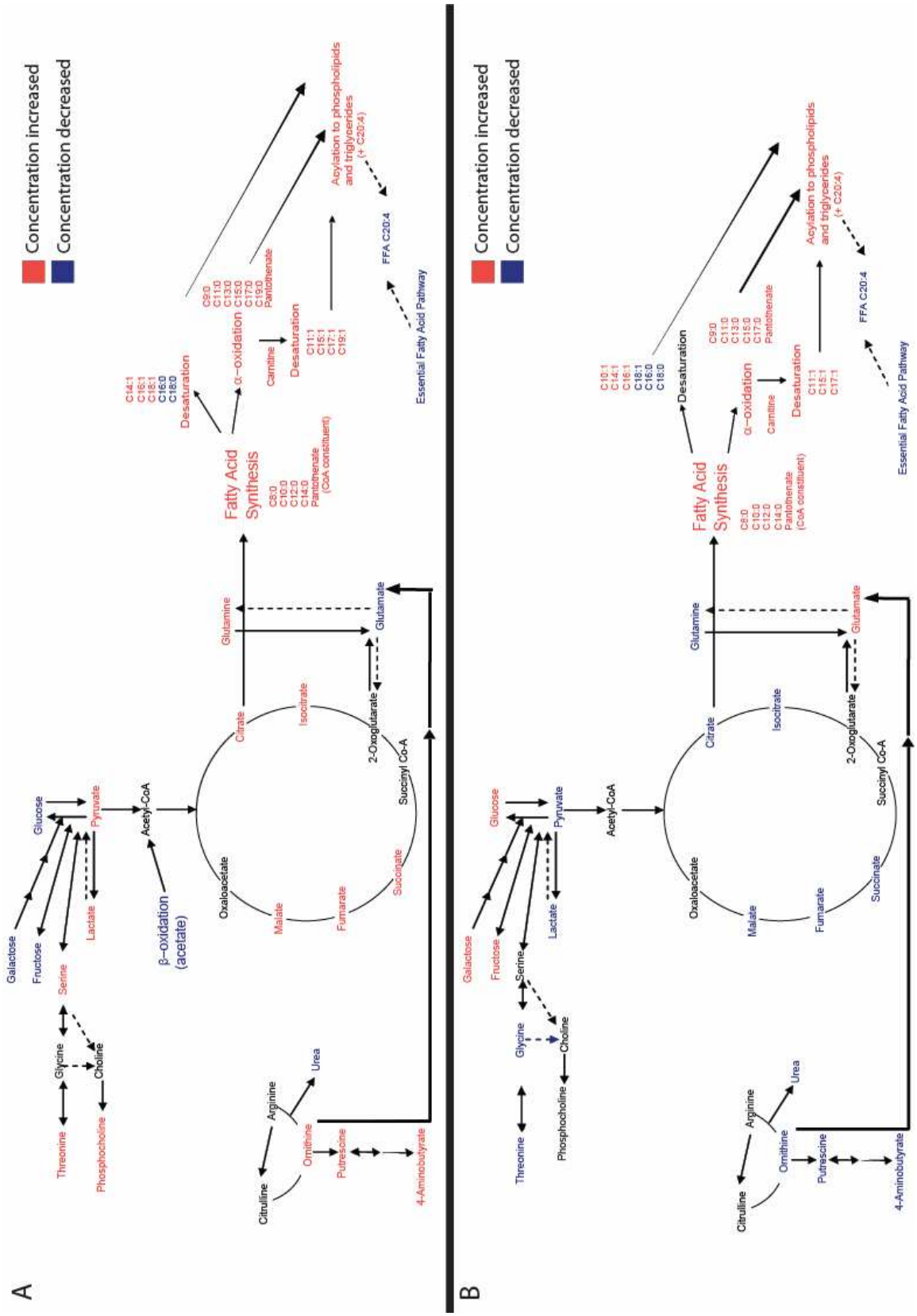
A
Concentration increased
Concentration decreased
Galactose
Fructose
Glucose
Lactate
Pyruvate
Serine
Glycine
Choline
Threonine
Phosphocholine
Acetyl-CoA
β–oxidation (acetate)
Oxaloacetate
Citrate
Isocitrate
2-Oxoglutarate
Succinyl Co-A
Succinate
Fumarate
Malate
Glutamine
Glutamate
Fatty Acid Synthesis
C8:0
C10:0
C12:0
C14:0
Pantothenate (CoA constituent)
Desaturation
C14:1
C16:1
C18:1
C16:0
C18:0
α–oxidation
C9:0
C11:0
C13:0
C15:0
C17:0
Pantothenate
Carnitine
Desaturation
C11:1
C15:1
C17:1
C19:1
Acylation to phospholipids and triglycerides (+ C20:4)
FFA C20:4
Essential Fatty Acid Pathway
Arginine
Urea
Citrulline
Ornithine
Putrescine
4-Aminobutyrate
B
Concentration increased
Concentration decreased
Galactose
Fructose
Glucose
Lactate
Pyruvate
Serine
Glycine
Choline
Threonine
Phosphocholine
Acetyl-CoA
Oxaloacetate
Citrate
Isocitrate
2-Oxoglutarate
Succinyl Co-A
Succinate
Fumarate
Malate
Glutamine
Glutamate
Fatty Acid Synthesis
C8:0
C10:0
C12:0
C14:0
Pantothenate (CoA constituent)
Desaturation
C10:1
C14:1
C16:1
C18:1
C16:0
C18:0
α–oxidation
C9:0
C11:0
C13:0
C15:0
C17:0
Pantothenate
Carnitine
Desaturation
C11:1
C15:1
C17:1
Acylation to phospholipids and triglycerides (+ C20:4)
FFA C20:4
Essential Fatty Acid Pathway
Arginine
Urea
Citrulline
Ornithine
Putrescine
4-Aminobutyrate

Figure 3.12: **A.** Metabolic pathways altered during the lipid accumulation phase of 3T3-L1 adipocyte differentiation (72-120 h). Metabolites increased in concentration are marked in Red; metabolites decreased in concentration are marked in Blue. **B.** Metabolic pathways altered at terminal differentiation of 3T3-L1 adipocytes (216 h). Metabolites increased in concentration are marked in Red; metabolites decreased in concentration are marked with Blue.

Metabolomic analysis of the differentiation of primary adipocytes was conducted to allow comparison of the metabolic changes that occur during differentiation of the primary cells with those identified in the differentiation of the 3T3-L1 adipocyte model, from which the relevance of applying metabolomic investigation to the 3T3-L1 cell line for the study of adipocytes could be assessed. Primary adipocyte metabolomic investigation focused on the lipid changes occurring within the primary adipocytes during differentiation as the composition of this metabolite class was found to be most significantly altered during the differentiation of the 3T3-L1 cells. The availability of primary adipocyte material was also limited.

The changes observed in the total fatty acid composition of the primary adipocytes as the cells differentiated was comparable with those seen in the 3T3-L1 cells. In both cell types there was an increase in the concentration of the short and mid chain fatty acids, odd chain fatty acids and the monounsaturated products of the Δ9 desaturase. As with the 3T3-L1 cells an increase in the incorporation of odd chain and monounsaturated fatty acids into TAGs was also detected An increase in the concentration of glycolytic and TCA cycle intermediates, analogous to the metabolic changes observed in the 3T3-L1 cells during differentiation, was also observed in differentiated primary adipocytes and may correspond to the utilisation of glucose to generate fatty acids as was confirmed in the 3T3-L1 cells using ^{13}C-labelled glucose.

3.6 Conclusions

Although the 3T3-L1 cell line is a robust and extensively used tool for the investigation of adipocyte biology it is worthy of note that, as with all immortalised cell lines, they do not behave identically to their primary cell line counterparts. However, the metabolic differences found between primary preadipocytes and primary differentiated adipocytes matched many of the findings observed in the 3T3-L1 cell line. Therefore it is hoped the current study will provide invaluable cues for research conducted in the 3T3-L1 cell line, primary cell lines and even white adipose tissue when following the changes in metabolism associated with differentiation.

In conclusion, global metabolic profiling has been used to study the changes in metabolism required to bring about differentiation of fibroblastic like cells into mature adipocytes. A diverse number of interacting metabolic pathways essential to differentiation have been highlighted as altered at key points in this process. The changes in metabolite concentrations during commitment to differentiate, lipid accumulation and the return to a resting state have been studied and the TCA cycle, glycolysis, fatty acid α-oxidation, synthesis and desaturation, polyamine biosynthesis and esterification of acyl groups to complex lipids have been identified as implicit to 3T3-L1 maturation.

Chapter 4

PPARδ Activation in White Adipose Tissue: Burning Fat by Upregulation of the TCA Cycle

4.1 Introduction

The WHO estimates over 180 million people worldwide suffer from TIIDM. The incidence of obesity, a major risk factor for the development of TIIDM, is also increasing globally. While a number of anti-diabetic treatments have been produced they rarely address the related obese state and consequently fail to confront this underlying risk factor. Therefore it becomes imperative that new treatment approaches with both anti-diabetic and anti-obesity properties are found.

The PPARs have already yielded viable targets for the treatment of TIIDM and dyslipidaemia; TZDs, PPARγ agonists, are currently used in the clinic for the treatment of TIIDM and fibrates, PPARα agonists, are routinely used to treat dyslipidaemia. Treatment with TZDs results in the recruitment of new metabolically active adipocytes causing an increase in lipid storage capacity and normalisation of adipocytokine levels[219]; whereas activation of PPARα by fibrates results in an increase in fatty acid catabolism in the heart and liver and decreases low-density lipoprotein-cholesterol concentrations[128].

A pharmacological agonist for PPARδ is yet to make it into the clinic, the receptor remains to be functionally defined and the physiological ligand for PPARδ is still to be

described. Nevertheless, the receptor has been shown to be activated by several 14 to 18 carbon containing polyunsaturated fatty acids, including eicosanoids such as prostaglandin A_1, iloprost and carbaprostacyclin, in the micromolar range[132]. The development of a number of high affinity synthetic ligands for PPARδ has shown the receptor holds considerable promise for the treatment of TIIDM, the metabolic syndrome, dyslipidaemia and obesity. Insulin resistant obese rhesus monkeys treated with the selective PPARδ agonist GW501516 demonstrated significant increases in HDL-cholesterol with concomitant decreases in TAGs and LDL-cholesterol[170]. PPARδ activation has also shown efficacy in reducing adiposity by decreasing intracellular TAG accumulation in mouse brown adipose tissue and liver[169] .

Investigation into the function of PPARδ in white adipose tissue has, thus far, demonstrated that the receptor has an important role in the regulation of metabolism and energy homeostasis. *In vitro* investigation has shown that expression of PPARδ is induced early in the differentiation of the 3T3-L1 murine adipocyte cell line[172] and during early brown adipogenesis[173]. PPARδ is also implicated in the stimulation of adipogenesis via the induction of PPARγ expression and mitotic clonal expansion[174, 175]. Tissue specific over-expression of PPARδ in the white adipose tissue of transgenic mice resulted in decreases in body weight, adipocyte TAG accumulation, circulating FFAs and circulating TAG[169]. The same transgenic mice were also protected against weight gain, adipocyte hypertrophy, hypertriglyceridaemia, and steatosis. PPARδ activation also leads to elevated expression of *Uncoupling protein-1* in white adipose tissue[169].

4.2 Aims and Objectives

In order to deconvolute the effect of PPARδ activation on the control of metabolism in white adipose tissue we have performed a metabolomics study using both *in vivo* analysis in the *ob/ob* mouse and *in vitro* analysis using the murine 3T3-L1 adipocyte cell line. A synthetic, high affinity pharmacological agonist, GW610742, was used to activate PPARδ in both the mice and the adipocyte cell line (GW610742 EC50 for murine PPARδ is 28 nM compared to 8,900 nM for PPARα and >10,000 nM for PPARγ)[185]. A combined GC-MS, ^{1}H-NMR, LC-MS and DI-MS approach was used in conjunction with multivariate statistics to probe the metabolic phenotype resulting from PPARδ activation. To unambiguously define the mechanisms by which PPARδ alters the metabolism of adipose tissue we then carried out ^{13}C-stable isotope substrate labelling studies using 1-^{13}C glucose and U-^{13}C palmitate, respirometric analysis using a Clark-type oxygen electrode and transcriptomic microarray analysis.

It was found that PPARδ activation was not only characterised by increased fatty acid oxidative metabolism as previously observed but also by glucose oxidation. This implicates PPARδ as a control for global oxidative energy metabolism and suggests a mechanism by which activation of the nuclear receptor, in part, brings about its anti-diabetic and anti-obesity properties by simultaneously reducing the quantity of TAGs and glucose in white adipose tissue.

4.3 Materials and Methods

4.3.1 *Ob/Ob* Mouse Study Tissue Collection and Extraction

Animals were kept as is outlined in **Chapter 2 Materials and Methods** (section *2.2.1. Animal handling*). Briefly, the *ob/ob* mice were dosed orally daily at 8 am with 0.5% Hydroxypropylmethylcellulose/0.1% Tween80 vehicle control (n=8) or a PPARδ agonist, GW610742 (n=8 at 30 mg/kg). Injection volume was adjusted daily according to body weight at 10 ml/kg. White adipose tissue was collected as summarised in **Chapter 2 Materials and Methods** (section *2.2.4. Tissue handling*).

4.3.2 3T3-L1 Cell Culture

3T3-L1 preadipocytes were grown and differentiated as described in **Chapter 2 Materials and Methods** (section 2.1.1 *3T3-L1 cell culture and adipocyte differentiation*).

4.3.3 3T3-L1 PPARδ Activation

3T3-L1 adipocytes were treated with the selective PPARδ agonist GW610742 as is outlined in **Chapter 2 Materials and Methods** (2.1.3. *Activation of PPARδ in 3T3-L1 adipocytes*). Briefly, adipocytes were treated with either DMSO (control n=6 T75 flasks) or GW610742 PPARδ selective agonist (n=6 T75 flasks at 100 nM and 1 μM) for 2 days.

4.3.4. Oil Red O Staining and Intracytoplasmic Lipid Accumulation

Six additional T75 flasks of 3T3-L1 adipocytes were grown per control, 100 nM and 1 μM treatment groups. Three flasks per group were stained prior to PPARδ agonist treatment to assess levels of differentiation; three flasks per groups were stained post PPARδ agonist treatment to assess the effects of PPARδ activation on the concentration of neutral lipid stored within the adipocytes. The cells were stained and the

intracytoplasmic lipid accumulation assessed as in **Chapter 2 Materials and Methods** (section 2.1.5 *Oil Red O staining and intracytoplasmic lipid accumulation*).

4.3.5 3T3-L1 Cell Collection

The cells were collected and their metabolites extracted as described in **Chapter 2 Materials and Methods** (sections 2.1.6 and 2.3 *Adipocyte cell collection*).

4.3.6 Tissue and 3T3-L1 Metabolite Extraction

Metabolites were extracted from white adipose tissue and 3T3-L1 cells using the modified Bligh and Dyer method[187]. The details are as in **Chapter 2 Materials and Methods (***section 2.3 3T3-L1 Cell, Primary Adipocyte and Tissue Metabolite Extraction*)**.**

4.3.7 ^{1}H-NMR Spectroscopy

All samples were analysed using a Bruker AVANCE II+ spectrometer operating at 500.13 MHz for the ^{1}H frequency using a 5 mm Broadband TXI Inverse ATMA probe. All procedures are as depicted in **Chapter 2 Materials and Methods** (sections 2.6.1. *Spectrometer*, 2.6.2. *Sample preparation*, 2.6.3. *1-dimensional ^{1}H-Nuclear Magnetic Resonance experimental method* and 2.6.4. *Processing 1-dimensional ^{1}H-Nuclear Magnetic Resonance data*).

4.3.8 GC-MS Analysis

The aqueous phase of extracts was derivatised as described in **Chapter 2 Materials and Methods** (section 2.7.1 *Derivatisation of aqueous phase metabolites*).

The organic phase of extracts was derivatised as described in **Chapter 2 Materials and Methods** (section 2.7.2 *Derivatisation of organic phase metabolites*).

GC-MS analyses were made using a Trace GC Ultra coupled to a Trace DSQ II single-quadrupole mass spectrometer. Parameters for the GC-MS analysis of aqueous phase metabolites and organic phase metabolites were as outlined in **Chapter 2 Materials and Methods** (sections 2.7.3.1 *Gas Chromatography-Mass Spectrometry methods for aqueous phase samples* and 2.7.3.2 *Gas Chromatography-Mass Spectrometry methods for organic phase samples*). Derivatised organic samples were injected with a split ratio of 60 for white adipose tissue and 8 for 3T3-L1 cells.

GC-MS chromatograms were processed using Xcaliber (version 2.0; Thermo Electron) as outlined in **Chapter 2 Materials and Methods** (2.7.5. *Processing Gas Chromatography-Mass Spectrometry data*).

4.3.9 UPLC-MS Analysis

Chromatography was performed using an ACQUITY UPLC® system equipped with an Acquity UPLC 1.7 μm BEH C8 column (2.1×100 mm) coupled to a Micromass QTof-*Ultima* with a Z-spray electrospray source. All chromatography and mass spectrometric parameters were as outlined in **Chapter 2 Materials and Methods (**section 2.8.1. *Chromatography and mass Spectrometry parameters*)

The organic phase of adipose tissue extracts was reconstituted in methanol-chloroform (2:1, 500 μl). This was further diluted 10-fold prior to injection onto the C8 column (5 μl). The column mobile phase was held at 85% solvent B for 0.5 min followed by an increase from 85%-100% solvent B over 0.5-8 min. The mobile phase was then held at 100% B for 4 min. Between 12 and 12.25 min the mobile phase was returned to 85% B and held for 1.75 min to re-equilibrate the column.

3T3-L1 Cell Organic phase metabolites were reconstituted in methanol-chloroform (2:1, 1 ml). Aliquots of diluted organic phase sample (5 μl) were injected onto the C8 column. The column mobile phase was held at 50% solvent B for 0.5 min followed by an increase from 50%-100% solvent B over 0.5-6.5 min. The mobile phase was then held at 100% B

for 3.5 min. Between 10 and 10.25 min the mobile phase was returned to 50% B and held for 3.75 min to re-equilibrate the column. The total UPLC cycle was 14 min and the eluent flow rate was 600 µl/min for both methods.

Tandem mass spectrometry procedures were as described in **Chapter 2 Materials and Methods** (2.8.3 *Tandem mass spectrometry method*).

Data was processed using Micromass MarkerLynx Applications Manager as depicted in **Chapter 2 Materials and Methods** (2.8.4. *Processing Liquid Chromatography-Mass Spectrometry data*).

4.3.10 DI-MS Analysis

Mass spectrometric analysis was performed using a Thermo Finnigan LTQ equipped with a Finnigan Surveyor pump and Finnigan Micro AS Autosampler.

The white adipose tissue organic phase samples for DI-MS were reconstituted in 1 ml methanol:THF (2:1 v/v). 60 µl of each sample was aliquoted into a 96 well plate where the samples were diluted by the addition of a further 600 µl methanol:THF (2:1 v/v).

The 3T3-L1 organic phase samples for DI-MS were reconstituted in 500 µl methanol:THF (2:1 v/v). 100 µl of each sample was added to a 96 well plate. Samples were analyzed in triplicate using both positive and negative mode.

All other direct infusion and mass spectrometric parameters were as described in **Chapter 2 Materials and Methods** (section 2.9.2. *Direct infusion and mass spectrometry parameters*).

DI-MS chromatograms were processed using Xcaliber as outlined in **Chapter 2 Materials and Methods** (2.9.3. *Processing of direct infusion mass spectrometry data*).

4.3.11 ^{13}C-glucose Substrate Labelling Study

At 2 days post differentiation media was removed from the T75 flasks and replaced with DMEM (10% (v/v) FBS, 50 units/ml penicillin, and 50 µg/ml streptomycin) and either 4.5 g/l unlabelled glucose with DMSO control (n=6) or with 1µM GW610742 PPARδ selective agonist (n=7) or 4.5 g/l 1-^{13}C-glucose with DMSO control (n=7) or with 1 µM GW610742 PPARδ selective agonist (n=7). After 2 days cells were collected and metabolites extracted as described in **Chapter 2 Materials and Methods** (sections 2.1.6 and 2.3 *Adipocyte cell collection*).

4.3.12 ^{13}C-palmitate Substrate Labelling Study

Preparation of ^{13}C labelled and unenriched palmitate solution is defined in **Chapter 2 Materials and Methods** (2.4.3. *Preparation of ^{13}C and ^{12}C palmitate solution*).

At 2 days post-differentiation media was removed from the T75 flasks and replaced with DMEM (serum free, 50 units/ml penicillin, and 50 µg/ml streptomycin) and either 70 µM unlabelled palmitate (n=6) with DMSO control (n=6) or with 1 µM GW610742 PPARδ selective agonist (n=7) or 70 µM U-^{13}C labelled palmitate (n=7) with DMSO control (n=6) or with 1 µM GW610742 PPARδ selective agonist (n=7). After 2 days cells were collected and metabolites extracted as previously described in **Chapter 2 Materials and Methods** (sections 2.1.6 *Adipocyte cell collection* and 2.3 *Adipocyte cell collection*).

4.3.13 ^{13}C-HSQC NMR Spectroscopy

Dried organic phase extracts were dissolved in 600 µl of deuterated chloroform. Samples were analyzed using a DRX Avance II+ spectrometer interfaced to a 5-mm TXI ATMA probe. All procedures are as depicted in Chapter 2 Materials and Methods (sections 2.6.5. *2-dimensional Heteronuclear Single-Quantum Coherence ^{13}C-Nuclear Magnetic Resonance experimental method and* 2.6.6. *Processing 2-dimensional Heteronuclear Single-Quantum Coherence ^{13}C-Nuclear Magnetic Resonance data*).

4.3.14 ^{13}C-labelled Substrate GC-MS Analysis

Analysis of organic and aqueous phases was carried out as previously described in **Chapter 2 Materials and Methods** (section 2.7.1 *Derivatisation of aqueous phase metabolites,* 2.7.2. *Derivatisation of organic phase metabolites,* 2.7.3.1 *Gas Chromatography-Mass Spectrometry methods for aqueous phase samples* and 2.7.3.2 *Gas Chromatography-Mass Spectrometry methods for organic phase samples*).

Enrichment of metabolites was identified by calculating isotope ratios of the M and M+1 ions for the parent ion of the fragmentation pattern in the case of ^{13}C-glucose metabolism analysis and TCA cycle intermediates originating from ^{13}C-palmitate oxidation. For fatty acid synthesis and desaturation products from ^{13}C-labelled palmitate an ion ratio of M+16/M was used and for fatty acids originating from oxidation of U-^{13}C-labelled palmitate an ion ratio of M+n/M, where n = the carbon chain length of the fatty acid was used. Statistical analysis was performed using a univariate t-test.

4.3.15 Multivariate Analysis

Multivariate data analysis was performed using SIMCA-P^{+} 11.0 (Umetrics AB, Umeå, Sweden). NMR, DI-MS and UPLC-MS data sets were mean-centered and Pareto-scaled prior to analysis. GC-MS data sets were scaled to UV. Data sets were analyzed using PCA, PLS and PLS-DA. Further details are summarised in **Chapter 2 Materials and Methods** (section 2.11.6 *Multivariate Statistical Analysis Methodology*).

4.3.16 Respirometric Analysis of PPARδ Agonist Treated 3T3-L1 Cells

Cells were grown, treated with PPARδ agonist and collected as is outlined in **Chapter 2 Materials and Methods (**section 2.1.1 *3T3-L1 cell culture and adipocyte differentiation,* 2.1.3. *Activation of PPARδ in 3T3-L1 adipocytes,* 2.1.6 and 2.3 *Adipocyte cell collection*) with the exception that they were collected into respiration medium (100 mM KCl, 50 mM MOPS, 1.0 mM KH_2PO_4, 1.0 mg/ml defatted BSA, pH 7.4). Respiratory rates of *in situ* permeabilised control and PPARδ agonist treated 3T3-L1 cells were measured

using a Clark-type oxygen electrode (Strathkelvin Instruments Ltd, Glasgow, UK) with methods developed by Kuznetsov *et al*[188]. Respiration rates were recorded and quantified using 782 Oxygen System v3.0 software (Strathkelvin Instruments). Procedures are defined in **Chapter 2 Materials and Methods (**section 2.5 *Respirometric analysis of PPARδ agonist treated 3T3-L1 cells*).

4.3.17 Microarray Analysis of PPARδ Agonist Treated 3T3-L1 Cells

Cells were grown, treated with PPARδ agonist and collected as is outlined in **Chapter 2 Materials and Methods (**section 2.1.1 *3T3-L1 cell culture and adipocyte differentiation,* 2.1.3. *Activation of PPARδ in 3T3-L1 adipocytes,* 2.1.6 and 2.3 *Adipocyte cell collection*) An RNeasy RNA extraction and purification kit was used to extract total RNA from 3T3-L1 adipocytes (Qiagen GmbH, Hilden, Germany). RNA extraction procedures were carried out according to the methods outlined in **Chapter 2 Materials and Methods** (section 2.10.1. *RNA extraction*).

Transcriptomic analysis was conducted by Cambridge Genomic Centre for Microarray Resources (Cambridge Genomic Services, Department of Pathology, University of Cambridge). An automated Illumina Infinium Gene Expression BeadArray (Illumina Inc, San Diego, CA) was used to perform mRNA transcriptional profiling. A mouse WG6 array platform was used with 45281 probes.

Quality control was carried out using the arrayQualityMetrics R package and no samples failed or were identified as outliers to their replicates. Statistical selection was performed using the detection p-value provided by Illumina. This value represents the confidence that a given transcript is expressed above the background defined by the negative control probe. The R package lumi was used for this analysis[191] . The detection p-value threshold was set to 0.01. Probes were required to be successfully detected (p-value<0.01 in lumi) in at least one sample to pass the selection. The data is transformed using variance stabilisation and then normalised using quantile normalisation[192]. Gene expression was compared between PPARδ agonist treated and control 3T3-L1 cells using

the R package limma[193]. The threshold utilised in this analysis was the 5% confidence interval with false discovery rate. The selected and normalised data was then analysed using the multivariate statistics in the Simca-P+ package as has been described. The 6% of transcripts most responsible for separation in the multivariate models were then examined (3% most increased and 3% most decreased in PPARδ agonist treated cells as identified in the multivariate models).

The Reactome Skypainter tool (www.reactome.org) was used to determine which pathways were statistically significant in the 3% of genes most increased and most decreased in transcription in PPARδ agonist treated cells. From a given set of genes known to participate in a pathway, the total genes for *mus musculus* and the submitted list of genes (the genes increased or decreased in expression in PPARδ activated cells) of which N genes participate in the given pathway, the probability of observing at least N genes from a pathway if that pathway is not overrepresented in the submitted list of genes is calculated using the one-tailed version of Fisher's exact test. Therefore a p-value smaller than or equal to the significance level suggests that the pathway is statistically significant in the submitted list of genes.

4.3.18 Univariate Statistical Analysis Methodology

Selected microarray transcriptomic data was analysed by univariate techniques. Univariate analysis was performed using an unpaired Student's t-*t*est with a significance level set to $p<0.05$. An F-test was also utilised to compare the variance of two distributions. All univariate analysis was conducted in the GraphPad Prism package (version 4).

4.4 Results

4.4.1 Metabolomic Analysis

^{1}H-NMR spectroscopy, GC-MS, LC-MS and DI-MS analysis, combined with multivariate pattern recognition were used to profile metabolism within the white adipose tissue of *ob/ob* mice and 3T3-L1 murine cultured adipocytes treated with a PPARδ agonist. The different analytical techniques had varying sensitivities. High resolution ^{1}H-NMR spectroscopy detected ~15 metabolites in white adipose tissue and 25 identifiable metabolites in 3T3-L1 cells. GC-MS detected 100-150 defined peaks from aqueous phase samples in both cultured cells and tissue and 30-40 defined peaks from tissue organic phase samples and 60-70 metabolites from 3T3-L1 cells. Matching the mass spectra detected with those held in the NIST library identified 40-60% metabolites for aqueous extracts and ~70% for lipids. Phospholipid targeted UPLC-MS detected ~600 unique metabolite species in positive mode. Identification of metabolite species was performed using MS/MS.

To assess metabolic changes in the dataset a common processing strategy was adopted throughout the analysis. To investigate metabolite perturbations common to PPARδ activation PCA and PLS-DA models were built for both the white adipose tissue and the 3T3-L1 adipocytes. PCA and PLS-DA models were generated for the white adipose tissue and the cultured cells, comparing the control group with the PPARδ agonist treated groups. Metabolites identified in the VIP/coefficients plots as significantly contributing to separation in the models were then considered to have changed globally. The metabolite changes in the white adipose tissue and 3T3-L1 adipocytes are considered below.

4.4.1.1 White adipose tissue

The most robust multivariate model generated from the profiling of white adipose tissue was from the analysis of GC-MS FAME data (**Figure 4.1A**) where significant changes in fatty acid metabolism were detected. The concentration of longer chain fatty acids (pentadecanoic acid and palmitic acid) was decreased with a concomitant increase in the

concentration of the shorter chain fatty acids (caprylic acid C8:0, capric acid C10:0, lauric acid C12:0 and myristic Acid C14:0). Analysis of DI-MS negative mode ionisation data of the organic phase metabolites also generated robust multivariate models (Figure 4.1B), which indicated that the composition of the FFAs in the white adipose tissue of the *ob/ob* mice was altered upon PPARδ activation. A decrease in the concentration of the saturated long chain fatty acids (nonadecanoic acid C19:0, arachidic acid C20:0, henicosanoic acid C21:0 and behenic acid C22:0) was detected alongside an increase in the concentrations of the ω-6 fatty acid pathway intermediates (γ-linolenic acid C18:3, dihomo-γ-linolenic acid C20:3 and arachidonic acid C20:4). The concentration of free stearic acid and palmitic acid also increased, as did the desaturation products C18:1 and C18:2. One problem with investigating metabolic changes in whole animals is that changes in tissue metabolism are also influenced by alterations in systemic metabolism across the animal. This is particularly true for a PPARδ agonist which will profoundly influence a number of tissues. Hence, to address these metabolic changes were investigated in a tissue specific cell culture system.

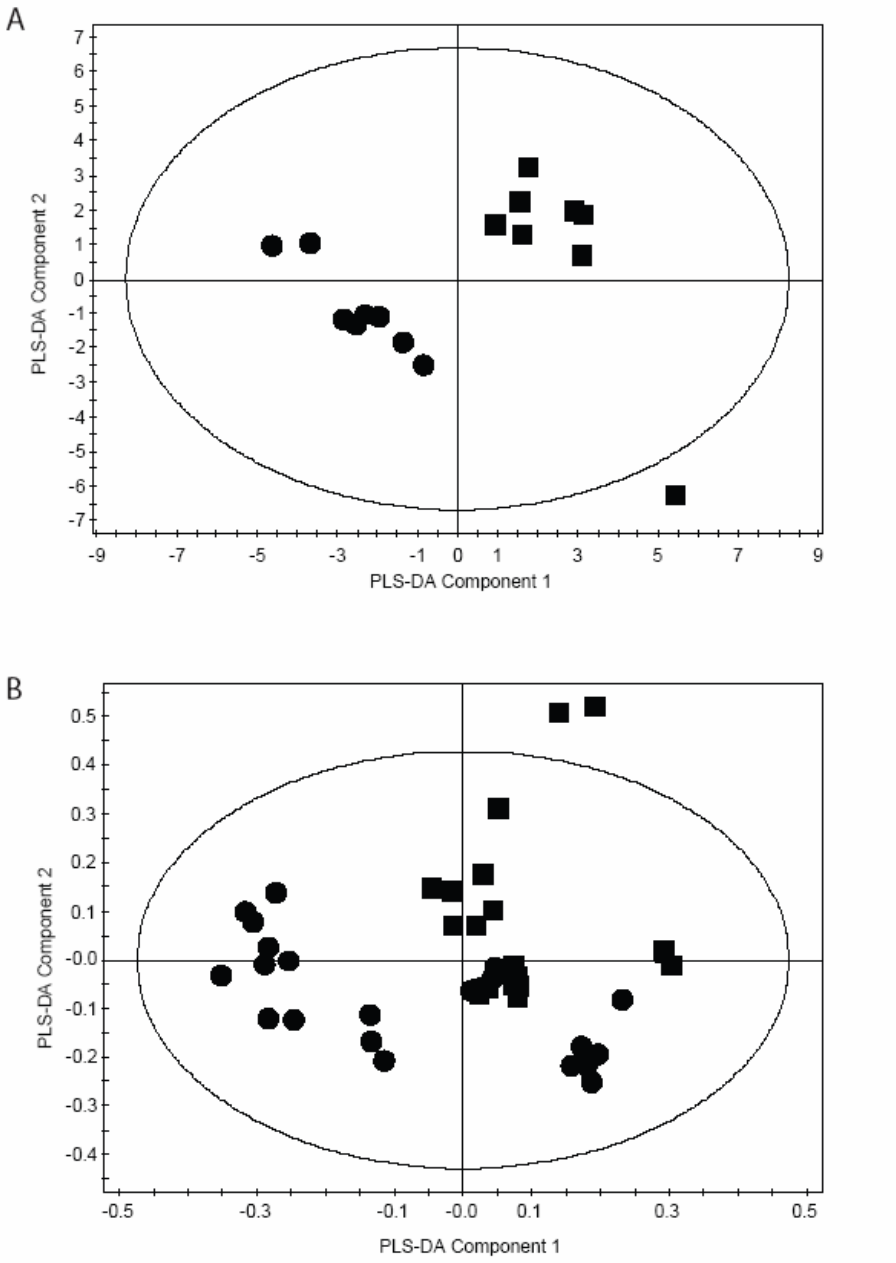

Figure 4.1: **A**. PLS-DA scores plot showing the clustering of GC-MS chromatograms from the organic fraction of the white adipose tissue from *ob/ob* mice treated with a PPARδ agonist compared with the control group. ●, PPARδ agonist treated, ■, control (R^2=0.321, Q^2=0.685). **B**. PLS-DA scores plot showing the clustering of DI-MS negative ionisation mode chromatograms from the organic phase of white adipose tissue extracts from *ob/ob* mice treated with a PPARδ agonist compared with control animals ●, PPARδ agonist treated, ■, control (R^2=0.724, Q^2=0.584). Two technical replicates were analysed.

4.4.1.2 3T3-L1 adipocytes

Investigation of the effects of PPARδ activation on the metabolism of the 3T3-L1 adipocyte tissue specific cell line within a cell culture system was conducted to generate an *in vitro* model of adipose tissue specific PPARδ activation. Oil red O staining for neutral lipids in the differentiated cells prior to treatment with the PPARδ agonist demonstrated that there were comparable levels of differentiation in the treatment groups (**Figure 4.2A**). Spectrophotometric measurement at 510 nm of eluted Oil Red O from stained cells post PPARδ agonist treatment determined that activation of PPARδ decreased the concentration of neutral lipid accumulated in the 3T3-L1 adipocytes (**Figure 4.2B**).

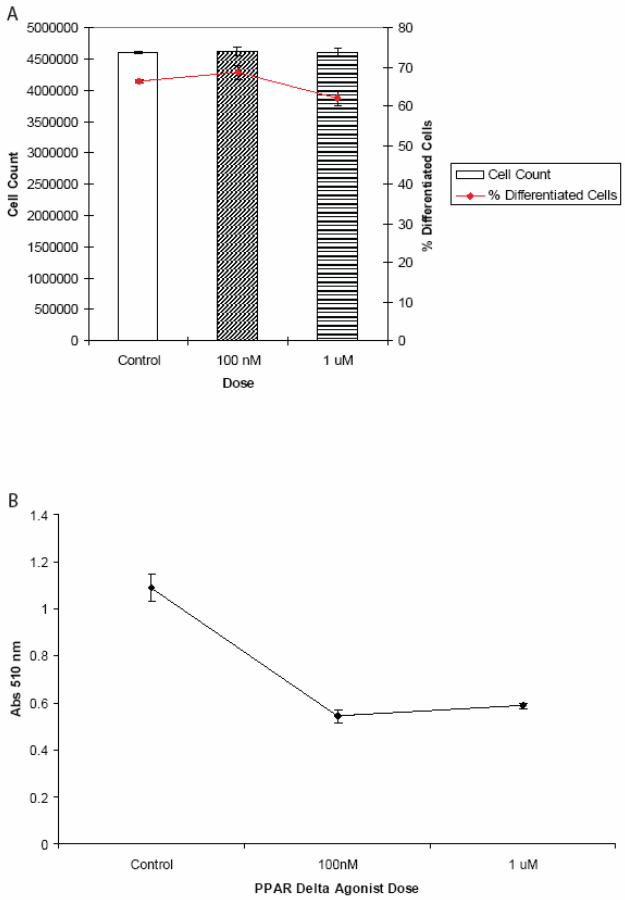

Figure 4.2: **A.** Graph showing cell counts and the percentage of differentiating cells prior to treatment with PPARδ agonist. **B.** Spectrophotometric measurement at 510 nm of Oil Red O eluted from stained 3T3-L1 cells treated with DMSO control, 100 nM and 1 μM GW610742 PPARδ agonist.

Global analysis of the 3T3-L1 metabolic response to PPARδ activation using the analytical platforms of GC-MS, LC-MS, DI-MS and ^{1}H-NMR spectroscopy and multivariate pattern recognition implicated a number of key pathways as being altered (**Figure 4.3**). A decrease in the concentration of a range of sugars including galactose, maltose and glucose and polyol pathway intermediates, glucitol and fructose was detected alongside an increase in the concentration of the TCA cycle intermediate isocitrate and glutamate, which is readily converted to 2-oxoglutarate. Also increased were the concentrations of the glucuronate and pentose interconversion pathway intermediates D-glucuronate-1-phosphate, myo-inositol and arabitol.

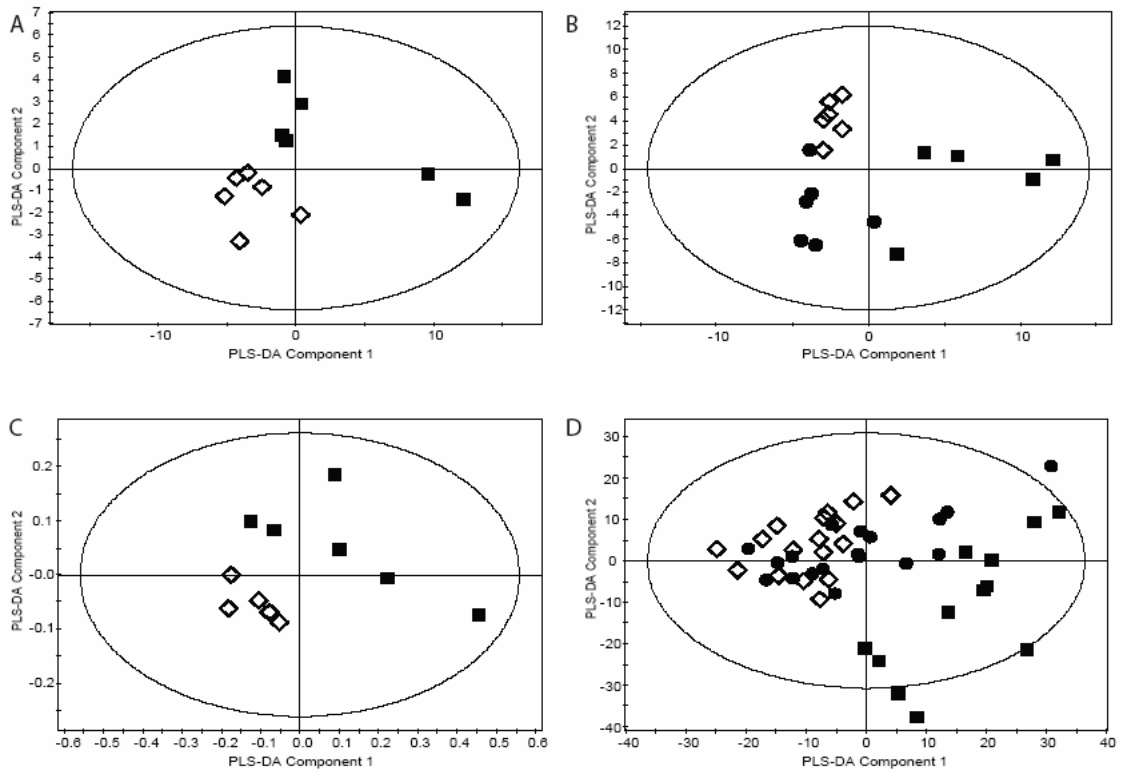

Figure 4.3: **A.** PLS-DA scores plot showing the clustering of GC-MS chromatograms from the organic fraction of 3T3-L1 adipocytes treated with 1 μM PPARδ agonist GW610742 compared with the control group. ◊, 1 μM PPARδ agonist dose, ■, control (R^2=0.82, Q^2=0.815). **B.** PLS-DA scores plot showing the clustering of GC-MS chromatograms from the aqueous fraction of 3T3-L1 adipocytes treated with 100 nM and 1 μM PPARδ agonist GW610742 compared with the control group. ◊, 1 μM PPARδ agonist dose, ●, 100 nM PPARδ agonist dose, ■, control (R^2=0.771, Q^2=0.746). **C.** PLS-DA scores plot showing the clustering of ^{1}H-NMR spectra from the aqueous fraction of 3T3-L1 adipocytes treated with 1 μM PPARδ agonist GW610742 compared with the control group. ◊, 1 μM PPARδ agonist dose, ■, control (R^2=0.871, Q^2=0.845). **D.** PLS-DA scores plot showing the clustering of DI-MS negative mode ionisation chromatograms from the organic fraction of 3T3-L1 adipocytes treated with 100 nM and 1 μM PPARδ agonist GW610742 compared with the control group. ◊, 1 μM PPARδ agonist dose, ●, 100 nM PPARδ agonist dose, ■, control (R^2=0.696, Q^2=0.853). Three technical replicates were analysed for DI-MS.

The high energy phosphate buffering capacity of the adipocytes was altered by PPARδ activation with a detected increase in the concentrations of both creatine and creatinine.

The essential fatty acid metabolism of the 3T3-L1 adipocytes was significantly affected by PPARδ activation. The concentration of the ω-6 fatty acid pathway intermediates and end products (dihomo-γ-linoleic acid C20:3, arachidonic acid C20:4 and docosatetraenoic acid C22:4) were increased as were the intermediates and end products of the ω-3 fatty acid pathway (eicosapentaenoic acid C20:5, docosapentaenoic acid C22:5 and docosahexaenoic acid C22:6).

The fatty acid oxidation/synthesis pathways were also altered by PPARδ activation. A range of fatty acids (undecanoic acid C11:0, tridecanoic acid C13:0, myristic acid C14:0, myristoleaic acid C14:1, 12-methyl myristic acid 12-methyl C14:0, pentadecanoic acid C15:0, pentadecenoic acid C15:1, palmitic acid C16:0, 14-methyl palmitic acid 14-methyl C16:0, palmitoleic acid C16:1, ethyl-9-palmitoleic acid ethyl-9-C16:1, margaric acid C17:0, heptadecenoic acid C17:1 and Oleate C18:1) were all identified as decreased in concentration with a concomitant increase in the concentration of the peroxisomal oxidation product, adipic acid.

Changes in the composition of complex lipids was observed in the PPARδ activated 3T3-L1 adipocytes. An increase in the concentration of a number of glycerophosphocholine (GPCho) species was ascertained (C34:1 GPCho, C32:0 16:0/16:0 GPCho, C36:1 GPCho, C34:1 GPCho, C36:2 GPCho, C36:3 GPCho, C35:5 GPCho, C34:0 GPCho). There was also a decrease in the concentration of specific TAGs (TAG C18:3/C17:0/C19:0), TAG C18:1/C17:1/C19:1, TAG C20:1/C17:1/C17:1, TAG C20:1/C15:0:C19:2, TAG C20:1/C15:1/C19:1, TAG C52:1, TAG C53:2, TAG C52:5, TAG C52:6).

4.4.2 ^{13}C-labelled Substrate Studies

In order to identify the metabolic mechanisms associated with PPARδ activation in 3T3-L1 adipocytes the ^{13}C-labelled substrates 1-^{13}C glucose and U-^{13}C-palmitate were used to monitor flux through glycolytic and fatty acid oxidative pathways.

4.4.2.1 1-^{13}C-glucose

Analysis by HSQC-NMR spectroscopy of the organic fraction of control and PPARδ agonist treated adipocytes incubated in media containing 1-^{13}C glucose showed that glycerol and esterified glycerol from PPARδ treated cells had reduced enrichment compared with the control group (**Figure 4.4**). Examination of the aqueous phase by GC-MS revealed that lactate, glutamate (readily labelled from the TCA cycle from labelled 2-oxoglutarate) and succinate from PPARδ agonist treated cells were enriched with ^{13}C when compared to control (**Figure 4.5**). GC-MS investigation of the organic fraction showed that palmitic acid from control adipocytes incubated in 1-^{13}C glucose had a greater concentration of ^{13}C enrichment than that of PPARδ agonist treated cells.

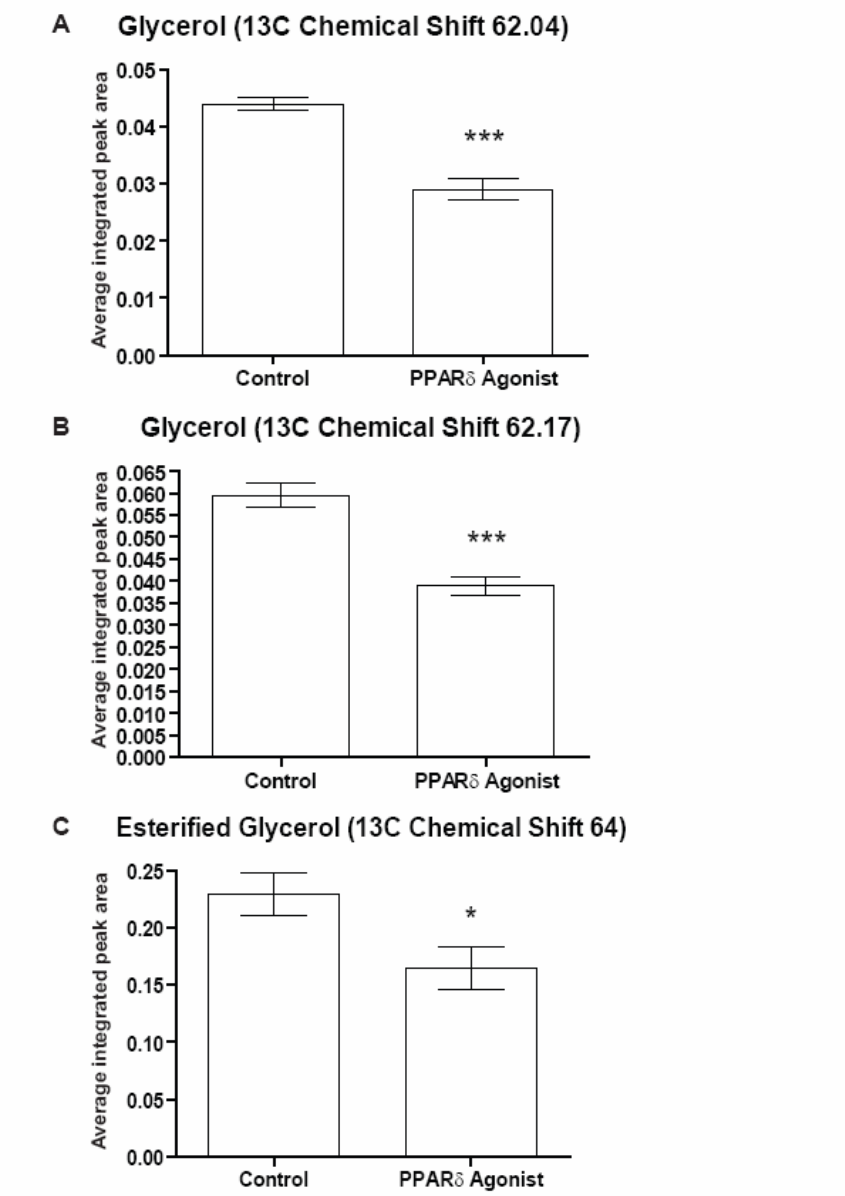

Figure 4.4: **A.** A graph of the average integrated area of the 2D-HSQC-NMR organic fraction glycerol peak (^{13}C Chemical shift 62.04) from control and 1 μM PPARδ agonist treated 3T3-L1 adipocytes incubated in 1-^{13}C-glucose. **B.** A graph of the average integrated area of the 2D-HSQC-NMR organic fraction glycerol peak (^{13}C Chemical shift 62.17) from control and 1 μM PPARδ agonist treated 3T3-L1 adipocytes incubated in 1-^{13}C-glucose. **C.** A graph of the average integrated area of the 2D-HSQC-NMR organic fraction esterified glycerol peak from control and 1 μM PPARδ agonist treated 3T3-L1 adipocytes incubated in 1-^{13}C-glucose. *P < 0.05, ***P < 0.005. Parent ions were used to calculate ion ratio.

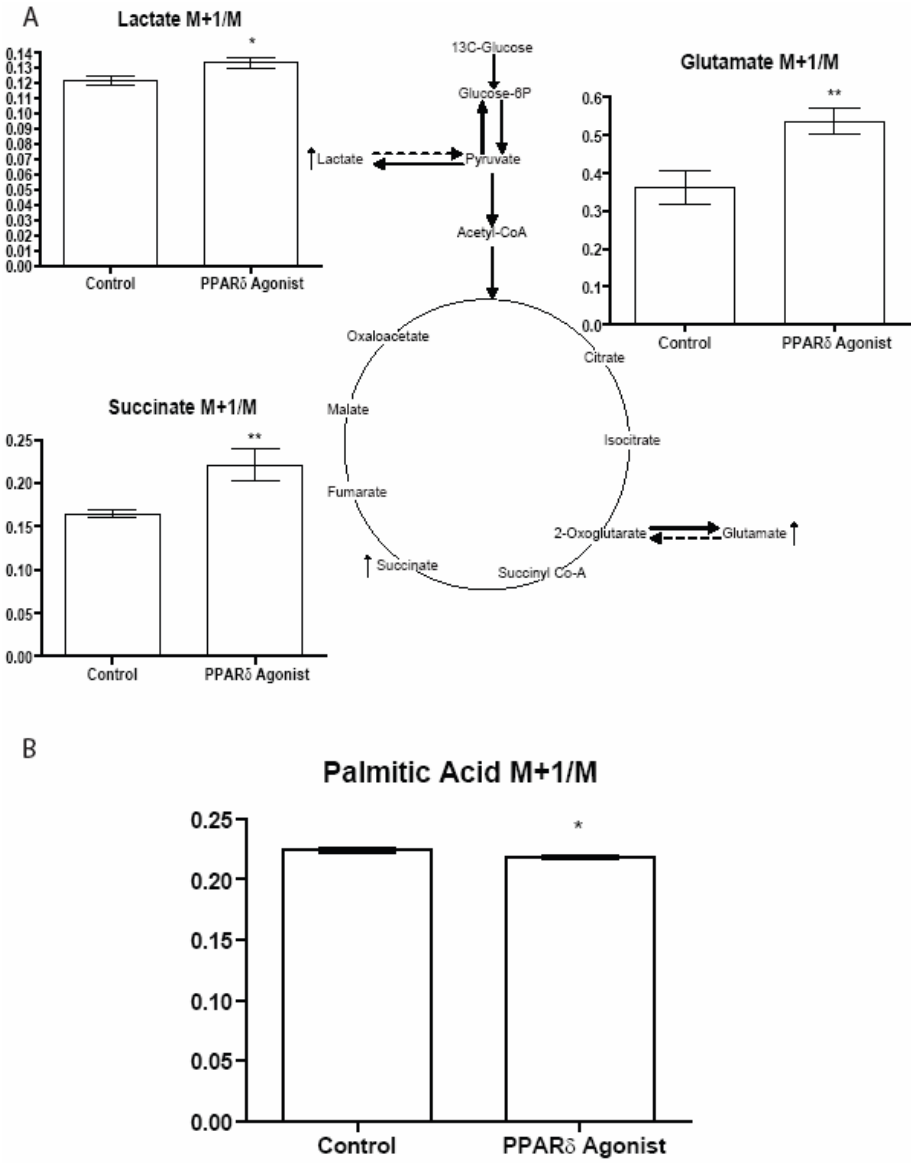

Figure 4.5: **A.** Graphs showing the M+1/M isotope ratio ^{13}C enrichment of lactate, glutamate and succinate analysed by GC-MS of the aqueous fraction from control and PPARδ agonist dosed 3T3-L1 cells incubated with 1-^{13}C-glucose. *P < 0.05, **P < 0.01. The metabolites have been mapped to the glycolysis and TCA cycle metabolic pathways. ↑ indicates a metabolite increased in ^{13}C enrichment by PPARδ activation. **B.** Graph showing the M+1/M isotope ratio ^{13}C enrichment of palmitic acid analysed by GC-MS of the organic fraction from control and PPARδ agonist dosed 3T3-L1 cells incubated with 1-^{13}C-glucose. *P < 0.05. Parent ions were used to calculate ion ratio.

4.4.2.2 U-^{13}C-palmitate

Assessment of the aqueous phase by GC-MS indicated that the TCA cycle intermediates malate, fumarate, succinate and glutamate from PPARδ agonist treated adipocytes were enriched compared to control cells (**Figure 4.6A**). Investigation of the organic phase by GC-MS demonstrated that the fatty acids downstream of palmitic acid in the β-oxidation pathway, myristic acid and lauric acid, showed greater ^{13}C enrichment in PPARδ agonist treated cells; as did palmitoleic acid, the Δ-9 desaturation product of palmitic acid. Simultaneously the enrichment of stearic acid and arachidic acid, which are upstream of palmitic acid in the fatty acid synthesis pathway, was reduced in PPARδ agonist treated cells (**Figure 4.6B**).

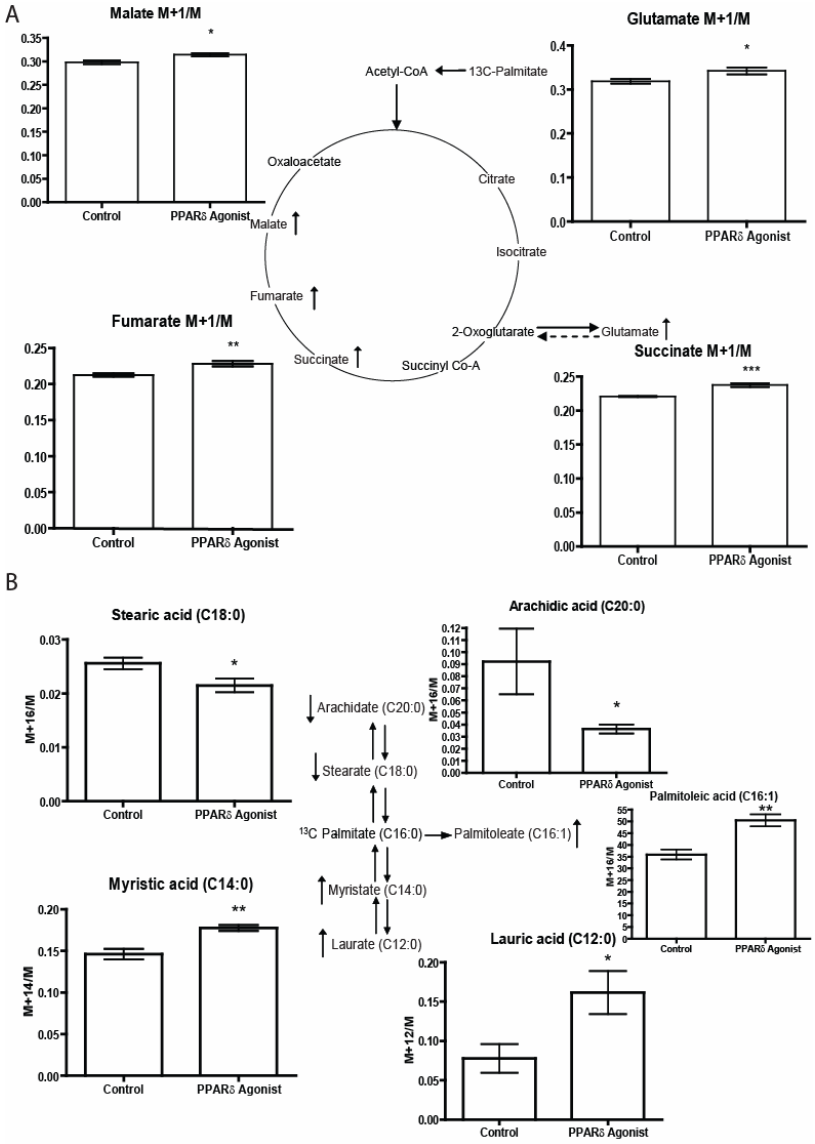

Figure 4.6: **A.** Graphs showing the M+1/M isotope ratio ^{13}C enrichment of malate, glutamate, fumarate and succinate analysed by GC-MS of the aqueous fraction from control and PPARδ agonist dosed 3T3-L1 cells incubated with U-^{13}C-palmitate. *P < 0.05, **P < 0.01,***P < 0.005. The metabolites have been mapped to the TCA cycle metabolic pathway. ↑ indicates a metabolite increased in ^{13}C enrichment by PPARδ activation. **B.** Graphs showing the isotope ratio ^{13}C enrichment of arachidic acid, stearic acid, palmitoleic acid, myristic acid and lauric acid analysed by GC-MS of the organic fraction from control and PPARδ agonist dosed 3T3-L1 cells incubated with U-^{13}C-palmitate. *P < 0.05, **P < 0.01. The metabolites have been mapped to the fatty acid synthesis/β-oxidation pathway. ↑ indicates a metabolite increased, and ↓ indicates a metabolite decreased in ^{13}C enrichment by PPARδ activation. Parent ions were used to calculate ion ratio.

4.4.3 Respirometric Analysis

Following the identification of increased flux through the glycolytic, TCA cycle and β-oxidation metabolic pathways in 3T3-L1 adipocytes treated with PPARδ agonist, respirometric analysis was conducted to investigate the influence of PPARδ activation on the rate of oxygen consumption of the cells. The oxygen consumption of PPARδ agonist treated and control 3T3-L1 cells was measured both when using fatty acid as substrate and isolated electron transport chain complex IV oxidation using *in situ* studies in a Clarke type oxygen electrode. Both complex IV and fatty acid oxidation were significantly increased in the adipocytes exposed to the PPARδ agonist when compared to control adipocytes (**Figure 4.7A** and **Figure 4.7B**).

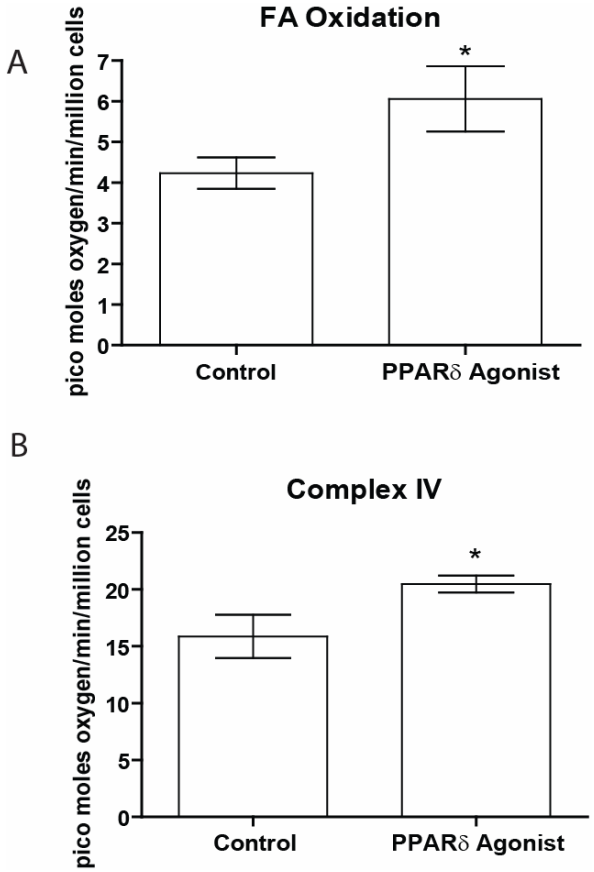

Figure 4.7: **A.** Graph showing the respiratory rates of *in situ* permeabilised control and PPARδ agonist treated 3T3-L1 cells performing β-oxidation using palmitoyl-carnitine measured using a Clark-type oxygen electrode. *P = 0.05. **B.** Graph showing the respiratory rates of the electron transport chain complex IV of *in situ* permeabilised control and PPARδ agonist treated 3T3-L1 cells measured using a Clark-type oxygen electrode. *P < 0.05.

4.4.4 Microarray Transcriptomic Analysis

The combination of steady state metabolomic changes in adipose tissue and adipocytes and isotope labelling studies indicated a profound upregulation of β-oxidation following PPARδ activation. These changes were investigated in further detail by scrutinising the transcriptome using microarray analysis of PPARδ activation in adipocytes. Of the 45281 probes utilised 13718 were expressed above the background defined by the negative control probe. From these 2349 were determined to be differentially expressed ($P < 0.05$) between PPARδ agonist treated and control 3T3-L1 adipocytes, with 117 estimated false positives using a threshold of 5% of differentially expressed probes. Multivariate models were built using the normalised data from the 13718 transcripts measured (**Figure 4.8**).

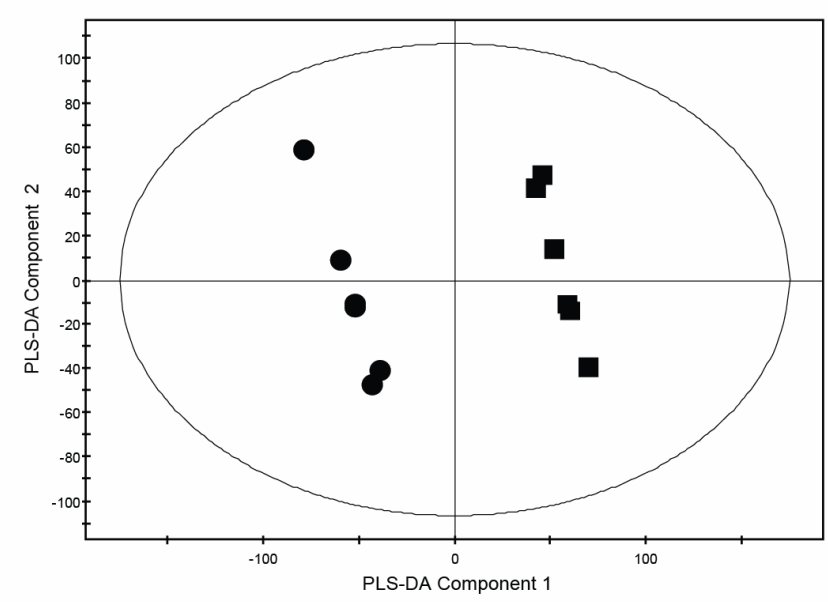

Figure 4.8: PLS-DA scores plot showing the clustering of gene transcription in control and PPARδ agonist treated 3T3-L1 adipocytes as measured with microarray analysis. ●, PPARδ agonist treated, ■, control (R^2=0.35, Q^2=0.9).

The 6% of transcripts most responsible for separation in the multivariate models were then examined (3% most increased and 3% most decreased in PPARδ agonist treated cells as identified in the multivariate models). The multivariate analysis indicated that the mRNA of genes involved in a number of key metabolic pathways was altered following PPARδ activation. The reactome skypainter tool was then utilised to

determine which pathways and reactions were statistically overrepresented by the 3% most increased (**Table 4.1**) and 3% most decreased transcripts in PPARδ agonist treated cells identified in the multivariate models.

P-value	Pathway	Transcripts increased in PPARδ agonist treated cells mapping to the pathway
6.3e-08	Glucose regulation of insulin secretion	Cycs, Etfa, Mdh2, Aldoa, Dld, Ndufb10, Ndufb9, Atp5a1, Ndufb5, Gpi1, Tpi1, Pgk1, mt-Co2, Sdhb, Sdhd, mt-Atp6, Cox7b, Ndufb2
1.3e-06	Integration of energy metabolism	Cycs, Etfa, Mdh2, Aldoa, Dld, Ndufb10, Ndufb9, Atp5a1, Cpt2, Ndufb5, Gpi1, Tpi1, Pgk1, mt-Co2, Sdhb, Sdhd, mt-Atp6, Cox7b, Ndufb2
1.3e-06	Diabetes pathways	Hspa8, Cycs, Wdr89, Etfa, Mdh2, Aldoa, Dld, Ndufb10, Myo5a, Ndufb9, Atp5a1, Rps21, Rps3a, Sec11c, Ndufb5, Gpi1, Tpi1, Pgk1, Sdhb, mt-Co2, Dnajb9, Sdhd, mt-Atp6, Cox7b, 2900062L11Rik, Ndufb2
8.5e-06	Electron transport chain	Cycs, Ndufb5, Etfa, mt-Co2, Ndufb10, Sdhb, Sdhd, Ndufb9, Cox7b, Ndufb2
3.4e-05	H2AX in recruitment of repair factors for DNA damage and double strand breaks	Hist1h2ah, Hist2h2ac, Hist1h2ao, Hist1h2af
7.1e-04	Citric acid cycle (TCA cycle)	Dld, Sdhb, Sdhd, Mdh2
1.4e-03	Mitochondrial fatty acid β-oxidation of saturated and unsaturated fatty acids	Hadhb, Acadl, Acadvl
1.6e-03	Glycolysis	Aldoa, Tpi1, Pgk1, Gpi1
1.7e-03	G1/S DNA damage checkpoints	Cdc25a, Rfwd2, Psmd12, Cdk2, Psmd14, Psmd11
2.1e-03	Gluconeogenesis	Aldoa, Tpi1, Pgk1, Mdh2, Gpi1
3.2e-03	Transfer of electrons through the succinate dehydrogenase complex	Sdhb, Sdhd
4.3e-03	Glucose metabolism	Pgm2, Aldoa, Tpi1, Pgk1, Dld, Mdh2, Gpi1
4.5e-03	Metabolism of lipids and lipoproteins	Agpat3, Hadhb, Ppp1cc, Slc27a1, Lass2, Angptl4, Cpt2, Akr1b3, Abcd3, Acadl, Sgpl1, Acaa2, Acadvl, Mod1, Hmgcs2, Adfp
5.3e-03	Metabolism of carbohydrates	Prps2, Mdh2, Gpi1, Aldoa, Pgm2, Pgk1, Tpi1, Dld
7.8e-03	Cdc25A mediated dephosphorylation of Cyclin A:phospho-Cdk2	Cdc25a, Cdk2
7.8e-03	Cleavage of the signal peptide of preproghrelin	Sec11c, 2900062L11Rik
7.8e-03	Notch 1 traffic and signalling	Notch1, Fbn1

7.8e-03	PEX-19 docks ABCD1/ABCD3 to peroximal membrane	Abcd3, Pex19
7.8e-03	Formation of acetoacetic acid in synthesis of ketone bodies	Hmgcs2, Acaa2
1.1e-02	Dephosphorylation of Cyclin:phospho-Cdc complexes in cell cycle regulation	Cdc25a, Cdk2
1.5e-02	Activation of the mRNA upon binding of the cap-binding complex and eIFs, and subsequent binding to 43S	Rps3a, Eif4b, Pabpc1, Eif4ebp1, Rps21
1.8e-02	Cyclin:Cdk-associated events at G1/S phase DNA damage checkpoint transition in the cell cycle	Cdc25a, Psmd12, Cdk2, Psmd14, Psmd11
2.0e-02	Proteasome mediated degradation of COP1	Rfwd2, Psmd12, Psmd14, Psmd11
2.0e-02	DARPP-32 events	Ppp1cc, Cdk2, Pde1b
2.2e-02	Synthesis of deoxyribonucleoside 5'-diphosphates from ribonucleoside 5'-diphosphates	Glrx2, Txn1
3.2e-02	Additional cell cycle checkpoints	Cdc25a, Cdc20, Rfwd2, Psmd12, Cdk2, Psmd14, Psmd11

Table 4.1: Table of the pathways and reactions statistically significant in the 3% most increased transcripts in PPARδ agonist treated cells identified in the multivariate models. From a given set of genes known to participate in a pathway, the total genes for *mus musculus* and the submitted list of genes (the genes increased in PPARδ activated cells) of which N genes participate in the given pathway, the probability of observing at least N genes from a pathway if that pathway is not overrepresented in the submitted list of genes is calculated using the one-tailed version of Fisher's exact test. A p-value smaller than or equal to the significance level suggests that the pathway is significantly represented. The genes increased in expression and contributing to each pathway are shown.

Key pathways of homeostatic regulation identified as statistically affected from the transcripts increased in expression by PPARδ activation as can be seen in table 1 include regulation of insulin secretion, integration of energy metabolism and pathways implicated in diabetes. Specific metabolic pathways and reactions were also influenced by PPARδ activation.

The expression of genes coding proteins involved in the mitochondrial β-oxidation pathway was increased. Transcription of several of the core enzymes including carnitine

palmitoyltransferase II, very long chain acyl-Coenzyme A dehydrogenase, long chain acyl-Coenzyme A dehydrogenase, hydroxyacyl-Coenzyme A dehydrogenase/3-ketoacyl-Coenzyme A thiolase/enoyl-Coenzyme A hydratase trifunctional enzyme and acetyl-CoA acyltransferases 2 were increased in PPARδ agonist treated cells. An increase in the expression of a number of genes functioning in peroxisomal fatty acid β-oxidation was also detected and includes peroxisomal D3,D2-enoyl-CoA isomerase, peroxisomal enoyl Coenzyme A hydratase 1 and ATP-binding cassette, sub-family D, member 3. Alongside these changes were an increase in the transcription of genes involved in both mitochondrial and peroxisomal biogenesis and maintenance (mitochondrial specific Single stranded DNA binding protein 1, mitochondrial ribosomal proteins S6 and S12 and peroxisomal biogenesis factors 14 and 19).

The transcription of several genes whose products play a role in the glycolytic metabolic pathway was also upregulated in PPARδ agonist treated cells. Affected transcripts include those for phosphoglucomutase 2, glucose phosphate isomerise 1, aldolase A, fructose-bisphosphate and phosphoglycerate kinase 1. The expression of genes encoding enzymes responsible for the catalysis of the reactions of the TCA cycle, malate dehydrogenase, components of the succinate dehydrogenase complex and dihydrolipoamide dehydrogenase, was also upregulated.

There was a detected increase in the expressed mRNA concentrations of components of the electron transport chain. Amongst the increased transcripts were NADH dehydrogenase and several of its accessory subunits, cytochrome c, cytochrome c oxidase II and ATP synthase.

The metabolomic data indicated that the Δ-9 desaturation of fatty acids was a key point in the PPARδ regulated processing of fatty acids. However, the transcripts coding for the fatty acid desaturase 3 and the stearoyl-CoA desaturase, enzymes responsible for the desaturation of fatty acids were not found in the 3% most increased transcripts from PPARδ agonist treated cells. Therefore the normalised data for these transcripts was selected for univariate statistical analysis. Using an unpaired Student's t-*t*est with a

significance level set to $p<0.05$ and an F-test, utilised to compare the variance of two distributions, the transcription of both fatty acid desaturase 3 and stearoyl-CoA desaturase was found to be significantly increased in PPARδ agonist treated adipocytes (**Figure 4.9**).

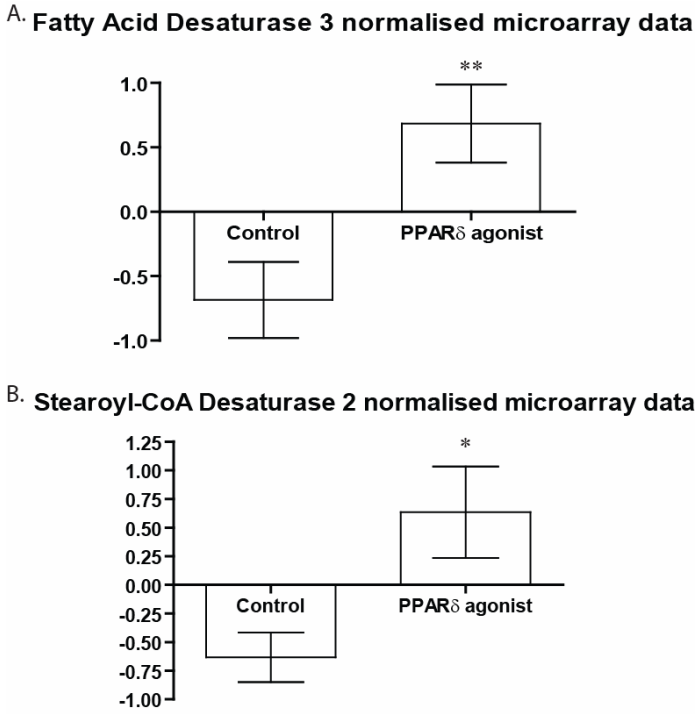

Figure 4.9 Graphs of the microarray normalised data for the transcripts of **A.** fatty acid desaturase 3 and **B.** stearoyl-CoA desaturase 2 in control and PPARδ agonist treated 3T3-L1 adipocytes analysed using an unpaired Student's t-*t*est. The transcription of both fatty acid desaturase 3 and stearoyl-CoA desaturase was found to be significantly increased in PPARδ agonist treated adipocytes. *P < 0.05, **P < 0.01.

4.5 Discussion

A comprehensive array of analytical techniques were used in a metabolomic investigation to study the metabolic changes occurring in white adipose tissue from *ob/ob* mice following PPARδ activation and to understand the role of PPARδ in treating the combined effects of type II diabetes and obesity. Experimentation was then progressed into a tissue specific cell line (3T3-L1 adipocytes) within a cell culture system to generate an *in vitro* model of PPARδ activation in adipose tissue, and in particular to investigate the upregulation of fatty acid oxidation in isolation from changes induced by PPARδ activation in other tissues, and systemic metabolism as a whole. However, steady state metabolite concentrations cannot fully define changes in flux. To elucidate the metabolic mechanisms responsible for the observed changes in metabolite concentrations, within adipose tissue, a ^{13}C stable isotope substrate labelling study, respirometric study and transcriptomic microarray study were employed.

PPARδ activation in white adipose tissue generated changes in the fatty acid composition whereby there was a decrease in the concentration of the longer chain fatty acids and a concomitant increase in the shorter chain fatty acids. The detected alterations in the constituent fatty acids were indicative of an increase in fatty acid β-oxidation resulting from PPARδ activation. When examining PPARδ activation in the 3T3-L1 adipocyte cell line it was again found that there was a decrease in the concentration of a range of fatty acids alongside an increase in the concentration of TCA cycle intermediates and adipic acid, the main end product of peroxisomal β-oxidation[220].

The mechanism by which PPARδ activation brought about the alterations in fatty acid composition was confirmed using U-^{13}C-palmitate and 1-^{13}C-glucose. The U-^{13}C-palmitate labelling study established that PPARδ activation resulted in an increase in flux through the β-oxidation pathway, as ^{13}C-enrichment was increased in shorter chain fatty acids from PPARδ treated adipocytes, found downstream of palmitate in the β-oxidation pathway, relative to the control group. The ^{13}C-enrichment of TCA cycle intermediates

was increased in adipocytes incubated in U-^{13}C-palmitate and treated with the PPARδ agonist relative to the enrichment in the control adipocytes, confirming increased oxidative breakdown of fatty acids. Concomitantly the fatty acid synthesis pathway was confirmed as downregulated; longer chain fatty acids found upstream in the synthesis pathway showed decreased ^{13}C-enrichment in 3T3-L1 adipocytes incubated in labelled palmitate and treated with the PPARδ agonist compared with the control group. A result reciprocated by the decreased ^{13}C-enrichment detected in palmitate from cells incubated with 1-^{13}C-glucose and treated with the PPAR agonist when compared to control adipocytes. This conclusion was supported by the respirometric data which confirmed that adipocytes treated with PPARδ had a higher oxidative rate when using fatty acids as a fuel source. Transcriptomic analysis supported the findings from the metabolic studies with identified increases in the transcription of genes involved in fatty acid mitochondrial and peroxisomal β-oxidation including carnitine palmitoyltransferase II, very long chain acyl-Coenzyme A dehydrogenase, long chain acyl-Coenzyme A dehydrogenase, hydroxyacyl-Coenzyme A dehydrogenase/3-ketoacyl-Coenzyme A thiolase/enoyl-Coenzyme A hydratase trifunctional enzyme, acetyl-CoA acyltransferases 2, D3,D2-enoyl-CoA isomerase, peroxisomal enoyl Coenzyme A hydratase 1 and ATP-binding cassette, sub-family D, member 3).

A further key finding was that PPARδ activation lead to an increase in the oxidation of glucose. The metabolomic studies demonstrated that upon PPARδ activation the steady state concentration of several sugars, including glucose was decreased and accompanied by an increase in several TCA cycle intermediates. An increase in the catabolism of glucose resulting from PPARδ activation was confirmed using 1-^{13}C-glucose with the observation that the enrichment of lactate, succinate and glutamate in cells treated with PPARδ agonist was greater than that of control adipocytes. Transcriptomic analysis substantiated this finding with the identification that the expression of genes with roles in glycolysis and the TCA cycle was significantly increased upon PPARδ activation. Genes affected include those for phosphoglucomutase 2, glucose phosphate isomerise 1, aldolase A, fructose-bisphosphate, phosphoglycerate kinase 1, malate dehydrogenase,

components of the succinate dehydrogenase complex and dihydrolipoamide dehydrogenase.

Additional evidence for an increase in global oxidative metabolism, over a view of exclusive fatty acid oxidation, comes from the respirometric studies, in which it was ascertained that independently of fatty acid oxidation the oxidative rate of electron transport chain complex IV was increased with PPARδ activation. An increase in global oxidation resulting from PPARδ activation is supported by transcriptomic analysis which shows that the receptor is responsible for increases in mitochondrial biogenesis and expression of key electron transport chain components such as cytochrome c, cytochrome c oxidase, complex II and ATP synthase.

Supporting the evidence for increased global oxidative metabolism is the finding that PPARδ activation increased the concentration of creatine and creatinine within the 3T3-L1 adipocytes and so altered the high energy phosphate buffering capacity of the cells. These findings are consistent with previously reported observations in skeletal muscle. A decrease in the intramyocellular lipid-to-total creatine ratio in the soleus and tibialis anterior muscles from Sprague-Dawley rats treated with selective PPARδ agonist GW610742 has been discerned using *in vivo* ^{1}H-MRS[221]. In addition an increase in the concentration of creatine and phosphocreatine was detected in the gastrocnemius of *ob/ob* mice following pharmacological activation of PPARδ[222].

The ω-6 essential fatty pathway and both the ω-3 and ω-6 essential fatty acid pathways were upregulated in PPARδ agonist treated *ob/ob* mice white adipose tissue and 3T3-L1 adipocytes, respectively. The Δ 6-desaturase is integral to both pathways; the enzyme introduces the initial double bond to linoleate forming γ-linolenate in the ω-6 pathway and introduces the double bond to linolenate forming stearidonic acid. The Δ 6-desaturase gene is known to contain a PPRE and is under PPAR transcriptional control[223] and therefore appears to be the point of PPARδ transcriptional control within the essential fatty acid pathways.

Using U-^{13}C-palmitate it was shown that when PPARδ is activated in 3T3-L1 adipocytes the enrichment of palmitoleate is increased relative to control and therefore desaturation of palmitate to palmitoleate is increased. Stearoyl-CoA desaturase, the enzyme responsible for the Δ-9 desaturation of saturated fatty acids to the monounsaturated form, is known to be under PPAR expressional control[224]. Univariate analysis of the normalised microarray data for stearoyl-CoA desaturase and fatty acid desaturase 3, an additional enzyme responsible for the Δ-9 desaturation of fatty acids, demonstrated that the expression of these enzymes was increased in the PPARδ agonist treated adipocytes.

A decrease in the concentration of a number of TAGs was observed in the 3T3-L1 adipocytes. Within white adipose tissue a number of FFAs, such as palmitic acid, were increased in concentration despite their total concentration within the tissue decreasing. These metabolic alterations are complicit with previously observed changes indicating that PPARδ activation in white adipose tissue results in an increase in lipolysis in the tissue[225]. The results are corroborated by our observation, made using HSQC-NMR, that there was a decrease in the enrichment of glycerol in adipocytes incubated with 1-^{13}C-glucose and treated with PPARδ agonist when compared to control cells; indicating reduced synthesis of glycerol from glucose on activation of PPARδ. This, in part, could also explain the decrease in the concentration of TAGs due to reduced synthesis. It is reasonable to conclude that PPARδ activation leads to a mobilisation of lipid stores and concomitant decrease in the synthesis of the complex lipids such as TAGs required for fatty acid storage.

It is worthy of note that the concentrations of several metabolites in the polyol pathway were decreased in concentration following PPARδ activation; a finding likely to be more attributable to increased glucose catabolism than direct control of the pathway by the receptor. However, given the role that the polyol pathway and aldose reductase have in the formation of toxic advance glycation end-products and resultant diabetic complications such as neuropathy, nephropathy and retinopathy, a decrease in the activity of this pathway may prove a significant anti-diabetic effect of PPARδ activation[226].

The increased concentrations of the glucuronate and pentose phosphate pathway intermediates can be explained by previous studies which demonstrate that PPARδ increases glucose flux through the pentose phosphate pathway contributing to the nuclear receptors ability to ameliorate hyperglycaemia; it has been suggested that the glyceraldehyde-3-phosphate, formed from the 5-carbon sugar phosphates during the pentose phosphate shunt, can then enter glycolysis[227].

4.6 Conclusions

To summarise, it has been shown that the anti-diabetic and anti-obesity effects of PPARδ activation are brought about, in part, by a decrease in fatty acid synthesis and fat storage within synthesised TAG depots and a concomitant mobilisation of complex lipid fat stores. The mobilisation of lipid energy stores is accompanied by upregulation of not only fatty acid oxidation but also by carbohydrate oxidative metabolism in white adipose tissue, a tissue not traditionally thought of as being energetic and oxidative. Essential to this process is the integration and co-ordination of the energy metabolism pathways, which PPARδ accomplishes by upregulating the transcription of a series of genes involved in glycolysis, the TCA cycle, the electron transport chain and fatty acyl β-oxidation (**Figure 4.10**) (**Table 4.1**).

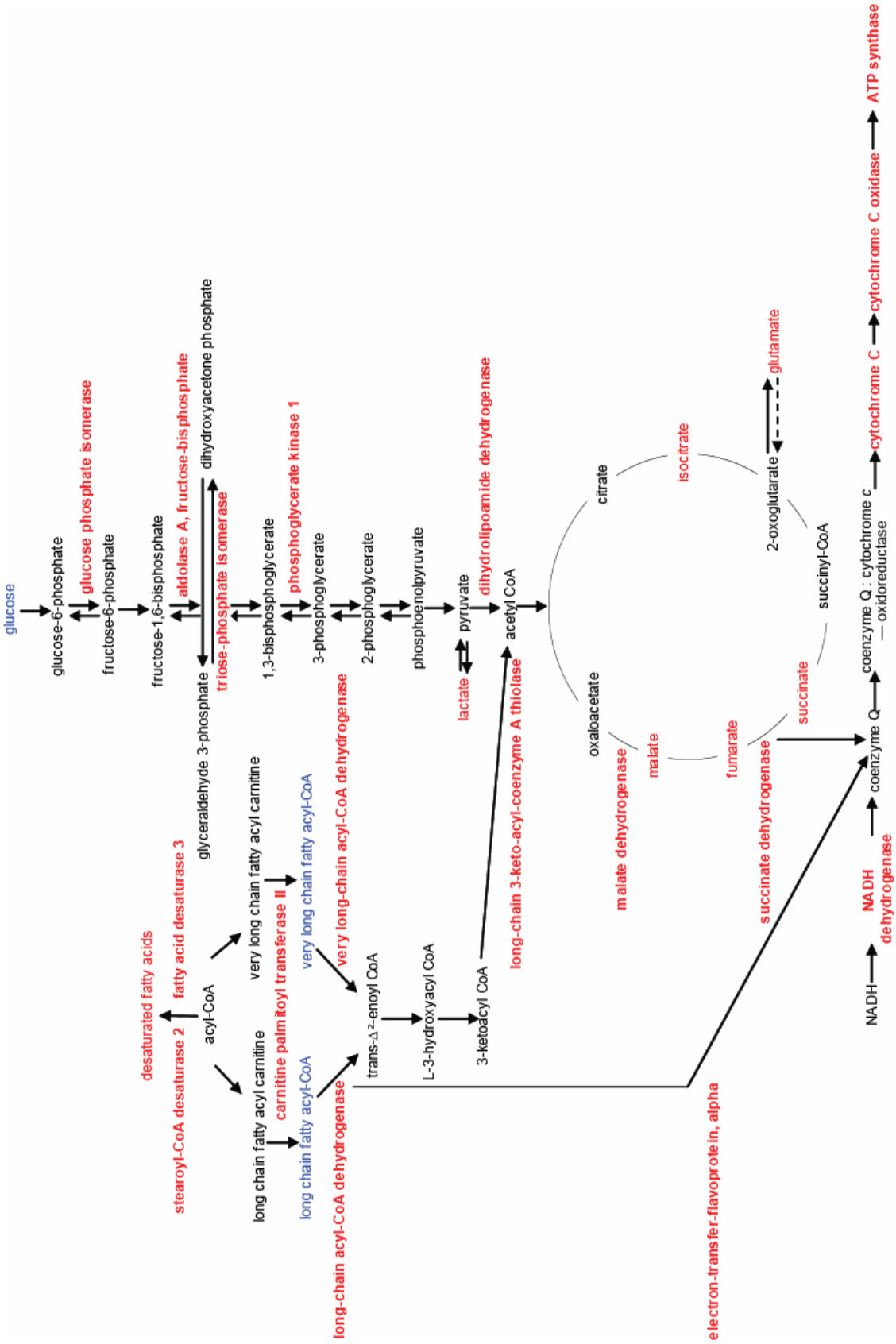
glucose
glucose-6-phosphate
glucose phosphate isomerase
fructose-6-phosphate
fructose-1,6-bisphosphate
aldolase A, fructose-bisphosphate
glyceraldehyde 3-phosphate
dihydroxyacetone phosphate
triose-phosphate isomerase
1,3-bisphosphoglycerate
phosphoglycerate kinase 1
3-phosphoglycerate
2-phosphoglycerate
phosphoenolpyruvate
pyruvate
lactate
dihydrolipoamide dehydrogenase
acetyl CoA
citrate
isocitrate
2-oxoglutarate
glutamate
oxaloacetate
malate dehydrogenase
malate
fumarate
succinate dehydrogenase
succinate
succinyl-CoA
desaturated fatty acids
fatty acid desaturase 3
stearoyl-CoA desaturase 2
acyl-CoA
very long chain fatty acyl carnitine
carnitine palmitoyl transferase II
long chain fatty acyl carnitine
very long chain fatty acyl-CoA
long chain fatty acyl-CoA
very long-chain acyl-CoA dehydrogenase
long-chain acyl-CoA dehydrogenase
trans-Δ²-enoyl CoA
L-3-hydroxyacyl CoA
3-ketoacyl CoA
long-chain 3-keto-acyl-coenzyme A thiolase
electron-transfer-flavoprotein, alpha
coenzyme Q
coenzyme Q : cytochrome c — oxidoreductase
cytochrome C
cytochrome C oxidase
ATP synthase
NADH
NADH dehydrogenase

Figure 4.10: Diagram showing the effect of PPARδ activation on the integration of the energy metabolism pathways of 3T3-L1 adipocytes based on the combination of results from the metabolomic, transcriptomic and stable isotope labelling studies. Red indicates an increase in concentration or expression in cells treated with the GW610742 PPARδ selective agonist. Blue indicates a decrease in concentration in cells treated with the GW610742 PPARδ selective agonist.

In conclusion PPARδ activation in white adipose tissue does not exclusively stimulate either fatty acid oxidation or carbohydrate oxidation but rather global oxidative metabolism; activation of the nuclear receptor burns fatty acids by stoking the carbohydrate fire.

Chapter 5

Tissue Specific PPARγ Activation Sequesters Glucose and Lipid into the White Adipose Tissue Storage Depot

5.1 Introduction

PPARγ is a ligand activated transcription factor belonging to the PPAR nuclear receptor family. Upon binding its ligand the receptor heterodimerises with the RXR and binds to specific sequences in target genes known as PPRE[135]. Once bound to ligand the PPARs undergo a conformational change, facilitating the release of corepressors and allowing the binding of transcriptional coactivators[228]. The receptor exists in two distinct protein isoforms, PPARγ$_1$ and PPARγ$_2$, which exhibit specific tissue expression patterns[229]. PPARγ$_1$ is found almost ubiquitously whereas the PPARγ$_2$ isoform is definitively expressed in adipose tissue[230].

White adipose tissue is vital to the control of energy metabolism and global lipid homeostasis. PPARγ plays an essential role within adipose tissue, where it is the master regulator of adipogenesis and key to mature adipocyte survival[158, 159]. The receptor is also a crucial regulator of lipid metabolism in mature adipocytes. Activation of PPARγ regulates expression of several lipid metabolism genes including oxidized LDL receptor 1, lipoprotein lipase, the glycerol transporter aquaporin 7, phosphoenolpyruvate carboxykinase and fatty-acid transport protein[231, 232, 233, 234]. Upregulation of these genes results in an increase in the uptake of circulating fatty acids and consequentially an enhancement of adipocyte lipid storage. PPARγ activation also inhibits lipolysis[235],

upregulates the expression of GLUT4 glucose transporter mRNA levels and increases glucose uptake in adipocytes[236].

Despite its role in adipose tissue formation, PPARγ is also a target for insulin sensitising drugs for the treatment of TIIDM[164]. The TZD class of compounds are PPARγ ligands currently available in the clinic that bring about insulin sensitisation[163]. Nevertheless, the use of TZDs for the treatment of TIIDM has not been without controversy. In 2007 meta-analyses of two TZDs, rosiglitazone and pioglitazone were published, suggesting that both drugs were associated with increased risk of heart failure (rosiglitazone 109% increase $P < 0.001$, pioglitazone 41% increase $P = 0.02$)[237, 238]. Although rosiglitazone was not found to increase cardiovascular mortality and pioglitazone was shown to reduce the risk of myocardial infarction, stroke and death in TIIDM patients. The world wide sales for the TZDs were significantly affected by these findings with the revenue generated by rosiglitazone dropping from $3.2 billion in 2006 to $1.49 billion in 2008. Pioglitazone sales were more stable and in 2008 generated $2.4 billion world wide. In spite of the contention over the use of TZDs they continue to share a substantial amount of the anti-diabetic drug market.

The insulin sensitising mode of action of PPARγ activation is thought to be a result of the fatty acid sequestration into TAGs and storage in adipocytes; lowering plasma FFA concentrations[239] and partitioning the lipids away from other peripheral tissues, such as skeletal muscle, where their accumulation is deleterious and may cause lipotoxicity[240]. However, other plasma lipid concentration lowering drugs do not share this insulin sensitising effect, suggesting additional mechanisms are at play.

5.2 Aims and Objectives

With the aim of identifying metabolic effects of PPARγ activation in adipose tissue that may be contributing to the nuclear receptor's anti-diabetic potential a metabolomics study using both *in vivo* analysis in the *ob/ob* mouse and *in vitro* analysis using the murine 3T3-L1 adipocyte cell line has been performed. A synthetic, high affinity, non-TZD, PPARγ agonist, GW347845, was used to activate the nuclear receptor in both the mice and the adipocyte cell line. To increase the coverage of the metabolome a combination of multiple analytical techniques was used. GC-MS, ^{1}H-NMR, LC-MS and DI-MS in conjunction with multivariate statistics were employed to probe the metabolic phenotype of PPARγ activated adipose tissue. Mechanistic analysis was then performed with ^{13}C-stable isotope substrate labelling studies, using 1-^{13}C-glucose and U-^{13}C-palmitate, and transcriptomic microarray analysis to explicitly define the pathways, as identified in the metabolomic analysis, by which PPARγ activation alters the metabolism of adipose tissue.

It was discovered that PPARγ activation in white adipose tissue not only resulted in the increased uptake, elongation and sequestration of circulating fatty acids into TAG pools and a decrease in fatty acid breakdown by β-oxidation but also an increase in de novo fatty acid synthesis directly from glucose. In addition PPARγ activation is implicated in the augmentation of calcium cellular signalling; a signalling pathway associated with insulin signalling and downstream metabolic effects. Providing additional mechanisms for the observed normalisation of blood glucose and dyslipidaemia in both human patients and murine subjects with the metabolic syndrome and TIIDM when treated with PPARγ agonists.

5.3 Materials and Methods

5.3.1 Ob/Ob Mouse Study Tissue Collection and Extraction

Animals were kept as is outlined in **Chapter 2 Materials and Methods** (section *2.2.1. Animal handling*). Briefly, the *ob/ob* mice were dosed orally daily at 8 am with 0.5% Hydroxypropylmethylcellulose/0.1% Tween80 vehicle control (n=8) or a PPARγ agonist, GW347845 (n=8 at 5 mg/kg). Injection volume was adjusted daily according to body weight at 10 ml/kg. White adipose tissue was collected as summarised in **Chapter 2 Materials and Methods** (section *2.2.4. Tissue handling*).

5.3.2 3T3-L1 Cell Culture

3T3-L1 preadipocytes were grown and differentiated as described in **Chapter 2 Materials and Methods** (section 2.1.1 *3T3-L1 cell culture and adipocyte differentiation*).

5.3.3 3T3-L1 PPARγ Activation

3T3-L1 adipocytes were treated with the selective PPARγ agonist GW347845 as is outlined in **Chapter 2 Materials and Methods** (2.1.4. *Activation of PPARγ in 3T3-L1 adipocytes*). Briefly, adipocytes were treated with either DMSO (control n=6; T75 flasks) or GW347845 PPARγ selective agonist (n=6; T75 flasks at 10 nM and 100 nM) for 2 days.

5.3.4. Oil Red O Staining and Intracytoplasmic Lipid Accumulation

Three additional T75 flasks of 3T3-L1 adipocytes were grown per control, 10 nM and 100 nM treatment groups. Three flasks per group were stained prior to PPARγ agonist treatment to assess levels of differentiation. The cells were stained and the

intracytoplasmic lipid accumulation assessed as in **Chapter 2 Materials and Methods** (section 2.1.5 *Oil Red O staining and intracytoplasmic lipid accumulation*).

5.3.5 3T3-L1 Cell Collection

The cells were collected and their metabolites extracted as described in **Chapter 2 Materials and Methods** (sections 2.1.6 and 2.3 *Adipocyte cell collection*).

5.3.6 Tissue and 3T3-L1 Metabolite Extraction

Metabolites were extracted from white adipose tissue and 3T3-L1 cells using the modified Bligh and Dyer method187. The details are as in Chapter 2 Materials and Methods (*section 2.3 3T3-L1 Cell, Primary Adipocyte and Tissue Metabolite Extraction*).

5.3.7 ^{1}H-NMR Spectroscopy

All samples were analysed using a Bruker AVANCE II+ spectrometer operating at 500.13 MHz for the ^{1}H frequency using a 5 mm Broadband TXI Inverse ATMA probe. All procedures are as depicted in **Chapter 2 Materials and Methods** (sections 2.6.1. *Spectrometer*, 2.6.2. *Sample preparation*, 2.6.3. *1-dimensional ^{1}H-Nuclear Magnetic Resonance experimental method* and 2.6.4. *Processing 1-dimensional ^{1}H-Nuclear Magnetic Resonance data*).

5.3.8 GC-MS Analysis

The aqueous phase of extracts was derivatised as described in **Chapter 2 Materials and Methods** (section 2.7.1 *Derivatisation of aqueous phase metabolites*).

The organic phase of extracts was derivatised as described in **Chapter 2 Materials and Methods** (section 2.7.2 *Derivatisation of organic phase metabolites*).

GC-MS analyses were made using a Trace GC Ultra coupled to a Trace DSQ II single-quadrupole mass spectrometer. Parameters for the GC-MS analysis of aqueous phase metabolites and organic phase metabolites were as outlined in **Chapter 2 Materials and Methods** (sections 2.7.3.1 *Gas Chromatography-Mass Spectrometry methods for aqueous phase samples* and 2.7.3.2 *Gas Chromatography-Mass Spectrometry methods for organic phase samples*). Derivatised organic samples were injected with a split ratio of 60 for white adipose tissue and 8 for 3T3-L1 cells.

GC-MS chromatograms were processed using Xcaliber (version 2.0; Thermo Electron) as outlined in **Chapter 2 Materials and Methods** (2.7.5. *Processing Gas Chromatography-Mass Spectrometry data*).

5.3.9 UPLC-MS Analysis

Chromatography was performed using an ACQUITY UPLC® system equipped with an Acquity UPLC 1.7 μm BEH C8 column (2.1×100 mm) coupled to a Micromass QTof-*Ultima* with a Z-spray electrospray source. All chromatography and mass spectrometric parameters were as outlined in **Chapter 2 Materials and Methods (**section 2.8.1. *Chromatography and mass Spectrometry parameters*)

The organic phase of adipose tissue extracts was reconstituted in methanol-chloroform (2:1, 500 μl). This was further diluted 10-fold prior to injection onto the C8 column (5 μl). The column mobile phase was held at 85% solvent B for 0.5 min followed by an increase from 85%-100% solvent B over 0.5-8 min. The mobile phase was then held at 100% B for 4 min. Between 12 and 12.25 min the mobile phase was returned to 85% B and held for 1.75 min to re-equilibrate the column.

3T3-L1 Cell Organic phase metabolites were reconstituted in methanol-chloroform (2:1, 1 ml). Aliquots of diluted organic phase sample (5 μl) were injected onto the C8 column. The column mobile phase was held at 50% solvent B for 0.5 min followed by an increase from 50%-100% solvent B over 0.5-6.5 min. The mobile phase was then held at 100% B

for 3.5 min. Between 10 and 10.25 min the mobile phase was returned to 50% B and held for 3.75 min to re-equilibrate the column. The total UPLC cycle was 14 min and the eluent flow rate was 600 µl/min for both methods.

Tandem mass spectrometry procedures were as described in **Chapter 2 Materials and Methods** (2.8.3 *Tandem mass spectrometry method*).

Data was processed using Micromass MarkerLynx Applications Manager as depicted in **Chapter 2 Materials and Methods** (2.8.4. *Processing Liquid Chromatography-Mass Spectrometry data*).

5.3.10 DI-MS Analysis

Mass spectrometric analysis was performed using a Thermo Finnigan LTQ equipped with a Finnigan Surveyor pump and Finnigan Micro AS Autosampler.

The white adipose tissue organic phase samples for DI-MS were reconstituted in 1 ml methanol:THF (2:1 v/v). 60 µl of each sample was aliquoted into a 96 well plate where the samples were diluted by the addition of a further 600 µl methanol:THF (2:1 v/v).

The 3T3-L1 organic phase samples for DI-MS were reconstituted in 500 µl methanol:THF (2:1 v/v). 100 µl of each sample was added to a 96 well plate. Samples were analyzed in triplicate for negative mode and duplicate for positive mode ionisation.

All other direct infusion and mass spectrometric parameters were as described in **Chapter 2 Materials and Methods** (section 2.9.2. *Direct infusion and mass spectrometry parameters*).

DI-MS chromatograms were processed using Xcaliber as outlined in **Chapter 2 Materials and Methods** (2.9.3. *Processing of direct infusion mass spectrometry data*).

5.3.11 ^{13}C-glucose Substrate Labelling Study

At 2 days post differentiation media was removed from the T75 flasks and replaced with DMEM (10% (v/v) FBS, 50 units/ml penicillin, and 50 µg/ml streptomycin) and either 4.5 g/l unlabelled glucose with DMSO control (n=6) or with 1 µM GW347845 PPARγ selective agonist (n=7) or 4.5 g/l 1-^{13}C-glucose with DMSO control (n=7) or with 1 µM GW347845 PPARγ selective agonist (n=7). After 2 days cells were collected and metabolites extracted as described in **Chapter 2 Materials and Methods** (sections 2.1.6 and 2.3 *Adipocyte cell collection*).

5.3.12 ^{13}C-palmitate Substrate Labelling Study

Preparation of ^{13}C labelled and unenriched palmitate solution is defined in **Chapter 2 Materials and Methods** (2.4.3. *Preparation of ^{13}C and ^{12}C palmitate solution*).

At 2 days post-differentiation media was removed from the T75 flasks and replaced with DMEM (serum free, 50 units/ml penicillin, and 50 µg/ml streptomycin) and either 70 µM unlabelled palmitate (n=6) with DMSO control (n=6) or with 1 µM GW347845 PPARγ selective agonist (n=7) or 70 µM U-^{13}C labelled palmitate (n=7) with DMSO control (n=6) or with 1 µM GW347845 PPARγ selective agonist (n=7). After 2 days cells were collected and metabolites extracted as previously described in **Chapter 2 Materials and Methods** (sections 2.1.6 *Adipocyte cell collection* and 2.3 *Adipocyte cell collection*).

5.3.13 ^{13}C-labelled Substrate GC-MS Analysis

Analysis of organic and aqueous phases was carried out as previously described in **Chapter 2 Materials and Methods** (section 2.7.1 *Derivatisation of aqueous phase metabolites,* 2.7.2. *Derivatisation of organic phase metabolites,* 2.7.3.1 *Gas Chromatography-Mass Spectrometry methods for aqueous phase samples* and 2.7.3.2 *Gas Chromatography-Mass Spectrometry methods for organic phase samples*).

Enrichment of metabolites was identified by calculating isotope ratios of the M and M+1 ions for the parent ion of the fragmentation pattern in the case of ^{13}C-glucose metabolism analysis and TCA cycle intermediates originating from ^{13}C-palmitate oxidation. For fatty acid synthesis and desaturation products from ^{13}C-labelled palmitate an ion ratio of M+16/M was used and for fatty acids originating from oxidation of ^{13}C-labelled palmitate an ion ratio of M+n/M, where n = the carbon chain length of the fatty acid was used. Statistical analysis was performed using a univariate t-test.

5.3.14 Multivariate Analysis

Multivariate data analysis was performed using SIMCA-P^{+} 11.0 (Umetrics AB, Umeå, Sweden). NMR, DI-MS and UPLC-MS data sets were mean-centered and Pareto-scaled prior to analysis. GC-MS data sets were scaled to UV. Data sets were analyzed using PCA, PLS and PLS-DA. Further details are summarised in **Chapter 2 Materials and Methods** (section 2.11.6 *Multivariate Statistical Analysis Methodology*).

5.3.15 Microarray Analysis of PPARγ Agonist Treated 3T3-L1 Cells

Cells were grown, treated with PPARγ agonist and collected as is outlined in **Chapter 2 Materials and Methods (**section 2.1.1 *3T3-L1 cell culture and adipocyte differentiation,* 2.1.4 *Activation of PPARγ in 3T3-L1 adipocytes,* 2.1.6 and 2.3 *Adipocyte cell collection*) An RNeasy RNA extraction and purification kit was used to extract total RNA from 3T3-L1 adipocytes (Qiagen GmbH, Hilden, Germany). RNA extraction procedures were carried out according to the methods outlined in **Chapter 2 Materials and Methods** (section 2.10.1. *RNA extraction*).

Transcriptomic analysis was conducted by Cambridge Genomic Centre for Microarray Resources (Cambridge Genomic Services, Department of Pathology, University of Cambridge). An automated Illumina Infinium Gene Expression BeadArray (Illumina Inc, San Diego, CA) was used to perform mRNA transcriptional profiling. A mouse WG6 array platform was used with 45281 probes.

Quality control was carried out using the arrayQualityMetrics R package and no samples failed or were identified as outliers to their replicates. Statistical selection was performed using the detection p-value provided by Illumina. This value represents the confidence that a given transcript is expressed above the background defined by the negative control probe. The R package lumi was used for this analysis[191]. The detection p-value threshold was set to 0.01. Probes were required to be successfully detected (p-value<0.01 in lumi) in at least one sample to pass the selection. The data is transformed using variance stabilisation and then normalised using quantile normalisation[192]. Gene expression was compared between PPARγ agonist treated and control 3T3-L1 cells using the R package limma[193]. The threshold utilised in this analysis was the 5% confidence interval. The selected and normalised data was then analysed using the multivariate statistics in the Simca-P+ package as has been described. The 6% of transcripts most responsible for separation in the multivariate models were then examined (3% most increased and 3% most decreased in PPARδ agonist treated cells as identified in the multivariate models).

The Reactome Skypainter tool (www.reactome.org) was used to determine which pathways were statistically significant in the 3% of genes most increased and most decreased in transcription in PPARγ agonist treated cells. From a given set of genes known to participate in a pathway, the total genes for *mus musculus* and the submitted list of genes (the genes increased or decreased in expression in PPARγ activated cells) of which N genes participate in the given pathway, the probability of observing at least N genes from a pathway if that pathway is not overrepresented in the submitted list of genes is calculated using the one-tailed version of Fisher's exact test. Therefore a p-value smaller than or equal to the significance level suggests that the pathway is statistically significant in the submitted list of genes.

5.4 Results

5.4.1 Metabolomic Analysis

^{1}H-NMR spectroscopy, GC-MS, LC-MS and DI-MS analysis, combined with multivariate pattern recognition were used to examine metabolism within the white adipose tissue of *ob/ob* mice and 3T3-L1 murine cultured adipocytes treated with a PPARγ agonist. To assess metabolic changes in the dataset a common processing strategy was adopted throughout the analysis. To investigate metabolite perturbations mutual to PPARγ activation PCA and PLS-DA models were built for both the white adipose tissue and the 3T3-L1 adipocytes. PCA and PLS-DA models were generated for the white adipose tissue and the cultured cells, comparing the control group with the PPARγ agonist treated groups. Metabolites identified in the VIP/coefficients plots as significantly contributing to separation in the models were then considered to have changed globally. The metabolite changes in the white adipose tissue and 3T3-L1 adipocytes are considered below.

5.4.1.1 White adipose tissue

Robust multivariate models were generated to describe the metabolic influence of PPARγ activation in the white adipose tissue of *ob/ob* mice from data collected by DI-MS analysis of the organic extracts and GC-MS analysis of both the aqueous and organic metabolite extracts (**Figure 5.1**).

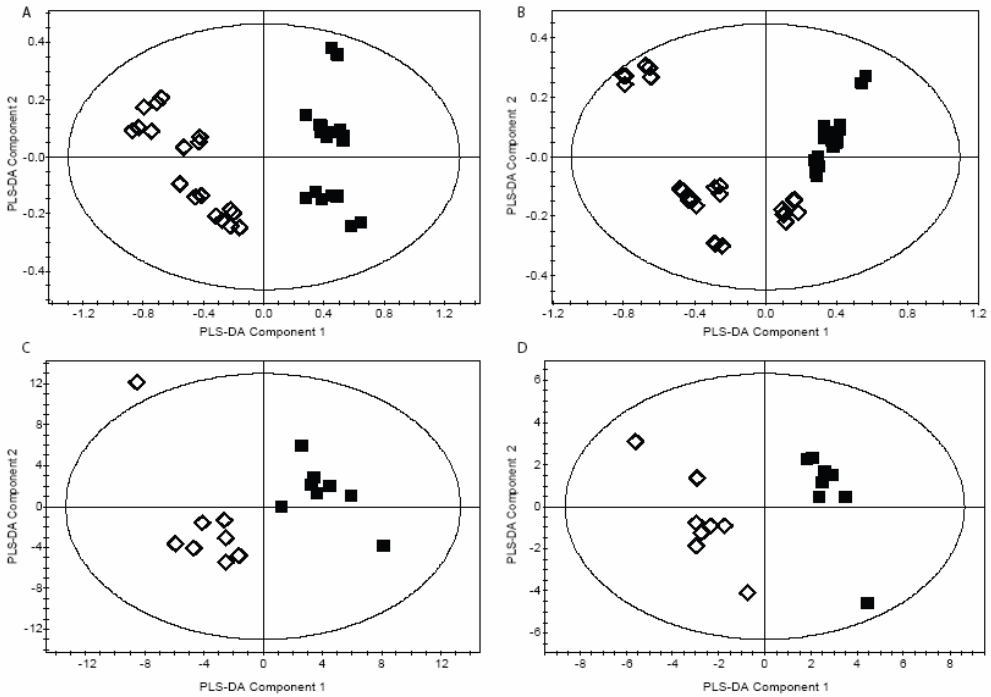

Figure 5.1: **A**. PLS-DA scores plot showing the clustering of DI-MS positive ionisation mode chromatograms from the organic phase of white adipose tissue extracts from *ob/ob* mice treated with a PPARγ agonist compared with control animals ◊, PPARγ agonist treated, ■, control (R^2=0.887, Q^2=0.949). Two technical replicates were analysed. **B**. PLS-DA scores plot showing the clustering of DI-MS negative ionisation mode chromatograms from the organic phase of white adipose tissue extracts from *ob/ob* mice treated with a PPARγ agonist compared with control animals ◊, PPARγ agonist treated, ■, control (R^2=0.926, Q^2=0.949). Two technical replicates were analysed. **C**. PLS-DA scores plot showing the clustering of GC-MS chromatograms from the aqueous fraction of white adipose tissue extracts from *ob/ob* mice treated with a PPARγ agonist compared with control animals ◊, PPARγ agonist treated, ■, control (R^2=0.499, Q^2=0.786). **D**. PLS-DA scores plot showing the clustering of GC-MS chromatograms from the organic fraction of white adipose extracts from *ob/ob* mice treated with a PPARγ agonist compared with control animals ◊, PPARγ agonist treated, ■, control (R^2=0.305, Q^2=0.738).

Activation of PPARγ in the white adipose tissue of *ob/ob* mice resulted in a decrease in the concentration of several carbohydrate and sugar species including galactose and glucose. Concomitantly acetic acid concentrations were observed to decrease. These changes in the glycolytic pathway are accompanied by a change in the steady state equilibrium of the TCA cycle and oxidative metabolism. The concentration of the early

TCA cycle intermediates isocitrate and succinate were increased whilst latter intermediates fumarate and malate were decreased in concentration.

Amino acid metabolism in the white adipose tissue was modified by the activation of PPARγ; the concentrations of threonine, glycine, serine, isoleucine, phenylalanine, valine, alanine, aspartate and proline were increased, whilst the concentration of β-alanine was decreased.

The fatty acid metabolic pathways of the adipose tissue were also modified by activation of the nuclear receptor. There was a detected increase in the concentrations of the Δ-9 desaturation products, myristoleate C14:1, cis-10-pentadecanoate C15:1, and palmitoleate C16:1. Also increased in concentration were the fatty acid myristate C14:0 and the long chain fatty acid arachidate C20:0.

DI-MS detected increases in the concentrations of free arachidonic acid C20:4 and docosahexaenoic acid 22:6, respectively, the ω-6 and ω-3 essential fatty acid pathway products.

The complex lipid metabolic pathways were altered upon PPARγ activation; the concentrations of a number of glycerophosphoinositols were decreased as was the concentration of their constituent, myo-inositol. Cholesterol ester concentrations were also increased in the white adipose tissue of PPARγ agonist treated animals.

5.4.1.2 3T3-L1 adipocytes

Investigation of the effects of PPARγ activation on the metabolism of the 3T3-L1 adipocyte tissue specific cell line within a cell culture system was conducted to generate an *in vitro* model of adipose tissue specific PPARγ activation. Oil red O staining for neutral lipids in the differentiated cells prior to treatment with the PPARγ agonist demonstrated that there were comparable levels of differentiation in the treatment groups (**Figure 5.2**).

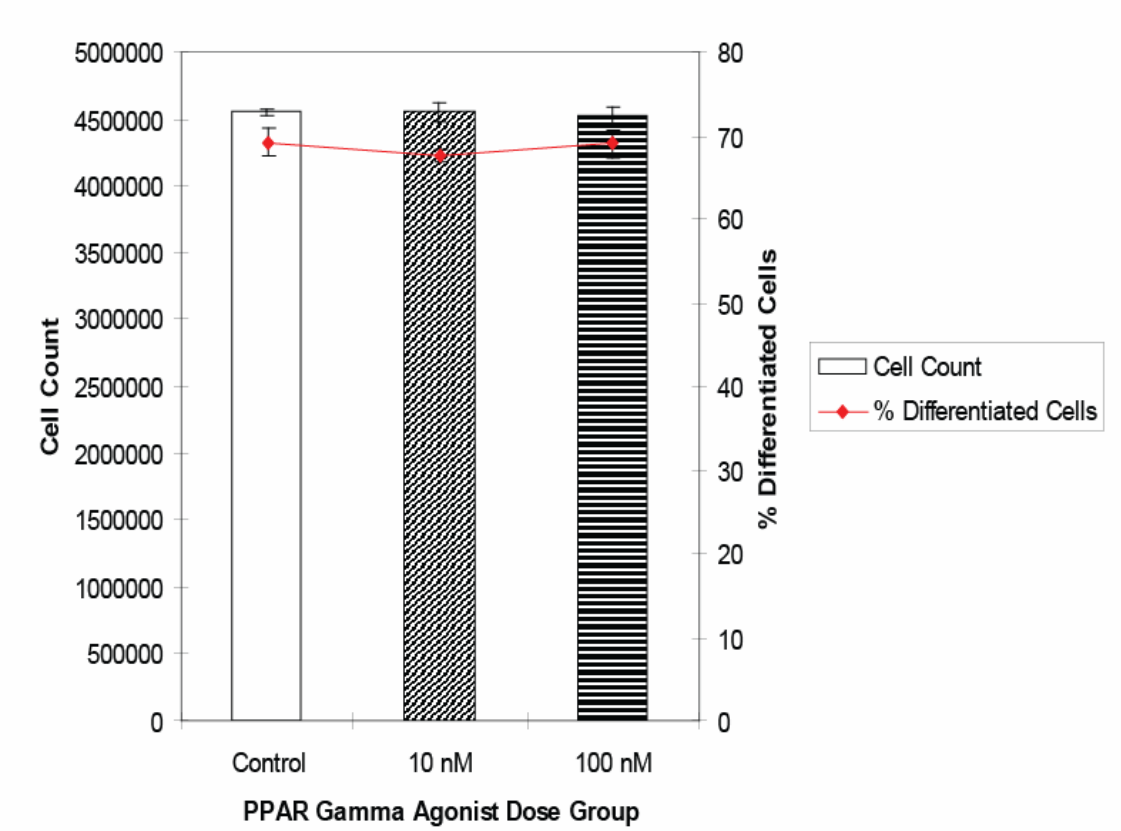

Figure 5.2: Graph showing cell counts and the percentage of differentiating cells prior to treatment with PPARγ agonist.

The metabolic effect of activation of PPARγ in 3T3-L1 adipocytes was investigated using a range of analytical platforms, including GC-MS, DI-MS, LC-MS and ^{1}H-NMR spectroscopy enabling extensive coverage of the metabolome; the data obtained from analysis was used in chemometric processing to create multivariate statistical models designating the metabolites that were altered upon stimulation of the nuclear receptor (**Figure 5.3**).

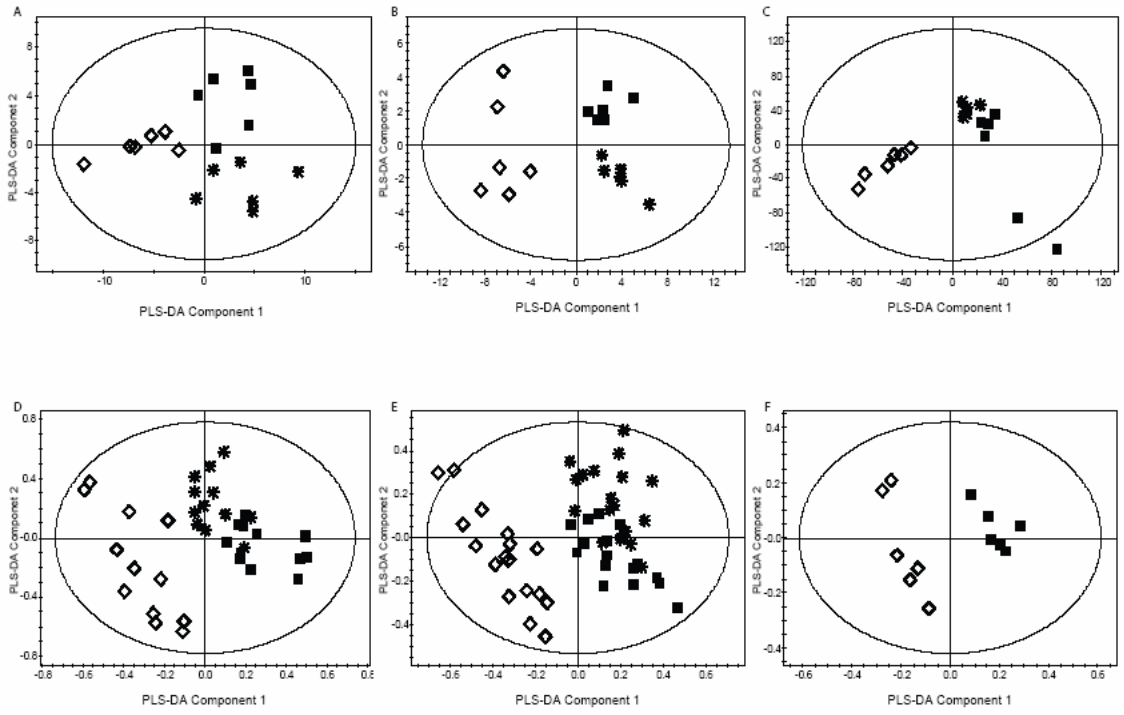

Figure 5.3: **A**. PLS-DA scores plot showing the clustering of GC-MS chromatograms from the aqueous fraction of 3T3-L1 adipocytes treated with 10 nM PPARγ agonist GW347845 and 100 nM PPARγ agonist GW347845 compared with the control group.∗, 10 nM PPARγ agonist dose ◊, 100 nM PPARγ agonist dose, ■, control (R^2=0.765, Q^2=0.735). **B.** PLS-DA scores plot showing the clustering of GC-MS chromatograms from the organic fraction of 3T3-L1 adipocytes treated with 10 nM PPARγ agonist GW347845 and 100 nM PPARγ agonist GW347845 compared with the control group.∗, 10 nM PPARγ agonist dose ◊, 100 nM PPARγ agonist dose, ■, control (R^2=0.87, Q^2=0.895). **C.** PLS-DA scores plot showing the clustering of LC-MS chromatograms from the organic fraction of 3T3-L1 adipocytes treated with 10 nM PPARγ agonist GW347845 and 100 nM PPARγ agonist GW347845 compared with the control group.∗, 10 nM PPARγ agonist dose ◊, 100 nM PPARγ agonist dose, ■, control (R^2=0.778, Q^2=0.564). **D.** PLS-DA scores plot showing the clustering of DI-MS positive mode ionisation chromatograms from the organic fraction of 3T3-L1 adipocytes treated with 10 nM PPARγ agonist GW347845 and 100 nM PPARγ agonist GW347845 compared with the control group.∗, 10 nM PPARγ agonist dose ◊, 100 nM PPARγ agonist dose, ■, control (R^2=0.781, Q^2=0.873). Two technical replicates were analysed. **E.** PLS-DA scores plot showing the clustering of DI-MS negative mode ionisation chromatograms from the organic fraction of 3T3-L1 adipocytes treated with 10 nM PPARγ agonist GW347845 and 100 nM PPARγ agonist

GW347845 compared with the control group.∗, 10 nM PPARγ agonist dose ◊, 100 nM PPARγ agonist dose, ■, control (R^2=0.856, Q^2=0.882). Three technical replicates were analysed. **F.** PLS-DA scores plot showing the clustering of ^{1}H-NMR spectra from the aqueous fraction of 3T3-L1 adipocytes treated with 100 nM PPARγ agonist GW347845 compared with the control group. ◊, 100 nM PPARγ agonist dose, ■, control (R^2=0.819, Q^2=0.978).

The 3T3-L1 adipocytes exposed to the PPARγ agonist were found to have reduced concentrations of glycolytic pathway intermediates including glucose, gluconic acid, pyruvate and lactate.

The polyol pathway is also profoundly affected by the activation of the ligand-gated receptor; the steady state concentrations of both glucitol and fructose were observed to be increased in the adipocytes treated with the PPARγ agonist.

Steady state concentrations of a number of TCA cycle intermediates, glutamate (a surrogate for α-ketoglutarate), succinate, fumarate and malate were decreased in PPARγ activated adipocytes indicating a role in oxidative metabolic control for the nuclear receptor.

The cells treated with PPARγ agonist also displayed altered amino acid metabolism with detected decreases in the concentration of aspartate, asparagine, glutamine, threonine and β-alanine.

Activation of PPARγ altered the metabolism of the fatty acid synthesis and oxidation pathways within the 3T3-L1 adipocytes; there was an observed decrease in the shorter chain fatty acids (tridecanoate C13:0, myristate C14:0, isomyristate, 12-methyl tetradecanoate, pentadecanoate C15:0, 10-pentadecanoate C15:1, palmitoleate C16:1, margaric acid C17:0, cis-10-heptadecenoic acid C17:1, isostearate and elaidate and oleate C18:1) and a concomitant increase in the steady state concentrations of the long chain fatty acids, arachidate C20:0 and behenic acid C22:0. The concentration of carnitine was also decreased in adipocytes treated with the PPARγ agonist. The ω-6 essential fatty acid

pathway was also perturbed as a consequence of PPARγ stimulation; the steady state concentration of γ-linolenate was decreased, concurrently the concentration of the consecutive pathway intermediate, dihomo-γ-linolenate was increased, again implicating the fatty acid elongase.

The concentrations of FFAs altered by PPARγ activation closely matched the detected changes in the total fatty acid population. Longer chain FFAs were increased in concentration (C22:0**,** C20:0**,** C22:6, C22:5**,** C22:3**,** C22:7**,** C22:4) whilst the concentration of shorter chain FFAs was observed to decrease (C15:0**,** C17:0, C18:0, C16:1**,** C18:1**,** C17:1**,** C19:1, C19:3**,** C18:2).

The substituent complex lipids of the 3T3-L1 adipocytes were also modified by activation of PPARγ. The TAG pool was restructured as a consequence of stimulation of the nuclear receptor; there was a detected increase in the desaturation and length of the acyl chains esterified to the TAGs (**Table 5.1**). The glycerophospholipids were observed to have changed upon stimulation of the ligand activated transcription factor; a decrease in the concentration of a number of phospholipid species including glycerophosphocholines, glycerophosphoethanolamines and glycerophosphoinositols were accompanied by a decrease in their constituents, α-glycerophosphoric acid and myo-inositol phosphate. In addition, 3T3-L1 adipocytes incubated with the PPARγ agonist had elevated concentrations of a number of cholesterol ester species.

TAG species increased in concentration in PPARγ agonist treated adipocytes	TAG species decreased in concentration in PPARγ agonist treated adipocytes
TAG 48:0 NH4+	TAG 44:2 NH4+
TAG 50:1 NH4+	TAG 44:1 (15:0/15:0/14:1) NH4+
TAG 52:4 NH4+	TAG 44:1 (15:1/14:0/15:0) NH4+
TAG 54:6 NH4+	TAG 45:2 NH4+
TAG 54:5 NH4+	TAG 46:2 NH4+
TAG 54:4 NH4+	TAG 47:3 NH4+
	TAG 47:2 NH4+
	TAG 48:3 NH4+
	TAG 48:2 NH4+
	TAG 49:3 NH4+
	TAG 50:3 NH4+

Table 5.1: TAG species altered in concentration in 3T3-L1 adipocytes treated with GW347845 PPARγ agonist. TAGs were detected using LC-MS. Lipids identified in the VIP/coefficients plots as significantly contributing to separation in the PCA and PLS-DA models built for the LC-MS analysis of the organic metabolite fraction. The control group was compared with the PPARγ agonist treated group.

5.4.2 ^{13}C-labelled Substrate Studies

The metabolic mechanisms of PPARγ activation in 3T3-L1 adipocytes were elucidated using the ^{13}C-labelled substrates 1-^{13}C glucose and U-^{13}C-palmitate to monitor flux through glycolytic, oxidative and fatty acid synthesis pathways.

5.4.2.1 1-^{13}C-glucose

Analysis by GC-MS of the aqueous fraction of control and PPARγ agonist treated adipocytes incubated in media containing 1-^{13}C glucose revealed that when treated with the PPARγ agonist, the glycolytic pathway product, lactate had reduced ^{13}C enrichment (**Figure 5.4A.**). The enrichment of the TCA cycle intermediates succinate and glutamate

was also decreased in adipocytes with activated PPARγ (**Figure 5.4B.C**.). In addition, the polyol pathway intermediate, glucitol, was increased in ^{13}C-enrichment when the adipocytes were treated with the PPARγ agonist. Investigation, by GC-MS, of the organic fraction from control and PPARγ agonist treated adipocytes incubated in 1-^{13}C glucose demonstrated that the long chain fatty acid arachidate had a greater concentration of ^{13}C enrichment in PPARγ agonist treated cells (**Figure 5.4D.**).

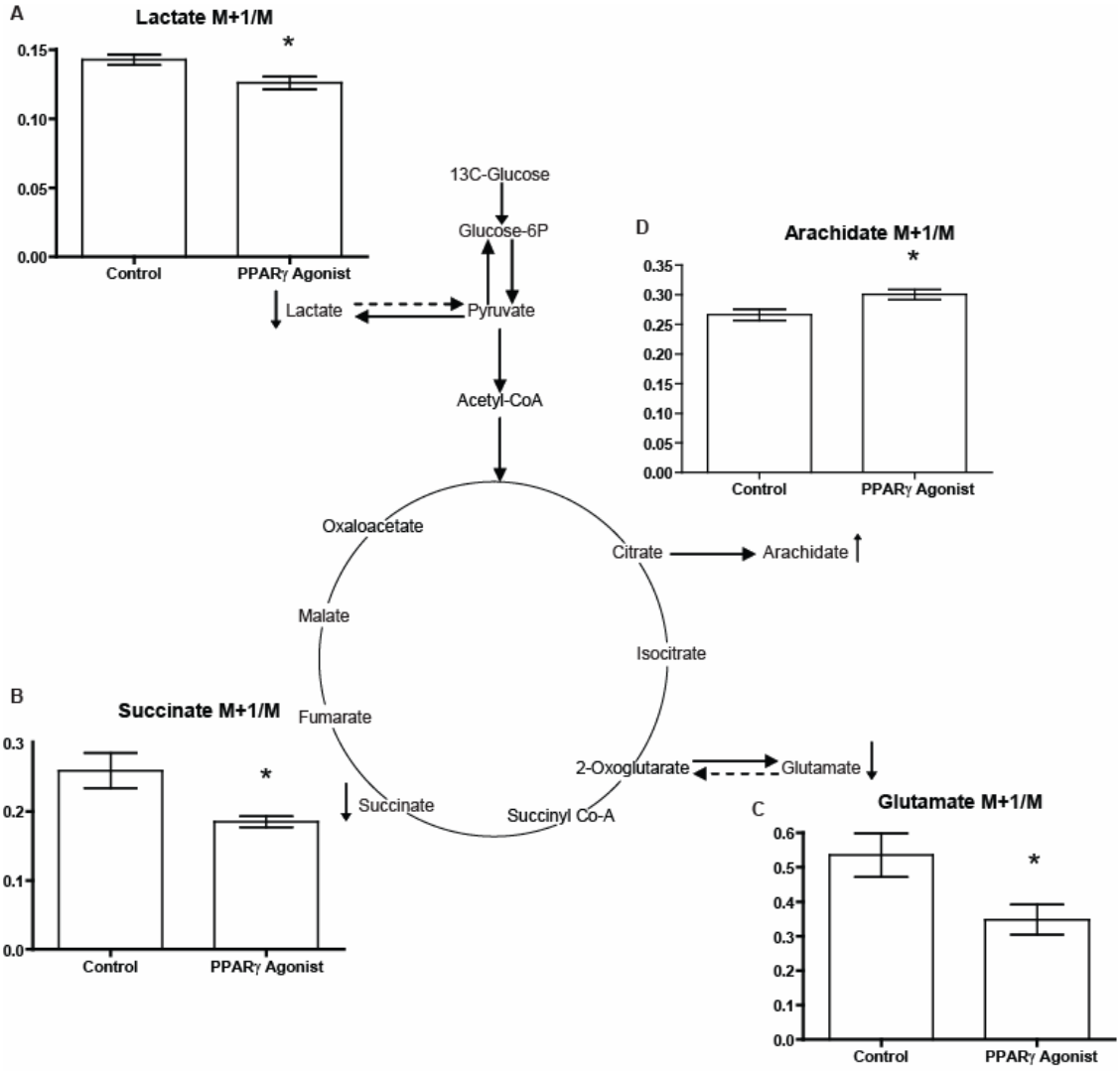

Figure 5.4: Graphs showing the M+1/M isotope ratio ^{13}C enrichment of **A.** lactate, **B.** succinate and **C.** glutamate analysed by GC-MS of the aqueous fraction from control and PPARγ agonist dosed 3T3-L1 cells incubated with 1-^{13}C-glucose. **D.** Graph showing the M+1/M isotope ratio ^{13}C enrichment of arachidate analysed by GC-MS of the organic fraction from control and PPARγ agonist dosed 3T3-L1 cells incubated with 1-^{13}C-glucose. *P < 0.05. The metabolites have been mapped to the glycolysis, TCA cycle and fatty acid synthesis metabolic pathways. ↑ indicates a metabolite increased in ^{13}C enrichment by PPARγ activation. ↓ indicates a metabolite decreased in ^{13}C enrichment by PPARγ activation. Parent ions were used to calculate ion ratio.

5.4.2.2 U-^{13}C-palmitate

GC-MS analysis of the aqueous phase of cells incubated in U-^{13}C-palmitate indicated that the early TCA cycle intermediates glutamate and isocitrate exhibited decreased ^{13}C enrichment in PPARγ agonist treated adipocytes when compared to control adipocytes (**Figure 5.5A.B.**). Assessment of the organic phase by GC-MS indicated that the ^{13}C-enrichment of the long chain fatty acid arachidate was increased in the PPARγ agonist treated cells when compared to control (**Figure 5.5C.**). Concurrently the ^{13}C-enrichment of the shorter chain fatty acid, myristate was detected by GC-MS to have decreased in the adipocytes treated with PPARγ agonist in comparison to control 3T3-L1 cells (**Figure 5.5D.**). An increase in the ^{13}C enrichment of palmitate in cells treated with PPARγ agonist, when compared to control adipocytes was also observed. (**Figure 5.5E.**).

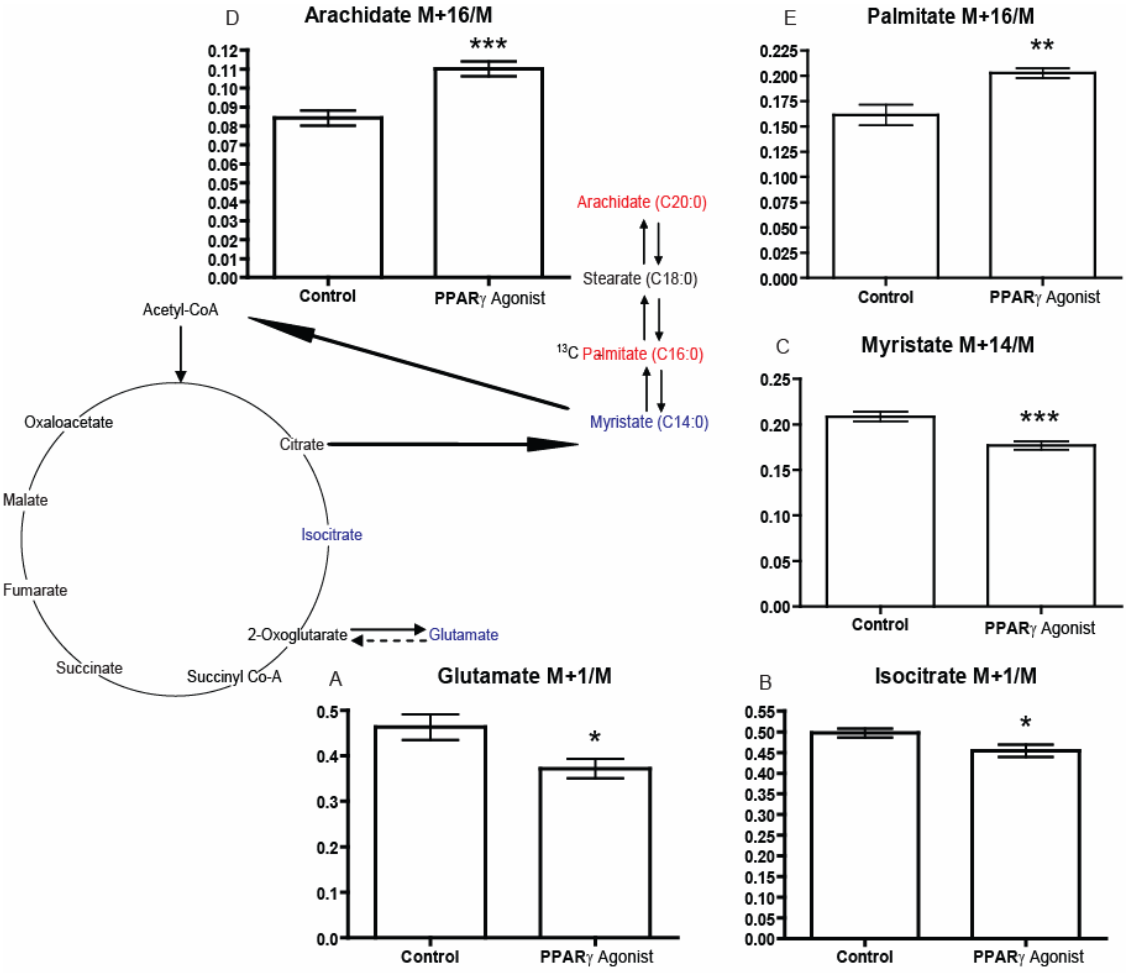

Figure 5.5: Graphs showing the M+1/M isotope ratio ^{13}C enrichment of **A.** glutamate and **B.** isocitrate analysed by GC-MS of the aqueous fraction from control and PPARγ agonist dosed 3T3-L1 cells incubated with ^{13}C-U-palmitate. Graphs showing the isotope ratio ^{13}C enrichment of **C.** myristate, **D.** arachidate and **E.** palmitate analysed by GC-MS of the organic fraction from control and PPARγ agonist dosed 3T3-L1 cells incubated with ^{13}C-U-palmitate. The metabolites have been mapped to the TCA cycle and fatty acid β-oxidation/synthesis metabolic pathways. Red indicates a metabolite increased in ^{13}C enrichment by PPARγ activation. Blue indicates a metabolite decreased in ^{13}C enrichment by PPARγ activation. *P < 0.05, **P < 0.01,***P < 0.005. Parent ions were used to calculate ion ratio.

5.4.3 Microarray Transcriptomic Analysis

The results from the steady state metabolomic experiments in adipose tissue and adipocytes and isotope labelling studies suggest PPARγ activation has a pronounced effect on glucose utilisation and fatty acid metabolism in adipocytes. To define these changes the focus of investigation was moved to the transcriptome using microarray analysis of PPARγ activation in adipocytes. Of the 45281 probes utilised 13755 were expressed above the background defined by the negative control probe. From these 3282 were determined to be differentially expressed ($P < 0.05$) with 164 estimated false positives using a threshold of 5% of differentially expressed probes. Multivariate models were built using the normalised data from the 13755 transcripts measured (**Figure 5.6**).

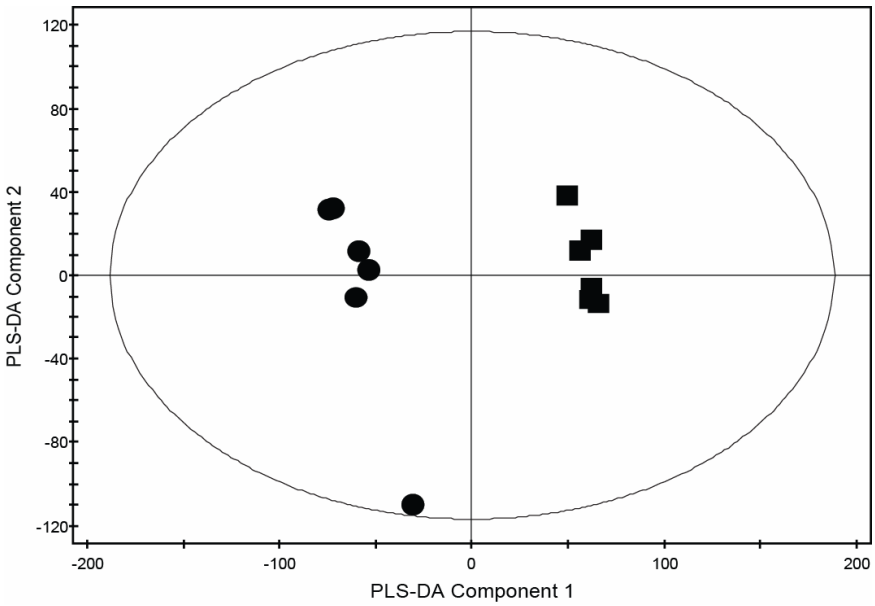

Figure 5.6: PLS-DA scores plot showing the clustering of gene transcription in control and PPARγ agonist treated 3T3-L1 adipocytes as measured with microarray analysis. ●, PPARγ agonist treated, ■, control (R^2=0.42, Q^2=0.84).

The 6% of transcripts most responsible for separation in the multivariate models were then examined (3% most increased and 3% most decreased in PPARγ agonist treated cells as identified in the multivariate models). The multivariate analysis indicated that the mRNA of genes involved in a number of key metabolic pathways was altered following PPARγ activation. The reactome skypainter tool was then utilised to determine which pathways and reactions were statistically overrepresented by the 3% most

increased (**Table 5.2**) and 3% most decreased transcripts in PPARγ agonist treated cells identified in the multivariate models.

P-value	Pathway	Transcripts increased in PPARγ agonist treated cells mapping to the pathway
6.4e-05	Glycolysis	Aldoa, Pgam1, Pfkl, Gapdh, Gpi1
1.1e-03	Gluconeogenesis	Aldoa, Slc25a11, Pgam1, Gapdh, Gpi1
1.2e-03	Ca^{2+} signalling via IP3 binding to the IP3 receptor, opening the endoplasmic reticulum Ca^{2+} channel	Itpr2, Itpr1
1.2e-03	Sar1p activation and membrane binding	Preb, Sar1b
1.8e-03	PLC mediated signalling events	Prkaca, Itpr2, Itpr1, Adcy6, Pde1b
2.5e-03	Hormone-sensitive lipase (HSL)-mediated triacylglycerol hydrolysis	Prkaca, Abhd5, Ppp1ca
2.6e-03	Metabolism of lipids and lipoproteins	Prkaca, Abhd5, Abcd3, Ppp1ca, Ncor1, Chd9, Slc27a1, Hsd17b4, Acaa2, Sin3b, Scd2, Hmgcl, Fads3, Csnk1g2, Angptl4
3.2e-03	Regulation of insulin secretion	Prkaca, Dlst, Ndufb6, Itpr1, Gpi1, Aldoa, Ndufs6, Pgam1, Itpr2, Pfkl, Gapdh
5.8e-03	Formation of acetoacetic acid in the synthesis of ketone bodies	Hmgcl, Acaa2
8.2e-03	Additional metabolism of carbohydrates	Aldoa, Slc25a11, Pgam1, Pfkl, Gapdh, Gpi1, G6pdx
1.1e-02	PKA mediated events	Prkaca, Pde1b
1.1e-02	Regulation of lipid metabolism by peroxisome proliferator-activated receptor alpha (PPARalpha)	Sin3b, Scd2, Fads3, Ncor1, Chd9, Slc27a1, Angptl4
1.4e-02	DARPP-32 events	Prkaca, Ppp1ca, Pde1b
1.7e-02	STAT signalling	Stat5a, Stat6
1.7e-02	Integration of energy metabolism	Prkaca, Dlst, Ndufb6, Gpi1, Aldoa, Ndufs6, Pgam1, Pfkl, Adcy6, Gapdh
2.0e-02	β-oxidation of very long chain fatty acids	Abcd3, Hsd17b4

2.4e-02	Adenylate cyclise mediated CREB phosphorylation	Prkaca, Adcy6
2.6e-02	Signalling by NGF/TRKA	Prkaca, Itpr1, Gbl, Arhgef11, Pde1b, Bcl2l11, Foxo1, Itpr2, Adcy6, Araf
3.1e-02	Peroxisomal lipid metabolism	Abcd3, Slc27a1, Hsd17b4

Table 5.2: The pathways statistically significant in the 3% most increased transcripts in PPARγ agonist treated cells identified in the multivariate models. From a given set of genes participating in a pathway, the total genes for *mus musculus* and the submitted genes (genes increased in PPARγ activated cells) of which N genes participate in a pathway, the probability of observing at least N genes from a pathway if that pathway is not overrepresented in the submitted list of genes is calculated using Fisher's exact test. A p-value smaller than the significance level suggests the pathway is significantly represented.

A number of primary cellular signalling pathways were identified as statistically affected from the transcripts increased in expression by PPARγ activation including inositol triphosphate, calcium, calmodulin and G-protein signalling. PPARγ activation also affected the expression of genes involved in specific metabolic energy pathways and reactions as well as the integration of energy metabolism.

The expression of genes encoding proteins involved in the glycolytic metabolic pathway was also upregulated in PPARγ agonist treated cells. Transcription of several of the key enzymes including glucose phosphate isomerise, phosphofructokinase, aldolase A fructose-bisphosphate, phosphoglycerate mutase 1 and glyceraldehyde-3-phosphate dehydrogenase was upregulated. Consistent with the metabolic changes observed in the polyol pathway the expression of sorbitol dehydrogenase, which catalyses the conversion of glucitol to fructose, was increased in PPARγ agonist treated 3T3-L1 cells. In addition, the expression of the gene encoding the TCA cycle enzyme isocitrate dehydrogenase was identified as decreased.

PPARγ activation was also discerned to significantly affect the transcription of genes responsible for the remodelling and metabolism of lipids. The fatty acid desaturases stearoyl-CoA desaturase 2 and fatty acid desaturase 3, a possible Δ-9 fatty acid

desaturase, were increased in expression following PPARγ activation ($P < 0.005$ for both stearoyl-CoA desaturase 2 and fatty acid desaturase 3). The transcripts of a number of genes that favour conditions of fatty acid synthesis are also increased in concentration in the adipocytes following treatment with the PPARγ agonist; these genes include sterol regulatory element binding transcription factor 2, a transcription factor required for lipid homeostasis that regulates the LDL receptor gene as well as the cholesterol and fatty acid synthesis pathways[241], holocarboxylase synthetase, which activates acetyl-CoA-carboxylase (and pyruvate carboxylase) by conjugating biotin to these enzymes[242], NAD kinase, which transfers a phosphate group of ATP to NAD generating NADP for use as an electron donor in biosynthetic reactions including fatty acid synthesis and malonyl CoA:ACP acyltransferase which catalyses the transfer of a malonyl moiety from malonyl-CoA to the phosphopantethenate moiety of the acyl carrier peptide in the first step of fatty acid synthesis. Concomitantly the expression of acyl-CoA thioesterase 7 and nudix-type motif 19 Coenzyme A diphosphatase, enzymes which catalyse the hydrolysis of medium and long chain acyl-CoAs to FFA and CoA[243], was upregulated in the treated adipocytes. In addition the transcription of solute carrier family 27a1 mRNA was increased in PPARγ agonist treated cells; this protein is an insulin responsive fatty acid transporter responsible for the import of long chain fatty acids into adipose tissue undergoing high levels of TAG synthesis[244].

Genes involved in the restructuring and remodelling of complex lipids were also affected by PPARγ activation. Lysophosphatidylcholine acyltransferases 3 acyltransferase expression was increased in adipocytes treated with PPARγ; this enzyme catalyses the conversion of lysophosphocholines, lysophosphoserines and lysophosphoethanolamines into phosphocholines, phosphoserines and phosphoethanolamines, respectively and favours polyunsaturated fatty acyl-CoAs as acyl donors[245]. Transcription of the platelet activating factor acetylhydrolase 2 lipase was also increased in the PPARγ activated adipocytes. Expression of angiopoietin-related protein 4, a protein regulating extracellular lipolysis through lipoprotein lipase, was increased in the agonist treated 3T3-L1 cells[246].

PPARγ activation also increased the expression of nuclear receptor corepressor 1 in the 3T3-L1 adipocytes. Nuclear receptor corepressor 1 is a transcriptional repressor responsible for the downregulation of gluconeogenesis, lipolysis and fatty acid β-oxidation[247]. Additionally transcription of the PPAR transcriptional coactivator, Chromodomain-helicase-DNA-binding protein 9, was upregulated in the PPARγ agonist treated adipocytes.

5.5 Discussion

A comprehensive metabolomics investigation was performed using a diverse range of analytical and chemometric techniques. The primary aim of this study was to probe the metabolic effects of PPARγ activation within the white adipose tissue of *ob/ob* mice to elucidate the metabolic influence stimulus of this receptor has on a tissue perceived to be the primary target for synthetic PPARγ ligands in their use as anti-diabetic agents. A 3T3-L1 adipocyte cell culture system was then employed to generate an *in vitro* model of PPARγ activation in adipose tissue, which was subsequently analysed using metabolomic methods. The metabolomic data was then complemented with investigations in 3T3-L1 adipocytes using ^{13}C-labelled substrates to monitor flux through glycolytic, oxidative and fatty acid synthesis pathways and RNA microarray analysis to explain alterations in gene transcription; these additional techniques were utilised to explicate the mechanisms by which PPARγ activation generates its metabolic properties.

Transcriptomic analysis highlighted the significant upregulation in the expression of genes involved in calcium and calmodulin signalling within adipocytes treated with the PPARγ agonist, GW347845. The calcium signalling pathway is implicated in the insulin responsive signalling pathway and influences many metabolic targets[248, 249]. Calcium signalling increases GLUT4 translocation to the plasma membrane, possibly through a phosphatidic acid lipid signalling mechanism mediated by phospholipase D[250], and increases glucose transportation into adipocytes[251]. PPARγ activation has previously been linked to an increase in glucose uptake and glycolysis in white adipose tissue[236, 252]. A consistent observation from both the white adipose tissue and 3T3-L1 adipocytes exposed to PPARγ agonist was a decrease in the concentration of glucose and other carbohydrate species. Transcriptomic analysis indicated that expression of a number of key enzymes catalysing the events of glycolysis was increased in PPARγ activated adipocytes. The glycolytic enzymes affected were glucose phosphate isomerase, phosphofructokinase, aldolase A fructose-bisphosphate, phosphoglycerate mutase 1 and glyceraldehyde-3-phosphate dehydrogenase. It would appear however that the utilisation of the

carbohydrates is not limited to glycolysis. The concentration of the end products of glycolysis, acetic acid in white adipose tissue and pyruvate and lactate in the 3T3-L1 cells decreased when PPARγ was activated. The decrease in ^{13}C-labelling of lactate from 1-^{13}C-glucose confirms this observation. Further to this, calcium signalling is known to activate pyruvate dehydrogenase[253], leading to examination of the TCA cycle, the consecutive step in oxidative breakdown of carbohydrate.

TCA cycle metabolism in both white adipose tissue and cultured adipocytes is modified by PPARγ activation to favour a reduction in oxidation of carbohydrates and an increase in fatty acid synthesis. In white adipose tissue the equilibrium of the cycle is altered in favour of the earlier intermediates (oxidation substrates), at the expense of the latter intermediates (oxidation products) and appears to occur at the electron transport chain complex II intersect with increases in the concentrations of isocitrate and succinate while the concentrations of fumarate and malate were decreased . The effect in adipocytes is even more pronounced with a decrease in the concentration of a range of latter intermediates. Analysis with ^{13}C-labelled glucose showed a reduction in ^{13}C-enrichment of TCA cycle intermediates and substantiated the reduction in oxidative metabolism. Augmenting these findings were the results of the transcriptomic analysis which identified a decrease in the concentration of the mRNA of the gene coding for the TCA cycle enzyme isocitrate dehydrogenase, which catalyses the oxidative decarboxylation of isocitrate to 2-oxoglutarate.

Alternative pathways of carbohydrate metabolism were also observed to be altered by activation of PPARγ. Intermediates of the polyol pathway, glucitol and fructose, were identified as increased in concentration in the 3T3-L1 adipocytes analysed by metabolomics. Further investigation using 1-^{13}C-glucose established increased flux through this pathway. Corroborating findings were detected in the transcriptomic analysis which verified an increase in the expression of sorbitol dehydrogenase, a polyol pathway enzyme that catalyses the conversion of glucitol to fructose. The polyol pathway has been implicated in the formation of advanced glycation end-products (AGEs)[254]. AGEs are formed by a reaction between carbohydrates and the free amino

groups of proteins, lipids and DNA. These glycation products are often found in excess with pathologies such as diabetes, where they are thought to contribute to macro- and micro-vascular complications via several deleterious mechanisms including the accumulation in circulatory vessel walls, the *in situ* glycation of substrates and direct binding to cellular receptors[255]. Therefore the implication that PPARγ activation increases activity of the polyol pathway in adipocytes potentially complicates the use of TZDs and other PPARγ agonists in the treatment of diabetes and the metabolic syndrome.

The activation of PPARγ in both the white adipose tissue and cultured cells generated changes in the composition of the cellular fatty acid pool. The effect of PPARγ activation on fatty acid metabolism, although more distinct in cultured cells, where there was a defined decrease in the concentrations of shorter chain fatty acids and an increase in the concentration of longer chain fatty acids as opposed to white adipose tissue where there was an increase in the long chain fatty acid arachidate, was indicative of fatty acid synthesis and elongation. The increased ^{13}C-enrichment of arachidate in adipocytes incubated in 1-^{13}C-glucose and treated with the PPARγ agonist verified an increase in fatty acid synthesis as a result of PPARγ activation; a finding further corroborated by the observed increase in ^{13}C-enrichment of arachidate in PPARγ activated adipocytes incubated in U-^{13}C -palmitate. Activation of PPARγ in white adipose tissue is known to upregulate the expression of a number of genes involved in fatty acid lipogenesis and elongation [233, 256], together with the results of the microarray analysis which show an increase in the concentration of mRNA for genes that promote fatty acid synthesis there is an indication of a switch to a lipogenic metabolic state upon receptor activation. An upregulation of transcription, in response to PPARγ activation, affected sterol regulatory element binding transcription factor 2, a transcription factor required for lipid homeostasis that regulates the LDL receptor gene as well as the cholesterol and fatty acid synthesis pathways[241], holocarboxylase synthetase, which activates acetyl-CoA-carboxylase (and pyruvate carboxylase) by conjugating biotin to these enzymes[242], NAD kinase, which catalyses the transfer of a phosphate group from ATP to NAD generating NADP forming an electron donor for biosynthetic reactions and malonyl CoA:ACP acyltransferase which catalyses the transfer of a malonyl moiety from malonyl-CoA to

the phosphopantethenate moiety of the acyl carrier peptide in the first step of fatty acid synthesis.

PPARγ activation also increases the uptake of fatty acids by adipocytes[257]. Evidence for the influence of PPARγ on fatty acid uptake can be seen within the U-^{13}C-palmitate study; where an increase in the ^{13}C-enrichment of palmitate in the PPARγ agonist treated 3T3-L1 adipocytes compared to control 3T3-L1 cells was detected. Increased expression of the insulin responsive fatty acid transporter solute carrier family 27 in PPARγ agonist treated cells is a further indication of the import of long chain fatty acids into adipose tissue undergoing high levels of TAG synthesis as a consequence of the activation of the nuclear receptor[244].

Evidence demonstrating decreased ^{13}C-enrichment of TCA cycle intermediates and shorter chain fatty acids in U-^{13}C-palmitate studies also suggests that PPARγ activation concurrently decreases flux through the fatty acid β-oxidation pathway alongside the upregulation of fatty acid synthesis. Supporting this finding was the decreased concentration of carnitine in PPARγ agonist treated adipocytes. Carnitine is required for the transport of fatty acids, in the form of acyl-carnitine from the cytosol to the mitochondrial matrix during β-oxidation. Transcriptomic analysis provides additional mechanisms by which activation of PPARγ may bring about the observed decrease in β-oxidation. The expression of acyl-CoA thioesterase 7 and nudix-type motif 19 Coenzyme A diphosphatase, enzymes which catalyse the hydrolysis of medium and long chain acyl-CoAs to FFA and CoA and therefore prevent the β-oxidation of medium and long chain fatty acids once they are formed[243], was upregulated in the treated adipocytes. Transcription of nuclear receptor corepressor (Ncor1) was also increased in the adipocytes treated with PPARγ agonist. Ncor1 is a transcriptional repressor indicated in the repression of gluconeogenesis, oxidative and ketotic metabolism and lipolysis[247].

A distinct restructuring of the TAG pool occurred as a consequence of PPARγ activation; the length and desaturation of fatty acids esterified to TAGs in cultured adipocytes was

increased, reinforcing the data substantiating increased activity of the fatty acid elongase and the observed increases in the Δ-9 desaturase products in white adipose tissue. This observation is consistent with previous studies that demonstrate that the gene for stearoyl-CoA desaturase, the enzyme responsible for Δ-9 desaturation of fatty acids, is under PPARγ transcriptional control[258], a finding supported by the microarray analysis conducted which found that the expression of the stearoyl-CoA desaturase 2 gene was upregulated in PPARγ agonist treated 3T3-L1 genes. PPARγ also directly regulates the glycerol kinase promoter and therefore is expected to promote the esterification of fatty acids into TAGs[259]. Microarray analysis indicated that lysophosphatidylcholine acyltransferases 3 acyltransferase expression was increased in adipocytes treated with PPARγ. The enzyme catalyses the conversion of lysophosphocholines, lysophosphoserines and lysophosphoethanolamines into phosphocholines, phosphoserines and phosphoethanolamines, respectively[245]. The protein favours polyunsaturated fatty acyl-CoAs as acyl donors. Platelet activating factor acetylhydrolase 2 lipase transcription was also increased in the PPARγ activated adipocytes. This lipase is selective for phospholipids with short acyl chains at the sn-2 position[260]. The concentration of angiopoietin-related protein 4 mRNA was increased in the agonist treated 3T3-L1 cells; the protein product of which inhibits lipoprotein lipase and therefore inhibits lipolysis[246]. Furthermore, the upregulation of the transcription of genes involved in calcium signalling as a consequence of PPARγ activation may play a role in defining the constituents of the complex lipid pool within the adipocytes. An increase in intracellular calcium stimulates the activity of fatty acid synthase, stimulates lipogenesis, inhibits basal lipolysis, and promotes TAG accumulation within murine and human adipocytes[261].

Essential fatty acid metabolism was identified as altered following activation of the nuclear transcription factor. The ω-3 and ω-6 fatty acid pathways are under the influence of PPARγ control, a result that not only corresponds to the previously discussed effect of activation of the nuclear receptor on fatty acid synthesis but also to the identification of a PPRE in the gene for the Δ-6 desaturase[262], an enzyme intrinsic to both essential fatty

acid pathways. Transcriptomic analysis further identified the increased expression of the Δ-6 desaturase in adipocytes upon PPARγ activation.

PPARγ activation was found to increase the cholesterol content of both white adipose tissue from *ob/ob* mice and cultured 3T3-L1 adipocytes. Given that PPARγ activity upregulates the expression of oxidized LDL receptor 1 in adipocytes[263]; it appears that increasing cholesterol concentrations are brought about by stimulation of the uptake of oxidized LDL into adipocytes, a process that may be mediated through the sterol regulatory element binding transcription factor 2, so sequestering potentially harmful circulating cholesterol into the adipose tissue depository.

5.6 Conclusions

In conclusion, it is proposed that PPARγ activation, in part, brings about its anti-diabetic effects on white adipose tissue via transcriptional control of an array of direct metabolic responses and indirect signalling mechanisms. PPARγ activation in white adipose tissue leads to an upregulation of glycolysis and catabolism of other carbohydrate species. Subsequently the TCA cycle is downregulated, an effect especially apparent by the disparity between the decreases in concentration of the latter intermediates compared with an increase in concentration of intermediates at the start of the cycle, demonstrating fatty acid synthesis rather than oxidative catabolism. In combination with de novo fatty acid synthesis, the cellular uptake of FFAs is increased; generating a pool of longer chain fatty acids which are incorporated into TAGs directly or else desaturated and incorporated into TAGs. Concomitantly fatty acid breakdown via β-oxidation is downregulated upon nuclear receptor activation (**Figure 5.7**).

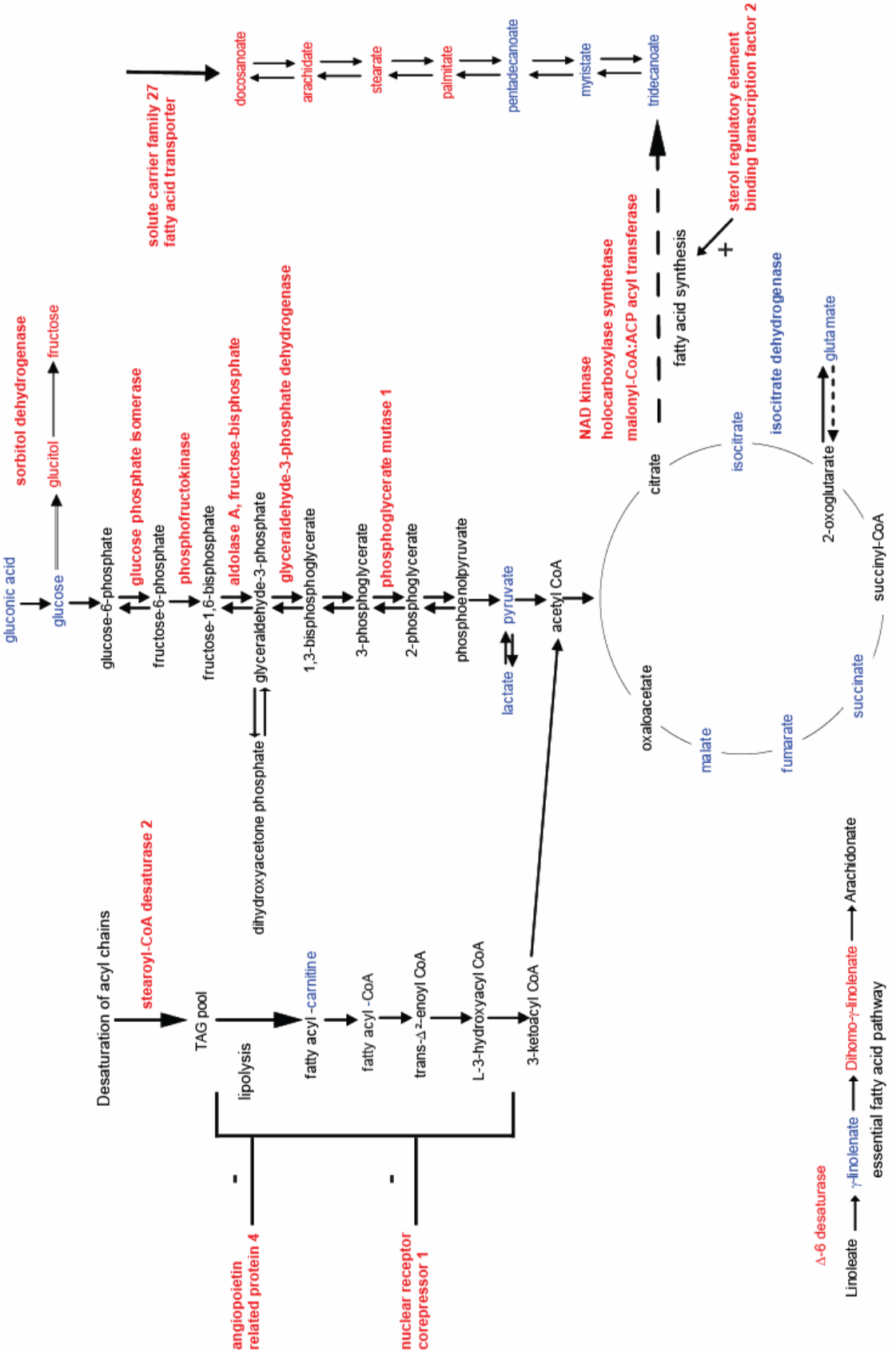
gluconic acid
glucose
sorbitol dehydrogenase
glucitol
fructose
glucose-6-phosphate
glucose phosphate isomerase
fructose-6-phosphate
phosphofructokinase
fructose-1,6-bisphosphate
aldolase A, fructose-bisphosphate
dihydroxyacetone phosphate
glyceraldehyde-3-phosphate
glyceraldehyde-3-phosphate dehydrogenase
1,3-bisphosphoglycerate
3-phosphoglycerate
phosphoglycerate mutase 1
2-phosphoglycerate
phosphoenolpyruvate
pyruvate
lactate
acetyl CoA
solute carrier family 27
fatty acid transporter
docosanoate
arachidate
stearate
palmitate
pentadecanoate
myristate
tridecanoate
NAD kinase
holocarboxylase synthetase
malonyl-CoA:ACP acyl transferase
fatty acid synthesis
sterol regulatory element
binding transcription factor 2
citrate
isocitrate
isocitrate dehydrogenase
2-oxoglutarate
glutamate
succinyl-CoA
succinate
fumarate
malate
oxaloacetate
Desaturation of acyl chains
stearoyl-CoA desaturase 2
TAG pool
lipolysis
fatty acyl -carnitine
fatty acyl -CoA
trans-Δ2-enoyl CoA
L-3-hydroxyacyl CoA
3-ketoacyl CoA
angiopoietin
related protein 4
nuclear receptor
corepressor 1
Δ-6 desaturase
Linoleate
γ-linolenate
Dihomo-γ-linolenate
Arachidonate
essential fatty acid pathway

Figure 5.7: Diagram showing the effect of PPARγ activation on the integration of the energy metabolism pathways of 3T3-L1 adipocytes based on the combination of results from the metabolomic, transcriptomic and stable isotope labelling studies. Red indicates an increase in concentration or expression in cells treated with the GW347845 PPARγ selective agonist. Blue indicates a decrease in concentration in cells treated with the GW347845 PPARγ selective agonist.

The extensive metabolic pathway regulation found to be under PPARγ control in white adipose tissue identifies a mechanism that contributes to the observed normalisation of blood glucose levels and dyslipidaemia[264], increase in glucose utilisation [236,252], and increase in body weight and subcutaneous adiposity previously reported in both human patients and rodent subjects treated with selective PPARγ agonists[265,266]. This sequestration of glucose and lipid into the white adipose tissue, as a safely contained storage depot, may reduce the damaging potential of increased levels of circulating glucose and lipid, whilst reducing lipid and cholesterol accumulation in peripheral tissues[267]. Given white adipose tissue appears to be the primary target for PPARγ agonist mediated insulin sensitisation[268] these findings provide a possible means by which PPARγ activation influences peripheral tissue insulin sensitivity, by reducing the accumulation of fat in peripheral tissue and therefore lipotoxicity through increased storage of lipid in adipose tissue, in accordance with the adipose tissue expandability model[269]. Through the dual mechanisms of augmenting facets of the calcium signalling pathway associated with insulin action and direct transcriptional regulation of metabolic enzymes PPARγ activation brings about metabolic changes that function to reinforce insulin sensitisation.

Chapter 6

The Effects of PPARδ and PPARγ Activation on the Cori Cycle and Systemic Metabolism in the *ob/ob* Mouse

6.1 Introduction

The role of PPARδ in hepatic metabolism remains to be fully elucidated and relatively little research has focussed on the effects of activation of the nuclear receptor in the liver. Nevertheless, it has been shown that treatment of *db/db* mice with a selective PPARδ agonist resulted in suppression of hepatic glucose production and release[227]. In addition PPARδ activation was found to increase hepatic glucose disposal, flux through the pentose phosphate pathway and to inhibit VLDL secretion from the livers of treated mice[227]. The disparity of research conducted into the function of PPARδ in the liver in comparison to peripheral tissues, and especially skeletal muscle, may have occurred because PPARα is known to act primarily in the liver, whereas PPARδ mRNA is expressed at 10 and 50 times the concentrations of PPARα and PPARγ mRNA[139], respectively, in skeletal muscle. Administration of PPARδ agonists to rodents results in an increase in expression of genes involved in fatty acid oxidation, mitochondrial respiration, oxidative metabolism and slow twitch contractile apparatus, decreasing muscle fatigability[171]. Treatment of L6 myotubes with GW610742, a PPARδ agonist, was shown to increase fatty acid oxidation whilst overexpression of PPARδ in C2C12 myotubes induced genes involved in fatty acid uptake and catabolism including lipoprotein lipase, FAT and carnitine palmitoyl transferase I[270]. Further to this,

an animal model of muscle specific PPARδ overexpression has been developed in which a remodelling of the soleus and tibialis anterior muscles in favour of oxidative fibres was observed[271]. The activity of several oxidative enzymes was also increased in the mice; enzymes affected include citrate synthase and β-hydroxyacyl-CoA dehydrogenase. Together these findings are suggestive of a regulatory role for PPARδ in the control of the Cori cycle and the metabolic interactions of the liver and skeletal muscle. Research conducted in this thesis, thus far, has been directed at the effects of both PPARδ and PPARγ activation in adipose tissue. However, it is likely that the observed increases in glucose tolerance and insulin sensitivity upon PPARδ and PPARγ activation *in vivo* may crucially involve combined hepatic and peripheral metabolic effects.

However, the ubiquitous expression of PPARδ may result in diverse and unwanted side effects upon activation of this receptor. PPARδ activation has been implicated as a cause of muscle atrophy[272]. The nuclear receptor has also been implicated in the acceleration of intestinal adenoma growth and increased growth in breast and prostate cancer cell lines, but conversely it also attenuates colon cancer[176, 177, 178]. The role of PPARδ in development and carcinogenesis is complex and has been extensively reviewed[179].

It is hypothesized that the insulin sensitising effects of PPARδ activation are brought about, in part, by changes in systemic metabolism. Given that TAG in liver contributes to insulin resistance it has been suggested that increased TAG oxidation in the liver, caused by PPARδ activation, may contribute to this improvement[227]. In this chapter the effect of both the selective PPARδ agonist GW610742 and PPARγ agonist GW347845 on the systemic metabolism of the *ob/ob* mouse is examined with specific focus directed at hepatic and skeletal muscle metabolism. The *ob/ob* mouse model of insulin resistance is robust, well characterised and used extensively to study TIIDM and its therapies. However, it is worthy of note that it is a monogenic paradigm of leptin deletion, whereas TIIDM is a polygenic disorder.

6.2 Aims and Objectives

This study aims to use metabolomics to examine the changes that occur in hepatic metabolism following PPARδ activation and the impact detected systemically through metabolite changes in blood serum and skeletal muscle in the *ob/ob* mouse. ^{1}H-NMR spectroscopy, GC-MS, UPLC-MS and DI-MS were used to examine metabolites from tissue extracts. This study has used a metabolomics approach in conjunction with traditional clinical chemistry end points to investigate and define the global physiological and pharmacological effects of PPARδ and PPARγ activation through the metabolic characterisation of blood serum, skeletal muscle and liver tissue from a pharmacological compound treatment study performed in the *ob/ob* mouse model of insulin resistance.

Analysis by multivariate statistics demonstrated that PPARδ activation profoundly affected glycolysis, gluconeogenesis, the TCA cycle and linoleic acid and α-linolenic acid essential fatty acid pathways. Although activation of both PPARδ and PPARγ led to increased insulin sensitivity and glucose tolerance; PPARδ activation was functionally distinct from PPARγ activation, and was characterised by increased hepatic and peripheral fatty acid oxidative metabolism, demonstrating the distinctive catabolic role of this receptor compared with PPARγ.

6.3 Materials and Methods

6.3.1. Clinical Chemistry

All clinical chemistry measurements were performed using an Olympus AU 400e analyser[186]. Insulin measurements were performed by ELISA as described in **Chapter 2 Materials and Methods** (section *2.2.2. Clinical Chemistry*).

6.3.2. Oral Glucose Tolerance Test

OGTT was performed as stated in **Chapter 2 Materials and Methods** (section *2.2.3.Oral Glucose Tolerance Test*).

6.3.3. Animal and Tissue Handling

Animals were kept as is outlined in **Chapter 2 Materials and Methods** (section *2.2.1. Animal handling*). Briefly, the *ob/ob* mice were assigned to three groups of eight and dosed orally daily at 8 am with 0.5% Hydroxypropylmethylcellulose/0.1% Tween80 vehicle control, a PPARδ agonist, GW610742 (30 mg/kg) and a PPARγ agonist, GW347845 (5 mg/kg). Injection volume was adjusted daily according to body weight at 10 ml/kg.

Liver, skeletal muscle and serum were collected as summarised in **Chapter 2 Materials and Methods** (section *2.2.4. Tissue handling*).

6.3.4. Metabolite Extraction

Metabolites were extracted from tissues using the modified Bligh and Dyer method[187]. The details are as in Chapter 2 Materials and Methods (*section 2.3 3T3-L1 Cell, Primary Adipocyte and Tissue Metabolite Extraction*).

6.3.5. ^{1}H-NMR Spectroscopy Analysis

All samples were analysed using a Bruker AVANCE II+ spectrometer operating at 500.13 MHz for the ^{1}H frequency using a 5mm Broadband TXI Inverse ATMA probe. All procedures are as depicted in **Chapter 2 Materials and Methods** (sections 2.6.1. *Spectrometer*, 2.6.2. *Sample preparation*, 2.6.3. *1-dimensional ^{1}H-Nuclear Magnetic Resonance experimental method* and 2.6.4. *Processing 1-dimensional ^{1}H-Nuclear Magnetic Resonance data*).

6.3.6. GC-MS Analysis

Aqueous phase samples were derivatised as described in **Chapter 2 Materials and Methods** (section 2.7.1).

Organic phase samples were derivatised as described in **Chapter 2 Materials and Methods** (section 2.7.2).

GC-MS analyses were made using a Trace GC Ultra coupled to a Trace DSQ II single-quadrupole mass spectrometer. Parameters for the GC-MS analysis of aqueous phase metabolites and organic phase metabolites were as described in **Chapter 2 Materials and Methods** (sections 2.7.3.1 *Gas Chromatography-Mass Spectrometry methods for aqueous phase samples* and 2.7.3.2 *Gas Chromatography-Mass Spectrometry methods for organic phase samples*). Derivatised aqueous phase samples were injected splitless and organic phase samples were injected with a split ratio of 8.

GC-MS chromatograms were processed using Xcaliber (version 2.0; Thermo Electron) as outlined in **Chapter 2 Materials and Methods** (2.7.5. *Processing Gas Chromatography-Mass Spectrometry data*).

6.3.7. UPLC-MS Analysis

Chromatography was performed using an ACQUITY UPLC® system equipped with an Acquity UPLC 1.7 μm BEH C8 column (2.1×100 mm) coupled to a Micromass QTof-

Ultima with a Z-spray electrospray source. All chromatography and mass spectrometric parameters were as outlined in **Chapter 2 Materials and Methods (**section 2.8.1. *Chromatography and mass Spectrometry parameters*)

6.3.7.1 Liver tissue preparation and chromatographic gradient

The organic phase of liver was reconstituted in methanol-chloroform (2:1, 500 µl). This was further diluted 7.5-fold prior to injection onto the C8 column (5 µl). The column mobile phase was held at 70% solvent B for 0.5 min followed by an increase from 70%-100% solvent B over 0.5-6.5 min. The mobile phase was then held at 100% B for 3.5 min. Between 10 and 10.25 min the mobile phase was returned to 70% B and held for 3.75 min to re-equilibrate the column. The total UPLC cycle was 14 min. The eluent flow rate was 600 µl/min.

6.3.7.2 Serum preparation and chromatographic gradient

The organic phase of serum was reconstituted in methanol-chloroform (2:1, 500 µl). This was further diluted 4 fold prior to injection onto the C8 column (10 µl). The column mobile phase was held at 70% solvent B for 0.5 min followed by an increase from 70%-100% solvent B over 0.5-6.5 min. The mobile phase was then held at 100% B for 3.5 min. Between 10 and 10.25 min the mobile phase was returned to 70% B and held for 3.75 min to re-equilibrate the column. The total UPLC cycle was 14 min. The eluent flow rate was 600 µl/min.

Tandem mass spectrometry procedures were as described in **Chapter 2 Materials and Methods** (2.8.3 *Tandem mass spectrometry method*).

Data was processed using Micromass MarkerLynx Applications Manager as depicted in **Chapter 2 Materials and Methods** (2.8.4. *Processing Liquid Chromatography-Mass Spectrometry data*).

6.3.8. Direct Infusion Mass Spectrometry

Mass spectrometric analysis was performed using a Thermo Finnigan LTQ equipped with a Finnigan Surveyor pump and Finnigan Micro AS Autosampler.

6.3.8.1 Liver tissue

The liver organic phase samples for DI-MS were reconstituted in 500 µl methanol:THF (2:1 v/v). 50 µl of each sample was aliquoted into a 96 well plate where the samples were diluted by the addition of a further 150 µl methanol:THF (2:1 v/v).

Analysis was performed in negative ionisation mode. All other direct infusion and mass spectrometric parameters were as described in **Chapter 2 Materials and Methods** (section 2.9.2. *Direct infusion and mass spectrometry parameters*).

DI-MS chromatograms were processed using Xcaliber as outlined in **Chapter 2 Materials and Methods** (2.9.3. *Processing of direct infusion mass spectrometry data*).

6.3.9. Multivariate Analysis

Multivariate data analysis was performed using SIMCA-P^+ 11.0 (Umetrics AB, Umeå, Sweden). NMR, DI-MS and UPLC-MS data sets were mean-centered and Pareto-scaled prior to analysis. GC-MS data sets were scaled to univariate scaling. Data sets were analyzed using PCA, PLS and PLS-DA. Further details are summarised in **Chapter 2 Materials and Methods** (section 2.11.6 *Multivariate Statistical Analysis Methodology*).

6.4 Results

6.4.1. Clinical Chemistry

All mice were examined ensuring they were physically normal and exhibited normal activity prior to both commencement and termination of the study. The concentrations of both insulin and glucose were found to be significantly decreased in both PPARδ and PPARγ agonist treated serum, indicating that the insulin resistant status of the *ob/ob* mice is improved by PPARδ and γ activation. This was also confirmed by the OGTT. The concentrations of β-hydroxybutyrate, total cholesterol and HDL-cholesterol were increased in the serum of PPARδ agonist treated mice, while non esterified fatty acids were decreased in concentration. While, serum TAG concentrations were increased in PPARδ agonist treated mice, this metabolite class decreased in PPARγ agonist treated mice (**Figure 6.1**).

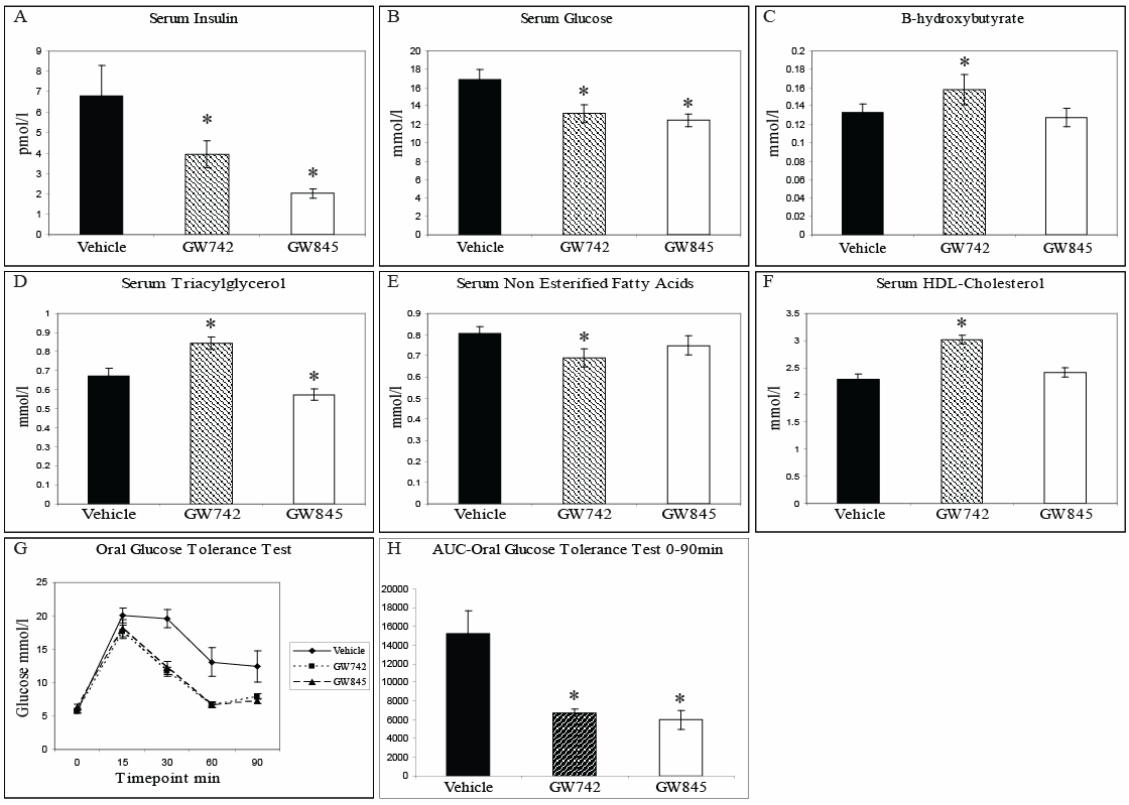

Figure 6.1: Clinical chemistry measurements from the serum of control, GW610742 PPARδ agonist and GW347845 PPARγ agonist treated *ob/ob* mice. A. Serum Insulin B. Glucose C. β-hydroxybutyrate D. TAG E. Non Esterified Fatty Acids F. HDL-Cholesterol G. Oral Glucose Tolerance Test H. Area Under Curve Oral Glucose Tolerance Test.* $P < 0.05$ with respect to vehicle control treated animals.

6.4.2. Metabolomics

^{1}H-NMR spectroscopy and GC-MS analysis, combined with multivariate pattern recognition were used to profile metabolism within the liver, serum and skeletal muscle of *ob/ob* mice treated with a PPARδ agonist and a PPARγ agonist. The different analytical techniques had varying sensitivities. High resolution ^{1}H-NMR spectroscopy detected 20-25 metabolites in both liver and skeletal muscle. GC-MS detected 100-150 defined peaks from aqueous phase samples and 30-40 defined peaks from organic phase samples. Matching the mass spectra detected with those held in the NIST library identified 40-60% metabolites for aqueous extracts and ~70% for lipids from the GC-MS datasets.

Phospholipid targeted UPLC-MS detected 100-150 unique metabolite species in positive mode. Identification of metabolite species was performed using MS/MS. Phosphatidylcholines were identified using the phosphocholine head group ion (detection of ion at 184 m/z).

To assess metabolic changes in the dataset a common processing strategy was adopted throughout the analysis. To investigate metabolite perturbations common to PPARδ and PPARγ activation PCA and PLS-DA models were built for the individual tissues treating the δ and γ agonists as part of a common group. Although the groups were shown to co-cluster and separate from the control group in this supervised analysis, the majority of the Q^2 values (testing model statistical robustness) were low, despite the δ and γ agonist treatment groups separating along the same scores plot axis. While similar changes were detected in the concentration of a large number of metabolites for both treatments, these occurred with different magnitudes (**Figure 6.2**). Activation of PPARδ in the liver and skeletal muscle caused a greater magnitude of changes compared to activation of PPARγ. These findings correspond to known tissue distribution of the PPAR subtypes and that the two receptors share a number of common metabolic effects.

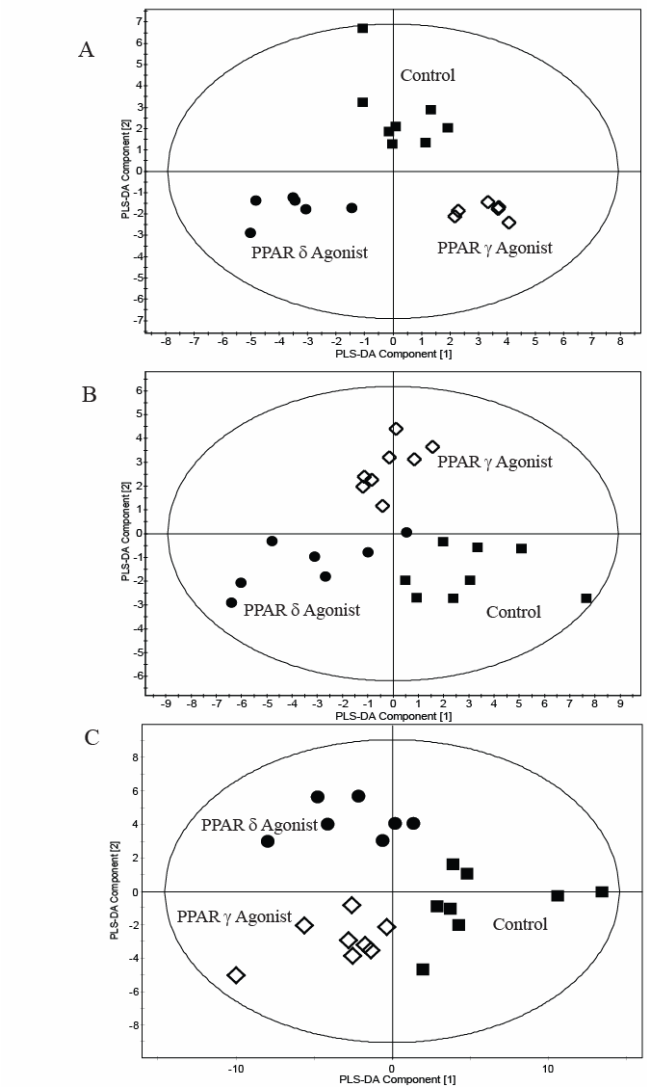

Figure 6.2: **A**. PLS-DA scores plot showing the clustering of GC-MS chromatograms from the organic fraction of the liver from mice treated with either a PPARδ or a PPARγ agonist compared with the control group. ●, PPARδ agonist treated, ◊, PPARγ agonist treated, ■, control (R^2=0.59, Q^2=0.82). **B.** PLS-DA scores plot showing the clustering of GC-MS chromatograms from the aqueous phase of skeletal muscle extracts from mice treated with either a PPARδ agonist or a PPARγ agonist compared with control animals. ●, PPARδ agonist treated, ◊, PPARγ agonist treated, ■, control (R^2=0.24, Q^2=0.32). **C.** PLS-DA scores plot showing clustering of GC-MS chromatograms from PPARδ agonist and PPARγ agonist treated mice serum aqueous phase metabolites following GC-MS analysis. ●, PPARδ agonist treated, ◊, PPARγ agonist treated, ■, control (R^2=0.563, Q^2=0.631).

Visual inspection of the ^{1}H-NMR spectra and GC-MS chromatograms indicated differences between the control and treated groups. PCA and PLS-DA models were built for the individual tissues comparing the control group with the PPARδ agonist treated group and the control group with the PPARγ agonist treated groups. Metabolites identified in the VIP/coefficients plots as significantly contributing to separation in the models were then considered to have changed globally. Metabolite changes were then compared between agonists (**Table 6.1**). The metabolite changes in the individual tissues are considered below.

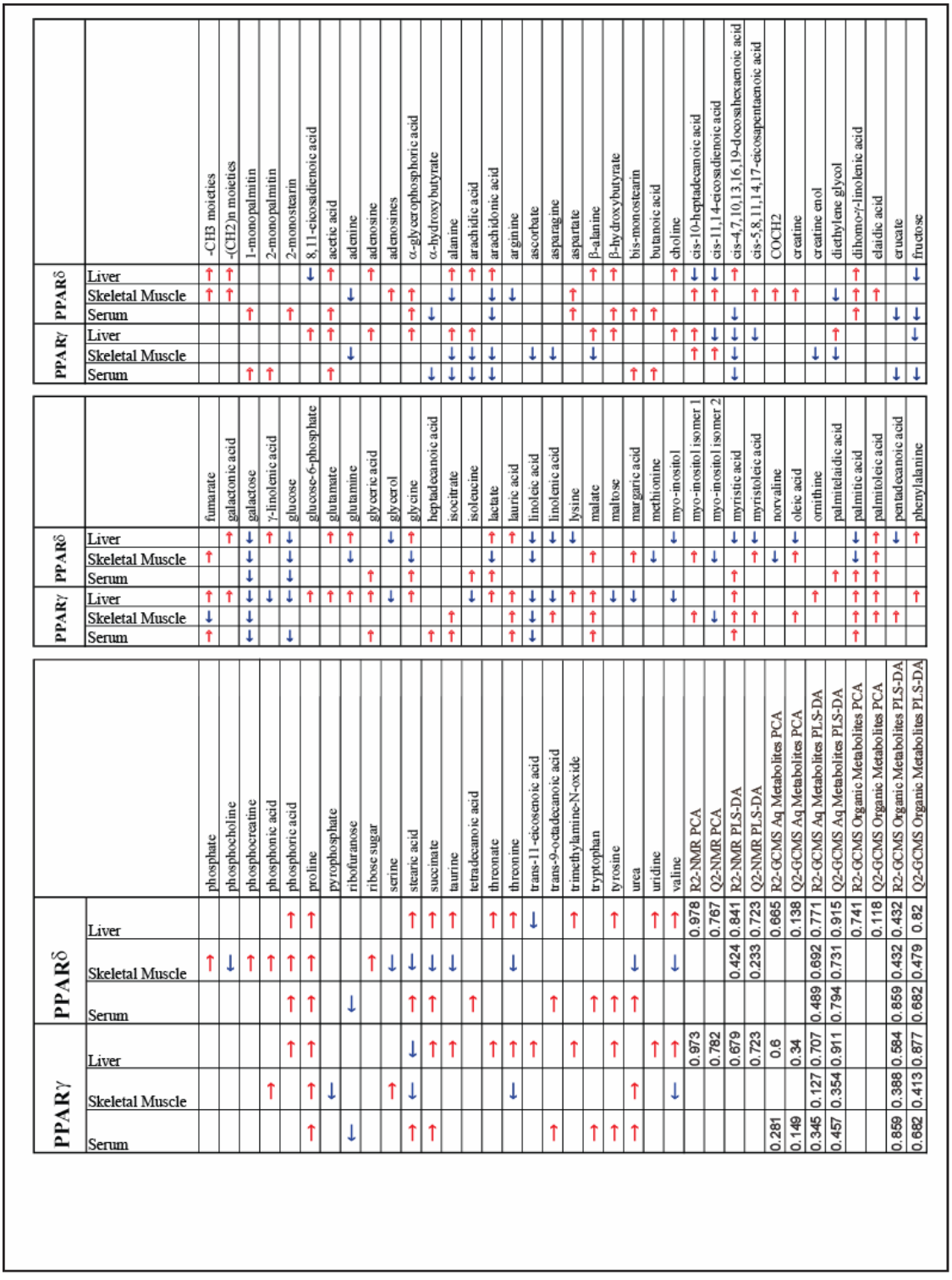
PPARγ
PPARδ
phosphate
phosphocholine
phosphocreatine
phosphonic acid
phosphoric acid
proline
pyrophosphate
ribofuranose
ribose sugar
serine
stearic acid
succinate
taurine
tetradecanoic acid
threonate
threonine
trans-11-eicosenoic acid
trans-9-octadecanoic acid
trimethylamine-N-oxide
tryptophan
tyrosine
urea
uridine
valine
R2-NMR PCA
Q2-NMR PCA
R2-NMR PLS-DA
Q2-NMR PLS-DA
R2-GCMS Aq Metabolites PCA
Q2-GCMS Aq Metabolites PCA
R2-GCMS Aq Metabolites PLS-DA
Q2-GCMS Aq Metabolites PLS-DA
R2-GCMS Organic Metabolites PCA
Q2-GCMS Organic Metabolites PCA
R2-GCMS Organic Metabolites PLS-DA
Q2-GCMS Organic Metabolites PLS-DA
fumarate
galactonic acid
galactose
γ-linolenic acid
glucose
glucose-6-phosphate
glutamate
glutamine
glyceric acid
glycerol
glycine
heptadecanoic acid
isocitrate
isoleucine
lactate
lauric acid
linoleic acid
linolenic acid
lysine
malate
maltose
margaric acid
methionine
myo-inositol
myo-inositol isomer 1
myo-inositol isomer 2
myristic acid
myristoleic acid
norvaline
oleic acid
ornithine
palmitelaidic acid
palmitic acid
palmitoleic acid
pentadecanoic acid
phenylalanine
-CH3 moieties
-(CH2)n moieties
1-monopalmitin
2-monopalmitin
2-monostearin
8,11-eicosadienoic acid
acetic acid
adenine
adenosine
adenosines
α-glycerophosphoric acid
α-hydroxybutyrate
alanine
arachidic acid
arachidonic acid
arginine
ascorbate
asparagine
aspartate
β-alanine
β-hydroxybutyrate
bis-monostearin
butanoic acid
choline
cis-10-heptadecanoic acid
cis-11,14-eicosadienoic acid
cis-4,7,10,13,16,19-docosahexaenoic acid
cis-5,8,11,14,17-eicosapentaenoic acid
COCH2
creatine
creatine enol
diethylene glycol
dihomo-γ-linolenic acid
elaidic acid
erucate
fructose
Liver
Skeletal Muscle
Serum
0.978
0.787
0.841
0.723
0.685
0.138
0.771
0.915
0.741
0.118
0.432
0.82
0.973
0.782
0.679
0.723
0.6
0.34
0.707
0.911
0.432
0.877
0.584
0.388
0.424
0.233
0.489
0.731
0.794
0.859
0.682
0.479
0.692
0.127
0.354
0.457
0.281
0.149
0.345
0.859
0.682
0.413

Table 6.1: Metabolite changes detected by GC-MS and ^{1}H-NMR spectroscopy in liver, serum and skeletal muscle of control, PPARδ agonist and PPARγ agonist treated ob/ob mice. Metabolites identified in the VIP/coefficients plots as significantly contributing to separation in the PCA and PLS-DA models built for the individual tissues. The control group was compared with the combined PPARδ agonist and PPARγ agonist treated groups. The R^2 and Q^2 values for the individual models are shown. ↑, indicates a detected increase in metabolite concentration. ↓, indicates a detected decrease in metabolite concentration.

6.4.3. Liver

6.4.3.1 Metabolite changes common to PPARδ and PPARγ activation

Activation of both PPARδ and γ caused increases in the concentrations of many amino acids including alanine, β-alanine, glutamate, glutamine, glycine, phenylalanine, proline, threonine, tyrosine and valine in liver tissue relative to tissue from control animals. Fatty acid metabolism was also affected in the liver with an observed increase in the concentration of lauric acid and palmitoleic acid accompanied by a decrease in the concentration of cis-11,14-eicosadienoic acid in the PPARδ and γ treated mice. The essential fatty acid pathways were altered by PPARδ and γ activation with an increase in the concentration of arachidonic acid and a concomitant decrease in linoleic acid and linolenic acid. In addition carbohydrate catabolism, anabolism and energy metabolism was influenced by the activation of both PPARδ and γ. An increase in the concentration of acetic acid, β-hydroxybutyrate, galactonic acid, lactate and succinate and a decrease in fructose, galactose, glucose and glycerol were detected in the livers of treated mice. UPLC-MS analysis identified a decrease in the concentration of a number of TAGs and a concomitant increase in phosphatidylcholine species in both PPARδ and PPARγ agonist treated livers (**Figure 6.3**), (**Table 6.2**). Of the 14 species identified as increased in concentration following PPARδ activation 12 were identified as phosphatidylcholines. Twelve species of TAG were observed to decrease in concentration following PPARδ activation.

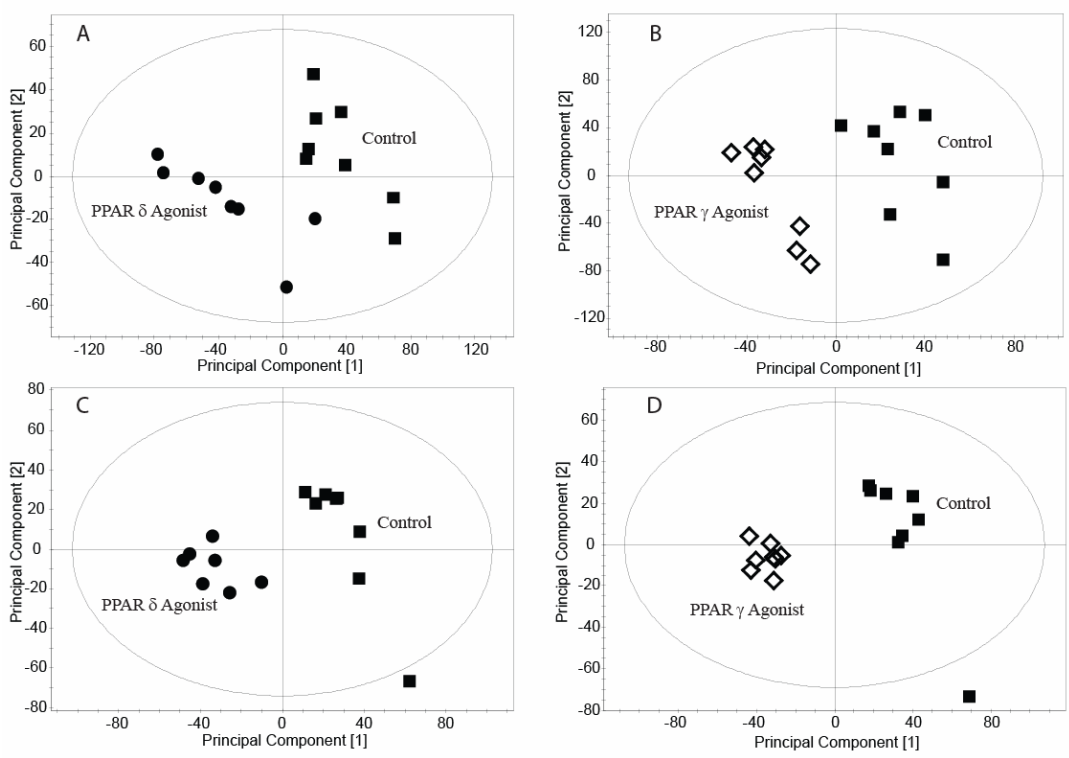

Figure 6.3: **A.** PLS-DA scores plot showing the clustering of the UPLC-MS chromatograms from the organic fraction of liver tissue from mice treated with a PPARδ agonist compared with control mice. ●, PPARδ agonist treated. ■, control (R^2=0.877, Q^2=0.574) **B.** PLS-DA scores plot showing the clustering of the UPLC-MS chromatograms from the organic fraction of liver tissue from mice treated with a PPARγ agonist compared with control mice. ◊, PPARγ agonist treated. ■, control (R^2=0.996, Q^2=0.852). **C.** PLS-DA scores plot showing the clustering of the UPLC-MS chromatograms from the organic fraction of serum from mice treated with a PPARδ agonist compared with control mice. ●, PPARδ agonist treated. ■, control (R^2=0.948, Q^2=0.821) **D.** PLS-DA scores plot showing the clustering of the UPLC-MS chromatograms from the organic fraction of serum from mice treated with a PPARγ agonist compared with control mice. ◊, PPARγ agonist treated. ■, control (R^2=0.985, Q^2=0.864).

A) PPARδ Agonist Treated Liver

Metabolites increased in PPARδ agonist treated mice relative to control	Metabolites decreased in PPARδ agonist treated mice relative to control
PC (32:1)	TAG (16:0/16:1/18:1)
PC (34:2)	TAG (16:1/18:1/18:2)
PC (34:1)	TAG (18:1/18:2/16:0)
PC (36:5)	TAG (18:1/18:0/16:1)
PC (36:4)	TAG (16:0/16:0/21:0)
PC (36:3)	TAG (18:2/18:2/18:3)
PC (36:1)	TAG (16:0/16:0/21:0)
PC (38:6)	TAG (18:2/18:2/18:3)
PC (38:5)	TAG (18:1/20:4/16:0)
PC (38:4)	TAG (18:1/16:0/20:1)
PC (38:3)	TAG (18:1/18:0/18:1)
PC (40:6)	TAG (18:1/16:0/21:0)
TAG (16:1/16:1/16:0)	
TAG (16:1/18:1/14:0)	

B) PPARγ Agonist Treated Liver

Metabolites increased in PPAR γ agonist treated mice relative to control	Metabolites decreased in PPAR γ agonist treated mice relative to control
PC (34:2)	PC (36:2)
PC (34:1)	PC (40:6)
PC (36:4)	TAG (16:1/18:1/18:2)
PC (36:3)	TAG (18:1/18:2/16:0)
PC (36:1)	TAG (16:0/16:0/21:0)
PC (38:5)	TAG (18:2/18:2/18:3)
PC (38:4)	TAG (18:1/20:4 16:0)
TAG (16:1/16:1/16:0)	TAG (18:1/18:1/18:1)
TAG (16:1/18:1/14:0)	TAG (18:1/18:0/21:0)

Table 6.2: Complex lipid changes detected in liver of control, PPARδ agonist and PPARγ agonist treated *ob/ob* mice using UPLC-MS. Lipids identified in the VIP/coefficients plots as significantly contributing to separation in the PCA and PLS-DA models built for the UPLC-MS analysis of the organic metabolite fraction. The control group was compared with the PPARδ agonist and PPARγ agonist treated groups from liver. (Glycerophosphatidylcholine PC)

DI-MS analysis of livers from PPARδ and PPARγ agonist treated *ob/ob* mice demonstrated an increase in the concentration of a range of glycerophosphoinositol species. Several of the species increased in concentration were common to both the PPARδ and PPARγ treated animals (**Table 6.3**). The increase in glycerophosphoinositols also coincided with the decrease in the free concentration of myoinositol in the livers of both treatment groups and may be indicative of the increased synthesis of the phospholipids.

GPIns species increased in PPARδ agonist treated mice relative to control	**GPIns species increased in PPARγ agonist treated mice relative to control**
GPIns (16:0/0:0)–H_2O	GPIns (20:4/16:0)
GPIns (18:1/0:0)	GPIns (16:0/20:3)
GPIns (16:0/18:2)	GPIns (18:1/18:2)
GPIns (20:4/16:0)	GPIns (18:0/18:2)
GPIns (16:0/20:3)	GPIns (16:0/20:2)
GPIns (18:1/18:2)	GPIns (18:1/18:1)
GPIns (18:0/18:2)	GPIns (20:4/18:1)
GPIns (16:0/20:2)	GPIns (20:3/18:0)
GPIns (20:4/18:2)	GPIns (22:5/18:0)
GPIns (16:0/22:6)	GPIns (18:0/22:4)
GPIns (20:4/18:1)	GPIns (18:1/22:3)
GPIns (20:3/18:0)	
GPIns (22:6/18:1)	
GPIns (22:6/18:0)	
GPIns (22:5/18:0)	
GPIns (18:0/22:4)	
GPIns (18:1/22:3)	
GPIns (18:0/22:3)	

Table 6.3: Glycerophosphoinositol (GPIns) species increased in concentration in the livers of PPARδ agonist and PPARγ agonist treated *ob/ob* mice detected using DI-MS. Lipids identified in the VIP/coefficients plots as significantly contributing to separation in the PCA and PLS-DA models built for the DI-MS analysis of the organic metabolite fraction. The control group was compared with the PPARδ agonist and PPARγ agonist treated groups from liver. GPIns species increased in concentration in both treatment groups are highlighted in red.

6.4.3.2 Metabolite changes unique to PPARδ activation

While only a decrease in the concentration of the ketogenic amino acid, lysine distinguished the animals treated with the PPARδ agonist from the other groups for aqueous soluble metabolites, this group was more readily distinguished by lipid metabolites. The PPARδ agonist produced an increase in the $–CH_3$ and $-(CH_2)_n$ lipid moieties, detected by ^{1}H-NMR spectroscopy. A decrease was detected in the concentrations of 8,11-eicosadienoic acid, cis-10-heptadecanoic acid, myristic acid, myristoleic acid, oleic acid, palmitic acid, pentadecanoic acid and trans-11-eicosenoic acid. The essential fatty acid pathways were also targeted with increases in arachidonic acid, dihomo-γ-linolenic acid, cis-4,7,10,13,16,19-docosahexaenoic acid and a decrease in γ-linolenic acid (**Figure 6.4**).

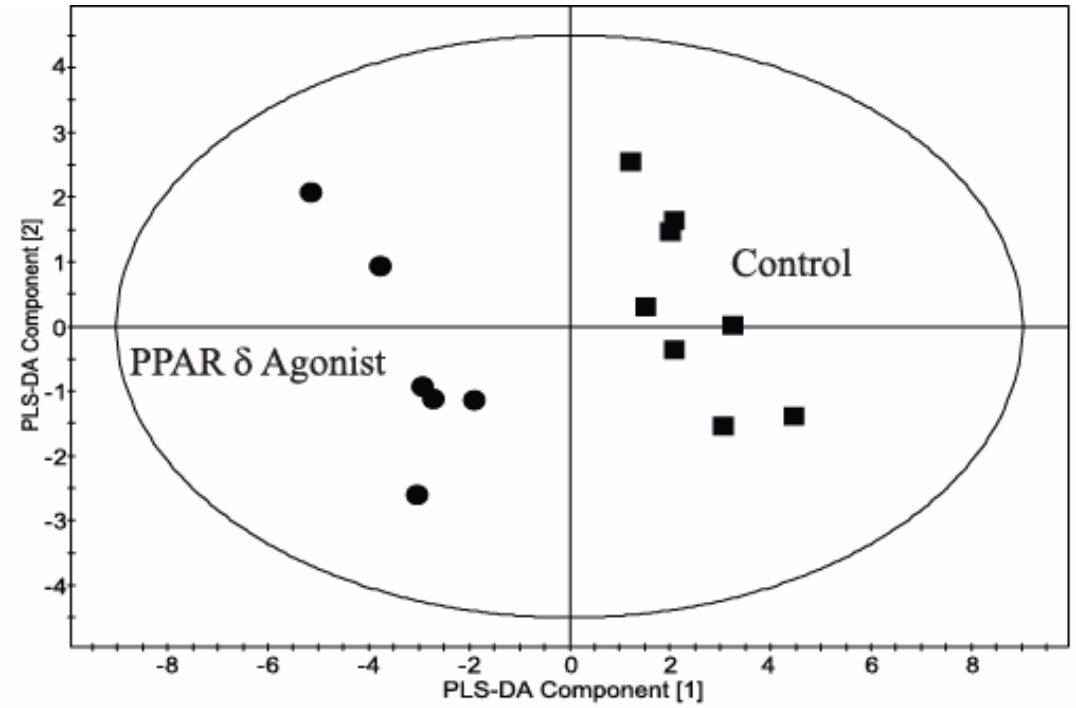

Figure 6.4: PLS-DA scores plot showing the clustering of the GC-MS chromatograms from the organic fraction of liver tissue from mice treated with a PPARδ agonist compared with control mice. ●, PPARδ agonist treated. ■, control (R^2=0.43, Q^2=0.82).

The FFA composition of the liver, as detected by DI-MS, was also altered in livers from mice treated with PPARδ agonist. There was an increase in the intermediates of the ϖ-6 fatty acid pathway (dihomo-γ-linolenic acid and adrenic acid) and an increase in the intermediates and end products of the ϖ-3 essential fatty acid pathway (cis-7,10,13,16,19-docosapentaenoic acid and cis-4,7,10,13,16,19-docosahexaenoic acid). In addition there was an increase in incorporation of the ϖ-6 fatty acid pathway end product, arachidonic acid, into phospholipids and a concomitant decrease in the free concentration of this fatty acid.

Given the increased ketogenesis and reduction in TAGs observed in the liver for both agonists it was deemed important to examine how these metabolic changes were influencing the metabolism systemically by analysing the serum.

6.4.4. Serum

6.4.4.1 Metabolite changes common to PPARδ and PPARγ activation

Treatment with either of the two PPAR agonists induced changes in amino acid metabolism (increases in proline, tryptophan and tyrosine) and glycolysis/TCA cycle intermediates (increases in acetic acid, glyceric acid and succinate; decreases in fructose, galactose and glucose) reflecting those detected in the liver. Also, in a similar manner to the liver, the largest changes occurred in lipid metabolism. The agonists caused increases in monopalmitin, bis-monostearin, myristic acid, palmitic acid, stearic acid, trans-9-octadecanoic acid and trans-11-eicosanoic acid and decreases in cis-4,7,10,13,16,19-docosahexaenoic acid and erucate. Arachidonic acid from the ϖ-6 essential fatty acid pathway was decreased in the serum of treated animals.

6.4.4.2 Metabolite changes unique to PPARδ activation

Amino acids increased in the PPARδ agonist treated mice serum relative to control were aspartate and isoleucine. The concentration of the ketone body, β-hydroxybutyrate was increased as were the concentration of the TCA cycle metabolite fumarate and the glycolytic product lactate. Fatty acid metabolism was also affected in the serum with

increases in the concentration of 2-monostearin, palmitelaidic acid, palmitoleic acid and tetradecanoic acid. The ϖ-6 essential fatty acid pathway intermediate, dihomo-γ-linolenic acid was also increased in PPARδ agonist treated mice serum. UPLC-MS analysis highlighted that the concentration of a range of TAGs was found to be elevated in PPARδ treated serum; this was the reverse of the observation upon PPARγ activation where the concentration of the same TAGs was found to be decreased (**Table 6.4**).

PPARδ Agonist Treated Serum

Metabolites increased in PPARδ agonist treated mice relative to control	Metabolites decreased in PPARδ agonist treated mice relative to control
PC (16:0/18:1)	PC (18:2/0:0)
PC (16:0/0:0)	PC (18:0/0:0)
PC (18:1/0:0)	PC (34:1)
PC (22:6/18:0)	PC (36:2)
TAG (16:1/18:1/18:2)	TAG (18:1/18:1/18:1)
TAG (16:1/18:1/18:1)	
TAG (18:1/18:2/16:0)	
TAG (18:1/18:1/16:0)	
TAG (16:1/16:0/18:1)	
PC (36:3)	

PPARγ Agonist Treated Serum

Metabolites increased in PPARγ agonist treated mice relative to control	Metabolites decreased in PPARγ agonist treated mice relative to control
PC (16:0/0:0)	PC (18:0/0:0)
PC (18:1/0:0)	PC (34:1)
PC (34:2)	PC (36:2)
PC (16:0/18:1)	PC (40:6)
PC (36:5)	TAG (16:1/18:1/18:2)
PC (36:4)	TAG (16:1/18:1/18:1)
PC (36:3)	TAG (18:1/18:2/16:0)
PC (36:1)	TAG (18:1/18:1/16:0)
	TAG (18:1/18:1/18:1)

Table 6.4: Complex lipid changes detected in serum of control, PPARδ agonist and PPARγ agonist treated *ob/ob* mice using UPLC-MS. Lipids identified in the VIP/coefficients plots as significantly contributing to separation in the PCA and PLS-DA models built for the UPLC-MS analysis of the organic metabolite fraction. The control group was compared with the PPARδ agonist and PPARγ agonist treated groups from serum. The TAGs increased in the PPARδ agonist treated mice marked in red are equivalent to those decreased in the PPARγ agonist treated mice marked in blue.

To examine the fate of the increased serum β-hydroxybutyrate produced by the liver through increased fatty acid oxidation following exposure to the PPARδ agonist and investigate the causes for the decrease in glucose in the blood serum of both agonist treated groups, the metabolome of skeletal muscle was examined.

6.4.5. Skeletal Muscle

6.4.5.1 Metabolite changes common to PPARδ and PPARγ activation

Amino acid metabolism was also altered in the skeletal muscle of PPARδ and γ agonist treated mice; concentrations of proline and threonine were increased and alanine and valine concentrations were decreased in treated mice relative to tissue from control animals. Cis-10-heptadecanoic acid, cis-11,14-eicosadienoic acid, myristoleic acid, oleic acid and palmitoleic acid were increased and stearic acid was decreased in the skeletal muscle of the PPARδ and γ agonist treated mice. The ϖ-6 essential fatty acid pathway was also altered with a decrease in linoleic acid and arachidonic acid.

6.4.5.2 Metabolite changes unique to PPARδ activation

In contrast to liver tissue amino acid metabolism, glycolysis and the TCA cycle were profoundly affected in the skeletal muscle of PPARδ agonist treated mice. Increases in the concentration of aspartate and α-glycerophosphoric acid and decreases in arginine, glutamine, glycine, methionine, norvaline, serine, glucose, lactate and succinate were detected (**Figure 6.5**). Fatty acid metabolism was changed in the skeletal muscle of PPARδ agonist treated mice, with an increase in the $-CH_3$, $COCH_2$ and $-(CH_2)_n$ lipid moieties and cis-5,8,11,14,17-eicosapentaenoic acid, elaidic acid and margaric acid. There was a concomitant decrease in palmitic acid. The ϖ-6 essential fatty acid pathway intermediate, dihomo-γ-linolenic acid was also increased.

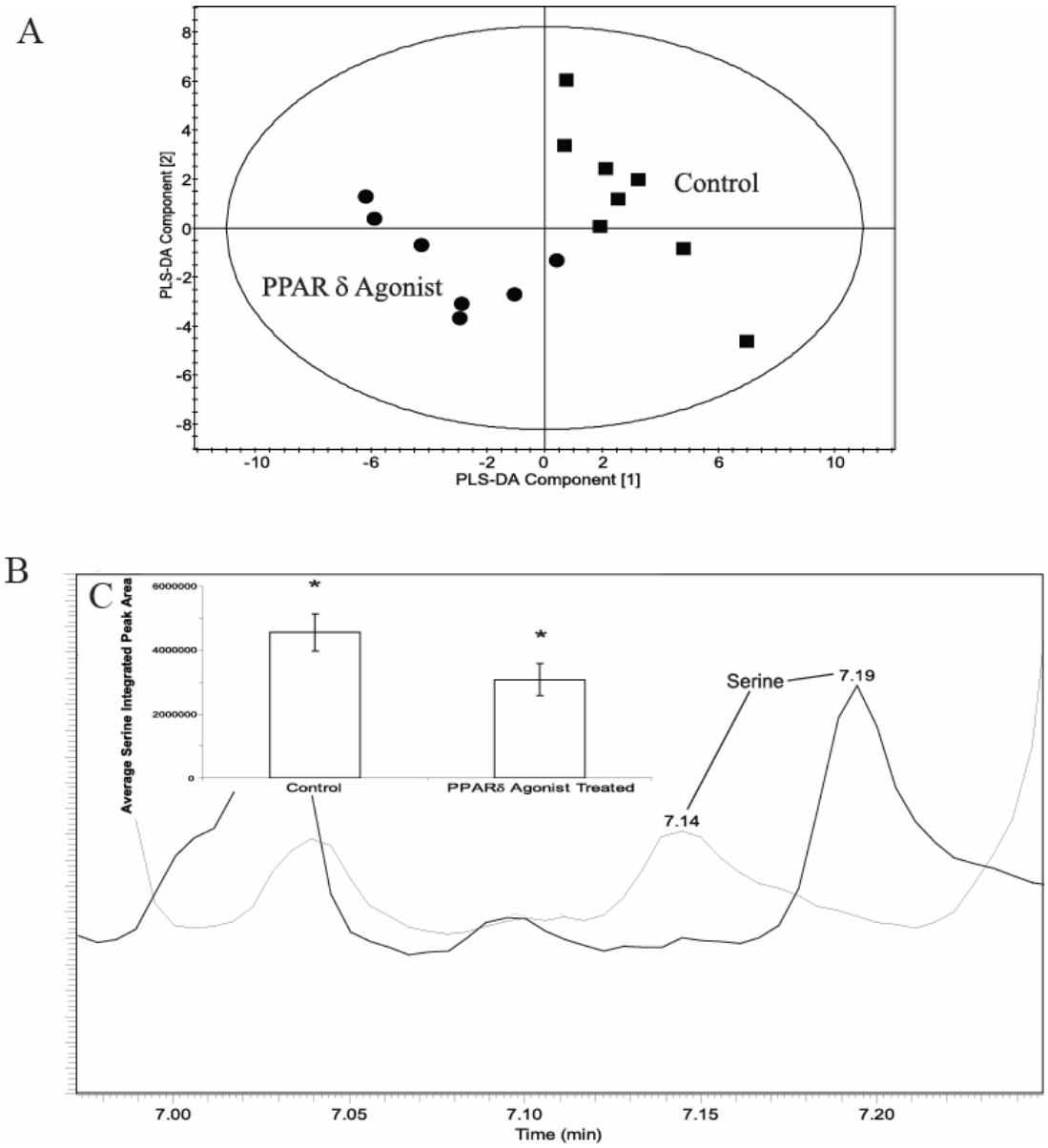

Figure 6.5: **A.** PLS-DA scores plot showing the clustering of the GC-MS chromatograms from the aqueous extracts from skeletal muscle from mice treated with a PPARδ agonist compared with control mice. ●, PPARδ agonist treated. ■, control (R^2=0.69, Q^2=0.73). **B.** Comparison of the region of typical GC-MS chromatograms of control skeletal muscle tissue (black) and skeletal muscle tissue from mice treated with a PPARδ agonist (grey) containing the serine peak. **C.** Bar graph demonstrating the difference in the average integrated area of the Serine peak from control and PPARδ agonist treated liver. Standard error bars are shown. * $P < 0.05$ with respect to vehicle control animals.

6.5 Discussion

A range of complementary metabolic profiling approaches were used to study key tissues involved in type II diabetes from *ob/ob* mice treated with a PPARδ or a PPARγ agonist to understand the role of PPARδ in regulating systemic metabolism with a particular focus on hepatic and skeletal muscle metabolism. In particular we investigated the core components of the Cori cycle to understand the implications altered liver metabolism has on muscle tissue. While similarities were present between the two agonists, and in particular activation of both PPARδ and PPARγ resulted in an increase in the insulin sensitivity and glucose tolerance of the *ob/ob* mice, PPARδ induced a number of unique responses particularly in liver and skeletal muscle. These findings are consistent with the high level of PPARδ protein expression in these tissues[273]. A decrease was detected in glucose and galactose in all tissues, and fructose in serum and liver from PPARδ agonist treated mice; the decrease in glucose in serum was confirmed by clinical chemistry. Concomitantly an increase in lactate was detected in the liver and serum of the treated mice, indicating a decrease in hepatic glucose production which has previously been observed following PPARδ activation[227]. It has been suggested that PPARδ activation increases glyceraldehyde-3-phosphate, formed from the 5-carbon sugar phosphates during the pentose phosphate shunt, which can then enter glycolysis[227], explaining the observed reduction of glucose, galactose and fructose in the serum and skeletal muscle.

During prolonged β-oxidation of fatty acids in the liver the production of acetyl-CoA can exceed the capacity of the TCA cycle. The excess acetyl-CoA is converted to β-hydroxybutyrate through ketogenesis in liver mitochondria. The increased liver and blood serum concentrations of β-hydroxybutyrate indicate the PPARδ agonist stimulates ketone body formation for the peripheral tissue, a change which is also observed by clinical chemistry assays. In addition acetic acid was increased in the treated livers; whilst a decrease in concentrations of non esterified fatty acids in the serum of PPARδ was indicative of increased tissue oxidative breakdown of fatty acids. The concentration

of serum TAGs was increased in PPARδ agonist treated mice, as they are mobilised for catabolism in muscle. These observations are consistent with previous studies showing activation of PPARδ increases fatty acid β-oxidation[274]. Furthermore activation of PPARγ lead to the reverse effect with a decrease in serum TAGs, consistent with this receptor being involved in regulating white adipose tissue storage of TAGs and adipocyte expandability[275]. The glucogenic amino acids (those that are precursors of glucose in gluconeogenesis), glycine, glutamate, glutamine, alanine, proline and valine and the amino acids which are glucogenic and ketogenic, threonine, tyrosine and phenylalanine were increased in the PPARδ agonist treated livers. In contrast the concentration of the ketogenic amino acid (those that are broken down to acetyl-CoA and converted to ketone bodies), lysine was decreased. These changes within the livers of PPARδ agonist treated mice indicate a decrease in gluconeogenesis and an increase in fatty acid oxidation and ketogenesis (**Figure 6.6**).

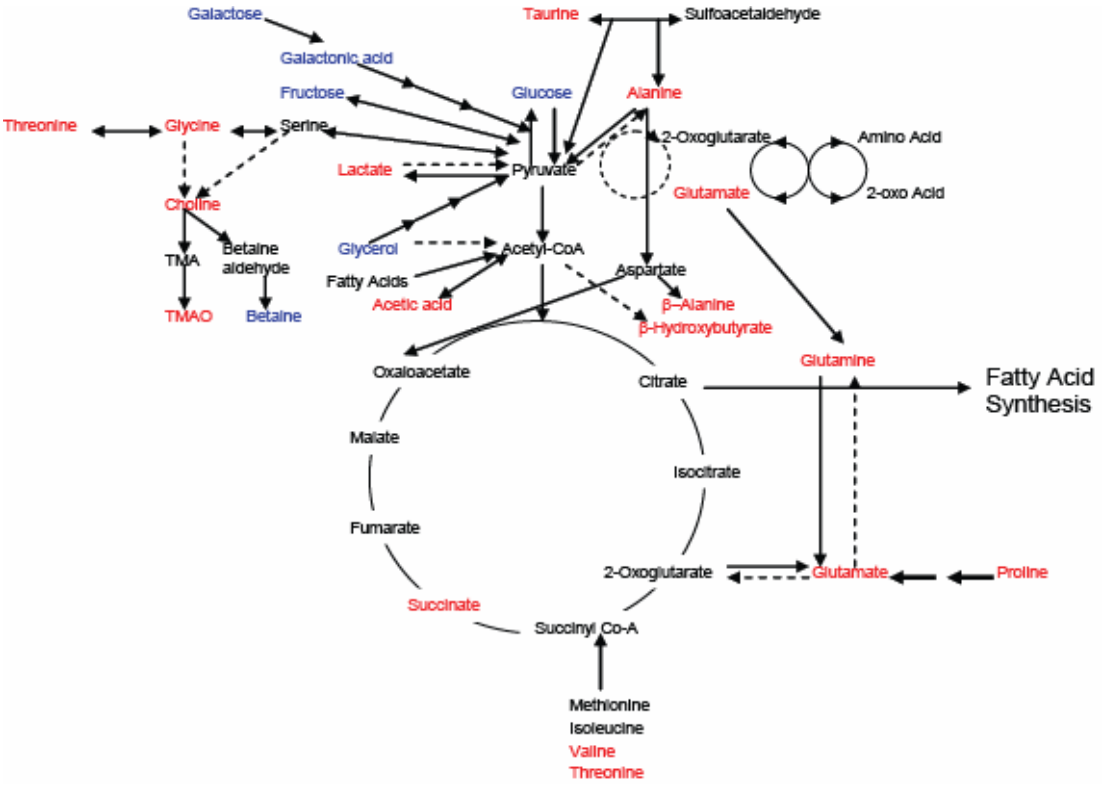

Figure 6.6: Metabolic pathways altered in PPARδ agonist treated liver from *ob/ob* mice. Metabolites increased relative to control tissue are red; metabolites decreased relative to control tissue are blue.

PPARδ agonist treated liver contained decreased linoleate and increased linoleate pathway intermediates, γ-linolenate and dihomo-γ-linolenate, and the pathway end product arachidonate (**Figure 6.7**). The Δ 6-desaturase introduces the initial double bond to linoleate forming γ-linolenate. The Δ 6-desaturase gene contains a PPRE and is known to be under PPARα transcriptional control[223]. From this study the desaturase also appears to be under PPARδ transcriptional control. Whilst it is worth considering that all pharmacological agonists are likely to exhibit some "off target" effects, this study has taken into account the high affinity, specificity and extensive characterisation of GW610742 for PPARδ, even over the highly related PPARα, which make the compound a very selective tool for the activation of the PPARδ nuclear receptor[185]. Van der Veen *et al* demonstrated that a dose of 20 mg/kg/day of GW610742 in mice gave an average plasma concentration of 1μM, given that the specificity of GW610742 for PPARδ is 28 nM compared to 8900 nM for PPARα and >10,000 nM for PPARγ then the dose used in the current study saturates the PPARδ receptor whilst only minimally activating the other PPAR isotypes[185]. Within the skeletal muscle linoleate was also decreased and dihomo-γ-linolenate increased but arachidonate was decreased. However, increased arachidonic acid metabolism is not necessary a contradictory result when PPARδ is activated. The exact balance between the concentrations of these pathways presumably arise from the balance between increased β-oxidation and the actual activity of the synthetic pathway across the different tissues, as well as potential cross-talk between the three different PPARs. Thus, while synthesis of polyunsaturated fatty acids may be increased by PPARδ stimulation, increased β-oxidation will also deplete intermediates, and a new steady state will be achieved.

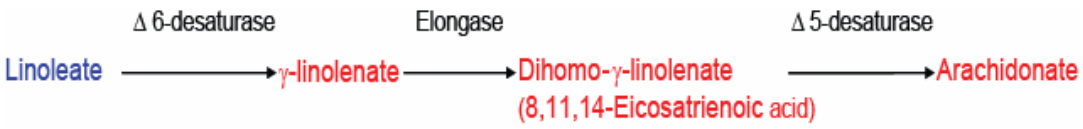

Figure 6.7: Linoleate pathway altered in PPARδ agonist treated liver from *ob/ob* mice. Metabolites increased relative to control tissue are red; metabolites decreased relative to control tissue are blue.

The α-linolenic acid essential fatty acid pathway was also altered in the liver of PPARδ agonist treated mice (**Figure 6.8**). There was a decrease in the initial metabolite in the pathway, α-linolenic acid and a concurrent increase in the pathways product 4,7,10,13,16,19-docosahexaenoic acid. Two steps in the pathway are again catalysed by the Δ 6-desaturase. Also the final step in the pathway, the formation of 4,7,10,13,16,19-docosahexaenoic acid from 6,9,12,15,18,21-C24:6, occurs via β-oxidation, which is upregulated in the livers of PPARδ treated mice. Nevertheless as the intermediates in the pathway were not detected, the exact target of PPARδ cannot be identified unambiguously from this data.

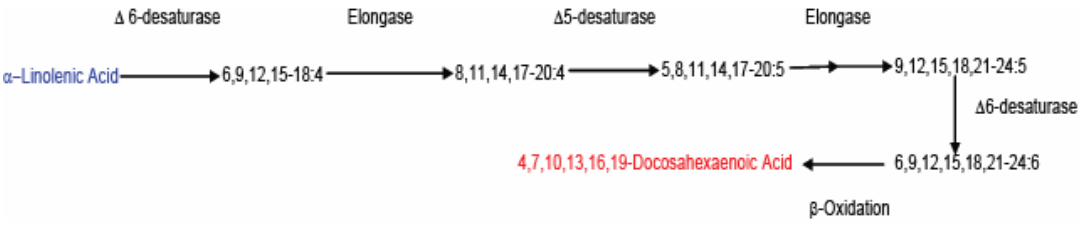

Figure 6.8: Linolenate pathway altered in PPARδ agonist treated liver from *ob/ob* mice. Metabolites increased relative to control tissue are red; metabolites decreased relative to control tissue are blue.

PPARδ mRNA is expressed in skeletal muscle at 10-fold higher levels than PPAR α and 50-fold higher levels compared with PPARγ mRNA[139]. The receptor is preferentially found in oxidative rather than glycolytic myofibers[139]. A major metabolic change exhibited by the PPARδ treated skeletal muscle was a decrease in the concentration of the majority of the observed amino acids (**Figure 6.9**). Since skeletal muscle lacks glucose-6-phosphatase the amino acids will not have been used as substrates in gluconeogenesis. An alternative fate for the amino acids is as substrates for the TCA cycle, which was also affected. The increased demand for TCA cycle substrates was also apparent from the decrease in succinate and concomitant increase in fumarate and malate. Succinate is the substrate for complex II of the electron-transport chain which catalyses the formation of fumarate and reduces coenzyme Q. PPARδ activation increases mitochondrial biogenesis, expression of electron transport chain components such as cytochrome c, cytochrome c oxidase and complex II and induces muscle fibre type switching to type I

fibres[171]. Within the treated skeletal muscle the concentrations of adenine were decreased and those of adenosines and ribose sugars from the adenosines were increased. Therefore, the decrease in amino acids may relate to increased oxidative metabolism occurring in this tissue. In addition we detected an increase in the concentration of creatine and phosphocreatine in muscle tissue which reflects an increase in the high energy phosphate buffering capacity of the cell in addition to the increase in ATP also detected. These changes are accompanied by a decrease in lactate concentration and increased β-oxidation, indicating a reduction in glycolysis and a switch to more oxidative metabolism. PPARδ activation has been implicated as a cause of skeletal muscle atrophy[272]. As demand for amino acids increases one mechanism indicated by our results is that proteins are broken down to supply substrates to the TCA cycle.

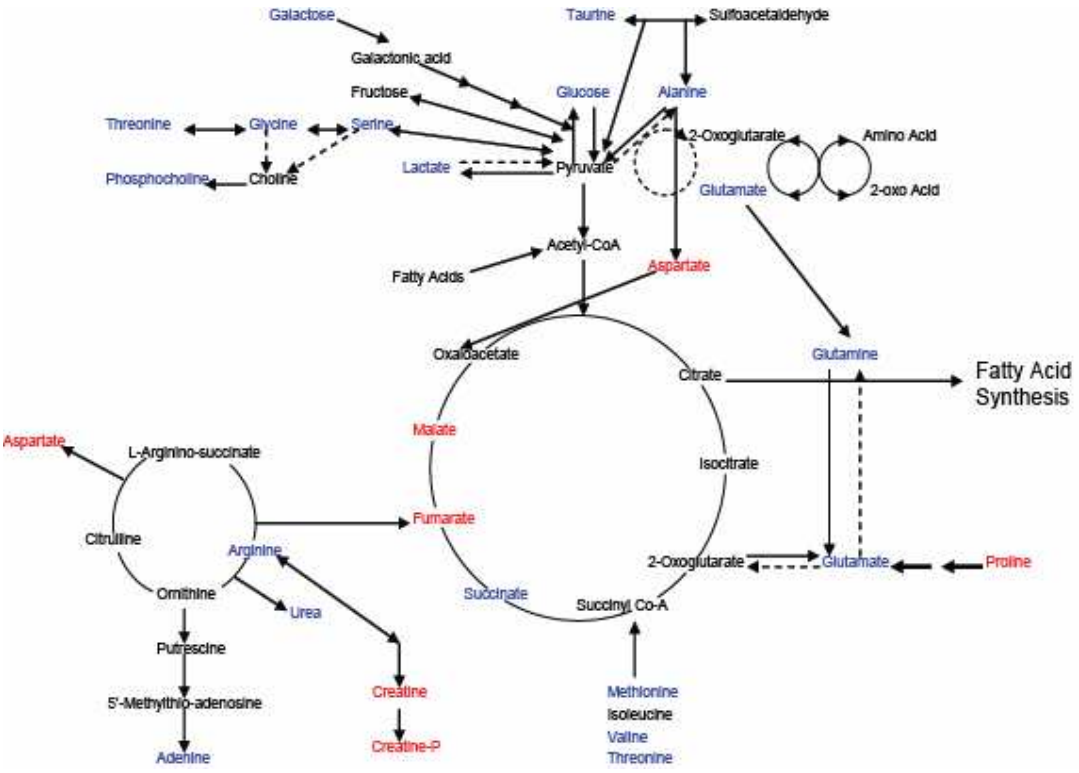

Figure 6.9: Metabolic pathways altered in PPARδ agonist treated skeletal muscle from *ob/ob* mice. Metabolites increased relative to control tissue are red; metabolites decreased relative to control tissue are blue.

PPARδ activation also reduced the degree of saturation of fatty acids in the skeletal muscle of the treated *ob/ob* mice. Palmitate and stearate concentrations were found to be decreased and their monounsaturated forms palmitoleate and oleate concentrations were increased. The enzyme catalysing these reactions, stearoyl-CoA desaturase, is under PPAR expressional control[224].

Activation of PPARδ further improved the dyslipidaemic state in the *ob/ob* mice by increasing the serum HDL cholesterol concentrations. Activation of PPARδ increases the expression of the cholesterol efflux pump ATP-binding cassette transporter1, promoting the efflux of cholesterol from peripheral tissues which may lead to the observed increase in HDL cholesterol[170].

6.6 Conclusions

A global summary of the observed changes leads to the conclusion that PPARδ activation generates a systemic change in energy balance in which the Cori cycle is profoundly affected. A decrease in hepatic glucose production produces an increase in hepatic and circulating lactate concentrations and a drop in circulating blood glucose; hepatic metabolism begins to favour fatty acid β-oxidation and ketogenesis, in order to maintain energy supply to peripheral tissues the ketone bodies are released into circulation. Furthermore glucose is decreased within skeletal muscle alongside increased TCA cycle intermediates but without an observed increase in lactate, correlating with the observed increase in oxidative metabolism. Therefore, the activation of PPARδ produces a marked switch from the Cori cycle to ketone and fatty acid metabolism between the liver and oxidative skeletal muscle which may contribute to the observed improvement in insulin sensitivity.

In conclusion, to understand the global physiological and pharmacological effects of PPARδ activation, which may give rise to further applications for PPARδ agonists, compound treatment studies have been performed on an *ob/ob* mouse background. The combined metabolomic study of liver, skeletal muscle and serum identified multiple changes in metabolism in the PPARδ agonist treated mice. These changes showed that PPARδ activation profoundly affected glycolysis, gluconeogenesis, the TCA cycle and linoleic acid and α-linolenic acid essential fatty acid pathways, many of the changes were found to correlate well with known PPAR controlled gene expression. While some of these metabolic perturbations could be induced by a selective PPARγ agonist, there were also specific changes associated with PPARδ, demonstrating the complexity of the PPAR system and cross-talk between different receptors when considering systemic metabolism.

Chapter 7

Summary and Discussion

7.1 General Discussion

The PPARs are orphan nuclear receptors that function as transcriptional regulators in a ligand dependent manner. They have been implicated in the expressional control of a plethora of genes vital to organogenesis, inflammation, cell differentiation and proliferation. The receptors have also been recognised as master regulators of lipid and carbohydrate metabolism and as such have been identified as targets for the treatment of metabolic diseases and in particular dyslipidaemia, obesity, TIIDM and the metabolic syndrome. Several classes of pharmacological agents currently available in the clinic function through PPAR agonism and include the fibrates, activators of PPARα used to treat dyslipidaemia, and thiazolidinediones, PPARγ agonists employed in the treatment of TIIDM. Thus far a clinically available therapeutic directed at PPARδ has eluded full development and clinical release despite implications that the receptor has potential as a treatment for obesity, TIIDM and the associated metabolic syndrome. In spite of their potential and widespread use as medication the mechanisms by which PPAR agonists can alleviate metabolic perturbations and bring about normalisation remain to be fully defined. Both PPARδ and PPARγ are crucially implicated in the regulation of metabolism within white adipose tissue; consequently it was the aim of this thesis to use a metabolomics approach to investigate and define the metabolic effects of PPARδ and PPARγ activation in both *in vivo* adipose tissue and in an *in vitro* model of adipose tissue.

To generate a metabolically phenotyped *in vitro* model of adipocyte differentiation and metabolism the metabolic changes occurring during differentiation of 3T3-L1 preadipocytes as they develop into mature adipocytes was defined using a multiplatform metabolomic and ^{13}C-isotope substrate labelling technique. The metabolic changes identified were then compared and contrasted to the metabolic differences between pre- and post-differentiation primary adipocytes. Distinct periods in the differentiation process could be defined by changes in metabolite concentrations. Alterations in metabolism, affecting a range of pathways, were ascertained to occur during adipocyte differentiation. Affected pathways included the TCA cycle, glycolysis, the production of odd chain fatty acids by α-oxidation, fatty acid synthesis, fatty acid desaturation, polyamine biosynthesis and trans-esterification to produce complex lipids. Moreover the usage of glucose in the generation of fatty acids during 3T3-L1 metabolism was confirmed utilising ^{13}C-labelled glucose to monitor the metabolic flux through glycolysis, the TCA cycle and into fatty acid synthesis. It was shown that upon synthesis, the fatty acids are subjected to desaturation by the Δ-9 desaturase or to α-oxidation, forming odd chain fatty acids as was confirmed through the use of U-^{13}C-labelled palmitate. Although the 3T3-L1 cell line is a widely utilised tool for the investigation of adipocyte biology it was found that, as with all immortalised cell lines, they do not behave identically to their primary cell line counterparts. Nevertheless, the modifications in metabolism discovered between primary preadipocytes and primary differentiated adipocytes equated to many of the findings observed in the 3T3-L1 adipocytes. Therefore it is hoped that alongside metabolically phenotyping an adipocyte model for use in the investigation of tissue specific PPARδ and PPARγ activation, the work conducted in this thesis will provide invaluable information for research conducted in the 3T3-L1 cell line, primary cell lines and even white adipose tissue when following the changes in metabolism associated with differentiation.

To evaluate and characterise the systemic and tissue specific metabolic effects of PPARδ activation in adipose tissue, a multifaceted metabolomic method was used to examine the effects of PPARδ activation, using a high affinity pharmacological agonist, in white adipose tissue from the *ob/ob* mouse model of insulin resistance, and the 3T3-L1

adipocyte cell line within a cell culture system, generating an *in vivo* and an *in vitro* model of adipose tissue specific PPARδ activation. In addition, to unambiguously define the mechanisms by which PPARδ alters the metabolism of adipose tissue, ^{13}C-stable isotope substrate labelling studies using 1-^{13}C-glucose and U-^{13}C-palmitate, respirometric analysis using a Clark-type oxygen electrode and transcriptomic microarray analysis were performed on PPARδ agonist treated 3T3-L1 adipocytes. In summary, possible metabolic mechanisms by which PPARδ activation actualises its observed anti-diabetic and anti-obesity effects were identified; activation of the nuclear receptor decreases fatty acid synthesis and fat storage within synthesised TAG depots and concomitantly mobilises complex lipid fatty acid stores. Mobilisation of the TAG lipid energy stores was found to be accompanied by upregulation of not only fatty acid oxidation but also by carbohydrate oxidative metabolism in the white adipose tissue, a tissue not conventionally thought of as being energetic or oxidative. Fundamental to this process is the consolidation and systematisation of the energy metabolism pathways, which PPARδ was identified as accomplishing by upregulating the transcription of a series of genes involved in glycolysis, the TCA cycle, the electron transport chain and fatty acyl β-oxidation. PPARδ activation in white adipose tissue was found to neither bring about exclusive stimulation of either fatty acid oxidation or carbohydrate oxidation but rather global oxidative metabolism; simultaneously reducing the quantity of TAGs and glucose in white adipose tissue. Therefore, despite the absence of PPARδ agonists in the clinic, the nuclear receptor may still prove a powerful target for the treatment of the metabolic syndrome.

It was an additional aim of this thesis to identify the potential metabolic effects of PPARγ activation in adipose tissue that may be contributing to the nuclear receptor's anti-diabetic potential. Consequently a metabolomics study of PPARγ activation both *in vivo* in the *ob/ob* mouse, to determine the systemic effect of PPARγ activation on adipose tissue, and *in vitro* using the murine 3T3-L1 adipocyte cell line, to independently establish adipose tissue specific activation of the nuclear receptor, was conducted. To delineate the metabolic changes established as associated with PPARγ activation in the

metabolomic analysis and to explicitly define the pathways by which activation of the ligand binding transcription factor influences the metabolism of adipose tissue, mechanistic analyses were performed using ^{13}C-stable isotope substrate labelling, employing 1-^{13}C-glucose and U-^{13}C-palmitate, and transcriptomic microarray analysis. Investigations led to the discovery that activation of the nuclear receptor in adipocytes leads to an upregulation of glycolysis and catabolism of other carbohydrate species. Correspondingly activity of the TCA cycle is decreased, an effect especially obvious in the later oxidative stages of the cycle as they are downregulated in preference of fatty acid synthesis from the early TCA cycle substrates. In addition to de novo fatty acid synthesis, cellular FFA uptake is increased; propagating a pool of longer chain fatty acids which are integrated into TAGs or desaturated and incorporated into TAG's. Preservation of the complex lipid pool is subsequently achieved via an inhibition of lipolysis. Concurrently the breakdown of fatty acids via β-oxidation is reduced. Furthermore, PPARγ activation was implicated in the augmentation of calcium cellular signalling. The calcium signalling pathway is associated with insulin signalling and its downstream metabolic effectors; identifying a potential accessory mechanism for PPARγ activation mediated normalisation of blood glucose and dyslipidaemia in both human patients and murine subjects with the metabolic syndrome and TIIDM. However, it was also discovered that PPARγ activation increases activity of the polyol pathway in 3T3-L1 adipocytes; a pathway in which increased flux has been associated with the development of diabetic complications. This finding casts a shadow over the use of thiazolidinediones and other PPARγ agonists in the clinic for the treatment of diabetes and the metabolic syndrome. Nevertheless, the observed sequestration of glucose and lipid into the white adipose tissue, as a safely contained storage depot, was described as a possible mechanism by which PPARγ activation reduces the damaging potential of increased levels of circulating glucose and lipid, whilst simultaneously reducing lipid and cholesterol accumulation in peripheral tissues; demonstrating a means by which PPARγ activation may initiate insulin sensitisation, not only in the white adipose tissue but also in the peripheral tissue. This thesis has proposed that through the dual mechanisms of augmenting facets of the calcium signalling pathway associated with insulin action and

direct transcriptional regulation of metabolic enzymes PPARγ activation brings about metabolic changes that function to reinforce insulin sensitisation.

Further to these aims, this thesis was intended to use a metabolomics approach to investigate and characterise the systemic physiological effects of PPARδ and PPARγ activation by definition of the hepatic and peripheral metabolic changes that occur in the *ob/ob* mouse following activation of the nuclear receptors. Consistent with many of the results from the studies of PPAR activation in adipocytes conducted in this thesis, a number of key metabolic pathways in liver and skeletal muscle were identified as affected by PPARδ agonism including glycolysis, gluconeogenesis, the TCA cycle and linoleic acid and α-linolenic acid essential fatty acid pathways. Moreover, through systemic analysis, it was discovered that PPARδ activation generates a system wide change in energy balance, profoundly impacting on the Cori cycle. Decreased hepatic gluconeogenesis was found to cause an increase in the concentration of hepatic and circulating lactate and a concomitant reduction in circulating blood glucose; to sustain energy balance hepatic metabolism switched to favour fatty acid β-oxidation and ketogenesis, the ketones were then released into circulation as a source of energy for the peripheral tissues. Furthermore the concentration of glucose within skeletal muscle was found to decrease upon PPARδ activation. Coinciding with this observation was a detected increase in TCA cycle intermediates, correlating with the increase in oxidative metabolism. It was concluded that the activation of PPARδ produced a significant modification in energy metabolism from the Cori cycle to ketone and fatty acid metabolism between the liver and oxidative skeletal muscle. Whilst some of these metabolic perturbations were also found to be induced by PPARγ activation and both activation of PPARδ and PPARγ lead to increased insulin sensitivity and glucose tolerance, activation of both nuclear receptors were identified as functionally distinct. Characterisation of PPARδ activation demonstrated the specific catabolic role of this receptor relative to PPARγ.

7.2 Future Directions

The research described in this thesis could be expanded upon using various experimental approaches to further the characterisation and understanding of the physiological role played by the PPARs in the control of metabolism and consequentially to assess their potential as a therapeutic target for the treatment of a myriad of metabolic diseases including TIIDM, dyslipidaemia and the metabolic syndrome. One such approach would be the development of additional tissue specific models of PPAR activation using cell lines, or even primary cells, derived from alternative metabolic tissues such as skeletal muscle, hepatic and cardiac tissue to complement that of the 3T3-L1 adipocytes studied in **Chapter 4** and **Chapter 5** of this thesis and to expand upon the observations made regarding systemic metabolism in **Chapter 6** of this thesis. Although there are a number of robust cell lines available for the study of hepatocytes and skeletal and cardiac myocytes, it is worthy of note that, as with all immortalised cell lines, they do not behave identically to their primary cell line or *in vivo* counterparts. Extensively used skeletal muscle cell lines include the rat L6 and mouse C2C12 cell lines that are easy to cultivate and can be induced to differentiate forming multinucleated myotubes in culture dishes. However, the differentiation of these cells is halted and they fail to recapitulate their contractile function, or generate different fibre types[276]. The Huh-7 and HepG2 cell lines have been widely employed for hepatocyte research, nevertheless these cells are derived from neoplastic tissues and are therefore de-differentiated from mature hepatocytes. To surmount the disadvantages in the hepatocyte cell lines available primary human hepatocytes have also been utilised in the study of liver functions. Even so primary hepatocytes can suffer from a rarity of supply, lack of homogeneity, mortality and intransigency to growth in culture[277]. Human hepatocyte lines have recently been developed that now retain a primary hepatocyte phenotype and may prove valuable for research into the metabolic processes that occur in the liver[278]. Immortalised cardiomyocyte cell lines capable of proliferation in culture include the AT-1[279] and MC29[280] cell lines. Alternative methods have been employed to generate cardiomyocyte cell lines including harvesting cells from transgenic mice expressing SV40 T-ag[281] and

transformation of foetal cardiomyocytes with the SV40 oncogene[282]. Again, these cell lines suffer from similar deficiencies the most common being a limited capacity to be passaged, de-differentiating in long term culture and deviation from a typical cardiomyocyte phenotype. To circumvent these inadequacies, a mouse atrial cardiomyocyte cell line, HL-1 a derivative of the AT-1 line, has been developed which maintains the phenotype of adult mouse atrial cardiomyocytes whilst obtaining the capacity for serial passage[283]. Through the use of a selection of these cell lines and the application of metabolomic techniques employed in combination with ^{13}C stable isotope substrate labelling, respirometry and transcriptomics, as detailed in **Chapter 4** and **Chapter 5** of this thesis, several tissue specific metabolic models of PPAR activation could be generated and studied.

To further define the physiological role of PPAR activation metabolomic investigations of *in vivo* models of tissue specific PPAR activation and ablation would be a pertinent approach. Although PPARδ knockout mice are viable they suffer from several developmental defects and homeostatic perturbations including placental abnormalities generating embryonic lethality, myelination defects, unusual skin inflammatory responses and reduced adipose tissue mass[284,285]. In addition, tissue dependent metabolic effects are convoluted due to systemic changes. However, tissue specific animal models of PPAR overexpression, activation and ablation have been developed. Rodent models of overexpression of PPARδ in both adipose tissue, under the control of the enhancer-promoter region of the adipocyte fatty acid binding protein (aP2) gene[169], and in skeletal muscle[171] have been developed to investigate the role that the nuclear receptor plays in these tissues.

To elaborate on future research possibilities, an approach whereby the exact points of PPAR directed control in metabolic pathways can be identified is provided by the RNAi techniques. Following on from the identification of pathways affected by PPAR activation in adipocytes, as outlined in this thesis, RNAi could be used to perturb the system and test potential PPAR control points in pathways highlighted by the metabolomic and transcriptomic analysis conducted in **Chapter 4** and **Chapter 5**. RNAi

provides a versatile tool, allowing knock-down of gene transcripts as opposed to knock-out and high selectivity when compared to a variety of metabolic inhibitors. The RNAi analysis could also be expanded to investigate PPAR control of metabolism in additional tissue specific cell lines as previously discussed.

The research conducted in **Chapter 3**, **Chapter 4** and **Chapter 5** of this thesis demonstrated the potential of ^{13}C labelled substrate studies to characterise the effect of PPAR activation on the spatio-temporal flux of metabolites through metabolic pathway networks. In addition to the investigation of glycolysis, the TCA cycle, fatty acid β-oxidation and fatty acid synthesis reported, the potential remains to investigate other metabolic pathways identified as affected by PPAR activation; a pertinent example would be to establish the fate of amino acids as likely substrates for the TCA cycle using myocytes incubated with ^{13}C-labelled amino acids, this would substantiate speculation made in **Chapter 6** regarding PPARδ activation in skeletal muscle.

Finally, an extra dimension of metabolomic analysis could be achieved through LC-MS profiling of the polar, aqueous soluble metabolites to further define PPAR activation in adipose tissue culture and animal studies. LC-MS conducted within this thesis has focussed on the more established lipidomic analysis. However, studies of the polar metabolites using LC-MS are becoming more widespread within metabolomics with the technique under continual development[286]. Currently many of the methods are targeted to biofluids, with the analysis of blood and urine most common[287]. Although advances are being made in the analysis of tissue extracts[288], the use of LC-MS investigation of polar metabolites would be advantageous in enlarging the coverage of the metabolome.

7.3 Conclusions

The research conducted within this thesis emphasises the benefit of combining omic methods with mechanistic studies to further characterise metabolic changes observed within metabolomic experiments. Moreover a multi-omic approach has been exploited, increasing the coverage of the strata defined by the central biochemical and molecular biological dogma to constitute a biological network; in doing so, the complex interactions between metabolites and genes can be further characterised, improving our understanding of the systems properties of biological networks and their perturbation.

In conclusion, through the use of a multi-platform metabolomic technique, employed in conjunction with transcriptomic, metabolite flux and respirometric techniques, the metabolic influence of both PPARδ and PPARγ in adipose tissue has been further defined. Although the metabolic effects of both PPARδ and PPARγ activation were indicative of an effective therapeutic target for the treatment of the metabolic syndrome, improving insulin sensitisation and glucose tolerance, the metabolic mechanisms initiated by receptor activation profoundly deviated. PPARδ activation was distinguished by oxidative catabolism of metabolites identified as potentially deleterious in the diabetic state. Conversely, PPARγ activation was identified by the sequestration of the same metabolites into safe storage depots. The role of the PPARs as master regulators of metabolism has been accentuated and their latent capacity as targets for the treatment of metabolic diseases of global consequence inferred.

References

[1] Hollywood, K., Brison, D.R., and Goodacre, R. (2006) Metabolomics: Current technologies and future trends. *Proteomics* **6**, 4716-23.

[2] Godovac-Zimmermann, J., and Brown, L.R. (2001) Perspectives for mass spectrometry and functional proteomics, *Mass Spectrom. Rev.* **20**, 1–57.

[3] Panisko, E.A., Conrads, T.P., Goshe, M.B., and Veenstra, T.B. (2002) The postgenomic age: characterization of proteomes, *Exp Hematol* **30**, 97–107

[4] Oliver, S.G. Winson, M.K. Kell, D.B. Baganz, F. (1998) Systematic functional analysis of the yeast genome. *Trends Biotechnol.* **16**, 373-378

[5] Nicholson, J.K. Lindon, J.C. Holmes, E. (1998) 'Metabonomics': understanding the metabolic responses of living systems to pathophysiological stimuli via multivariate statistical analysis of biological NMR spectroscopic data. *Xenobiotica*. **29**, 1181-1189

[6] Lindon, J.C. Holmes, E. Nicholson, J.K. (2003) So what's the deal with metabonomics? **75**, 384A-391A

[7] Griffin, J.L., Nicholls, A.W., Keun, H.C., Mortishire-Smith, R.J., Nicholson, J.K., and Kuehn, T. (2002) Metabolic profiling of rodent biological fluids via 1H NMR spectroscopy using a 1 mm microlitre probe. *Analyst*. **127**, 582-584.

[8] Goodacre, R. (2003) Metabolic Profiling: Its role in Biomarker Discovery and Gene Function Analysis, *Kluwer Academic Publishers, London*.

[9] Goodacre, R., Vaidyanathan, S., Dunn, W.B., Harrigan, G.G. and Kell D.B. (2004) Metabolomics by numbers: acquiring and understanding global metabolite data. *Trends Biotechnol.* **22**, 245-252.

[10] Forster, J., Famili, I., Fu, P., Palsson, B.O., and Nielsen , J. (2003) Genome-scale reconstruction of the Saccharomyces cerevisiae metabolic network. **13**, 244-253.

[11] Fiehn, O. (2001) Combining genomics, metabolome analysis, and biochemical modelling to understand metabolic networks. *Comp. Funct. Genomics*. **2**, 155-168.

[12] Atherton, H.J. Bailey, N.J. Zhang, W. Taylor, J. Major, H. Shockcor, J. Clarke, K. and Griffin, J.L. (2006) A combined ^{1}H-NMR spectroscopy- and mass spectrometry-based metabolomic study of the PPAR-α null mutant mouse defines profound systemic changes in metabolism linked to the metabolic syndrome. *Physiol Genomics*. **27**, 178-186.

[13] Spencer, F., Lagarde, M., Geloen, A., Record, M. What is lipi- domics? (2003) *Eur. J. Lipid Sci. Technol.* **105** 481-482.

[14] Hu, C., van der Heijden, R., Wang, M., van der Greef, J., Hankemeier, T., Xu, G. (2009) Analytical strategies in lipidomics and applications in disease biomarker discovery. *J. Chromatogr. B Analyt. Technol. Biomed. Life Sci*. **877**, 2836-46.

[15] Roberts, L.D., McCombie, G., Titman, C.M., Griffin, J.L. (2008) A matter of fat: an introduction to lipidomic profiling methods. **871**, 174-81.

[16] Jia, L., Wang, C., Zhao, S., Lu, X., Xu, G. (2007) Metabolomic identification of potential phospholipid biomarkers for chronic glomerulonephritis by using high performance liquid chromatography-mass spectrometry. J. Chromatogr. B. **860**, 134-40.

[17] Hillery, C.A., Du, M.C., Montgomery, R.R. and Scott, J.P. (1996) Increased adhesion of erythrocytes to components of the extracellular matrix: isolation and characterization of a red blood cell lipid that binds thrombospondin and laminin. *Blood.* **87**, 4879-4886.

[18] Virella, G., Derrick, M.B., Pate, V., Chassereau, C., Thorpe, S.R. and Lopes-Virella, M.F.. (2005) Development of capture assays for different modifications of human Low-Density Lipoprotein. Clinical and Diagnostic Laboratory Immunology. **12**, 68-75.

[19] Pagano, R.E., Puri, V., Dominguez, M., and Marks, D.L. (2000) Membrane traffic in sphingolipid storage diseases. Traffic. **1**, 807-815.

[20] Kraegen, E.W., Cooney, G.J., Ye, J.E., Thompson, A.L., Furler, S.M. (2001) The role of lipids in the pathogenesis of muscle insulin resistance and beta cell failure in type II diabetes and obesity. Exp Clin Endocrinol Diabetes. **109**, 189-201.

References

[21] Ma, Q.L., Teter, B., Ubeda, O.J., Morihara, T., Dhoot, D., Nyby, M.D., Tuck, M.L., Frautschy, S.A., Cole, G.M. (2007) Omega-3 fatty acid docosahexaenoic acid increases sorLA/LR11, a sorting protein with reduced expression in sporadic Alzheimer's disease (AD): Relevance to AD prevention. *J. Neuroscience.* **27**, 14299-14307.

[22] Wenk, M.R. (2005) The emerging field of lipidomics Nat. Rev. Drug Discov. **4**, 594-610.

[23] Griffin, J.L., Cemal, C.K., Pook, M.A. (2004) Defining a metabolic phenotype in the brain of a transgenic mouse model of spinocerebellar ataxia 3. *Physiol. Genomics*. **16**, 334-340.

[24] Han, X., Holtzman, D,M., McKeel Jr, D.W., Kelley, J., Morris, J.C. (2002) Substantial sulfatide deficiency and ceramide elevation in very early Alzheimer's disease: Potential role in disease pathogenesis, *J. Neurochem*. **82**, 809-818.

[25] Odunsi, K., Wollman, R.M., Ambrosone, C.B., Hutson, A., McCann, S.E., Tammela, J., Geisler, J.P., Miller, G., Sellers, T., Cliby, W., Qian, F., Keitz, B., Intengan, M., Lele, S., Alderfer, J.L. (2005) Detcetion of epithelial ovarian cancer using 1H-NMR-based metabonomics. **113**, 782-8.

[26] Giffiths, J.R., McSheehy, P.M., Robinson, S.P., Troy, H., Chung, Y.L., Leek, R.D., Williams, K.J., Stratford, I.J., Harris A.L., Stubbs, M. (2002) Metabolic changes detected by in vivo magnetic resonance studies of HEPA-1 wild-type tumours deficient in hypoxis-inducible factor-1 beta(HIF-1beta) evidence of an anabolic role for the HIF-1 pathway. **62**, 688-95.

[27] Oursel, D., Loutelier-Bourhis, C., Orange, N., Chevalier, S., Norris, V., and Lange, C.M. (2007) Identification and relative quantification of fatty acids in Escherichia coli membranes by gas chromatography/mass spectrometry. *Rapid Commun. Mass Spectrom.* **21**, 3229-3233.

[28] Wakelam, M.J., Pettitt, T.R., Postle, A.D. (2007) Lipidomic analysis of signaling pathways. *Methods Enzymol.* **432**, 233-46.

[29] Festa, A. Williams, K., Hanley, A.J., Otvos, J.D., Goff, D.C., Wagenknecht, L.E., and Haffner, S.M. (2005) Nuclear magnetic resonance lipoprotein abnormalities in prediabetic subjects in the Insulin Resistance Atherosclerosis Study. *Circulation*. **111**, 3465-3472.

[30] Sabatine, M.S., Liu, E., Morrow, D.A., Heller, E., McCarroll, R., Wiegand, R., Berriz, G.F., Roth, F.P., Gerszten, R.E. (2005) Metabolomic identification of novel biomarkers of myocardial ischemia, *Circulation.* **112**, 3868–3875.

[31] Brindle, J.T., Nicholson, J.K., Schofield, P.M., Grainger, D.J., and Holmes, E. (2003) Application of chemometrics to 1H NMR spectroscopic data to investigate a relationship between human serum metabolic profiles and hypertension. *Analyst*. **128**, 32-36.

[32] Salek, R.M., Maguire, M.L., Bentley, E., Rubtsov, D.V., Hough, T., Cheeseman, M., Nunez,D., Sweatman, B.C., Haselden, J.N., Cox, R.D., Connor, S.C., Griffin, J.L. (2007) A metabolomic comparison of urinary changes in type 2 diabetes in mouse, rat, and human (2007) *Physiol. Genomics*. **29**, 99-108.

[33] Han, X. and Gross, R.W. (2003) Global analyses of cellular lipidomes directly from crude extracts of biological samples by ESI mass spectrometry: a bridge to lipidomics. *J. Lipid. Res.* **44**, 1071-1079.

[34] Morris, M., and Watkins, S.M. (2005) Focused metabolomic profiling in the drug development process: advances from lipid profiling. *Curr. Opin. Chem. Biol.* **9**, 407-412.

[35] Yetukuri, L., Katajamaa, M., Medina-Gomez, G., Seppanen-Laakso, T., Vidal-Puig, A., and Oresic, M. (2007) Bioinformatics strategies for lipidomics analysis: characterization of obesity related hepatic steatosis. BMC Syst. Biol. **1**, 12.

[36] Pietilainen, K.H., Sysi-Aho, M., Rissanen, A., Seppanen-Laakso, T., Yki-Jarvinen, H., Kaprio, J., and Oresic, M. (2007) Acquired obesity is associated with changes in the serum lipidomic profile independent of genetic effects - a monozygotic twin study. *PLoS ONE* **2**, e218.

[37] Pruzanski, W., Stefanski, E., de Beer, F.C., de Beer, M.C., Ravandi, A., and Kuksis, A. (2000) *J. Lipid Res.* **41**, 1035-1047.

[38] Wang, C., Kong, H., Guan, Y., Yang, J., Gu, J., Yang, S., Xu, G. (2005) Plasma phospholipid metabolic profiling and biomarkers of type 2 diabetes mellitus based on high-performance liquid chromatography/electrospray mass spectrometry and multivariate statistical analysis. *Anal. Chem*. **77**, 4108-16.

[39] Raamsdonk, L.M., Teusink, B., Broadhurst, D., Zhang, N., Hayes, A., Walsh, M.C., Berden, J.A., Brindle, K.M., Kell, D.B., Rowland, J.J., Westerhoff, H.V., van Dam, K., Oliver, S.G. (2001) A functional genomics strategy that uses metabolome data to reveal the phenotype of silent mutations. *Nat. Biotechnol.* **19**, 45-50.

[40] Allen, J., Davey, H.M., Broadhurst, D., Heald, J.K., Rowland, J.J, Oliver, S.G. and Kell, D.B. (2003) High-throughput classification of yeast mutants for functional genomics using metabolic footprinting. *Nat. Biotechnol.* **21**, 692-696.
[41] Fiehn, O., Kopka, J., Dormann, P., Altmann, T., Trethewey, R.N., and Willmitzer, L. (2000) Metabolite profiling for plant functional genomics. *Nat. Biotech.* **18**, 1157-1161.
[42] Roberts, L.D., Virtue, S., Vidal-Puig, A.J., Nicholls, A.W., Griffin, J.L. (2009) Metabolic phenotyping of a model of adipocyte differentiation. *Physiol. Genomics*. **39**, 109-19.
[43] Jones, G.L., Sang E., Goddard, C., Mortishire-Smith, R.J., Sweatman, B.C., Haselden, J.N., Davies, K., Grace, A.A., Clarke, K., Griffin, J.L. (2005) A functional analysis of mouse models of cardiac disease through metabolic profiling. *J. Biol. Chem.* **280**, 7530-9.
[44] Kim, H., Choi, Y.H., Erkelens, C., Lefeber, A.W., Verpoorte, R. (2005) Metabolic fingerprinting of Ephedra species using 1H-NMR spectroscopy and principal componet analyis. *Chem. Pharm. Bull.* **53**, 105-109.
[45] Smedsgaard, J., Nielsen, J. (2005) Metabolit profiling of fungi and yeast: from phenotype to metabolome by MS and informatics. *J. Exp. Bot.* **56**, 273-286.
[46] Bundy, J.G, Willey, T.L., Castell, R.S., Ellar, D., Brindle K.M. (2005) Discrimination of pathogenic clinical isolates and laboratory strains of Bacillus cereus by NMR-based metabolomic profiling. *FEMS Microbiol. Lett.* **242**, 127-136.
[47] Nicholls, A.W., Nicholson, J.K., Haselden, J.K., and Waterfield. C.J. (2000) A metabonomic approach to the investigation of drug-induced phospholipidosis: An NMR spectroscopy and pattern recognition study. *Biomarkers*. **5**, 410-423.
[48] Nicholls, A.W. , Holmes, E., Lindon, J.C., Shockor, J.P., Farrant, R.D., Hasleden, J.N., Damment, S.J., Waterfield, C.J., and Nicholson, J.K. (2001) Metabonomic investigations into hydrazine toxicity in the rat. *Chem. Res. Toxicol.* **14**, 975-987.
[49] Gartland, K.P., Bonner, F.W., and Nicholson, J.K. (1989) Investigations into the biochemical effects of region-specific nephrotoxins. *Mol, Pharmacol.* **35**, 242-250.
[50] Anthony, M.L., Gartland, K.P., Beddell, C.R., Lindon, J.C., and Nicholson, J.K. (1994) Studies of the biochemical toxicology of uranyl nitrate in the rat. *Arch. Toxicol.* **68**, 43-53.
[51] Beckonert, O., Bollard, M.E., Ebbels, T.M.D., Keun, H.C., Antti, H., Holmes, E., Lindon, J.C., Nicholson, J.K. (2003) NMR-based metabonomic toxicity classification: hierarchical cluster analysis and k-nearest-neighbour approaches. *Anal. Chim. Acta.* **490**, 3-15.
[52] Griffin, J.L., Bonney, S.A., Mann, C., Hebbachi, A.M., Gibbons, G.F., Nicholson, J.K., Shoulders, C.C., and Scott, J. (2004) An integrated reverse functional genomic and metabolomic approach to understanding orotic acid induced fatty liver. *Physiol. Genom.* **17**, 140-149.
[53] Clish, C.B., , Davidov, E., Oresic, M., Plasterer, T.N., Lavine, G., Londo, T., Meys, M., Snell, P., Stochaj, W., Adourian, A., Zhang, X., Morel, N., Neumann, E., Verheij, E., Vogels, J.T.W.E., Havekes, L.M., Afeyan, N., Regnier, F., Van Der Greef, J., Naylor, S. (2004) Integrative biological analysis of the APOE*3-leiden transgenic mouse. *Omics*. **8**, 3-15.
[54] Mayr, M., Yusuf, S., Weir, G., ,Chung, Y., Mayr, U., X. Yin, Ladroue, C. Madhu, B., Roberts, N., De Souza, A., Fredericks, S., Stubbs, M. Griffiths, J.R., Jahangiri, M., Xu Q.,and Camm, A.J. (2008) Combined metabolomic and proteomic analysis of human atrial fibrillation, *J. Am. Coll. Cardiol.* **51**, 585–594.
[55] Samani, N.J., Erdmann J., Hall A.S., Hengstenberg, C., Mangino, M., Mayer, B., Dixon, R.J., Meitinger, T., Braund, P., Wichmann, H., Barrett, J.H., König, I.R., Stevens, S.E., Szymczak, S., Tregouet, D-A., Iles, M.M., Pahlke, F., Pollard, H., Lieb, W., Cambien, F., Fischer, M., Ouwehand, W., Blankenberg, S., Balmforth, A.J., Baessler, A., Ball, S.G., Strom, T.M., Brænne, I., Gieger, C., Deloukas, P., Tobin, M.D., Ziegler, A., Thompson, J.R., Schunkert, H. (2007) Genomewide association analysis of coronary artery disease. *N. Engl. J. Med.* **357**, 443–453.
[56] McPherson, R., Pertsemlidis, A., Kavaslar, N., Stewart, A., Roberts, R., Cox, D.R., Hinds, D.A., Pennacchio, L.A., Tybjaerg-Hansen, A., Folsom, A.R., Boerwinkle, E., Hobbs, H.H., Cohen, J.C. (2007) A common allele on chromosome 9 associated with coronary heart disease. *Science.* **316**, 1488–1491.
[57] Helgadottir, A., Thorleifsson, G., Manolescu, A., Gretarsdottir, S., Blondal, T., Jonasdottir, A., Jonasdottir, A., Sigurdsson, A., Baker, A., Palsson, A., Masson, G., Gudbjartsson, D.F., Magnusson, K.P., Andersen, K., Levey, A.I., Backman, V.M., Matthiasdottir, S., Jonsdottir, T., Palsson, S., Einarsdottir, H.,

Gunnarsdottir, S., Gylfason, A., Vaccarino, V., Hooper, W.C., Reilly, M.P., Granger, C.B., Austin, H., Rader, D.J., Shah, S.H., Quyyumi, A.A., Gulcher, J.R., Thorgeirsson, G., Thorsteinsdottir, U., Kong, A., Stefansson, K. (2007) A common variant on chromosome 9p21 affects the risk of myocardial infarction, *Science*. **316**, 1491–1493.

[58] Coen, M., Ruepp, S.U., Lindon, J.C. Nicholson, J.K., Pognan, F., Lenz, E.M, and Wilson, I.D. (2004) An integrated metabonomic investigation of acetaminophen toxicity in the mouse using NMR spectroscopy. *J. Pharm. Biomed. Anal.* **35**, 93-105.

[59] Brown, S.C., Kruppa, G., Dasseux, J.L. (2005) Metabolomics applications of FT-ICR mass spectrometry. *Mass Spectrom Rev.* **24**, 223-31.

[60] Kraly, J.R., Holcomb, R.E., Guan, Q., Henry, C.S. (2009) Review: Microfluidic applications in metabolomics and metabolic profiling. *Anal. Chim. Acta*. **653**, 23-35.

[61] Xia, J.F., Liang, Q.L., Liang, X.P., Wang, Y.M., Hu, P., Li, P., Luo, G.A. (2009) Ultraviolet and tandem mass spectrometry for simultaneous quantification of 21 pivotal metabolites in plasma from patients with diabetic nephropathy. *J. Chromatogr. B Analyt. Technol. Biomed. Life Sci.* **877**, 1930-6.

[62] Downard, K. (2004). Mass Spectrometry - A Foundation Course. Cambridge UK, Royal Society of Chemistry.

[63] Wong, S.F., Meng, C.K. , Fenn, J.B. (1988) Multiple Charging in Electrospray Ionization of Poly(ethylene glycols). *J. Phys. Chem.* **92**, 546-550.

[64] Jemal, M., Xia, Y.Q. (2006) LC-MS Development strategies for quantitative bioanalysis. *Curr. Drug Metab.* **7**, 491-502.

[65] Kebarle, P., and Ho, Y. (1997) Electrospray Ionization Mass Spectrometry; Fundamentals Instrumentation & Applications. R. B. Cole. New York, John Wiley & Sons, Inc.

[66] Prakash, C., Shaffer, C.L., Nedderman, A. (2007) Analytical strategies for identifying drug metabolites. **26**, 340-69.

[67] Michopoulos, F., Lai, L., Gika, H., Theodoridis, G., Wilson, I. (2009) UPLC-MS-Based Analysis of Human Plasma for Metabonomics Using Solvent Precipitation or Solid Phase Extraction. *J. Proteome Res.* **8**, 2114–2121.

[68] Hodson, M.P., Dear, G.J., Roberts, A.D., Haylock, C.L., Ball, R.J., Plumb, R.S., Stumpf, C.L., Griffin J.L., Haselden, J.N. (2007) A gender-specific discriminator in Sprague-Dawley rat urine: the deployment of a metabolic profiling strategy for biomarker discovery and identification. *Anal. Biochem* **362**, 182-92.

[69] Whitehouse, C.M., Dreyer, R.N., Yamashita, M., Fenn, J.B. (1985) Electrospray interface for liquid chromatographs and mass spectrometers. *Anal. Chem.* **57**, 675-679.

[70] Cech, N.B., Enke, C.G. (2001) Practical implications of some recent studies in electrospray ionization fundamentals. *Mass Spectrom. Rev.* **20**, 362-387.

[71] Blades, A.T., Ikonomou, M.G., Kerbale, P. (1991) Mechanism of electrospray mass-spectrometry as an electrolysis cell. *Anal. Chem.* **63**, 2109.

[72] Taflin, D.C., Ward, T.L., and Davis E.J. (1988) Electrified Droplet Fisiion and the Rayleigh Limit. *Langmuir*. **5**, 376-384.

[73] Kebarle, P., Peschke, M. (2000) On the mechanisms by which the charged droplets produced by electrospray lead to gas phase ions. **406**. 11-35.

[74] Han, X., and Gross, R.W. (2005) Shotgun lipidomics: multi-dimensional mass spectrometric analysis of cellular lipidomes. *Gross. Expert Rev Proteomics*. **2**, 253-264.

[75] Milne, S., Ivanova, P., Forrester, J., and Alex Brown, H. (2006) Lipidomics: an analysis of cellular lipids by ESI-MS. *Methods*. **39**, 92-103.

[76] Schiller, J., and Arnold, K. Mass Spectrometry in Sturctural Biology (2000) Encyclopedia of Analytical Chemistry. R. A. Meyers. Chichester, Willey and Sons.

[77] Koulman, A., Tapper, B.A., Fraser, K. , Cao, M., Lane, G.A., and Rasmussen, S. (2007) High-throughput direct-infusion linear ion trap mass spectrometry: a new method for mass spectrometry. *Rapid Commun. Mass Spectrom.* **21**, 421-428.

[78] Douglas, D.J., Frank, A.J., and Mao D. (2003) Linear Ion Traps in Mass Spectrometry. *Mass Spectrom. Rev.* **24**, 1-29.

[79] March, R.E., Strife, R.J. (1995) Practical aspects of ion trap mass spectrometry: chemical biomedical, and environmental applications. *Modern Mass Spectrometry Series, vol.2. CRC Press, Boca Raton, FL.*

[80] Petkovic, M., Schiller, J., Muller ,M., Benard, S., Reichl, S., Arnold, K. and Arnhold, J. (2001) Detection of individual phospholipids in lipid mixtures by matrix-assisted laser desorption/ionization time-of-flight mass spectrometry: phosphatidylcholine prevents the detection of further species. *Anal. Biochem.* **289**, 202-216.

[81] Knochenmuss, R. (2003) A quantitative model of ultraviolet matrix-assisted laser desorption/ionization including analyte ion generation. *Anal. Chem.* **75**, 2199-207.

[82] Peterson, B.L., and Cummings, B.S (2006) A review of chromatographic methods for the assessment of phospholipids in biological samples. Biomed. Chromatogr. **20,** 227-243.

[83] Han, X., Yang, J., Cheng, H., Yang, K., Abendschein, D.R., and R.W. Gross. (2005) Shotgun lipidomics identifies cardiolipin depletion in diabetic myocardium linking altered substrate utilization with mitochondrial dysfunction. *Biochem.* **44**, 16684-16694.

[84] Han, X., Yang, K., Yang, J. , Cheng, H., and Gross., R.W. (2006) Shotgun lipidomics of cardiolipin molecular species in lipid extracts of biological samples *J. Lipid Res.* **47**, 864-879.

[85] Hsu, F.F., Bohrer, A., and Turk, J. (1998) Formation of lithiated adducts of glycerophosphocholine lipids facilitates their identification by electrospray ionization tandem mass spectrometry. *J. Am. Soc. Mass Spectrom.* **9**, 516-526.

[86] Schwudke, D., Oegema, J., Burton, L., Entchev, E., Hannich, J.T., Ejsing, C.S., Kurzchalia, T., and Shevchenko, A. (2006) Lipid profiling by multiple precursor and neutral loss scanning driven by the data-dependent acquisition. *Anal. Chem.* **78**, 585-595.

[87] Wenk, M.R., Lucast, L., Di Paolo, G., Romanelli, A.J., Suchy, S.F., Nussbaum, R.L., Cline, G.W., Shulman, G.I., McMurray, W., and De Camilli., P. (2003) Phosphoinositide profiling in complex lipid mixtures using electrospray ionization mass spectrometry. *Nat. Biotech.* **21**, 813-817.

[88] Hvattum, E., Uran, S., Sandbaek, A.G., Karlsson, A.A., and Skotland., T. Quantification of phosphatidylserine, phosphatidic acid and free fatty acids in an ultrasound contrast agent by normal-phase high-performance liquid chromatography with evaporative light scattering detection (2006) *J. Pharm. Biomed. Anal.* **42**, 506-512.

[89] McNabb, T.J., Cremesti, A.E., Brown, P.R., and Fischl, A.S. (1999) The Separation and Direct Detection of Ceramides and Sphingoid Bases by Normal-Phase High-Performance Liquid Chromatography and Evaporative Light-Scattering Detection. *Anal. Biochem.* **276**, 242-250.

[90] Saldanha, T., Sawaya, A.C.H.F., Eberlin, M.N., and Bragagnolo, N. (2006) HPLC separation and determination of 12 cholesterol oxidation products in fish: Comparative study of RI, UV, and APCI-MS detectors. *J. Agric. Food Chem.* **54**, 4107-4113.

[91] Wang, C., Xie, S., Yang, J., Yang, Q., and Xu, G. (2004) Structural identification of human blood phospholipids using liquid chromatography/quadrupole-linear ion trap mass spectrometry**.** *Anal. Chim. Acta* **525**, 1-10.

[92] Malavolta, M., Bocci, F., Boselli, E., and Frega, N.G. (2004) Normal phase liquid chromatography-electrospray ionization tandem mass spectrometry analysis of phospholipid molecular species in blood mononuclear cells: application to cystic fibrosis. *J. Chromatogr. B.* **810**, 173-186.

[93] Olsson, N.U., and Salem, N. (1997) Molecular species analysis of phospholipids. *J. Chromatogr. B.* **692** 245-256.

[94] Rainville, P.D., Stumpf, C.L., Shockcor, J.P., Plumb, R.S., and Nicholson, J.K. (2007) Novel application of reversed-phase UPLC-oaTOF-MS for lipid analysis in complex biological mixtures: A new tool for lipidomics. *J. Proteome Res.* 6, 552-558.

[95] Chernushevich, I.V., Loboda, A.V. and Thomson, B.A. (2001) An introduction to quadrupole-time-of-flight mass spectrometry. *J. Mass Spectrom.* **36**, 849-865.

[96] Morris, H.R., Paxton, T., Dell, A., Langhorne, J., Berg, M., Bordoli, R.S., Hoyes, J., Bateman, R.H. (1996) High sensitivity collisionally-activated decomposition tandem mass spectrometry on a novel quadrupole/orthogonal acceleration time-of-flight mass spectrometer. *Rapid Commun. Mass Spectrom.* **10**, 889-896.

[97] Halket, J.M., Waterman, D., Przyborowska, A.M., Patel, R.K., Fraser, P.D. and Bramley, P.M. (2005) Chemical derivatization and mass spectral libraries in metabolic profiling by GC/MS and LC/MS/MS. *J. Exp. Bot*. **56** 219-243.

[98] Schmelzer, K., Fahy, E., Subramaniam, S., Dennis, E.A., and Brown, H.A. (2007) The LIPID MAPS initiative in lipidomics. *Methods in Enzymology* (Academic Press) **432**, 171-183.

[99] Caffrey, M, and Hogan, J. (1992) LIPIDAT: a database of lipid phase transition temperatures and enthalpy changes. DMPC data subset analysis. *Chem Phys Lipids.* **61**, 1-109.
[100] Martin, A.J.P., Synge R.L.M. (1941) A new form of chromatogram employing two liquid phases *Biochem. J.* **35**, 1358-1368.
[101] Gohlke, R.S., McLafferty, F.W. (1993) Early gas chromatography/mass spectrometry. *J. Am. Soc. Mass Spectrom.* **4**, 367-371.
[102] Halket, J.M., and Zaikin, V.G. (2003) Derivatisation in mass spectrometry—1. Silylation. *Eur. J. Mass Spectrom.* **9**, 1-21.
[103] Schlenk, H., Gellerman, J.L. (1960) Esterification of fatty acids with diazomethane on a small scale. *Anal. Chem.* **32**, 1412-14.
[104] Morrison, W.R., Smith, L.M. (1964) Preparation of fatty acid methyl esters and dimethylacetal from lipids with boron fluoridemethanol. *J. Lipid Res.* **5**, 600 – 608.
[105] Nicholson, J.K. Higham, D.P. Timbrell, J.A. Sadler, P.J. (1989) Quantitative high resolution 1H NMR urinalysis studies on the biochemical effects of cadmium in the rat. *Mol. Pharmacol.* **36**, 398-404.
[106] Bell, J.D. Brown, J.C. Sadler, P.J. (1989) NMR studies of body fluids. *NMR Biomed.* **2**, 246-56.
[107] Griffin, J.L., and Shockcor, J.P. (2004) Metabolic profiles of cancer cells. *Nat. Rev.Cancer.* **4**, 551-561.
[108] Ugurbil, K., Brown, T.R., den Hollander, J.A., Glynn, P., Shulman, R.G. (1978) High resolution ^{13}C NMR studies of glucose metabolism in *E.coli*. *Proc. Natl. Acad. Sci. USA*. **75**, 3742-46.
[109] Cohen, S.M., Shulman, R.G., McLaughlin, A.C. (1979) Effects of ethanol on alanine metabolism in perfused mouse liver studied by ^{13}C NMR. *Proc. Natl. Acad. Sci.* **76**, 4808-12.
[110] Alger, J.R., Sillerud, L.O., Behar, K.L., Gillies, R.J., Shulman, R.G. Gordon, R.E., Shae, D., Hanley, P.E. (1981) In vivo ^{13}C NMR studies of mammals. *Science.* **214**, 660-62.
[111] Jue, T., Rothman, D.L., Tavitian, B.A., Shulman, R.G. (1989) Natural-abundance ^{13}C NMR study of glycogen repletion in human liver and muscle. *Proc. Natl. Acad. Sci.* **86**, 1439-42.
[112] Wold, S., Albano, C., Dunn, W.J., Edlund, U., Esbensen, K., Geladi, P., Hellberg, S., Johansson, E., Lindberg, W., and Sjostrom, M. (1984) Chemometrics: Mathematics and Statistics in Chemistry: D. Reidel Publishing Company, Dordrecht, Holland.
[113] Valafar, F. (2002) Pattern recognition techniques in microarray data analysis: a survey. *Ann. N.Y. Acad. Sci.* **980**, 41-64.
[114] James, D.E., Piper, R.C. (1994) Insulin resistance, diabetes, and the insulin-regulated trafficking of GLUT-4. *J. Cell Biol.* **126**, 1123-6.
[115] Reaven, G., Abbasi, F., and McLaughlin, T. (2004) Obesity, insulin resistance, and cardiovascular disease. *Recent Prog. Horm. Res.* **59**, 207-223.
[116] Reaven, G.M. (2005) Insulin resistance, the insulin resistance syndrome, and cardiovascular disease. *Panminerva Med.* **47**, 201-210.
[117] Alexander, C.M., Landsman, P.B., Teutsch, S.M., and Haffer, S.M. (2003) NCEP-defined metabolic syndrome, diabetes, and prevalence of coronary heart disease among NHANES III participants age 50 years and older. *Diabetes*. **52**, 1210-1214.
[118] Reaven, G.M. (1988). Banting lecture 1988. Role of insulin resistance in human disease. *Diabetes*. **37**, 1595-1607.
[119] Austin, M.A., King, M.C., Vranizan, K.M., and Krauss, R.M. (1990) Atherogenic lipoprotein phenotype. A proposed genetic marker for coronary heart disease risk. *Circulation*. **82**, 495-506.
[120] Festa, A., Williams, K., Tracy, R.P., Wagenknecht, L.E., and Haffner, S.M. (2006) Progression of plasminogen activator inhibitor-1 and fibrinogen levels in relation to incident type 2 diabetes. *Circulation*. **113**. 1753-1759.
[121] Gurnell, M., Savage, D.B., Chatterjee, V.K., and O'Rahilly, S. (2003) The metabolic syndrome: peroxisome proliferator-activated receptor gamma and its therapeutic modulation. *J. Clin. Endocrinol. Metab.* **88**, 2412-2421.
[122] Reaven, G.M. (2006) The metabolic syndrome: is this diagnosis necessary? *Am. J. Clin. Nutr.* **83**, 1237-1247.
[123] Barroso, I., Gurnell, M., Crowley, V.E., Agostini, M., Schwabe, J.W., Soos, M.A., Maslen, G.L., Williams, T.D., Lewis, H., Schafer, A.J., Chatterjee, V.K., and O'Rahilly, S. (1999) Dominant negative mutations in human PPARgamma associated with severe insulin resistance, diabetes mellitus and hypertension. *Nature*. **402**, 880-883.

[124] Kahn, R., Buse, J., Ferrannini, E., and Stern, M. (2005) The metabolic syndrome: time for a critical appraisal: jopint statement from the Americal Diabetes Association and the European Association for the Study of Diabetes. *Diabetes Care.* **28**, 2289-2304.
[125] Huang, P.L. (2009) A comprehensive definition for metabolic syndrome. *Dis Model Mech.* **2**, 231-237.
[126] Isseman, I., and Green, S. (1990) Activation of a member of the steroid hormone receptor superfamily by peroxisome proliferators. *Nature*. **347**, 645-650.
[127] Celi, F.S. Shuldiner, A.R. (2002) The role of peroxisome proliferator-activated receptor gamma in diabetes and obesity. *Curr Diab Rep*. **2**, 179-185
[128] van Bilsen, M. van der Vusse, G.J. Gilde, A.J. Lindhout, M. van der Lee, K.A.(2002) Peroxisome proliferator-activated receptors: lipid binding proteins controlling gene expression. *Mol Cell Biochem*. **239**, 131-138.
[129] Ferre, P. (2004) The biology of peroxisome proliferator-activated receptors: relationship with lipid metabolism and insulin sensitivity. *Diabetes*. **53 Suppl. 1**, S43-50.
[130] Dreyer, C., Krey, G., Keller, H., Givel, F., Helftenbein, G., and Wahli, W. (1992) Control of the peroxisomal beta-oxidation pathway by a novel family of nuclear hormone receptors. *Cell*. **68**, 879-887.
[131] Michalik, L., Auwerx, J., Berger, J.P., Chatterjee, V.K., Glass, C.K., Gonzalez, F.J., Grimaldi, P.A., Kadowaki, T., Lazar, M.A., O'Rahilly, S., Palmer, C.N., Plutzky, J., Reddy, J.K., Piegelman, B.M., Staels, B., and Wahli, W. (2006) International Union of Pharmacology. LXI. Peroxisome proliferator-activated receptors. *Pharmacol, Rev.* **58**, 726-741.
[132] Forman, B.M.,Chen, J., and Evans, R.M. (1997) Hypolipidemic drugs, polyunsaturated fatty acids, and eicosanoids are ligands for peroxisome proliferator-activated receptors alpha and delta. *Proc. Natl. Acad. Sci. U.S.A.* **94**, 4312-4317.
[133] Desvergne, B., and Wahli, W. (1999) Peroxisome proliferator-activated receptors: nuclear control of metabolism. *Endocr. Rev.* **20**, 649-688.
[134] Nolte, R.T., Wisely, G.B., Westin, S., Cobb, J.E., Lambert, M.H., Kurokawa, R., Rosenfeld, M.G., Willson, T.M., Glass, C.K., and Milburn, M.V. (1998) Ligand binding and co-activator assembly of the peroxisome proliferator-activated receptor-gamma. *Nature*. **395**, 137-143.
[135] Castelein, H. Gulick, T. Declercq, P.E. Mannaerts, G.P. Moore, D.D. Baes, M.I. (1994) The peroxisome proliferator activated receptor regulates malic enzyme gene expression. *J Biol Chem*, **269**, 26754-8
[136] Jepsen, K., and Rosenfeld, M.G. (2002) Biological roles and mechanistic actions of co-repressor complexes. *J. Cell. Sci.* **115**, 689-698.
[137] Privalsky, M.L. (2004) The role of corepressors in transcriptional regulation by nuclear hormone receptors. *Annu. Rev. Physiol.* **66**, 315-360.
[138] Kliewer, S.A., Xu, H.E., Lambert, M.H., and Willson, T.M. (2001) Peroxisome Proliferator-Activated Receptors: From Genes to Physiology. *Recent Progress in Hormone Research* **56**, 239-265.
[139] Braissant, O., Foufelle, F., Scotto, C., Dauca, M., and Wahli. (1996) Differential expression of peroxisome proliferator-activated receptors (PPARs): tissue distribution of PPAR-alpha, -beta, and gamma in the adult rat. *Endocrinology*. **137**, 354-366.
[140] Barbier, O. Torra, JP. Duguay, Y. Blanquart, C. Fruchart, J.C. Glineur, C.(2002) Pleiotropic actions of peroxisome proliferator-activated receptors in lipid metabolism and atherosclerosis. *Arterioscle , Thromb Vasc. Biol.* **22**, 716-726.
[141] Berger, J., and Moller, D.E. (2002) The mechanisms of action of PPARs. *Annu. Rev. Med.* **53**, 409-435.
[142] Brandt, J.M., Djouadi, F., and Kelly, D.P. (1998). Fatty acids activate transcription of the muscle carnitine palmitoyltransferase I gene in cardiac myocytes via the peroxisome proliferator-activated receptor alpha. *J. Biol. Chem.* **273**, 23786-23792.
[143] Gulick, T., Cresci, S., Chiara, T., Moore, D.D., and Kelly, D.P. (1994). The peroxisome proliferator-activated receptor regulates mitochondrial fatty acid oxidative enzyme gene expression. *Proc. Natl. Acad. Sci. U.S.A.* **91**, 11012-11016.
[144] Berger, J., Leibowitz, M.D., Doebber, T.W., Elbrecht, A., Zhang, B., Zhou, G., Biswas, C, Cullinan, C.A., Hayes, N.S., Li, Y., Tanen, M., Ventre, J., Wu, M.S., Berger, G.D., Mosley, R., Marquis, R., Santini, C., Sahoo, S.P., Tolman, R.L., Smith ,R.G., and Moller, D.E. (1999) Novel peroxisome proliferator-activated receptor (PPAR) gamma and PPARdelta ligands produce distinct biological effects. *J. Biol. Chem.* **274**, 6718-6725.

[145] Vega, R.B., Huss, J.M., Kelly, D.P. (2000) The coactivator PGC-1 cooperates with peroxisome proliferator-activated receptor alpha in transcriptional control of nuclear genes encoding mitochondrial fatty acid oxidation enzymes. *Mol. Cell. Biol.* **20**, 1868-1876.
[146] Cabrero, A., Alegret, M., Sanchez, R.M., Adzet, T., Laguna, J.C., and Vazquez, M. (2001) Bezafibrate reduces mRNA levels of adipocyte markers and increases fatty acid oxidation in primary culture of adipocytes. *Diabetes*. **50**, 1883-1890.
[147] Costet, P., Legendre, C., More, J., Edgar, A., Glatier, P., and Thierry Pineau (1998) Peroxisome proliferator-activated receptor alpha-isoform deficiency leads to progressive dyslipidemia with sexually dimorphic obesity and steatosis. *J. Biol. Chem.* **273**, 29577-29585.
[148] Staels, B., and Fruchart, J.C. (2005) Therapeutic roles of peroxisome proliferator-activated receptor agonists. *Diabetes*. **54**, 2460-2470.
[149] Berger, J.P., Aikayama, T.E., and Meinke, P.T. (2005) PPARs: therapeutic targets for metabolic diseases. *Trends*. *Pharmacol*. *Sci.* **26**, 244-251.
[150] Knight, B.L., Patel, D.D., Humphreys, S.M., Wiggins, D., and Gibbons, G.F. (2003) Inhibition of cholesterol absorption associated with a PPAR alpha-dependent increase in ABC binding cassette transporter A1 in mice. *J. Lipid. Res.* **44**, 2049-2058.
[151] Hennuyer, N., Tailleux, A., Torpier, G., Mezdour, H., Fruchart, J.C., Staels, B., and Fievet, C. (2005) PPARalpha, but not PPARgamma, activators decrease macrophage-laden atherosclerotic lesions in a nondiabetic mouse model of mixes dyslipidemia. *Arterioscler. Thromb. Vasc. Biol.* **25**, 1897-1902.
[152] Zhu, Y., Alvares, K., Huang, Q., Rao, M., Reddy, J. (1993) Cloning of a new member of the peroxisome proliferator-activated receptor gene family from mouse liver. *J. Biol. Chem.* **268**, 26817-20.
[153] Graves, R.A., Tontonoz, P., Spiegelman, B.M. (1992) Analysis of a tissue-specific enhancer: ARF6 regulates adipogenic gene expression. *Mol. Cell. Biol.* **12**, 1202-8.
[154] Rosen, E. D., Hsu, C. H., Wang, X., Sakai, S., Freeman, M. W., Gonzalez, F. J., Spiegelman, B. M. (2002) C/EBPalpha induces adipogenesis through PPARgamma: a unified pathway. *Genes Dev*. **16**,22–6.
[155] Castillo, G., Brun, R.P., Rosenfield, J.K., Hauser, S., Park, C.W., Troy, A.E., Wright, M.E., and Spiegelman, B.M. (1999) An adipogenic cofactor bound by the differentiation domain of PPARγ. *EMBO J.* **18**, 3676-3687.
[156] Vidal-Puig, A.J., Considine, R.V., Jimenez-Liñan, M., Werman, A., Pories, W.J., Caro, J.F., Flier, J.S. (1997) Peroxisome proliferator-activated receptor gene expression in human tissues. Effects of obesity, weight loss, and regulation by insulin and glucocorticoids. *J. Clin .Invest.* **99**, 2416-2422.
[157] Barak, Y., Nelson, M.C., Ong, E.S., Jones, Y.Z., Ruiz-Lozano, P., Chien, K.R., Koder, A., Evans, R.M. (1999) PPAR gamma is required for placental, cardiac, and adipose tissue development. *Mol. Cell.* **4**, 585-595.
[158] Rosen, E.D., Sarraf, P., Troy, A.E., Bradwin, G., Moore, K., Milstone, D.S., Spiegelman, B.M., Mortensen, R.M. (1999) PPAR gamma is required for the differentiation of adipose tissue in vivo and in vitro. *Mol. Cell.* **4**, 611-617.
[159] Imai, T., Takakuwa, R., Marchand, S., Dentz, E., Bornet, J.M., Messaddeq, N., Wendling, O., Mark, M., Desvergne, B., Wahli, W., Chambon, P., Metzger, D. (2004) Peroxisome proliferator-activated receptor gamma is required in mature white and brown adipocytes for their survival in the mouse. *Proc. Natl. Acad. Sci. U.S.A.*.**101**, 4543-4547.
[160] Barrosa, I., Gurnell, M., Crowley, V.E., Agostini, M., Schwabe, J.W., Soos, M.A., Maslen, G.L., Williams, T.D., Lewis, H., Schafer, A.J., Chatterjee, V.K., O'Rahilly, S. (1999) Dominant negative mutations in human PPARgamma associated with severe insulin resistance, diabetes mellitus, and hypertension. *Nature*. **402**, 880-883.
[161] Christodoulides, C., Vidal-Puig, A. (2009) PPARs and adipocyte function. *Mol. Cell. Endocrin.* Epub ahead of print.
[162] Nishino, N., Tamori, Y., Tateya, S., Kawaguchi, T., Shibakusa, T., Mizunoya, W., Inoue, K., Kitazawa, R., Kitazawa, S., Matsuki, Y., Hiramatsu, R., Masubuchi, S., Omachi, A., Kimura, K., Saito, M., Amo, T., Ohta, S., Yamaguchi, T., Osumi, T., Cheng, J., Fujimoto, T., Nakao, H., Nakao, K., Aiba, A., Okamura, H., Fushiki, T., Kasuga, M. (2008) FSP27 contributes to efficient energy storage in murine white adipocytes by promoting the formation of unilocular lipid droplets. *J. Clin. Invest.* **118**, 2808-2821.
[163] Nolan, J.J., Ludvik, B., Beerdsen, P., Joyce, M., Olefsky, J. (1994) Improvement in glucose tolerance and insulin resistance in obese subjects treated with troglitazone. *N. Engl. J. Med.* **331**, 1188-93.

[164] Lehmann, J.M., Moore, L.B., Smith-Oliver, T.A., Wilkinson, W.O., Willson, T.M., Kliewer, S.A. (1995) An antidiabetic thiazolidinedione is a high affinity ligand for peroxisome proliferator-activated receptor gamma. *J. Biol. Chem.* **270**, 12953-56.
[165] Rangwala, S.M., Lazar, M.A. (2004) Peroxisome proliferator-activated receptor gamma in diabetes and metabolism. *Trends Pharmacol. Sci.* **25**, 331-336.
[166] Ye, J.M., Dzamko, N., Cleasby, M.E., Hegarty, B.D., Furler, S.M., Cooney, G.J., Kraegen, E.W. (2004) Direct demonstration of lipid sequestration as a mechanism by which rosiglitazone prevents fatty-acid-induced insulin resistance in the rat: comparison with metformin. *Diabetologia.* **47**, 1306-13.
[167] Sinha, R., Dufour, S., Petersen, K., LeBon, V., Enoksson, S., Ma, Y.Z., Savoye, M., Rothman, D.L., Shulman, G.I., Caprio, S. (2002) Assessment of skeletal muscle triglyceride content by (1)H nuclear magnetic resonance spectroscopy in lean and obese adolescents: relationships to insulin sensitivity, total body fat, and central adiposity. *Diabetes*. **51**, 1022-27.
[168] Girroir, E.E., Hollingshead, H.E., He, P., Zhu, B., Perdew, G.H., Peters, J.M. (2008) Quantitative expression patterns of peroxisome proliferator-activated receptor-beta/delta (PPARbeta/delta) protein in mice. *Biochem Biophys Res Commun.*, **371**, 456-61.
[169] Wang Y.X., Lee, C.H., Tiep, S., Yu, R.T., Ham, J., Kang, H., Evans. R.M. (2003) Peroxisome-proliferator-activated receptor delta activates fat metabolism to prevent obesity. *Cell*. **113**, 159-170.
[170] Oliver, W.R. Shenk J.L. Snaith, M.R. Russell, C.S. Plunket, K.D. Bodkin, N.L. Lewis, M.C. Winegar, D.A. Sznaidman, M.L. Lambert, M.H. Xu, H.E. Sternbach, D.D. Kliewer, S.A. Hansen, B.C. Willson, T.M. (2001) A selective peroxisome proliferator-activated receptor delta agonist promotes reverse cholesterol transport. *Proc. Natl. Acad. Sci. U. S. A.* **98**, 5306-11
[171] Wang, Y.X. Zhang, C.L. Yu, R.T. Cho, H.K. Nelson, M.C. Bayuga-Ocampo,C.R. Ham, J. Kang, H. Evans, R.M. (2004) Regulation of muscle fibre type and running endurance by PPAR delta.*PLoS Biol.***2**, e294
[172] Grimaldi, P.A. (2001) The roles of PPARs in adipocyte differentiation. *Prog. Lipid Res*. **40**; 269-281.
[173] Valmaseda, A., Carmona, M.C., Barbera, M.J., Vinas, O., Mampel, T., Iglesias, R., Villarroya, F., Giralt, M. (1999) Opposite regulation of PPAR-alpha and –gamma gene expresión by both their ligands and retinoico acid in brown adipocytes. *Mol. Cell Endocrinol.* **154**, 101-9.
[174] Bastie, C. Luquet, S., Holst, D., Jehl-Pietri, C., and Grimaldi, P.A. (2000) Alterations of peroxisome proliferator-activated receptor delta activity affect fatty acid-controlled adipose differentiation. *J. Biol. Chem.* **275**, 38768-38773.
[175] Hansen, J.B., Zhang, H., Rasmussen, T.H., Petersen, R.K., Flindt, E.N., Kristiansen, K. (2001) Peroxisome proliferator-activated receptor delta (PPARdelta)-mediated regulation of preadipocyte proliferation and gene expression is dependent on cAMP signalling. *J. Biol. Chem.* **276**, 3175-3182.
[176] Gupta, R.A. Wang, D. Katkuri, S. Wang, H. Dey, S.K. DuBois, R.N. (2004) Activation of nuclear hormone receptor peroxisome proliferator-activated receptor-δ accelerates intestinal adenoma growth. *Nat Med*. **10**, 245-247.
[177] Stephen, R.L. Gustafsson, M.C.U. Jarvis, M. Tatoud, R. Marshall, B.R. Knight, D. Ehrenborg, E. Harris, A.L. Wolf, C.R. Palmer, C.N.A.(2004) Activation of Peroxisome Proliferator-Activated Receptor δ Stimulates the Proliferation of Human Breast and Prostate Cancer Cell Lines. *Cancer Research*. **64**, 3162-3170.
[178] Harman, F.S. Nicol, C.J. Marin, H.E. Ward, J.M. Gonzalez, F.J. Peters, J.M.(2004) Peroxisome proliferator-activated receptor-delta attenuates colon carcinogenesis. *Nat Med.* **10**, 481-3.
[179] Peters, J.M., Hollingshead, H.E., Gonzalez, F.J. (2008) Role of peroxisome-proliferator-activated receptor beta/delta (PPARbeta/delta) in gastrointestinal tract function and disease. *Clin. Sci.* **115**, 107-27.
[180] Xu, J., Chang, V., Joseph, S.B., Trujillo, C., Bassilian, S., Saad, M.F., Lee W.N.P., and Kurland I.J. (2004) Peroxisomal proliferator-activated receptor alpha deficiency diminishes insulin responsiveness of gluconeogenic/glycolytic/pentose gene expression and substrate cycle flux. *Edocrinology*. **145**, 1087-1095.
[181] Xu, J., Xiao, G., Trujillo, C., Chang, V., Blanco, L., Joseph, S.B., Bassilian, S., Saad, M.F., Tontonoz, P., Lee W.N.P., and Kurland, I.R. (2002) Peroxisome proliferator-activated receptor α (PPARα) influences substrate utilization for hepatic glucose production. *J. Biol. Chem.* **277**, 50237-50244.
[182] Atherton, H.J., Gulston, M.K., Bailey, N.J., Cheng, K.K., Zhang, W., Clarke, K., Griffin, J.L. (2009) Metabolomics of the interaction between PPAR-alpha and age in the PPAR-alpha-null mouse. *Mol. Syst. Biol.* **5**, 259-268.

[183] Watkins, S.M., Reifsnyder, P.R., Pan, H.J., German, J.B., Leiter, E.H. (2002) Lipid metabolome-wide effects of the PPARγ agonist rosiglitazone. *J. Lipid Res.* **43**, 1809-1817.
[184] Ringeissen, S., Connor, S.C., Brown, H.R., Sweatman, B.C., Hodson, M.P., Kenny, S.P., Haworth, R.I., McGill, P., Price, M.A., Aylott, M.C., Nunez, D.J., Haselden, J.N., Waterfield, C.J. (2003) Potential urinary and plasma biomarkers of peroxisome proliferation in the rat: identification of N-methylnicotinamide and N-methyl-4-pyridone-3-carboxamide by 1H nuclear magnetic resonance and high performance liquid chromatography. *Biomarkers*. **8**, 240-71.
[185] Van der Veen, J.N., Kruit, J.K., Havinga, R., Baller, J.F., Chimini, G., Lestavel, S., Staels, B., Groot, B.H., Groen, A.K., and Kuipers, F. (2005) Reduced cholesterol absorption upon PPARdelta activation coincides with decreased intestinal expression of NPC1L1. *J. Lipid Res*. **46**, 526-534.
[186] Bilić, A., Alpeza, I., Rukavina, A.S. (2000) Evaluation of the Olympus AU 400 clinical chemistry analyzer. *Clin. Lab*, **46**, 1-6.
[187] Bligh EG, Dyer WJ**.** (1959) A rapid method of total lipid extraction and purification. *Can J Biochem Physiol.* **37**, 911-7.
[188] Kuznetsov, A.V., Veksler, V., Gellerich F.N., Saks, V., Margreiter, R. & Kunz, W.S. (2008) Analysis of mitochondrial function in situ in permeabilized muscle fibers, tissues and cells. *Nat. Protoc*. **3**, 965-76.
[189] Gullberg, J., Jonsson, P., Nordstrom, A., Sjostrom, M., and Moritz, T. (2004) Design of experiments: an efficient strategy to identify factors influencing extraction and derivatization of Arabidopsis thaliana samples in metabolomic studies with gas chromatography/mass spectrometry. *Anal. Biochem.* **331**, 283-295.
[190] Pietiläinen, K.H., Marko, S., Rissanen, A., Seppänen-Laakso, T., Yki-Järvinen, H., Kaprio, J. and Orešič, M. (2007) Acquired obesity is associated with changes in the serum lipidomic profile independent of genetic effects - a monozygotic twin study. *PLoS ONE*. **2,** e218.
[191] Du, P., Kibbe, W.A., Lin S.M. (2008) lumi: a pipeline for processing Illumina microarray. *Bioinformatics*. **24**, 1547-8.
[192] Lin, S.M., Du, P., Huber, W., Kibbe, W.A. (2008) Model-based variance-stabilizing transformation for Illumina microarray data. *Nucleic Acids Res*. **36**, e11.
[193] Smyth, G. K. (2004) Linear models and empirical Bayes methods for assessing differential expression in microarray experiments. *Stat. Appl. Genet. Mol. Biol*. **3**, Article 3.
[194] Green, H., Kehinde, O. (1974) Sublines of mouse 3T3 cells that accumulate lipid. *Cell.* **1**, 113-116.
[195] Green, H., Kehinde, O. (1976) Spontaneous heritable changes leading to increased adipose conversion in 3T3 cells. *Cell.* **7**, 105-113.
[196] Green, H., Kehinde, O. (1975) An established preadipose cell line and its differentiation in culture. II. Factors affecting the adipose conversion. *Cell.* **5**, 19-27.
[197] Green, H., Meuth, M. (1974) An established pre-adipose cell line and its differentiation in culture. *Cell.* **3**, 127-133.
[198] Rubin, C.S., Hirsch, A., Fung, C., Rosen, O.M. (1978) Development of hormone receptors and hormonal responsiveness in vitro. Insulin receptors and insulin sensitivity in the preadipocyte and adipocyte forms of 3T3-L1 cells. *J. Biol. Chem.* **253**, 7570-7578.
[199] Rosen, O.M., Smith, C.J., Fung, C., Rubin, C.S. (1978) Development of hormone receptors and hormone responsiveness in vitro. Effect of prolonged insulin treatment on hexose uptake in 3T3-L1 adipocytes. *J. Biol. Chem.* **253**, 7579-7583.
[200] Savage, D.B., Petersen, K.F., Shulman, G.I. (2005) Mechanisms of Insulin Resistance in Humans and Possible Links with Inflammation. *Hypertension*. **45**, 828-833.
[201] Im, S.S., Kwon, S.K., Kang, S.Y., Kim, T.H., Kim, H.I., Hur, M.W., Kim, K.S., Ahn, Y.H. (2006) Regulation of GLUT4 gene expression by SREBP-1c in adipocytes. *Biochem. J.* **399**, 131-9.
[202] Jitrapakdee, S., Slawik, M., Medina-Gomez, G., Campbell, M., Wallace, J.C., Sethi, J.K., O'rahilly, S., Vidal-Puig, A.J. (2005) The peroxisome proliferator-activated receptor-gamma regulates murine pyruvate carboxylase gene expression in vivo and in vitro. *J. Biol. Chem.* **280**, 27466-76.
[203] Wheatcroft, S.B., Kearney, M.T., Shah, A.M., Ezzat, V.A., Miell, J.R., Modo, M., Williams, S.C., Cawthorn, W.P., Medina-Gomez, G., Vidal-Puig, A., Sethi, J.K., Crossey, P.A. (2007) IGF-binding protein-2 protects against the development of obesity and insulin resistance. *Diabetes*. **56**, 285-94.
[204] Bethell, D.R., Pegg, A.E. (1981) Polyamines are needed for the differentiation of 3T3-L1 fibroblasts into adipose cells. *Biochem. Biophys. Res. Comm*. **102**, 272-278.

[205] Tanabe, Y., Matsunnaga, Y., Saito, M., Nakayama, K. (2008) Involvement of cyclooxygenase-2 in synergistic effect of cyclic stretching and eicosapentaenoic acid on adipocyte differentiation. *J. Pharmacol. Sci.* **106**, 478-484.
[206] Madsen, L., Petersen, R.K., Sorensen, M.B., Jorgensen, C., Hallenborg, P., Pridal, L., Fleckner, J., Amri E-Z., Krieg, P., Furstenberger, G., Berge, R.K., Kristiansen, K. (2003) Adipocyte differentiation of 3T3-L1 preadipocytes is dependent on lipoxygenase activity during the initial stages of the differentiation process. *Biochem. J.* **375**, 539-549.
[207] Christianson, J.L., Nicoloro, S., Straubhaar, J., Czech, M.P. (2008) Stearoyl-CoA desaturase 2 is required for peroxisome proliferator-activated receptor gamma expression and adipogenesis in cultured 3T3-L1 cells. *J. Biol. Chem*. **283**, 2906-2916.
[208] Weiss, G.H., Rosen, O.M., Rubin, C.S. (1980) Regulation of fatty acid synthetase concentration and activity during adipocyte differentiation. Studies on 3T3-L1 cells. *J. Biol. Chem*. **255**, 4751-4757.
[209] Kajimoto, K., Terada, H., Baba, Y., Shinohara, Y. (2005) Essential role of citrate export from mitochondria at early differentiation stage of 3T3-L1 cells for their effective differentiation into fat cells, as revealed by studies using specific inhibitors of mitochondrial di- and tricarbodylate carriers. *Mol. Gen. Metab*. **85**, 46-53.
[210] Pantoja, C., Huff, J.T., Yamamoto, K.R. (2008) Glucocorticoid signaling defines a novel commitment state during adipogenesis in vitro. *Mol Biol Cell*. **19**, 4032-41.
[211] Sadowski, H.B., Wheeler, T.T., Young, D.A. (1992) Gene expression during 3T3-L1 adipocyte differentiation. *J. Biol. Chem.* **266**, 4722-4731.
[212] Gene Expression Omnibus Datasets, Accession Number GDS2660. Adipogenesis in vitro.
[213] Gene Expression Omnibus Datasets, Accession Number GDS2659. Adipogenesis in vitro.
[214] Su, X., Han, X., Yang, J., Mancuso, D.J., Chen, J., Bickel, P.E., Gross, R.W. (2004) Sequential Ordered Fatty Acid α-Oxidation and Δ9 Desaturation Are Major Determinants of Lipid Storage and Utilization in Differentiating Adipocytes. *Biochem*. **43**, 5033-5044.
[215] Westin, M.A.K., Hunt, M.C., Alexson, S.E.H. (2008) Short- and medium-chain carnitine acyltransferases and acyl-CoA thioesterases in mouse provide complementary systems for transport of beta-oxidation products out of peroxisomes. *Cell. Mol. Life Sci.* **65**, 982-990.
[216] Kim, H-K., Della-Fera, M., Lin, J., Baile, C.A. (2006) Docosahexaenoic acid inhibits adipocyte differentiation and induces apoptosis in 3T3-L1 preadipocytes. *J Nutr*. **136**, 2965-9.
[217] Flower, R.J. (1988) Lipocortin and the mechanism of action of the glucocorticoids. *Br. J. Pharmacol.* **94**, 987-1015.
[218] Petersen, R.K., Jorgensen, C., Rustan, A.C., Froyland, L., Muller-Decker, K., Furstenberger, G., Berge R.K., Kristiansen, K., Madsen, L. (2003) Arachidonic acid-dependent inhibition of adipocyte differentiation requires PKA activity and is associated with sustained expression of cyclooxygenases. *J. Lipid Res*. **44**, 2320-2330.
[219] Larsen, T.M., Toubro, S., Astrup, A. (2003) PPARgamma agonists in the treatment of type II diabetes: is increased fatness commensurate with long term efficacy. *Int. J. Obes. Relat. Metab. Disord.* **27**, 147-161.
[220] Cerdan, S., Kunnecke, B., Dolle, A., and Seelig, J. (1988) In situ metabolism of 1,omega medium chain dicarboxylic acids in the liver of intact rats as detected by 13C and 1H NMR. *J. Biol. Chem*. **263**, 11664-11674.
[221] Jucker, B.M., Yang, D., Casey, W.M., Olzinski, A.R., Williams, C., Lenhard, S.C., Legos, J.J., Hawk, C.T., Sarkar, S.K., Newsholme, S.J. (2007) Selective PPARdelta agonist treatment increases skeletal muscle lipid metabolism without altering mitochondrial energy coupling: an in vivo magnetic resonance spectroscopy study. *Am J Physiol Endocrinol Metab.* **293**, E1256-64.
[222] Roberts, L.D., Hassall, D.G., Winegar, D.A., Haselden, J.N., Nicholls, A.W., Griffin, J.L (2009) Increased hepatic oxidative metabolism distinguishes the action of Peroxisome Proliferator-Activated Receptor delta from Peroxisome Proliferator-Activated Receptor gamma in the Ob/Ob mouse. *Genome Med*. **1**, 115.
[223] Kawashima, Y., Musoh, K., Kozuka, H. (1990) Peroxisome proliferators enhance linoleic acid metabolism in rat liver. Increased biosynthesis of omega 6 polyunsaturated fatty acids. *J. Biol. Chem*. **265**, 9170-5.
[224] Miller, C.W., Ntambi, J.M. (1996) Peroxisome proliferators induce mouse liver stearoyl-CoA desaturase 1 gene expression. *Proc. Natl. Acad. Sci. U S A*. **3**, 9443-8.

[225] de Lange, P., Lombardi, A., Silvestri, E., Goglia, F., Lanni, A., Moreno, M. (2008) Peroxisome Proliferator-Activated Receptor Delta: A Conserved Director of Lipid Homeostasis through Regulation of the Oxidative Capacity of Muscle. *PPAR Res*. **2008**, 172676.
[226] Sato, T., Iwaki, M., Shimogaito, N., Wu, X., Yamagishi, S., Takeuchi, M. (2006) TAGE (toxic AGEs) theory in diabetic complications. *Curr Mol Med.* **6,** 351-8.
[227] Lee, C-H., Olson, P., Hevener, A., Mehl, I., Chong, L-W., Olefsky, J.M., Gonzalez, F.J., Ham, J., Kang, H., Peters, J.M., and Evans, R.M. (2006) PPARdelta regulates glucose metabolism and insulin sensitivity. *PNAS.* **103**, 3444-3449.
[228] Mckenna, N.J., and O'Malley, B.W. (2002) Combinatorial control of gene expression by nuclear receptors and coregulators. *Cell*. **108**; 465-474.
[229] Zhu, Y., Qi, C., Korenberg, J.R., Chen, X.N., Noya, D., Roa, M.S., Reddy, J.K. (1995) Structural organization of mouse peroxisome proliferator-activated receptor gamma (mPPAR gamma) gene:alternative promoter use and different splicing yield two mPPAR gamma isoforms. *Proc. Natl. Acad. Sci. U.S.A.* **92**, 7921-5
[230] Tontonoz, P., Hu, E.,Graves, R.A., Budavari, A.I., Spiegelman, B.M. (1994) mPPAR gamma 2:tissue-specific regulator of an adipocyte enhance. *Genes Dev.* **8**, 1224-34.
[231] Tontonoz, P., Nagy, L., Alvarez, J.G., Thomazy, V.A., Evans, R.M. (1998) PPARgamma promotes monocyte/macrophage differentiation and uptake of oxidized LDL. *Cell.* **93**, 241-52.
[232] Schoonjan, K., Peinnado-Onsurbe, J., Lefebvre, A.M., Heyman, R.A., Briggs, M. et al. (1996) PPARalpha and PPARgamma activators direct a distinct tissue-specific transcriptional response via a PPRE in the lipoprotein lipase gene. *EMBO J.* **15**, 5336-48.
[233] Martin, G., Schoonjans, K., Lefebvre, A.M., Staels, B., Auwerx, J. (1997) Coordinate regulation of the expression of the fatty acid transport protein and acyl-CoA synthetase genes by PPARalpha and PPARgamma activators. *J. Biol. Chem.* **272**, 28210-17.
[234] Kishida, K., Shimomura, I., Nishizawa, H., Maeda, N., Kuriyama, H., et al. (2001) Enhancement of the aquaporin adipose gene expression by a peroxisome proliferator-activated receptor gamma. *J. Biol. Chem.* **276**, 48572-79.
[235] He, W., Barak, Y., Hevener, A., Olson, P., Liao, D., Le, J., Nelson, M., Ong, E., Olefsky, J.M., and Evans R.M. (2003) Adipose-specific peroxisome proliferator-activated receptor gamma knockout causes insulin resistance in fat and liver but not in muscle. *Proc. Natl, Acad. Sci. U.S.A.* **100**; 15712-15717.
[236] Wu, Z., Xie, Y., Morrison, R.F., Bucher, N.L., Farmer, S.R. (1998) PPARγ induces the insulin-dependent glucose transporter GLUT4 in the absence of C/EBPα during the conversion of 3T3 fibroblasts into adipocytes. *J. Clin. Invest.* **101**; 22-32.
[237] Singh, S., Loke, Y.K., Furberg, C.D. (2007) Long-term Risk of Cardiovascular Events with Rosiglitazone: A Meta-analysis. *JAMA*. **298**, 1189-1195.
[238] Lincoff, M., Wolski, K., Nicholls, S.J., Nissen, S.E. (2007) Pioglitazone and Risk of Cardiovascular Event in Patients with Type 2 Diabetes Mellitus: A Meta-analysis of Randomized Trials. *JAMA*. **298**, 1180-1188.
[239] Boden, G., Homko, C., Mossoli, M., Showe, L., Nichols, C., Cheung, P. (2005) Thiazolidinediones upregulate fatty acid uptake and oxidation in adipose tissue of diabetic patients. *Diabetes*. **54**, 880-85.
[240] Medina-Gomez, G., Gray, S., Vidal-Puig, A. (2007) Adipogenesis and lipotoxicity: role of peroxisome proliferator-activated receptor gamma (PPARgamma) and PPARgammacoactivator-1 (PGC1). *Public Health Nutr.* **10**, 1132-7.
[241] Eberlé, D., Hegarty, B., Bossard, P., Ferré, P., Foufelle, F. (2004) SREBP transcription factors: master regulators of lipid homeostasis. *Biochimie.* **86**, 839-48.
[242] Pacheco-Alvarez, D., Solórzano-Vargas, R.S., Del Río, A.L (2002) Biotin in metabolism and its relationship to human disease. *Arch. Med. Res.* **33**, 439-47
[243] Hunt, M.C., and Alexson, S.E.H. (2002) The role acyl-CoA thioesterases play in mediating intracellular lipid metabolism. *Prog. Lipid Res.* **41**, 99–130.
[244] Stahl, A. (2004) A current review of fatty acid transport proteins (SLC27). *Pflugers Arch.* **447**, 722-7.
[245] Kazachkov, M., Chen, Q., Wang, L., Zou, J. (2008) Substrate preferences of a lysophosphatidylcholine acyltransferase highlight its role in phospholipid remodeling. *Lipids*. **43**, 895-902.
[246] Hato, T., Tabata, M., Oike, Y. (2008) The role of angiopoietin-like proteins in angiogenesis and metabolism. *Trends Cardiovasc. Med.* **18**, 6-14.

[247] Alenghat, T., Meyers, K., Mullican, S.E., Leitner, K., Adeniji-Adele, A., Avila, J., Bucan, M., Ahima, R.S., Kaestner, K.H., Lazar, M.A. (2008) Nuclear receptor corepressor and histone deacetylase 3 govern circadian metabolic physiology. *Nature*. **456**, 997-1000.
[248] Clausen, T., Elbrink, J., Martin, B.R. (1974) Insulin controlling calcium distribution in muscle and fat cells. *Acta Endocrinol*. **77**, 137-143.
[249] Yang, C., Watson, R.T., Elmendorf J.S., Sacks D.B., Pessin, J.E. (2000) Calmodulin antagonists inhibit insulin-stimulated GLUT4 (glucose transporter 4) translocation by preventing the formation of phosphatidylinositol 3,4,5-triphosphate in 3T3-L1 adipocytes. *Mol. Endocrinol.* **14**, 317-326.
[250] Heyward, C.A., Pettitt, T.R., Leney, S.E., Welsh, G.I., Tavaré, J.M., Wakelam, M.J. (2008) An intracellular motif of GLUT4 regulates fusion of GLUT4-containing vesicles. *BMC Cell Biol.* **9,** 25.
[251] Sears Worral, D. and Olefsky, J.M. (2002) The effects of intracellular calcium depletion on insulin signalling in 3T3-L1 adipocytes. *Mol. Endocrinol.* **16**, 378-389.
[252] Anghel, S.I., Bedu, E., Delucinge, C., Descombes, V.P., Desvergne, B. and Wahli, W. (2007) Adipose Tissue Integrity as a Prerequisite for Systemic Energy Balance: A CRITICAL ROLE FOR PEROXISOME PROLIFERATOR-ACTIVATED RECEPTOR γ. *J. Biol. Chem*., **282,** 29946-29957.
[253] McCormack, G., Halestrap, A.P. and Denton, R.M. (1990) Role of calcium ions in regulation of mammalian intramitochondrial metabolism. *Physiol. Rev.* **70**, 391–425.
[254] Reddy, A.B., Ramana, K.V. (2009) Aldose reductase inhibition: Emerging drug target for the treatment of cardiovascular complications. *Recent Pat. Cardiovasc. Drug Discov.* Epub ahead of print.
[255] Boulanger, E., Wautier, J.L., Dequiedt, P., Schmidt, A.M. (2006) Glycation, glyoxidation and diabetes mellitus. *Nephrol. Ther.* **1**, S8-16.
[256] Yamauchi, T., Kamon, J., Waki, H., Murakami, K., Motojima, K., Komeda, K., Ide, T., Kubota, N., Terauchi, Y., Tobe, K., Miki, H., Tsuchida, A., Akanuma, Y., Nagai, R., Kimura, S., Kadowaki, T. 2001 The mechanisms by which both heterozygous peroxisome proliferator-activated receptor gamma (PPARgamma) deficiency and PPARgamma agonist improve insulin resistance. *J. Biol. Chem.* **276**, 41245-54.
[257] Laplante, M., Festuccia, W.T., Soucy, G., Gélinas, Y., Lalonde, J., Berger, J.P., Deshaies, Y. (2006) Mechanisms of the depot specificity of peroxisome proliferator-activated receptor gamma action on adipose tissue metabolism. *Diabetes.* **55**, 2771-8.
[258] Yao-Borengasser, A., Rassouli, N., Varma, V., Bodles, A.M., Rasouli, N., Unal, R., Phanavanh, B., Ranganathan, G., McGehee, R.E. Jr., Kern, P.A. (2008) Stearoyl-coenzyme A desaturase 1 gene expression increases after pioglitazone treatment and is associated with peroxisomal proliferator-activated receptor-gamma responsiveness. *J. Clin. Endocrinol. Metab.* **93**, 4431-9.
[259] Guan, H.P., Li, Y., Jensen, M.V., Newgard, C.B., Steppan, C.M. and Lazar, M.A. (2002) A futile metabolic cycle activated in adipocytes by antidiabetic agents. *Nat. Med.* **8,** 1122–1128.
[260] Steinbrecher, U.P., Pritchard, P.H. (1989) Hydrolysis of phosphatidylcholine during LDL oxidation is mediated by platelet-activating factor acetylhydrolase. *J. Lipid Res.* **30**, 305-15.
[261] Shi, H., Halvorsen, Y-D., Ellis, P.N., Wilkison, W.O., and Zemel M. (2000) Role of intracellular calcium in human adipocyte differentiation. *Physiol. Genomics.* **3**, 75-82.
[262] Tang, C., Cho, H.P., Nakamura, M.T., and Clarke S.D. (2003) Regulation of human delta-6 desaturase gene transcription: identification of a functionaln direct repeat-1 element. *J. Lipid Res.* **44**, 686-695.
[263] Chui, P.C., Guan, H-P, Lehrke, M., and Lazar M.A. (2005) PPARγ regulates adipocyte cholesterol metabolism via oxidized LDL receptor 1**.** *J Clin Invest.* **115**, 2244-56.
[264] Lebovitz HE, Dole JF, Patwardhan R, Rappaport, E.B., Freed, M.I. (2001) Rosiglitazone monotherapy is effective in patients with type 2 diabetes. *J. Clin. Endocrinol. Metab.* **86**, 280–8.
[265] Bays, H., Mandarino, L., DeFronzo, R.A. (2004) Role of the adipocyte, free fatty acids, and ectopic fat in pathogenesis of type 2 diabetes mellitus: peroxisomal proliferators-activated receptor agonists provide a rational therapeutic approach. *J Clin Endocrinol Metab.* **89**, 463–78.
[266] Carmona, M.C., Louche, K., Nibbelink, M., Prunet, B., Bross, A., Desbazeille, M., Dacquet, C., Renard, P., Casteilla, L., Pénicaud, L. (2005) Fenofibrate prevents Rosiglitazone-induced body weight gain in ob/ob mice. *Int. J. Obes.* **29**, 864-71.
[267] Martin, G., Schoonjans, K., Staels, B., Auwerx, J. (1998) PPARgamma activators improve glucose homeostasis by stimulating fatty acid uptake in the adipocytes. Atherosclerosis **137** Suppl, S75-80.

[268] Kintscher, U., Law, R.E. (2005) PPARgamma-mediated insulin sensitization: the importance of fat versus muscle. **288**, 287-91.
[269] Gray, S.L., Vidal-Puig, A.J. (2007) Adipose tissue expandability in the maintenance of metabolic homeostasis. *Nutr Rev*. **65**, S7-12.
[270] Luquet, S., Gaudel, C., Holst, D., Lopez-Soriano, J., Jehl-Pietri, C., Fredenrich, A., Grimaldi, P.A. (2005) Roles of PPAR delta in lipid absorption and metabolism: a new target for the treatment of type 2 diabetes. *Biochim. Biophys. Acta.* **1740**, 313-317.
[271] Luquet, S., Lopez-Soriano, J., Holst, D., Fredenrich, J., Melki, M., Rassoulzadegan, M., Grimaldi P.A. (2003) Peroxisome proliferator-activated receptor δ controls muscle development and oxidative capability. *FASEB J*. **17**, 2299-2301.
[272] Constantin, D., Constantin-Teodosiu, D., Layfield, R., Tsintzas, K., Bennett, A.J., Greenhaff, P.L. (2007) PPARdelta agonism induces a change in fuel metabolism and activation of an atrophy programme, but does not impair mitochondrial function in rat skeletal muscle. *J Physiol*. **15**, 381-90.
[273] Higashiyama, H., Billin, A.N., Okamoto, Y., Kinoshita, M., Asano, S. (2007) Expression profiling of peroxisome proliferator-activated receptor-delta (PPAR-delta) in mouse tissues using tissue microarray. *Histochem. Cell. Biol.* **127**, 485-94.
[274] Brunmair, B., Staniek, K., Dorig, J., Szocs, Z., Stadlbauer, K., Marian, V., Gras, F., Anderwald, C., Nohl, H., Waldhausl, W., Furnsinn, C. (2006) Activation of PPAR-delta in isolated rat skeletal muscle switches fuel preference from glucose to fatty acids. *Diabetologia.* **49**, 2713-22.
[275] Tan, C.Y., Vidal-Puig, A. (2008) Adipose tissue expandability: the metabolic problems of obesity may arise from the inability to become more obese. *Biochem. Soc. Trans.* **36**, 935-40.
[276] Neville, C., Rosenthal, N., McGrew, M., Bogdanova, N. and Hauschka, S. (1997) Skeletal muscle cultures. *Methods in Cell Biology*. **52**, 85-116.
[277] Runge, D., Runge, D. M., Jager, D., Lubecki, K.A., Beer Stolz, D., Karathanasis, S., Kietzmann, T., Strom, S.C., Jungermann, K., Fleig, W.E., and Michalopoulos, G.K. (2000) Serum-free, long-term cultures of human hepatocytes: maintenance of cell morphology, transcription factors, and liver-specific functions. *Biochem. Biophys. Res Commun*. **269**, 46–53.
[278] Clayton, R.F., Rinaldi, A., Kandyba, E.E, Edward, M., Willberg, C., Klenerman, P., Patel, A.H. (2005) Liver cell lines for the study of hepatocyte functions and immunological response. *Liver Int*. 25, 389-402.
[279] Steinhelper, M.E., Lanson Jr., N.A., Dresdner, K.P., Delcarpio, J.B., Wit, A.L. and Claycomb, W.C. and Field, L.J. (1990) Proliferation in vivo and in culture of differentiated adult atrial cardiomyocytes from transgenic mice, *Am. J. Physiol.* **259,** 1826–1834.
[280] Jaffredo, T., Chestier, A., Bachnou, N. and Dieterlen-Lievre, F. (1991) MC29-immortalized clonal avian heart cell lines can partially differentiate in vitro, *Exp. Cell Res.* **192**, 481–491.
[281] Katz, E.B., Steinhelper, M.E., Delcarpio, J.B., Daud, A.I., Claycomb, W.C. and Field, L.J. (1992) Cardiomyocyte proliferation in mice expressing alpha-cardiac myosin heavy chain-SV40 T-antigen transgenes, *Am. J. Physiol*. **262**, 1867–1876.
[282] Wang, C., Neckelmann, N., Mayne, A., Herskowitz, A., Srinivasan, A., Sell, K.W. Ahmed-Ansari, A. (1991) Establishment of a human fetal cardiac myocyte cell line, *In Vitro Cell. Dev. Biol.* **27**, 63–74.
[283] Claycomb, W., Lanson, N., Stallworth, B., Egeland, D., Delcaprio, J., Bahinski, A., Izzo, N. (1998) HL-1 cells: a cardiac muscle cell line that contracts and retains phenotypic characteristics of adult cardiomyocyte, *Proc. Natl. Acad. Sci. USA* . **95**, 2979–2984.
[284] Barak, Y., Liao, D., He, W., Ong, E.S., Nelson, M.C., Olefsky, J.M., Boland, R., Evans, R.M. (2002) Effects of peroxisome proliferator-activated receptor delta on placentation, adiposity, and colorectal cancer. *Proc. Natl. Acad. Sci. U.S.A.* **99**, 303-8.
[285] Peters, J.M., Lee, S.S., Li, W., Ward, J.M., Gavrilova, O., Everett, C., Reitman, M.L., Hudson, L.D., Gonzalez, F.J. (2000) Growth, adipose, brain, and skin alterations resulting from targeted disruption of the mouse peroxisome proliferator-activated receptor beta(delta). *Mol. Cell Biol*. **20**, 5119-28.
[286] Hodson, M.P., Dear, G.J., Griffin, J.L., Haselden, J.N. (2008) An approach for the development and selection of chromatographic methods for the high-throughput metabolomic screening of urine by ultra pressure LC-ESI-ToF-MS. *Metabolomics*. **5**, 166-182.
[287] Theodoridis, G., Gika, H.G., and Wilson, I.D. (2008) LC-MS-based methodology for global metabolite profiling in metabonomics/metabolomics. *TrAC Trends in anal. chem.* **3**, 251-260.

[288] Rammouz, R.E., Létisse, F., Durand, S., Portais, J.C., Moussa, Z.W., Fernandez, X. (2009) Analysis of skeletal muscle metabolome: Evaluation of extraction methods for targeted metabolite quantification using liquid chromatography tandem mass spectrometry. *Anal. Biochem.* Epub ahead of print.